REPORT NO.
UCB/EERC-82/20
NOVEMBER 1982

EARTHQUAKE ENGINEERING RESEARCH CENTER

GENERALIZED PLASTIC HINGE CONCEPTS FOR 3D BEAM-COLUMN ELEMENTS

by

PAUL FU-SONG CHEN
GRAHAM H. POWELL

Report to Sponsor:
National Science Foundation

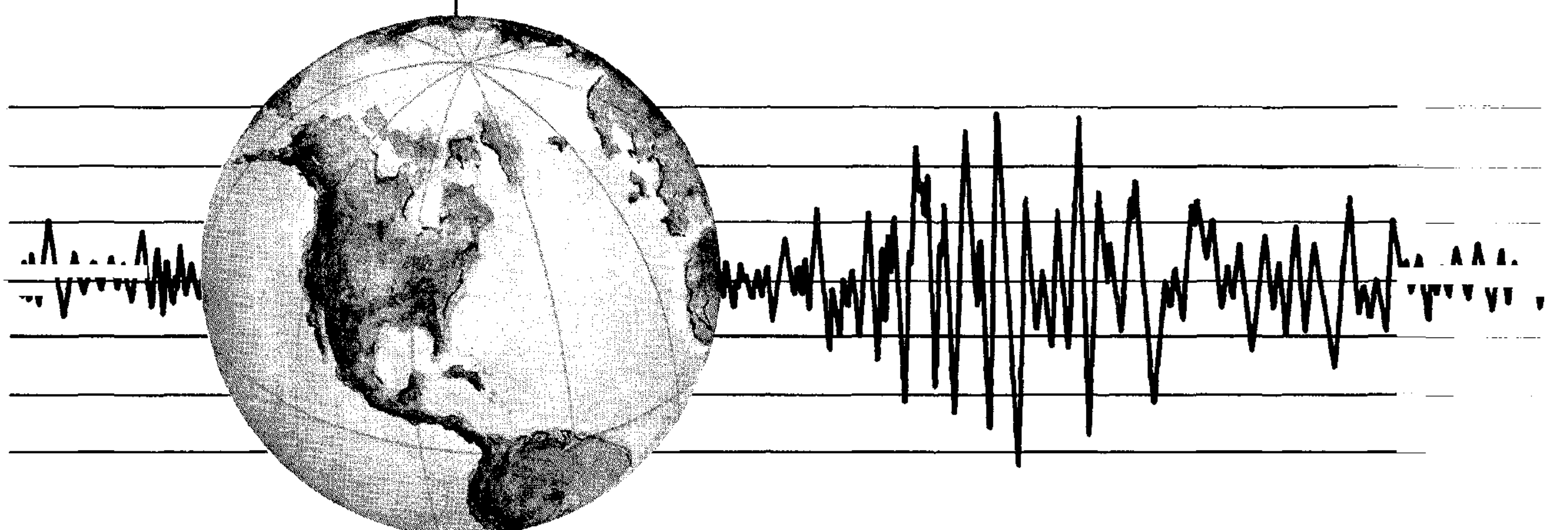

COLLEGE OF ENGINEERING

UNIVERSITY OF CALIFORNIA · Berkeley, California

For sale by the National Technical Information Service, U.S. Department of Commerce, Springfield, Virginia 22161.

See back of report for up to date listing of EERC reports.

50272-101

REPORT DOCUMENTATION PAGE	1. REPORT NO. NSF/CEE-82062	2.	3. Recipient's Accession No. PB3 247981

4. Title and Subtitle Generalized Plastic Hinge Concepts for 3D Beam-Column Elements	5. Report Date November 1982
	6.
7. Author(s) Paul F.-Song Chen and Graham H. Powell	8. Performing Organization Rept. No. UCB/EERC-82/20
9. Performing Organization Name and Address Earthquake Engineering Research Center, University of California, Berkeley, 47th Street and Hoffman Blvd., Richmond, Calif. 94804	10. Project/Task/Work Unit No. 3371609
	11. Contract(C) or Grant(G) No. (C) (G) CEE-8105790
12. Sponsoring Organization Name and Address National Science Foundation, 1800 G Street, N.W., Washington, D.C. 20550	13. Type of Report & Period Covered
	14.

15. Supplementary Notes

16. Abstract (Limit: 200 words)

In the "section" type of model, inelastic behavior is defined for the cross section as a whole, rather than for individual fibers. Action-deformation relationships for the cross section must be devised, considering the stress-strain characteristics of the cross section material. Models of this type are less accurate than fiber models, but more efficient computationally.

This report presents the theory and computational techniques for the "section" type of model and analyzes five example structures. In developing the model, inelastic interaction between bending moments, torque and axial force has been considered by means of yield interaction surfaces and a flow-rule type of plasticity theory. Emphasis has been placed on the ability to consider arbitrary loading-unloading cycles of the type likely to be induced by an earthquake. Both stable hysteretic action-deformation characteristics and relationships involving stiffness degradation are considered.

Three inelastic beam-column elements have been developed for the computer programs WIPS and/or ANSR: an element with distributed plasticity and nondegrading stiffness suitable for modeling inelastic behavior in piping systems; an element with lumped plasticity and nondegrading stiffness suitable for modeling inelastic steel beams and columns in buildings; an element, suitable for modeling inelastic reinforced concrete beams and columns in buildings, with lumped plasticity and degrading stiffness.

17. Document Analysis a. Descriptors

b. Identifiers/Open-Ended Terms

c. COSATI Field/Group

18. Availability Statement: Release Unlimited	19. Security Class (This Report)	21. No. of Pages 277
	20. Security Class (This Page)	22. Price

(See ANSI-Z39.18) See Instructions on Reverse OPTIONAL FORM 272 (4-77) (Formerly NTIS-35)

GENERALIZED PLASTIC HINGE CONCEPTS FOR 3D BEAM-COLUMN ELEMENTS

by

Paul Fu-Song Chen
Graduate Student

and

Graham H. Powell
Professor of Civil Engineering

Report to
National Science Foundation
under Grant No. CEE 8105790

Report No. UCB/EERC-82/20
Earthquake Engineering Research Center
College of Engineering
University of California
Berkeley, California

November 1982

i-b

ABSTRACT

Two basic procedures may be used for modeling the inelastic behavior of beams and columns. In the "fiber" type of model, the element cross section is divided into a number of small areas (fibers), and the behavior is governed by the stress-strain characteristics of the fiber material. Detailed and accurate results can be obtained, but the computational cost is high. In the "section" type of model, inelastic behavior is defined for the cross section as a whole, not for individual fibers. Action-deformation relationships for the cross section must be devised, considering the stress-strain characteristics of the cross section material. Models of this type are less accurate than fiber models, but more efficient computationally.

The purpose of the research has been to explore in depth the theory and computational techniques for the "section" type of model. In developing the model, inelastic interaction between bending moments, torque and axial force has been considered by means of yield interaction surfaces and a flow-rule type of plasticity theory. Emphasis has been placed on the ability to consider arbitrary loading-unloading cycles of the type likely to be induced by an earthquake. The study has considered both stable hysteretic action-deformation characteristics and relationships involving stiffness degradation.

Three separate inelastic beam-column elements, which share similar concepts, have been developed, as follows.

(a) An element with distributed plasticity and nondegrading stiffness, for the computer programs ANSR and WIPS. This element is most suitable for modeling inelastic behavior in piping systems.

(b) An element with lumped plasticity and nondegrading stiffness, for the ANSR program. This element is most suitable for modeling inelastic steel beams and columns in buildings.

(c) An element with lumped plasticity and degrading stiffness, for the ANSR program. This element is most suitable for modeling inelastic reinforced concrete beams and columns in buildings.

The theory and computational procedure are described in detail for each element.

Five example structures have been analyzed to test the elements and to assess their acceptability for different applications. The examples include a steel tubular beam-column; a steel tubular braced frame; a reinforced concrete cantilever beam under biaxial bending; a reinforced concrete frame subjected to earthquake excitation; and a pipe undergoing large displacements following pipe rupture.

ACKNOWLEDGEMENTS

The research described in this report was supported in part by the National Science Foundation under Grant No. CEE8105790 and in part by Lawrence Livermore National Laboratory under Subcontract No. 3371609. The authors wish to express their sincere appreciation for this support.

Sincere appreciation is also expressed to Linda Calvin for preparation of the typescript and to Gail Feazell and Mary Edmunds-Boyle for preparation of the figures.

TABLE OF CONTENTS

Preceding page blank

Page

Page

Page

A. OBJECTIVE AND SCOPE

A1. INTRODUCTION

A1.1 GENERAL

In frame structures the multi-dimensional motion of an earthquake has its greatest effect on column loading. The columns, especially those at the building corners, are subjected to biaxial bending from combined longitudinal, transverse, and torsional motion of the structure, with added axial loads due to overturning. It is well known that the bending strength in any particular direction is decreased by the existence of a simultaneous moment along another axis. Recently, a number of papers have been published on the earthquake damage to building structures during the 1971 San Fernando earthquake. In these studies, the effect of two-dimensional earthquake motion on the response of structural members was recognized to be substantially more significant than had been previously anticipated [14,15,16,18,29].

In order to obtain true evaluations of seismic safety, strong motion response analyses which consider the dynamic structural properties in the inelastic range are essential. Such analyses must be able to trace the damage process of the structural members in detail. A detailed analysis of the dynamic evolution of a structure subjected to intense ground motion requires realistic modeling of the restoring force characteristics of the constituent members. One of the difficulties in this regard is the idealization of the three-dimensional interaction of the restoring forces in members subjected to biaxial bending with varying axial force. An identification of the characteristics of this class of dynamic behavior is important to the understanding of the nature of severe damage in structures of a variety of types.

Two basic procedures may be used for modeling the inelastic behavior of beams and columns. In the "fiber" type of model, the member cross section is divided into a number of small areas (fibers). Each area is assumed to be uniaxially stressed and to have behavior governed by the hysteretic stress-strain characteristics of the material it stimulates. Detailed and accurate results can be obtained from models of this type, but the computational effort required makes them expensive for practical application. In the "section" type of model, it is assumed that inelastic behavior is defined for the cross section as a whole, not for individual fibers. Force-deformation relationships for the cross section must be specified, each governed by the cross section dimensions and the hysteretic force-deformation characteristics of the member material. Models of this type tend to be more difficult to use and less accurate than fiber models, but more efficient computationally. The research described in this report has been concerned only with the "section" type of model.

There are two basic approaches used in modeling the inelastic behavior of a structural element using a "section" model, as follows.

(a) "Distributed" Plasticity Approach:

It is assumed that yielding is distributed over the element length. The structural characteristics of the element are calculated by assuming a displaced shape for the element axis, with internal forces calculated at various sections from the resulting curvatures and axial strains. The element stiffness is then determined by integrating along the element. Mutli-dimensional action-deformation relationships must be specified for the cross sections, so that the effects of interaction among bending moment, axial force, and other actions can be taken into account. These relationships will be in terms of action quantities, such as moment and axial force, and deformation quantities, such as curvature and axial strain.

(b) "Lumped" Plasticity (Plastic Hinge) Approach:

Yield is assumed to take place only at generalized plastic hinges of zero length, and the beam between hinges is assumed to remain linearly elastic. In this approach, multi-dimensional action-deformation relationships must be specified for the hinges, in terms of moment and axial force actions, as before, but with deformations such as hinge rotations and axial extensions.

Lumped plasticity models are particularly suitable for the analysis of building frames under seismic loads, because plastic action in such structures is usually confined to small regions at the beam and column ends. The distributed plasticity approach tends to be preferable for structures in which the plastic zone locations are not known in advance. A particular application is the analysis of pipe whip, in which a plastic wave may move along the pipe.

A1.2 HISTORICAL BACKGROUND

Many studies of inelastic frames under earthquake forces have been described in recent years. Comprehensive surveys of early investigations of plane frames have been provided by Powell [1] and Otani [2]. A brief history of more recent studies is presented here.

The action-deformation relationships assigned to a member can have a significant influence on the calculated response. As a result, nonlinear analysis has concentrated on the modeling of stiffness changes in the members and the establishment of realistic hysteretic behavior.

Hidalgo and Clough [3] investigated a number of analytical models for the response prediction of a two-story, single bay frame, which they also tested on a shaking table. Starting with a two-component, elasto-plastic element, they attempted to improve the correlation between analysis and experiment by adding degradation effects to the model. One method of including degradation effects was to impose empirical changes in the value of the elastic modulus at specified times during the excitation. A second technique was based on degradation of the generalized stiffness of the first mode of vibration of the structure. Although these techniques can provide accurate results for specific frames, they are not convenient for general purpose application.

Takeda [4] examined the experimental results from cyclic loading of a series of reinforced concrete connections, and proposed a hysteresis model which was in agreement with these results. Several investigators have used this model, in both its original and modified forms. Litton [5] adopted a modified Takeda model for a reinforced concrete beam element for the DRAIN-2D computer program. This element consists of an elastic beam element with inelastic rotational springs at each end. A similar type of element has been suggested by Otani [6]. This element consists of a bilinear beam element with an inelastic rotational spring and a rigid link at each end. Neither of these models considered biaxial interaction effects.

Riahi and Powell [7] have described a 3D beam-column element and incorporated it into the ANSR [8,9] computer program. The element is assumed to be made up of three parallel components, two elasto-plastic components to represent yielding and one elastic component to model strain hardening. Interaction for biaxial bending and axial force are considered, but the element does not have stiffness degrading characteristics.

Takizawa and Aoyama [10] have developed the basic formulation for a reinforced concrete column model acted upon by biaxial bending moments. This model incorporates a two-dimensional extension of various nonlinear models for one-dimensional response analysis, in particular a degrading trilinear stiffness model. The theory demonstrates how degradation effects can be considered, but it does not account for axial forces and was not applied in a complete beam-column element.

Morris [11] presented a procedure for three-dimensional frames by employing an approximate interaction equation by Tebedge and Chen [12] for I section columns under biaxial bending. However, complete loading-unloading cycles and hysteretic behavior at the plastic hinges were not studied. Uzgider [13] adapted this method to study the hysteretic behavior at plastic hinges for three-dimensional dynamically loaded frames. The elasto-plastic action-deformation relationship at the ends of the frame member was represented by an equation which corresponds essentially to the inverse of the Ramberg-Osgood representation. Inelastic interaction of biaxial end moments and axial force was included.

A1.3 SCOPE OF STUDY

The purpose of the study described in this thesis has been to explore in depth the theory and computational techniques for the "section" type of model, considering both the distributed plasticity and lumped plasticity approaches. In developing the model, inelastic interaction between bending moments, torque and axial force was considered by means of yield interaction surfaces and a flow-rule type of plasticity theory. Emphasis has been placed on the ability to consider arbitrary loading-unloading cycles of the type likely to be induced by an earthquake. The study has considered both stable hysteretic action-deformation characteristics and relationships involving stiffness degradation.

Three separate inelastic beam-column elements, which share similar concepts, have been developed, as follows.

(a) An element with distributed plasticity and nondegrading stiffness has been developed and incorporated into the computer programs ANSR [8,9] and WIPS [31]. This element is most suitable for modeling inelastic behavior in piping systems.

(b) An element with lumped plasticity and nondegrading stiffness has been developed and incorporated into the computer program ANSR. This element is most suitable for modeling inelastic steel beams and columns in buildings.

(c) An element with lumped plasticity and degrading stiffness has been developed and incorporated into ANSR. This element is most suitable for modeling inelastic reinforced concrete beams and columns in buildings.

A1.4 REPORT LAYOUT

Sections B, C, and D are self-contained reports, one for each of the three elements. Examples using all three of the elements and general conclusions are contained in Section E.

B. DISTRIBUTED PLASTICITY BEAM-COLUMN ELEMENT

Preceding page blank

B1 INTRODUCTION

The *beam* type element provides a more economical means of modeling inelastic pipe behavior than the *pipe* type element.

In the *pipe* element, the stress-strain relationship for the pipe material is specified. The inelastic material behavior is then monitored at several points on the pipe cross section, and the moment-curvature and torque-twist relationships are calculated by the computer code. In the *beam* element, the moment-curvature and torque-twist relationships must be specified by the analyst, and the inelastic behavior is monitored for the cross section as a whole, not at individual points. The *beam* element is more efficient computationally, but it is likely to be less accurate than the pipe element, and less information is calculated on the stresses and strains in the pipe. Only straight *beam* elements are permitted, and preliminary calculation is required to determined the moment-curvature and torque-twist relationships.

The essential features of the element are as follows:

(1) The element may be arbitrarily oriented in space, but it must be straight. Elbows can be approximated using a number of straight elements.

(2) The element is an inelastic beam-column. Inelastic behavior is defined using stress resultant-strain resultant (e.g. moment-curvature) relationships.

(3) Multilinear stress resultant-strain resultant relationships may be specified. Kinematic strain hardening is assumed for cyclic loading. Strain rate effects may be considered if desired.

(4) Interaction between bending moments, torque and axial force is considered by means of yield interaction surfaces. The kinematic hardening rule corresponds to translation of the yield surface without change of size or shape.

(5) The effects of cross section ovalling and internal pressure cannot be considered directly. If these effects are important, they must be reflected in the stress resultant-strain resultant

relationships.

(6) Cross section plasticity is monitored at two cross sections in the element and is assumed to be distributed over the element length. Element lengths must be chosen so that yielding takes place more or less uniformly over the length of any element (i.e. is not concentrated in short plastic hinge regions at the element ends).

(7) Large displacement effects may be considered, if desired, using an *engineering* theory (i.e. not a consistent continuum mechanics approach).

A general description of the element properties is presented in Section B2. Theoretical details are presented in Sections B3 and B4. Details of the computer logic are described in Section B5. An element user guide for the ANSR program is presented in Section B6.

B2 ELEMENT PROPERTIES

B2.1 AXES

Element properties and results are specified in the local coordinate system x,y,z, defined as shown in Fig. B2.1. If node K is not specified, its location is assumed as follows.

(a) If IJ is not vertical, node K is at $Y = +\infty$. The xy plane is then the vertical plane containing the element.

(b) If IJ is vertical, node K is at $X = +\infty$. The xy plane is then parallel to the XY plane.

B2.2 MODELING OF INELASTIC BEHAVIOR

B2.2.1 General

It is assumed that yielding is distributed over the element. To satisfy this assumption in regions of large moment gradient, it will generally be necessary to specify fairly short elements.

Yielding is monitored at two cross sections in the element, located at the Gauss points (Fig. B2.1). Tangent stiffness relationships between the stress and strain resultants at the Gauss points are modeled using a plasticity theory similar to the Mroz theory for yield of metals. The element stiffness is then determined by Gauss integration (i.e. the conventional finite element technique).

B2.2.2 Section Properties

The relationships between actions (stress resultants) and deformations (strain resultants) must be specified for the cross sections at the Gauss points. The relationships at the two points in any element will typically be the same, but may be different if desired.

Relationships must be specified as shown in Fig. B2.2 for each of four action-deformation pairs, namely (1) bending moment, M_y, and corresponding curvature, ψ_y; (2) bending moment, M_z, and corresponding curvature, ψ_z; (3) torque, M_x, and corresponding rate of twist, ψ_x; and (4) axial force, F, and corresponding strain, ϵ. Each relationship may have up to four linear segments, as shown. The relationships may be of different shape for each stress resultant. For example, for material with an elastic-perfectly-plastic stress-strain relationship, the torque-twist and force-extension relationships will also be elastic-perfectly-plastic, whereas the moment-curvature relationships will exhibit strain hardening behavior (Fig. B2.3). It is necessary, however, for the deformation values at changes in stiffness to have the same ratios for all relationships, as shown in Fig. B2.2. This restriction is necessary to avoid inconsistencies in the plasticity theory, as explained later.

The relationships between actions and deformations may be determined by separate analysis or may be obtained from experiments. If *beam* elements are used to represent pipe elbows, the relationships should account for ovalling effects.

B2.2.3 Interaction Surface for First Yield

The actions M_y, M_z, M_x, and F interact with each other to produce initial yield of the cross section. For modeling of pipes, the influence of axial force on yield will usually be small and can be ignored. For other applications, however, all four actions may have significant effects. Because the *beam* element is not intended only for piping, a general theoretical formulation is used. For the special case of piping, it is recommended that the influence of axial force on yield be eliminated by specifying a very large value of S_{u1} (Fig. B2.2) for axial effects.

The interaction effect is determined by an interaction surface (yield surface). To allow for a variety of applications, provision is made in the theory for five different interaction surfaces. These surfaces are all four-dimensional (i.e. M_y, M_z, M_x, and F), and hence cannot be shown easily using diagrams. The surfaces differ, however, mainly in the way in which the axial force interacts with the three moments. Hence, the differences can be illustrated using the three-dimensional diagrams in Fig. B2.4. In these figures, the M_i and M_j axes indicate any two of the moments, and the F axis indicates axial force. The equations defining the interaction surfaces are shown in the figure.

Surface 1 is elliptical and is the simplest mathematically. Surfaces 2, 3, and 4 allow more realistic modeling of moment-force interaction for cases in which axial force effects are substantial. For all of these four surfaces, the interaction among M_y, M_z, and M_x is elliptical, and only the force-moment interaction changes. For piping, the influence of axial force on yield can be ignored, and hence the four surfaces are the same for practical purposes. Interaction surface 5 is of a different form than the other four and is included for greater generality in special cases. For piping, it is recommended that interaction surface 1 be specified, with a very large value for yield under axial force.

B2.2.4 Interaction Surfaces for Subsequent Yield

For modeling a slice with nonlinear material properties, it is assumed that the behavior is elastic-plastic-strain-hardening, as shown in Fig. B2.5. First yield is governed by the initial yield surface; and for each change of stiffness, there is a corresponding "subsequent" yield surface. These surfaces are assumed to have the same *basic* form as the surface for first yield. However, because the action-deformation relationships may be of different shape for each action, the surfaces for the first and subsequent yield will generally not have identical actual shapes. An example in 2D stress resultant space is shown in Fig. B2.5. In this example, yield surfaces considering axial force and moment are produced from corresponding force-strain and moment-curvature relationships.

B2.2.5 Elastic and Plastic Stiffnesses

The initial slopes, K_1, for the action-deformation relationships are defined as the *elastic stiffnesses* and are expressed as:

$$\underline{K}_{se} = diag \; [\; EI_y \; EI_z \; GJ \; EA \;] \tag{B2.1}$$

where E = Young's modulus, G = shear modulus, I = flexural inertia, J = torsional inertia, and A = section area. The slopes of subsequent segments of the action-deformation relationships are denoted as K_2, K_3, and K_4 and are defined as the *post-yield stiffnesses.* They must be specified to provide appropriate post-yield behavior.

The assumed multi-linear action-deformation relationship for each force component can be modeled as a set of springs, consisting of an elastic spring and a series of rigid plastic springs, as shown in Fig. B2.6. The plastic stiffnesses, K_p, of the rigid-plastic springs can be related to the post-yield stiffness values, K. The relationship between plastic stiffness, K_{pi}, and post-yield stiffnesses, K_i and K_{i+1}, can be obtained as:

$$K_{pi} = \frac{K_i K_{i+1}}{K_i - K_{i+1}} \tag{B2.2}$$

For each rigid plastic spring, a plastic stiffness matrix is defined as:

$$\underline{K}_{sp} = diag\ [\ K_{M_y}\ K_{M_z}\ K_{M_x}\ K_F\ ] \tag{B2.3}$$

where KM_y, KM_z, KM_x, and K_F are the plastic stiffnesses of the individual action-deformation relationships, obtained from Eqn. B2.2.

B2.2.6 Hardening Behavior

After first yield, the yield surfaces are assumed to translate in stress resultant space, obeying a kinematic hardening rule (translation without change of shape or size). An extension of the Mroz theory of material plasticity is used to define the hardening behavior. Because the interaction surfaces are generally not exactly similar, overlapping of the surfaces can occur (as described in detail in Section B3.7); and, as a result, the hardening behavior is more complex than in the basic Mroz theory. For example, in Fig. B2.5b, the current stress resultant point, A, lies on yield surfaces YS_1, YS_2, and YS_3. Hence, all three plastic springs (Fig. B2.6) have yielded, and the direction of plastic flow is a combination of the normal vectors $\underline{n}_1$, $\underline{n}_2$, and $\underline{n}_3$.

B2.2.7 Plastic Flow

Interaction among the stress resultants is considered as shown diagrammatically in Fig. B2.5. Yield begins when the first yield surface is reached. The surface then translates in stress resultant space, the motion being governed by the plastic flow of this first yield surface. Translation of the first surface continues until the second surface is reached. Both surfaces then translate together, governed by a combination of plastic flow on both of the surfaces. For any yield surface, plastic flow is assumed to take place normal to that surface. If two or more surfaces are moving together, the total plastic deformation is equal to the sum of the individual plastic deformations for each yield surface, directed along the respective normal directions at the action point. After some arbitrary amount of plastic deformation, the situation might be as illustrated in Fig. B2.5b.

On unloading, the elastic stiffness values, K_1, govern until the first surface is again reached (Fig. B2.5b). The surface then translates as before.

B2.3 END ECCENTRICITY

Plastic hinges in frames and coupled frame-shear wall structures will form near the faces of the joints rather than at the theoretical joint centerlines. This effect can be approximated by postulating rigid, infinitely strong connecting links between the nodes and the element ends, as shown in Fig. B2.7.

B2.4 INITIAL FORCES

For structures in which static analyses are carried out separately (i.e. outside the ANSR program), initial member forces may be specified. The sign convention for these forces is as shown in Fig. B2.8. These forces are not converted to loads on the nodes of the structure but are simply used to initialize the element end actions. For this reason, initial forces need not constitute a set of actions in equilibrium. The only effects they have on the behavior of the system are (a) to influence the onset of plasticity and (b) to affect the geometric stiffnesses.

B3. THEORY

B3.1 DEGREES OF FREEDOM

The element has two external nodes and two internal Gauss stations, as shown in Fig. B3.1a. The external nodes connect to the complete structure and have six degrees of freedom each, three global translations and three global rotations. After deletion of the six rigid body modes for the complete element and transformation to the local element coordinates, the six deformation degrees of freedom shown in Fig. B3.1b remain.

The transformation from global displacements to element deformations is:

$$\underline{v} = \underline{a}\,\underline{r} \tag{B3.1}$$

in which

$\underline{v}^T = [v_1, v_2, \cdots v_6]$ are the element deformations (Fig. B3.1b);

$\underline{r}^T = [r_1, r_2, \cdots r_{12}]$ are the global displacements (Fig. B3.1a);

and the transformation $\underline{a}$ is well known.

B3.2 SHAPE FUNCTIONS

The element *slice* at each Gauss station has six deformations, namely, axial deformation, rotational deformation about each of the local x, y, z axes, and shear deformation along the y and z axes. These deformations are arranged in the vector $\underline{w}$, where $\underline{w}^T = [w_1, w_2, ..., w_6]$. The shape functions for a uniform elastic beam are assumed to be applicable, in both the elastic and yielded states. These shape functions define the deformations at any location as:

$$\underline{w}(x) = \underline{B}(x)\,\underline{v} \tag{B3.2}$$

in which

$$\underline{B}(x) = \begin{bmatrix} B_{11} & B_{12} & 0 & 0 & 0 & 0 \\ 0 & 0 & B_{23} & B_{24} & 0 & 0 \\ 0 & 0 & 0 & 0 & 1/L & 0 \\ 0 & 0 & 0 & 0 & 0 & 1/L \\ B_{51} & B_{52} & 0 & 0 & 0 & 0 \\ 0 & 0 & B_{63} & B_{64} & 0 & 0 \end{bmatrix} \tag{B3.3}$$

Preceding page blank

and

$$B_{11} = \frac{1}{1+\beta_y}\left\{-4/L + 6x/L^2 - \beta_y/L\right\};$$

$$B_{12} = \frac{1}{1+\beta_y}\left\{-2/L + 6x/L^2 + \beta_y/L\right\};$$

$$B_{23} = \frac{1}{1+\beta_z}\left\{-4/L + 6x/L^2 + \beta_z/L\right\};$$

$$B_{24} = \frac{1}{1+\beta_z}\left\{-2/L + 6x/L^2 + \beta_z/L\right\};$$

$$B_{51} = B_{52} = -\frac{\beta_y}{2(1+\beta_y)};$$

$$B_{63} = B_{64} = -\frac{\beta_z}{2(1+\beta_z)};$$

$$\beta_y = \frac{12EI_y}{GA_y' L^2};$$

$$\beta_z = \frac{12EI_z}{GA_z' L^2};$$

$$\delta_y = \frac{-\beta_y}{2(1+\beta_y)};$$

$$\delta_z = \frac{-\beta_z}{2(1+\beta_z)};$$

$\underline{w}^T_{(x)} = [w_1(x), w_2(x), ..., w_6(x)] =$ deformations at location x in the element; and

$\underline{v}^T = [v_1, v_2, \cdots, v_6] =$ element deformations defined by Eqn. B3.1.

The slice deformations are simply the deformations at the slice locations.

B3.3 SLICE FLEXIBILITY

B3.3.1 General

In one-dimensional stress resultant space, a slice can be modeled as an elastic spring connected in series with rigid-plastic springs (Fig. B2.6). This concept can be expanded to multi-dimensional space, as follows.

The tangent slice stiffness changes as the cross section yields. For any state of the element, a 4 x 4 elastic slice flexibility matrix is first formed, in terms of the section actions (stress resultants) M_y, M_z, M_x, and F_x at each Gauss station. This matrix is then modified by adding in the plastic flexibility on each *active* yield surface to give a 4 x 4 elasto-plastic slice flexibility. This flexibility is inverted to obtain a 4 x 4 slice stiffness (computationally, the Sherman-Morrison formula rather than inversion is used). This stiffness is then expanded to a 6 x 6 slice stiffness by adding stiffnesses to account for shear deformations along the y and z axes. These stiffnesses are

$$K_y = GA_y' \tag{B3.4}$$

$$K_z = GA_z' \tag{B3.5}$$

in which GA_y' = effective shear rigidity along the y axis and GA_z' = effective shear rigidity along the z axis.

In the elasto-plastic state, it is assumed that any deformation increment can be divided into elastic and plastic parts. That is,

$$d\underline{w} = d\underline{w}_e + \sum_i d\underline{w}_{pi} \tag{B3.6}$$

in which

i = active yield surface number;

$d\underline{w}$ = total deformation increment;

$d\underline{w}_e$ = elastic deformation increment; and,

$d\underline{w}_{pi}$ = plastic deformation increment for each active yield surface.

The slice flexibility relationship can thus be written as:

$$d\underline{w} = \underline{f}_s \, d\underline{S} = \left(\underline{f}_{se} + \sum_i \underline{f}_{sp_i}\right) d\underline{S} \tag{B3.7}$$

in which

$\underline{f}_s$ = total slice flexibility;

$\underline{f}_{se}$ = elastic slice flexibility (diagonal, containing inverses of the elastic stiffnesses, $\underline{K}_{se}$); and,

$\underline{f}_{sp_i}$ = plastic flexibilities of each active yield surface.

It is necessary to determine $\underline{f}_{sp_i}$ for each active yield surface and then sum to obtain the total plastic flexibility $\underline{f}_{sp}$.

B3.3.2 Yield Function

Each slice is affected by four stress resultants (M_y, M_z, M_x, and F) with four corresponding deformations. The behavior is elastic-plastic-strain-hardening for each stress resultant individually, as shown in Fig. B2.2. Different yield values and stiffnesses may be specified for each stress resultant.

Initial yield of any slice is governed by a yield function (interaction relationship). Any one of five different yield functions may be specified, as considered in Section B2. After yield, each slice follows a kinematic hardening rule (that is, the yield surface translates in stress resultant space without change of shape or size). The hardening theory is a modification of the Mroz theory for plasticity in metals.

B3.3.3 Plastic Flexibility for a Single Yield Surface

Consider a single yield surface. Let $\underline{S}$ be the vector of stress resultants, where

$$\underline{S}^T = \left[M_y \; M_z \; M_x \; F\right] \tag{B3.8}$$

Assume that the slice is *rigid-plastic*, and let $\underline{w}_p$ be the vector of plastic slice deformations. That is, w_{p1} = plastic flexural deformation about axis y; w_{p2} = plastic flexural deformation about axis z; w_{p3} = plastic rate of twist about axis x; and w_{p4} = plastic rate of extension along axis x.

A flexibility relationship for the slice is required in the form

$$d\underline{w}_p = \underline{f}_{sp} \, d\underline{S} \tag{B3.9}$$

in which $\underline{f}_{sp}$ = slice flexibility matrix. The following assumptions are made:

(1) Let ϕ be the yield function, as considered in Section B3.3.2. The yield surface translates in stress resultant space. After some amount of hardening has taken place, the yield function is $\phi(\underline{S}-\underline{\alpha})$, where $\underline{\alpha}$ = vector defining the new location of the yield surface origin. In two-dimensional space, this is illustrated in Fig. B3.2.

(2) From any given plastic state (i.e. a point on the yield surface), any action increment ($d\underline{S}$) will produce increments of deformation ($d\underline{w}_p$) and yield surface translation ($d\underline{\alpha}$). The direction of $d\underline{S}$ may be arbitrary. It is assumed that the direction of $d\underline{w}_p$ is normal to the yield surface (i.e. an associated flow rule is assumed). The direction of $d\underline{\alpha}$ is determined by the hardening rule (as defined later) and is not necessarily parallel to either $d\underline{S}$ or $d\underline{w}_p$. This is illustrated in Fig. B3.2 for a two-dimensional space.

(3) The direction of the outward normal to the yield surface is the gradient of the yield function. That is,

$$\underline{n} = \frac{\underline{\phi},_s}{\left[\underline{\phi},_s^T \cdot \underline{\phi},_s\right]^{1/2}} \tag{B3.10}$$

in which

$$\underline{\phi},_s^T = \left[\partial\phi/\partial M_y \quad \partial\phi/\partial M_z \quad \partial\phi/\partial M_x \quad \partial\phi/\partial F\right] \tag{B3.11}$$

= yield function gradient; and

$\underline{n}$ = unit normal vector.

Hence, the deformation increment, $d\underline{w}_p$ is given by

$$d\underline{w}_p = \underline{n} \cdot dw_p^* \tag{B3.12}$$

in which dw_p^* = scalar which defines the magnitude of the plastic deformation.

(4) Let the component of $d\underline{S}$ in the direction of $\underline{n}$ be $d\underline{S}_n$ (Fig. B3.2). Hence,

$$d\underline{S}_n = \underline{n} \cdot (\underline{n}^T \cdot d\underline{S}) \tag{B3.13}$$

(5) Assume that $d\underline{S}_n$ and $d\underline{w}_p$ are related by

$$d\underline{S}_n = \underline{K}_{sp} d\underline{w}_p \tag{B3.14}$$

in which

$$\underline{K}_{sp} = diag\,[K_{M_y}\ K_{M_z}\ K_{M_x}\ K_F] \tag{B3.15}$$

is a diagonal matrix of the *plastic* stiffnesses from the individual action-deformation relationships for the slice, as defined in Section B2.2.5.

(6) From the definition of $\underline{dS}_n$ (Eqn. B3.13), it follows that

$$\underline{n}^T d\underline{S} = \underline{n}^T d\underline{S}_n \tag{B3.16}$$

Substitute Eqns. B3.14 and B3.12 into Eqn. B3.16 to get

$$\underline{n}^T \cdot \underline{dS} = \underline{n}^T \cdot \underline{K}_{sp} \cdot \underline{n} \cdot dw_p^* \tag{B3.17}$$

(7) Solve for dv_p^* as

$$dw_p^* = \frac{\underline{n}^T \cdot \underline{dS}}{\underline{n}^T \cdot \underline{K}_{sp} \cdot \underline{n}} \tag{B3.18}$$

(8) Hence, substitute Eqn. B3.18 into Eqn. B3.12 and use Eqn. B3.9 to get

$$d\underline{w}_p = \frac{\underline{n} \cdot \underline{n}^T}{\underline{n}^T \cdot \underline{K}_{sp} \cdot \underline{n}} d\underline{S} = \underline{f}_{sp}\, d\underline{S} \tag{B3.19}$$

Equation B3.19 is the required plastic flexibility relationship for any *active* yield surface.

B3.3.4 Elasto-Plastic Flexibility for Multiple Yield Surfaces

The 4 x 4 elasto-plastic flexibility of the slice, f_s, follows from Eqn. B3.7 as:

$$\underline{f}_s = \underline{f}_{se} + \sum_i \underline{f}_{sp_i} \tag{B3.20}$$

where i = active yield surface. The flexibility for any active yield surface, as derived in Section B3.3.3, can be written as:

$$\underline{f}_{sp_i} = \frac{\underline{n}_i \cdot \underline{n}_i^T}{\underline{n}_i^T \cdot \underline{K}_{sp_i} \cdot \underline{n}_i} \tag{B3.21}$$

in which

$\underline{n}_i$ = normal vector to the surface; and,

$\underline{K}_{sp_i}$ = plastic stiffness matrix for the surface.

B3.3.5 Relationship to Basic Mroz Theory

In the special case where the action-deformation relationships for the four actions are all directly proportional to each other, the yield surfaces are all of the same shape and the plastic stiffnesses for each active yield surface are in the same proportion. The plastic stiffness matrix for each active yield surface can then be formed in terms of the elastic stiffness matrix. That is,

$$\underline{K}_{sp_i} = \alpha_i \, \underline{K}_e \tag{B3.22}$$

where α_i defines the plastic stiffness as a proportion of the elastic stiffness. The plastic flexibility of a slice can then be written as:

$$\underline{f}_{sp} = \sum_i \underline{f}_{sp_i} = \sum_i \left(\frac{1}{\alpha_i}\right) \frac{\underline{n}_i \cdot \underline{n}_i^T}{\underline{n}_i^T \cdot \underline{K}_e \cdot \underline{n}_i} \tag{B3.23}$$

Because all the yield surfaces are the same shape, the $\underline{n}_i$ are all the same. Hence, if $\underline{n}_i = \underline{n}$, Eqn. B3.23 can be written as:

$$\underline{f}_{sp} = \frac{\underline{n} \cdot \underline{n}^T}{\underline{n}^T \cdot (\sum_i \alpha_i) \underline{K}_e \cdot \underline{n}} \tag{B3.24}$$

The flexibility given by this equation is the same as that from the basic Mroz material theory. This shows that the Mroz material theory is a special case of the extended theory derived here.

B3.4 SLICE STIFFNESS CALCULATION

For a nonlinear slice, a tangent action-deformation relationship is required in the form:

$$d\underline{S} = \underline{C}_{st} \, d\underline{w} \tag{B3.25}$$

in which

$\underline{C}_{st}$ = tangent stiffness matrix for a slice.

The procedure used is to develop a tangent flexibility matrix, then invert this flexibility to obtain the stiffness matrix, $\underline{C}_{st}$. Computationally, the Sherman-Morrison formula is used rather than direct inversion. The flexibility of any active yield surface is:

$$\underline{f}_{sp_i} = \frac{\underline{n}_i \cdot \underline{n}_i^T}{\underline{n}_i^T \cdot \underline{K}_{sp_i} \cdot \underline{n}_i} \tag{B3.26}$$

Define

$$\underline{u}_i = \frac{\underline{n}_i}{\left(\underline{n}_i^T \cdot \underline{K}_{sp_i} \cdot \underline{n}_i\right)^{1/2}} \tag{B3.27}$$

The elasto-plastic flexibility can thus be expressed as:

$$\underline{f}_s = \underline{f}_{se} + \sum \underline{f}_{sp_i} = \underline{f}_{se} + \sum \underline{u}_i \underline{u}_i^T \tag{B3.28}$$

The Sherman-Morrison formula states that:

$$[\underline{A} + \underline{u}\,\underline{u}^T]^{-1} = A^{-1} - \frac{A^{-1} u\, u^T A^{-1}}{\underline{u}^T \underline{A}^{-1} \underline{u} + 1} \tag{B3.29}$$

Application of the formula to the inversion of $\underline{f}_s$ gives:

$$\underline{C}_t = \underline{C}_{t(l-1)} - \frac{\underline{C}_{t(l-1)} \underline{u}_l \underline{u}_l^T \underline{C}_{t(l-1)}}{\underline{u}_l^T \underline{C}_{t(l-1)} \underline{u}_l + 1} \tag{B3.30}$$

in which l = current highest active yield surface.

$\underline{C}_{t(l-1)}$ is obtained using the recursion relationships:

$$\underline{C}_{t1} = \underline{f}_{se}^{-1} = \underline{K}_{se} \tag{B3.31a}$$

$$\underline{C}_{ti} = \underline{C}_{t(i-1)} - \frac{\underline{C}_{t(i-1)} \underline{u}_i \underline{u}_i^T \underline{C}_{t(i-1)}}{\underline{u}_i^T \underline{C}_{t(i-1)} \underline{u}_i + 1} \tag{B3.31b}$$

Hence, substitute Eqn. B3.27 into Eqn. B3.30 to get:

$$\underline{C}_t = \underline{C}_{t(l-1)} - \frac{\underline{C}_{t(l-1)} \underline{n}_l \underline{n}_l^T \underline{C}_{t(l-1)}}{\underline{n}_l^T \underline{C}_{t(l-1)} \underline{n}_l + \underline{n}_l^T \underline{K}_{sp_l} \underline{n}_l} \tag{B3.32}$$

The stiffness $\underline{C}_t$ is a 4 x 4 matrix. It is expanded to a 6 x 6 matrix by adding the shear stiffnesses along the y and z axes. The resulting tangent stiffness matrix for the slice, $\underline{C}_{st}$, has the form:

$$\underline{C}_{st} = \begin{bmatrix} C_{t11} & C_{t12} & C_{t13} & C_{t14} & 0 & 0 \\ C_{t21} & C_{t22} & C_{t23} & C_{t24} & 0 & 0 \\ C_{t31} & C_{t32} & C_{t33} & C_{t34} & 0 & 0 \\ C_{t41} & C_{t42} & C_{t43} & C_{t44} & 0 & 0 \\ 0 & 0 & 0 & 0 & GA'_y & 0 \\ 0 & 0 & 0 & 0 & 0 & GA'_z \end{bmatrix} \tag{B3.33}$$

in which

C_{tij} = $\underline{C}_t(i,j)$ in matrix $\underline{C}_t$;

GA_y' = shear rigidity along the element y axis; and,

GA_z' = shear rigidity along the element z axis.

B3.5 ELEMENT STIFFNESS

The element tangent stiffness matrix is given by

$$\underline{K}_t = \int_L \underline{B}^T \underline{C}_{st} \underline{B} \, dx \tag{B3.34}$$

in which

$\underline{C}_{st}$ = tangent stiffness matrix for an element slice at any point; and,

$\underline{B}$ = transformation relating node displacements to slice deformations, defined by Eqn. B3.2.

The integration is carried out numerically using Gauss quadrature. Hence, tangent stiffnesses are needed only for the two slices at the Gauss stations.

B3.6 EQUILIBRIUM NODAL LOADS

Nodal loads in equilibrium with the slice actions in any given state are given by

$$\underline{R} = \int_L \underline{B}^T \underline{S} \, dx \tag{B3.35}$$

in which

$$\underline{S}^T = \left[S_1, S_2, S_3, S_4, S_5, S_6\right]$$

(i.e. the actions corresponding to the element deformations $\underline{v}$); and the matrix $\underline{B}$ is given by Eqn. B3.2. The integral is evaluated numerically using Gauss quadrature.

B3.7 HARDENING RULE

B3.7.1 Geometrical Interpretation

The relationship between the actions and deformations at a slice is multi-linear. The interaction among the stress resultants (M_y, M_z, M_x, and F) is defined by the yield interaction function, as described earlier. After initial yield occurs, the behavior at a slice obeys a kinematic hardening rule (that is, the yield surface translates in action space without change of shape or size). The specific rule followed is a modification of the Mroz strain hardening rule which has been proposed for yield in metals.

B3.7.2 Modified Mroz Hardening Rule

For purposes of illustration, consider a two-dimensional M-F space as shown in Fig. B3.3a. In this figure, it is assumed that the current state (point P_i) is on yield surface YS_i, and that loading is taking place towards surface YS_j. It is necessary to define the direction in which surface YS_i translates.

As indicated in Fig. B3.3a, corresponding points P_i and P_j can be identified on YS_i and YS_j. The relationship between the actions at these two points ($\underline{S}_i$ at P_i and $\underline{S}_j$ at P_j) is obtained as follows.

Figure B3.3b shows a yield surface transformed into a normalized action space. In this space, surfaces YS_i and YS_j have identical shapes. Hence, points P_i and P_j coincide. The locations of P_i and P_j in Fig. B3.3a follow by transforming back to the natural action space. If the vector of actions at P_i is $\underline{S}_i$, it follows that the vector of actions at P_j is given by:

$$\underline{S}_j = \underline{S}_{uij}(\underline{S}_i - \underline{\alpha}_i) + \underline{\alpha}_j \tag{B3.36}$$

in which

$\underline{S}_j$ = vector of stress resultants at point P_j,

$\underline{\alpha}_i$ and $\underline{\alpha}_j$ = vectors defining the current origins, O_i and O_j, of yield surfaces YS_i and YS_j, respectively,

$$\underline{S}_{uij} = diag\left[\frac{M_{yuj}}{M_{yui}} \ \frac{M_{zuj}}{M_{zui}} \ \frac{T_{uj}}{T_{ui}} \ \frac{F_{uj}}{F_{ui}}\right]$$

It is assumed that the direction of translation of yield surface YS_i is along the line connecting point P_i to point P_j, as shown in Fig. B3.3a. That is, the direction of motion of surface YS_i is defined by:

$$d\underline{\alpha}_i = \left(\underline{S}_j - \underline{S}_i\right) d\alpha^* \tag{B3.37}$$

in which

$d\alpha^*$ = scalar which defines the magnitude of translation of yield surface YS_i;

$d\underline{\alpha}_i$ = vector defining the incremental shift of the origin of yield surface YS_i.

The magnitude of $d\alpha^*$ is determined as explained in the following section. For the hardening rule originally formulated by Mroz, all yield surfaces are geometrically similar in natural action space. The rule then ensures that the surfaces never overlap. For the modified Mroz rule, the yield surfaces are assumed to be geometrically similar only in normalized action space. As a result, overlapping of yield surfaces is allowed. This aspect of the model is considered further in a later section.

B3.7.3 Mathematical Formulation

Substitute Eqn. B3.36 in Eqn. B3.37 to get:

$$d\underline{\alpha}_i = \left[(\underline{S}_{uij} - \underline{I})\underline{S}_i - (\underline{S}_{uij}\underline{\alpha}_i - \underline{\alpha}_j)\right] d\alpha^* \tag{B3.38}$$

The usual normality rule for plastic flow is assumed. That is, the plastic deformation increment, $d\underline{w}_p$, is assumed to be directed along the outward normal to the yield surface at point P_i. The yield surface can be defined by:

$$\phi(\underline{S}_i - \underline{\alpha}_i) = 1 \tag{B3.39}$$

The requirement that the action point remain on the yield surface is:

$$d\phi = 0 = \underline{\phi}_{,s}^T \cdot d\underline{S}_i - \underline{\phi}_{,s}^T \cdot d\underline{\alpha}_i \tag{B3.40}$$

Substitute Eqns. B3.37 and B3.38 into Eqn. B3.40 to get:

$$d\alpha^* = \frac{\underline{\phi}_{,s}^T d\underline{S}_i}{\underline{\phi}_{,s}^T\left[(\underline{S}_{uij} - \underline{I})\underline{S}_i - (\underline{S}_{uij}\underline{\alpha}_i - \underline{\alpha}_j)\right]} \tag{B3.41}$$

Hence, substitute Eqn. B3.41 into Eqn. B3.37 to get $d\underline{\alpha}_i$ as:

$$d\underline{\alpha}_i = \frac{\left[(\underline{S}_{uij}-\underline{I})\underline{S}_i - (\underline{S}_{uij}\underline{\alpha}_i-\underline{\alpha}_j)\right]\underline{\phi}_{,s}^T d\underline{S}_i}{\underline{\phi}_{,s}^T\left[(\underline{S}_{uij}-\underline{I})\underline{S}_i - (\underline{S}_{uij}\underline{\alpha}_i-\underline{\alpha}_j)\right]} \tag{B3.42}$$

For any current state, defined by $\underline{S}_i$, $\underline{\alpha}_i$, and $\underline{\alpha}_j$, Eqn. B3.42 defines, for an action increment $d\underline{S}_i$, the translation of yield surface YS_i for loading towards surface YS_j.

B3.7.4 Last Yield Surface

For the case when the action point lies on the largest yield surface, the hardening rule can be obtained by assuming that an additional infinitely large yield surface exists. The direction of translation for this case is then along the radial direction connecting the origin of the current yield surface to the current action point. This is exactly Ziegler's hardening rule. It can be expressed as:

$$d\underline{\alpha}_n = (\underline{S}_n - \underline{\alpha}_n)d\alpha^* \tag{B3.43}$$

in which

n = number of largest yield surface;

$d\alpha^*$ = scalar which defines the magnitude of translation of the yield surface, as before;

$\underline{\alpha}_n$ = vector defining the yield surface origin;

$d\underline{\alpha}_n$ = vector defining the incremental shift of the origin.

For this case, Eqn. B3.42 becomes:

$$d\underline{\alpha}_n = \frac{(\underline{S}_n-\underline{\alpha}_n)\underline{\phi}_{,s}^T \cdot d\underline{S}_n}{\underline{\phi}_{,s}^T(\underline{S}_n-\underline{\alpha}_n)} \tag{B3.44}$$

B3.7.5 Overlapping of Yield Surfaces

In the original Mroz hardening rule, it is assumed that the yield surface, YS_i, is geometrically similar to the yield surface YS_j. This assumption is reasonable for metal plasticity in stress space because it is reasonable to assume as isotropic material. However, for dealing with stress resultants, each action-deformation relationship ($M_y-\psi_y$, $M_z-\psi_z$, $M_x-\psi_x$, and $F-\epsilon$), depends on the cross section shape in a different way, and the behavior is not isotropic in action space. That is, the yield surfaces will, in general, not be geometrically similar. The authors have considered a number of strategies in an attempt to obtain "correct" behavior while preventing yield surface overlap. None of these strategies proved satisfactory, and it was finally concluded that overlapping should be allowed.

B3.8 PLASTIC DEFORMATIONS

The equations for calculation of plastic strain resultants are derived as follows. The deformation increment for a slice is given by:

$$d\underline{w} = \underline{f}_{se}\, d\underline{S} + d\underline{w}_p \tag{B3.45}$$

in which

$d\underline{w}_p = \sum_i d\underline{w}_{pi}$ is the increment of plastic deformation, summed over all active yield surfaces.

Premultiply Eqn. B3.45 by $\underline{f}_{sp}\,\underline{K}_{se}$ to get:

$$\underline{f}_{sp}\,\underline{K}_{se}\, d\underline{w} = \underline{f}_{sp}\, d\underline{S} + \underline{f}_{sp}\,\underline{K}_{se}\, d\underline{w}_p \tag{B3.46}$$

in which

$\underline{f}_{sp} = \sum_i \underline{f}_{sp_i}$ is the plastic flexibility of the slice; and,

$$\underline{f}_{sp} d\underline{S} = d\underline{w}_p \tag{B3.47}$$

Substitute Eqn. B3.47 into Eqn. B3.46 to get:

$$(I + \underline{f}_{sp}\,\underline{K}_{se})\, d\underline{w}_p = \underline{f}_{sp}\,\underline{K}_{se}\, d\underline{w} \tag{B3.48}$$

From Eqn. B3.48, the plastic deformation increments can be obtained in terms of the total deformation increment as:

$$d\underline{w}_p = (I + \underline{f}_{sp}\,\underline{K}_{se})^{-1}\,\underline{f}_{sp}\,\underline{K}_{se}\, d\underline{w} \tag{B3.49}$$

B3.9 LOADING/UNLOADING CRITERION

The loading/unloading criterion enables continuing plastic flow to be distinguished from elastic unloading, for any current plastic state and any specified deformation increment. Two procedures are of general applicability, as follows.

(1) Postulate that the slice has unloaded an infinitesimal amount, so that the current state lies just within the yield surface. Calculate the elastic action increment, $d\underline{S}_e$, corresponding to the specified deformation increment. If the state moves outside the yield surface, the assumed elastic state is incorrect, indicating continuing plastic flow. If the state moves within the yield surface, the elastic assumption is correct, indicating unloading.

(2) For the specified deformation increment, calculate the magnitude parameter for the plastic deformation increment. A positive magnitude indicates continuing plastic flow, and a negative magnitude indicates unloading.

By the first of these two procedures, continued loading on yield surface i is indicated if $d\underline{S}_e$ has a positive component along the outward normal, $\underline{n}_i$, of the yield surface. That is, continued loading occurs if

$$\underline{n}_i^T \cdot d\underline{S}_e \geqslant 0 \tag{B3.50}$$

To consider the second procedure, first assume that the current plastic flow directions of all active yield surfaces are the same (that is, $\underline{n}_i = \underline{n}$ for all i). Hence, the plastic deformation increment for the slice is given by:

$$d\underline{w}_p = \underline{n}\ dw_p^* \tag{B3.51}$$

Premultiply Eqn. B3.45 by $\underline{n}^T \cdot \underline{f}_{sp} \cdot \underline{K}_{se}$ to get:

$$dw_p^* = \frac{\underline{n}^T \underline{f}_{sp} \underline{K}_{se}\, d\underline{w}}{1 + \underline{n}^T \cdot \underline{f}_{sp} \cdot \underline{K}_{se} \cdot \underline{n}} \tag{B3.52}$$

Substitute Eqn. B3.21 into Eqn. B3.52 to get:

$$dw_p^* = \frac{r_2 \underline{n}^T d\underline{S}_e}{1 + r_1} \tag{B3.53}$$

in which r_1 and r_2 are scalars defined as follows:

$$r_1 = \sum_i \frac{n^T \cdot \underline{K}_{se} \cdot \underline{n}}{\underline{n}^T \cdot \underline{K}_{spi} \cdot \underline{n}} \tag{B3.54}$$

$$r_2 = \sum_i \frac{1}{\underline{n}^T \cdot \underline{K}_{spi} \cdot \underline{n}} \tag{B3.55}$$

Because the matrices $\underline{K}_{spi}$ and $\underline{K}_{se}$ are always positive definite, the scalars r_1 and r_2 always exceed zero. Hence, the sign of dw_p^* is the same as the sign of $\underline{n}^T \cdot d\underline{S}_e$. This is the same criterion as Eqn. B3.50.

In general, the plastic flow directions for the active yield surfaces are not the same. Hence, it is possible for $\underline{n}_i^T d\underline{S}_e$ to be greater than zero for some yield surfaces and less than zero for others (i.e. continued loading on some, but unloading on others). This possibility is illustrated in Fig. B3.4. For computation, it is assumed that unloading is governed by the *highest active yield surface.* If unloading occurs on this surface, unloading is assumed to occur on all active surfaces. If the situation happens to be as shown in Fig. B3.4 (which is unlikely), reloading will immediately occur on one or more of the lower yield surfaces, and the analysis will continue.

B3.10 END ECCENTRICITY

Plastic hinges in frames and coupled frame-shear wall structures will form near the faces of the joints rather than at the theoretical joint centerlines. This effect can be approximated by postulating rigid, infinitely strong connecting links between the nodes and the element ends, as shown in Fig. B2.7. The displacement transformation relating the increments of node displacements, $d\underline{r}_u$, to increments of displacement at the element ends is easily established and can be written as:

$$d\underline{r} = \underline{a}_e \, d\underline{r}_u \tag{B3.56}$$

This transformation is used to modify the stiffness and state determination calculations to allow for end eccentricity effects.

B3.11 TOLERANCE FOR STIFFNESS REFORMULATION

Each time a new hinge yields or an existing hinge unloads, the element stiffness changes. Moreover, because the direction of plastic flow may change, the stiffness of a yielding element will generally change continuously. The change in stiffness results from differences in the directions of the normal to the yield surface as the actions at the hinge change. If the angle change is small, the change in stiffness will be small and can be neglected to avoid recalculating the stiffness. In the computer program, an option is provided for the user to set a tolerance for the angle. If a nonzero tolerance is specified, the element stiffness is reformed only when the change in state is such that the angle between the current yield surface normal and that when the stiffness was last reformed exceeds the tolerance. A tolerance of about 0.1 radians is recommended.

B4. STRAIN RATE EFFECTS

B4.1 GENERAL

The mathematical formulation for an element slice with rate-independent elasto-plastic behavior was presented in the preceding chapter. An extension to include strain rate effects is presented in this chapter.

A physical model for a slice is first constructed for one-dimensional behavior. This model is then generalized for the multi-dimensional case.

B4.2 MODELING OF STRAIN RATE EFFECTS

B4.2.1 Physical Model

In one dimension, elasto-plastic-strain-hardening behavior can be modeled using a linear spring in series with a number of rigid-plastic springs (Fig. B2.6). To include strain rate effects, a dashpot is added to the assemblage as shown in Fig. B4.1. With this model, the elastic behavior is independent of the strain rate, but the post-yield resistance is the sum of the static resistance plus that of the dashpot. The dashpot resistance depends on its stiffness and on the *plastic* strain rate in the material.

B4.2.2 Dashpot Properties

In order to establish a stiffness coefficient for the dashpot, information is needed on the strength increase of the element for different *plastic* deformation rates. If the physical model represents steel loaded in uniaxial tension or compression, the dashpot coefficient can be obtained from test results measuring the strength of the steel as a function of strain rate. Although the plastic strain rate is not necessarily equal to the total strain rate, the two will be essentially equal as the maximum strength is approached. Hence, a graph of strength increase versus total strain rate can, for practical purposes, be assumed to be the same as a graph of strength increase versus plastic strain rate. Such a graph might be as shown in Fig. B4.2.

For numerical analysis, the graph is assumed to be approximated by linear segments, as shown in Fig. B4.2. The relationship between force in the dashpot and the dashpot deformation rate can be written, for any linear segment, as:

$$dS_d = C_r \, d\dot{w}_p \tag{B4.1}$$

in which

dS_d = increment in dashpot force;

$d\dot{w}_p$ = increment in dashpot deformation rate; and

C_r = slope of segment.

For application to the beam element, this concept is generalized to the multi-dimensional action-deformation case and implemented numerically.

B4.2.3 Damping Matrix for a Slice

For a slice of a beam element, a relationship in the form of Eqn. B4.1 is required, relating damping action increments to corresponding increments of plastic deformation rate. That is, the relationship must be in the form:

$$d\underline{S}_d = \underline{C}_r \, d\underline{\dot{w}}_p \tag{B4.2}$$

in which

$d\underline{S}_d$ = vector of damping action increments;

$d\underline{\dot{w}}_p$ = vector of plastic deformation rate increments corresponding to $d\underline{S}_d$; and

$\underline{C}_r$ = diagonal matrix containing the slopes of the individual relationships between action and deformation rate (dashpot coefficient values).

For axial force, F, the strain rate effect is the same as that of the beam material. For bending moment, however, a somewhat different relationship can be expected, because the strain rate varies over the cross section as the beam bends (the strain rate effect can thus be expected to be relatively somewhat less for bending than for axial force). For torque, a different strain rate effect may also be obtained, because it depends on the relationship between shear strength and shear strain rate, which may be different from that for behavior in tension. In practice, it is unlikely that detailed knowledge of the strain rate effects will be available. Hence, for simplicity in the theoretical formulation, different dashpot coefficient values are not allowed for each of the four actions. Instead, a single generalized relationship is used for all four actions. The relationship is derived as follows.

(1) For the steel of which the pipe is made, first obtain the σ_d versus $\dot{\epsilon}_p$ relationship (stress increase versus strain rate) as in Fig. B4.3.

(2) Reduce to a dimensionless relationship (except for time) by dividing σ_d by the yield stress (or nominal yield stress) of the steel and dividing $\dot{\epsilon}_p$ by the yield strain (yield stress divided by Young's modulus).

(3) Approximate the relationship by a multi-linear curve. Let the slope of any segment be C_r^*, a generalized dashpot coefficient relating dimensionless stress to dimensionless strain rate increment. That is,

$$\frac{d\sigma_d}{\sigma_y} = C_r^* \frac{d\dot{\epsilon}_p}{\sigma_y/E} \tag{B4.3}$$

in which σ_y = yield stress and E = Young's modulus.

Hence,

$$d\sigma_d = C_r^* \; E \; d\dot{\epsilon}_p$$

so that, from Eqns. B4.2 and B4.3,

$$C_r = C_r^* E$$

(4) Assume that the same dimensionless relationship can be extended to actions and deformations of a slice, as illustrated in Fig. B4.4. For example, for bending about the z axis, assume the relationship is:

$$dM_{zd} = C_r^* \; EI_z \; d\dot{\psi}_z \tag{B4.4}$$

in which C_r^* is as before. It follows that the matrix $\underline{C}_r$ is given by:

$$\underline{C}_r = C_r^* \underline{K}_{se} \tag{B4.5}$$

in which $\underline{K}_{se}$ = elastic (diagonal) slice stiffness matrix.

B4.3 MATHEMATICAL FORMULATION

B4.3.1 Basic Equations

The equations for strain rate effects are derived as follows.

(1) Force Equilibrium:

$$d\underline{S} = d\underline{S}_e = d\underline{S}_p + d\underline{S}_d \tag{B4.6}$$

in which

$d\underline{S}$ = total action increment;

$d\underline{S}_e$ = elastic action increment;

$d\underline{S}_p$ = action increment due to plastic deformation;

$d\underline{S}_d$ = action increment due to strain rate effects.

(2) Deformation Compatibility:

$$d\underline{w} = d\underline{w}_e + d\underline{w}_p = d\underline{w}_e + \sum_i d\underline{w}_{pi} \tag{B4.7}$$

in which

$d\underline{w}_e$ = elastic deformation increment;

$d\underline{w}_p$ = plastic deformation increment;

$d\underline{w}_{pi}$ = plastic deformation increment for active yield surface i; and

i = active yield surface number.

(3) Rate Independent Flow Rule:

$$d\underline{w}_{pi} = \underline{n}_i \; d\dot{w}_{pi} \tag{B4.8}$$

in which

$\underline{n}_i$ = normal vector for current active yield surface i; and

dw_{pi}^* = scalar which defines the magnitude of plastic deformation along the normal direction of yield surface i.

(4) Step-by-Step Integration:

The dashpot relationship depends on the step-by-step integration rule being used. Two options have been considered, as follows:

(a) B4.ackwards difference rule:

$$d\underline{S}_d = \underline{C}_r\left(\frac{d\underline{w}_p}{dt} - \dot{\underline{w}}_p\right) = C_r^* \underline{K}_{se}\, \underline{n}\left(\frac{dw_p^*}{dt} - \dot{w}_p^*\right) \tag{B4.9a}$$

in which

$\underline{C}_r$ = diagonal matrix of dashpot coefficients, as defined previously.

(b) Trapezoidal rule:

$$d\underline{S}_d = 2\underline{C}_r\left(½\frac{d\underline{w}_p}{dt} - \dot{\underline{w}}_p\right) \tag{B4.9b}$$

These equations strictly apply only for finite time increments, Δt. The theory is developed on terms of dt for consistency with previous equations, but a finite Δt is used for actual numerical implementation. The backwards difference rule is used in the following derivations and is recommended for use in actual computation.

(5) Plastic Relationships:

$$d\underline{w}_p = \sum_i \underline{f}_{sp_i}\, d\underline{S}_p = \sum_i \frac{\underline{n}_i \cdot \underline{n}_i^T}{\underline{n}_i^T \cdot \underline{K}_{sp_i} \cdot \underline{n}_i}\, d\underline{S}_p \tag{B4.10}$$

Define:

$$\underline{f}_{sp} = \sum_i \underline{f}_{sp_i}$$

Hence,

$$d\underline{w}_p = \underline{f}_{sp}\, d\underline{S}_p \tag{B4.11}$$

(6) Elastic Relationships:

$$d\underline{S}_e = \underline{K}_{se}\, d\underline{w}_e \tag{B4.12}$$

or

$$d\underline{w}_e = \underline{f}_{se}\, d\underline{S}_e \tag{B4.13}$$

in which $\underline{K}_{se}$ and $\underline{f}_{se}$ are the elastic slice stiffness and flexibility matrices, respectively.

B4.3.2 Derivation of Stiffness Equation

Substitute Eqns. B4.11 and B4.13 into Eqn. B4.7 to get:

$$d\underline{w} = \underline{f}_{se}\, d\underline{S} + \underline{f}_{sp}\, d\underline{S}_p \tag{B4.14}$$

Substitute Eqns. B4.6 into Eqn. B4.14 to get:

$$d\underline{w} = (\underline{f}_{se} + \underline{f}_{sp})\, d\underline{S} - \underline{f}_{sp}\, d\underline{S}_d \tag{B4.15}$$

Substitute Eqns. B4.9, B4.7, and B4.13 into Eqn. B4.15 and rearrange to get:

$$(\underline{f}_{se} + \underline{f}_{sp} + \underline{f}_{sp}\,\underline{C}_r \frac{1}{dt} \underline{f}_{se})\, d\underline{S} = (\underline{I} + \underline{f}_{sp}\,\underline{C}_r \frac{1}{dt})\, d\underline{w} - \underline{f}_{sp}\,\underline{C}_r\,\underline{\dot{w}}_p \tag{B4.16}$$

Substitutve Eqn. B4.5 into Eqn. B4.16 to get:

$$(\underline{f}_{se} + (1 + \frac{C_r^*}{dt})\, \underline{f}_{sp})\, d\underline{S} = (\underline{I} + \underline{f}_{sp}\,\underline{C}_r \frac{1}{dt})\, d\underline{w} - \underline{f}_{sp}\,\underline{C}_r\,\underline{\dot{w}}_p \tag{B4.17}$$

Premultiply Eqn. B4.17 by $(\underline{f}_{se} + (1 + C_r^*/dt)\underline{f}_{sp})^{-1}$ to obtain:

$$d\underline{S} = \underline{C}_t\, d\underline{w} + d\underline{S}_q \tag{B4.18}$$

in which

$$\underline{C}_t = (\underline{f}_{se} + (1 + \frac{C_r^*}{dt})\, \underline{f}_{sp})^{-1}\, (\underline{I} + \underline{f}_{sp}\,\underline{C}_r \frac{1}{dt}) \tag{B4.19}$$

and

$$d\underline{S}_q = -(\underline{f}_{se} + (1 + \frac{C_r^*}{dt})\, \underline{f}_{sp})^{-1}\, \underline{f}_{sp}\,\underline{C}_r\,\underline{\dot{w}}_p \tag{B4.20}$$

Eqn. B4.18 is the required tangent stiffness relationship for a slice, including the effects of plastic strain rate. The term $\underline{C}_t$ is the tangent stiffness of the slice. The term $d\underline{S}_q$ is an initial stress effect associated with the strain rate effect. For a finite time step, Δt, an initial stress term $\Delta\underline{S}_q$ is included in the element effective load vector for the time step.

When strain rate effects are zero, the terms C_r^* and $d\underline{S}_q$ become zero, and the relationship of Eqn. B4.18 becomes the rate-independent relationship:

$$d\underline{S} = \underline{C}_t \, d\underline{w} \tag{B4.21}$$

in which

$$\underline{C}_t = (\underline{f}_{se} + \underline{f}_{sp})^{-1} \tag{B4.22}$$

B4.3.3 Plastic Deformation

The plastic deformation increments are obtained as follows. Substitute Eqns. B4.13 and B4.6 into Eqn. B4.7 to get:

$$d\underline{w} = \underline{f}_{se}(d\underline{S}_p + d\underline{S}_d) + d\underline{w}_p \tag{B4.23}$$

Premultiply Eqn. B4.23 by $\underline{f}_{sp}\,\underline{K}_{se}$ to get:

$$\underline{f}_{sp}\,\underline{K}_{se}\,d\underline{w} = \underline{f}_{sp}\,d\underline{S}_p + \underline{f}_{sp}\,d\underline{S}_d + \underline{f}_{sp}\,\underline{K}_{se}\,d\underline{w}_p \tag{B4.24}$$

Substitute Eqns. B4.9 and B4.11 into Eqn. B4.24 and rearrange to obtain:

$$(\underline{I} + \underline{f}_{sp}\,\underline{C}_r \frac{1}{dt} + \underline{f}_{sp}\,\underline{K}_{se})\,d\underline{w}_p = \underline{f}_{sp}\,\underline{K}_{se}\,d\underline{w} + \underline{f}_{sp}\,\underline{C}_r\,\dot{\underline{w}}_p \tag{B4.25}$$

or

$$d\underline{w}_p = (\underline{I} + \underline{f}_{sp}\,\underline{C}_r \frac{1}{dt} + \underline{f}_{sp}\,\underline{K}_{se})^{-1}\,(\underline{f}_{sp}\,\underline{K}_{se}\,d\underline{w} + \underline{f}_{sp}\,\underline{C}_r\,\dot{\underline{w}}_p) \tag{B4.26}$$

Eqn. B4.26 gives the plastic deformation increment in terms of the total deformation increment, including strain rate effects.

B4.4 LOADING/UNLOADING CRITERION

The unloading criterion remains unchanged from the rate-independent case. That is,

$$\underline{n}_l^T \cdot d\underline{S}_e \geqslant 0 \tag{B4.27}$$

indicates continued loading, in which $\underline{n}_l$ is the normal vector for the highest active yield surface.

B5. COMPUTER LOGIC

B5.1 STATE DETERMINATION

The state determination calculation for an inelastic element requires evaluation of the equation

$$\Delta \underline{S} = \int_0^{\Delta v} \underline{K}_t \, d\underline{v} \qquad \text{(B5.1)}$$

in which

$\Delta \underline{S}$ = finite action increment for element corresponding to the finite deformation increment $\Delta \underline{v}$; and

$\underline{K}_t$ = element tangent stiffness, which in general varies during the increment.

The computation procedure for state determination of the element is as follows:

(1) From the given nodal displacement increments, calculate the element deformation increments from

$$\Delta \underline{v} = \underline{a} \, \Delta \underline{r} \qquad \text{(B5.2)}$$

in which

$\Delta \underline{r}$ = vector of nodal displacement increments, in global system;

$\Delta \underline{v}$ = vector of element deformation increments, in local system; and

$\underline{a}$ = displacement transformation matrix.

(2) Calculate the slice deformation increments at the Gauss stations from

$$\Delta \underline{w} = \underline{B(x)} \Delta \underline{v} \qquad \text{(B5.3)}$$

in which

$\Delta \underline{w}$ = slice deformation increment;

$\Delta \underline{v}$ = element deformation increment; and

$\underline{B(x)}$ = shape function matrix defined by Eqn. B3.2.

Preceding page blank

(3) Perform state determination calculations at each slice, as follows:

(a) Check unloading. If unloading occurs, do elastic state determination. Otherwise, continue.

(b) Calculate plastic deformation, $\Delta \underline{w}_p$, using Eqn. B4.26.

(c) Calculate dashpot forces, $\Delta \underline{S}_d$, using Eqn. B4.9.

(d) Calculate total force increments, $\Delta \underline{S}$, using:

$$\Delta \underline{S} = \underline{K}_{se} (\Delta \underline{w} - \Delta \underline{w}_p) \tag{B5.4}$$

(e) Calculate plastic force increments, $\Delta \underline{S}_p$, using:

$$\Delta \underline{S}_p = \Delta \underline{S} - \Delta \underline{S}_d \tag{B5.5}$$

The new action point, $\underline{S}_p + \Delta \underline{S}_p$, must lie on the yield surface. If the error is within a specified tolerance, the state determination is complete. If the error exceeds the tolerance, or if a new yield event occurs, the deformation increments are subdivided into smaller increments. The procedure is described in the following section.

(4) Calculate the internal resisting forces for the element from the slice forces, using

$$\underline{R} = \int_0^L \underline{B(x)}^T \underline{S} \, dx \tag{B5.6}$$

in which

$\underline{S}$ = slice force vector; and

$\underline{B(x)}$ = strain displacement transformation matrix defined by Eqn. B3.2.

B5.2 YIELD SURFACE TOLERANCE

It is possible for the new action point, calculated assuming constant $\underline{K}_t$, to lie significantly outside the current yield surface. This will occur particularly when $\Delta \underline{S}$ and $\Delta \underline{\alpha}$ are distinctly nonparallel (Fig. B5.1). In this case, the calculation is assumed to be sufficiently accurate, provided the new action point lies within a tolerance zone (typically 1% of the yield surface size). If not, $\Delta \underline{w}$ is scaled, $\underline{K}_t$ is reformed, and the calculation is repeated for the balance of $\Delta \underline{w}$.

The scale factor is conveniently determined by the procedure illustrated for M-F space in Fig. B5.1. In this figure, the current action point is P, and the new action point, obtained by applying Eqn. B5.4, is at Q. Hardening is affected only by the component of $\Delta \underline{S}$ parallel to the yield surface normal. Hence, the yield surface translates as shown. Point Q lies outside the new yield surface, the amount being defined by e_r, which is the length of the "radial" error vector, $\underline{e}_r$. This error must not exceed the allowable tolerance.

Computationally, it is convenient to consider the "tangential" error, $\underline{e}_t$, which is the length of vector P'Q. If the yield surface is assumed to be locally quadratic, then

$$e_r \doteq 0.5\, e_t^2 \tag{B5.7}$$

The value of e_r is calculated from this equation. If e_r is within the allowable tolerance, point Q is scaled to the new yield surface and the computation continues (this scaling introduces an error which is assumed to be acceptable). If e_r exceeds the allowable tolerance, it is assumed that e_t varies linearly with slice deformation. A scale factor to set e_r equal to the tolerance is then calculated using Eqn. B5.7; the $\Delta \underline{S}$ and $\Delta \underline{\alpha}$ increments are scaled by this factor; and the new action point is scaled to the yield surface. The slice stiffness is then reformed, and the process is repeated for the remainder of the deformation increment. If $\Delta \underline{S}$ is parallel to $\underline{S} - \underline{\alpha}$, no scaling will be required. If $\Delta \underline{S}$ makes a large angle with $\underline{S} - \underline{\alpha}$, the slice deformation increment may be subdivided into several subincrements, depending on the magnitude of $\Delta \underline{w}$ and the value specified for the error tolerance.

The slice deformation increment is also subdivided if a new yield surface is reached. In this case, the new action point is permitted to go beyond the yield surface by an amount equal to the allowable radial error. The proportion of the deformation increment required to reach this state is calculated; the new action point is scaled to the yield surface; the slice stiffness is reformed; and the calculation proceeds for the remainder of the deformation increment.

B6. USER GUIDE

3D DISTRIBUTED PLASTICITY BEAM-COLUMN ELEMENT

The ANSR element does not allow for strain rate effects. These effects are considered only in the WIPS version of the element [31].

B6.1 CONTROL INFORMATION - Two Cards

B6.1.1 First Card

Columns	Note	Name	Data
5(I)		NGR	Element group indicator (=7).
6-10(I)		NELS	Number of elements in group.
11-15(I)		MFST	Element number of first element in group. Default = 1.
16-25(F)		DKO	Initial stiffness damping factor, β_o.
26-35(F)		DKT	Tangent stiffness damping factor, β_T.
41-80(A)		GRHED	Optional group heading.

B6.1.2 Second Cards

Columns	Note	Name	Data
1-5(I)		NMBT	Number of different strength types (max. 20). Default = 1.
6-10(I)		NECC	Number of different end eccentricity types (max. 15). Default = zero.
11-15(I)		NPAT	Number of different initial force patterns (max. 30). Default = zero.

B6.2 STRENGTH TYPES

NMBT sets of cards.

B6.2.1 Strength Type Number

Columns	Note	Name	Data
1-5(I)			Strength type number, in sequence beginning with 1.

B6.2.2 Bending Properties About Local y-axis

Columns	Note	Name	Data

Preceding page blank

1-10(F)			Flexural rigidity (effective elastic EI value, EI_1) about y axis.
11-20(F)			Flexural rigidity (EI_2) about y-axis.
21-30(F)			Flexural rigidity (EI_3) about y-axis.
31-40(F)			Flexural rigidity (EI_4) about y-axis.
41-50(F)			Yield moment (YS1) about y-axis.
51-60(F)			Yield moment (YS2) about y-axis.
61-70(F)			Yield moment (YS3) about y-axis.
71-80(F)			Elastic shear rigidity (GA_s) for bending about y-axis. May be zero.

B6.2.3 Bending Properties about Local z-axis

Columns	Note	Name	Data
1-80(F)			z-axis bending rigidities, yield moments, and shear rigidity, in the same sequence as in Card B6.2.2.

B6.2.4 Torsional Properties

Columns	Note	Name	Data
1-70(F)			Torsional rigidities (effective GJ) and yield torques, in same sequence as in Card 5.2(b).

B6.2.5 Axial Properties

Columns	Note	Name	Data
1-70(F)			Axial rigidities (effective EA) and yield forces, in the same sequence as in Card 5.2(b).

B6.3 END ECCENTRICITY TYPES

NECC Cards.

Columns	Note	Name	Data
1-5(I)	(1)		End eccentricity type number, in sequence beginning with 1.
6-15(F)			X_i = X eccentricity at end i.
16-25(F)			X_j = X eccentricity at end j.
26-35(F)			Y_i = Y eccentricity at end i.

36-45(F)			Y_j = Y eccentricity at end j.
46-55(F)			Z_i = Z eccentricity at end i.
56-65(F)			Z_j = Z eccentricity at end j.

B6.4 INITIAL ELEMENT FORCE PATTERNS

NPAT Cards.

Columns	Note	Name	Data
1-5(I)	(2)		Pattern number, in sequence beginning with 1.
6-15(F)			Initial moment M_{yy} at end i.
16-25(F)			Initial moment M_{zz} at end i.
26-35(F)			Initial moment M_{yy} at end j.
36-45(F)			Initial moment M_{zz} at end j.
46-55(F)			Initial axial force, F.
56-65(F)			Initial torque, M_{xx}.

B6.5 ELEMENT DATA GENERATION

As many sets of cards as needed to generate all elements in group.

B6.5.1 Card One

Columns	Note	Name	Data
1-5(I)	(3)		Element number, or number of first element in a sequentially numbered series of elements to be generated by this card.
6-10(I)		NODI	Node Number I.
11-15(I)		NODJ	Node Number J.
16-20(I)		INC	Node number increment for element generation. Default = 1.
21-25(I)			Number of a third node, K, lying in the xy plane, for definition of the local y axis orientation. Default = automatic orientation of y-axis.
26-30(I)			Strength type number at element Gauss point 1. No default.
31-35(I)			Strength type number at element Gauss point 2. No default.

Columns	Note	Name	Data
36-40(I)			End eccentricity type number. Default = no end eccentricity.
41-45(I)			Initial force pattern number. Default = no initial forces.
46-50(I)			Interaction surface type.
51-55(I)			Displacements code:
			(a) Blank or zero = small displacements.
			(b) 1 = large displacements (engineering theory).
56-60(I)			Large displacement theory code:
			(a) Blank or zero = Euler procedure.
			(b) 1 = midpoint procedure.
61-65(I)			Response output code:
			(a) Blank or zero = no response printout.
			(b) 1 = response output required.
66-75(F)	(4)		Stiffness reformulation angle tolerance, α (radians). Default = zero.

B6.5.2 Card Two

Columns	Note	Name	Data
1-10(F)			Parameter for yield surface type, a_1.
11-20(F)			Parameter for yield surface type, a_2.
21-30(F)			Parameter for yield surface type, a_3.
31-40(F)			Parameter for yield surface type, a_4.

B6.6 NOTES

(1) All eccentricities are measured *from* the node *to* the element end (Fig. B2.7), positive in the positive coordinate directions.

(2) See Fig. B2.8 for the positive directions for initial element actions. Refer to Section B2.4 for a description of the effects of initial element actions.

(3) Cards must be input in order of increasing element number. Cards for the first and the last elements must be included (that is, data for these two elements cannot be generated). Cards may be provided for all elements, in which case each card specifies the data for one element, and the generation is not used. Alternatively, cards for a series of elements may be omitted, in which case data for the missing elements is generated as follows:

(a) All missing elements are assigned the same node "K" (NODK), slave nodes (NSI and NSJ), strength types, end eccentricity type, initial force pattern type, interaction surface type, codes for large displacements and response output, and stiffness reformulation angle tolerance, as those for the element preceding the missing series of elements.

(b) The node numbers I and J for each missing element are obtained by adding the increment (INC) to the node numbers of the preceding element. That is,

$$\mathrm{NODI(N)} = \mathrm{NODI(N\text{-}1)} + \mathrm{INC}$$

$$\mathrm{NODJ(N)} = \mathrm{NODJ(N\text{-}1)} + \mathrm{INC}$$

The node increment, INC, is the value specified with the element *preceding* the missing series of elements.

(4) Refer to Section B3.11 for a description of the stiffness reformulation tolerance.

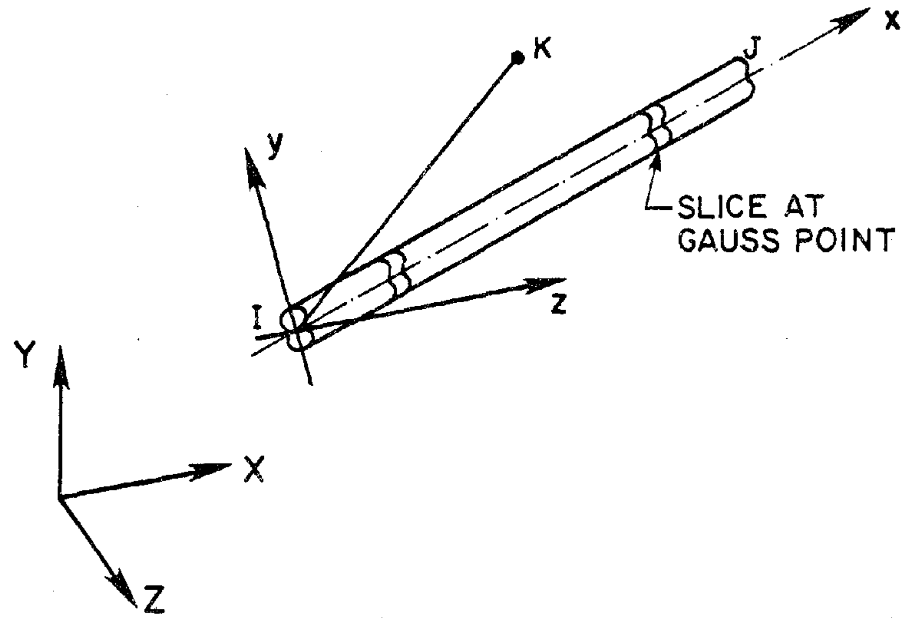

FIG. B2.1 ELEMENT AXES

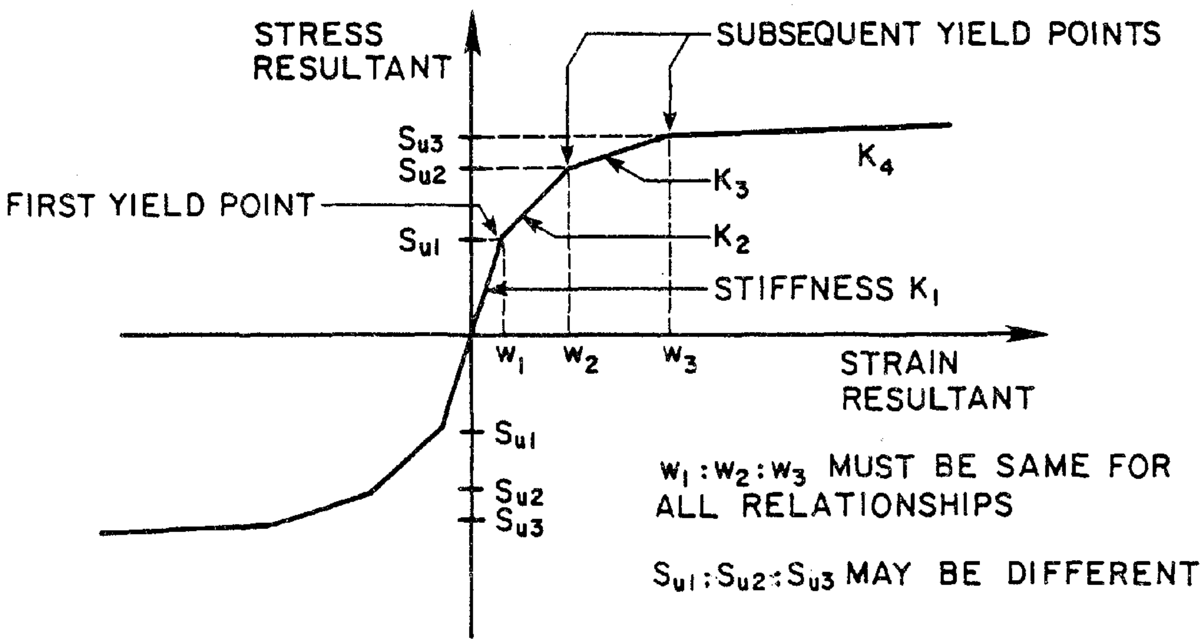

FIG. B2.2 STRESS VS. STRAIN RESULTANT RELATIONSHIP

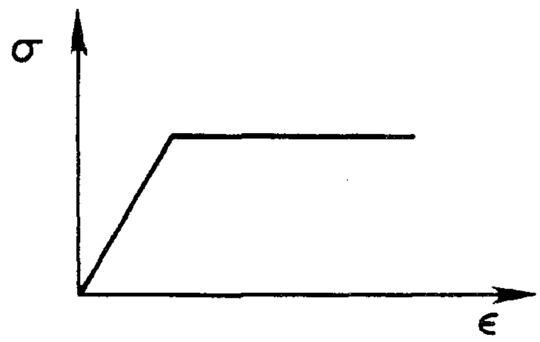

(a) ELASTIC-PLASTIC STRESS-STRAIN RELATIONSHIP

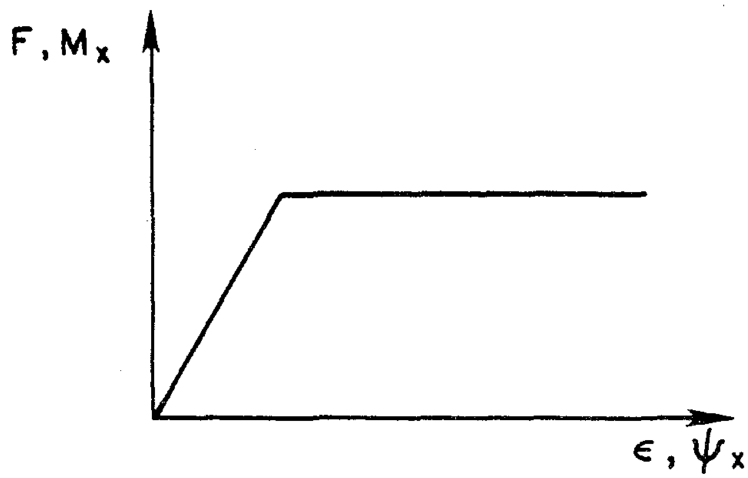

(b) FORCE-EXTENSION AND TORQUE-TWIST

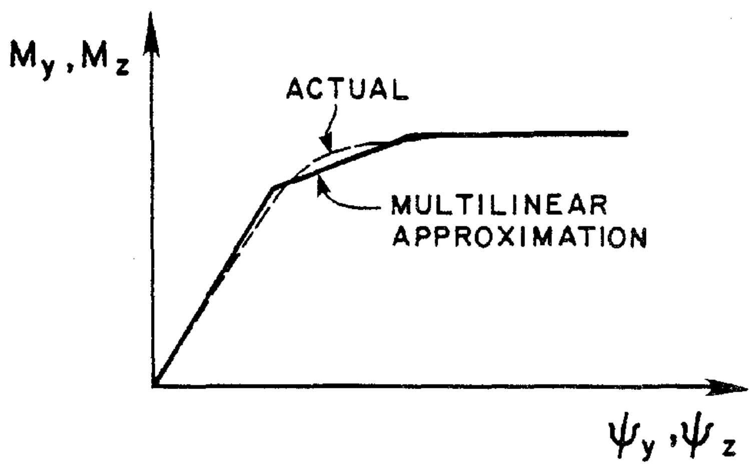

(c) MOMENT-CURVATURE

FIG. B2.3 DIFFERENCES IN SHAPES OF RELATIONSHIPS

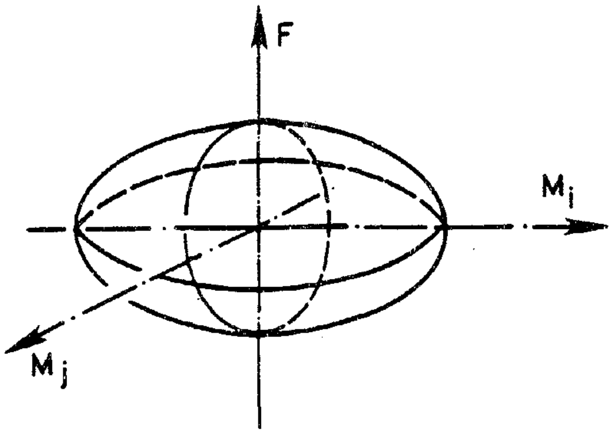

$$\phi = \left(\frac{M_y}{M_{yu}}\right)^2 + \left(\frac{M_z}{M_{zu}}\right)^2 + \left(\frac{M_x}{M_{xu}}\right)^2 + \left(\frac{F}{F_u}\right)^2 = 1$$

(A) SURFACE TYPE 1

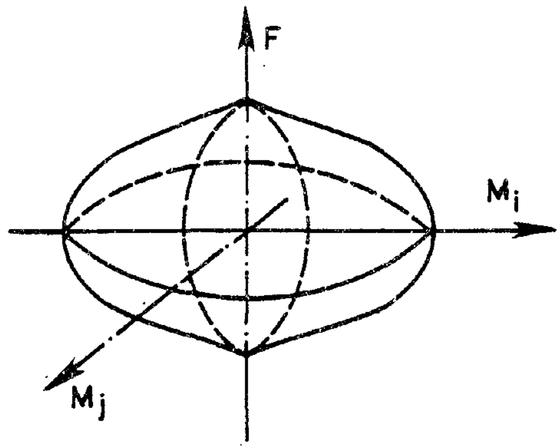

$$\phi = \left[\left(\frac{M_y}{M_{yu}}\right)^2 + \left(\frac{M_z}{M_{zu}}\right)^2 + \left(\frac{M_x}{M_{xu}}\right)^2\right]^{1/2} + \left(\frac{F}{F_u}\right)^2 = 1$$

(B) SURFACE TYPE 2

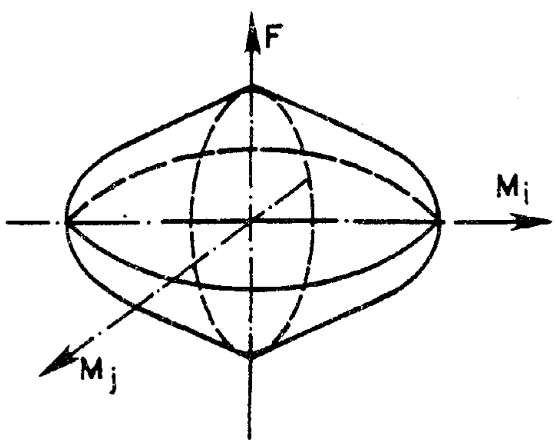

$$\phi = \left[\left(\frac{M_y}{M_{yu}}\right)^2 + \left(\frac{M_z}{M_{zu}}\right)^2 + \left(\frac{M_x}{M_{xu}}\right)^2\right]^{1/2} + \left(\frac{F}{F_u}\right)^{a_1} = 1$$

(C) SURFACE TYPE 3

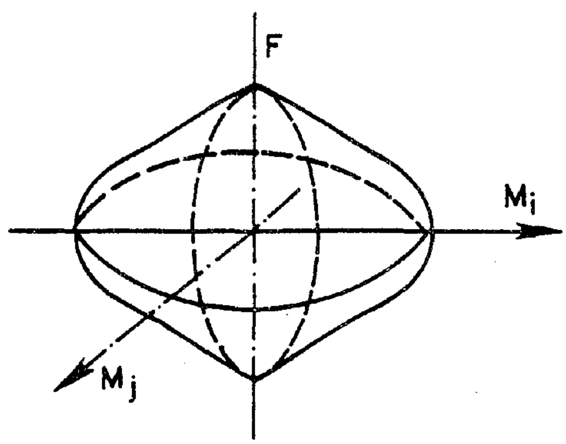

$$\phi = \left[\left(\frac{M_y}{M_{yu}}\right)^2 + \left(\frac{M_z}{M_{zu}}\right)^2 + \left(\frac{M_x}{M_{xu}}\right)^2\right]^{a_1} + \left(\frac{F}{F_u}\right)^{a_2} = 1$$

(D) SURFACE TYPE 4

FIG. B2.4 INTERACTION SURFACES

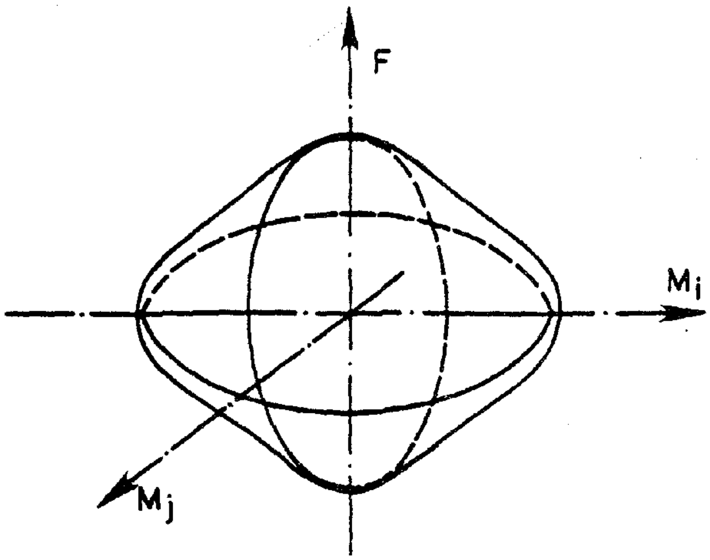

$$\phi = \left(\frac{M_y}{M_{yu}}\right)^{a_1} + \left(\frac{M_z}{M_{zu}}\right)^{a_2} + \left(\frac{T}{T_u}\right)^{a_3} + \left(\frac{F}{F_u}\right)^{a_4} = 1$$

(E) SURFACE TYPE 5

FIG. B2.4 INTERACTION SURFACES (CONT'D)

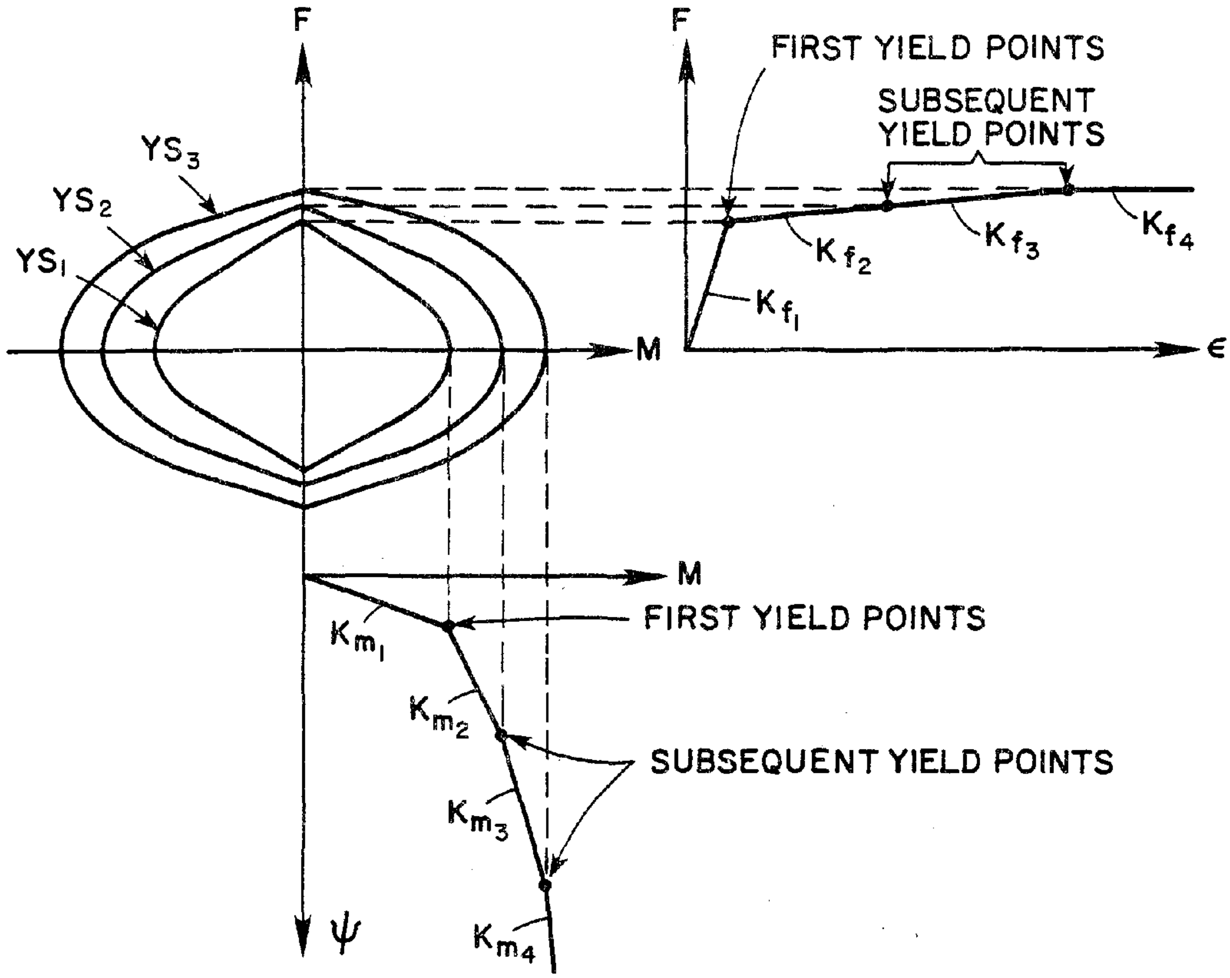

(a) INITIAL LOCATIONS OF SURFACES

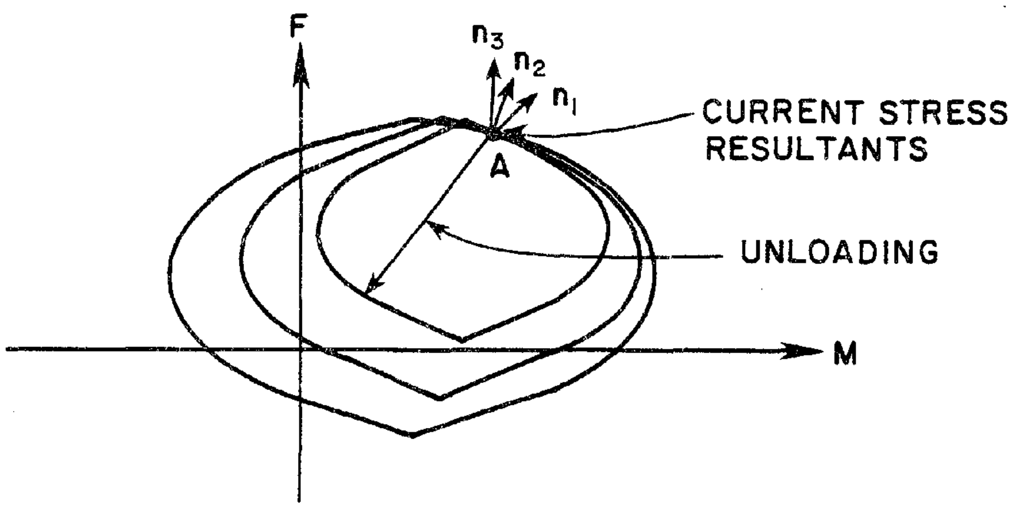

(b) DISPLACED SURFACES AFTER HARDENING

FIG. B2.5 STRAIN HARDENING BEHAVIOR

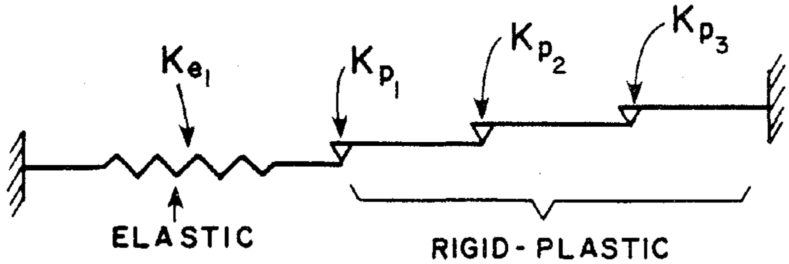

FIG. B2.6 1-D MODEL

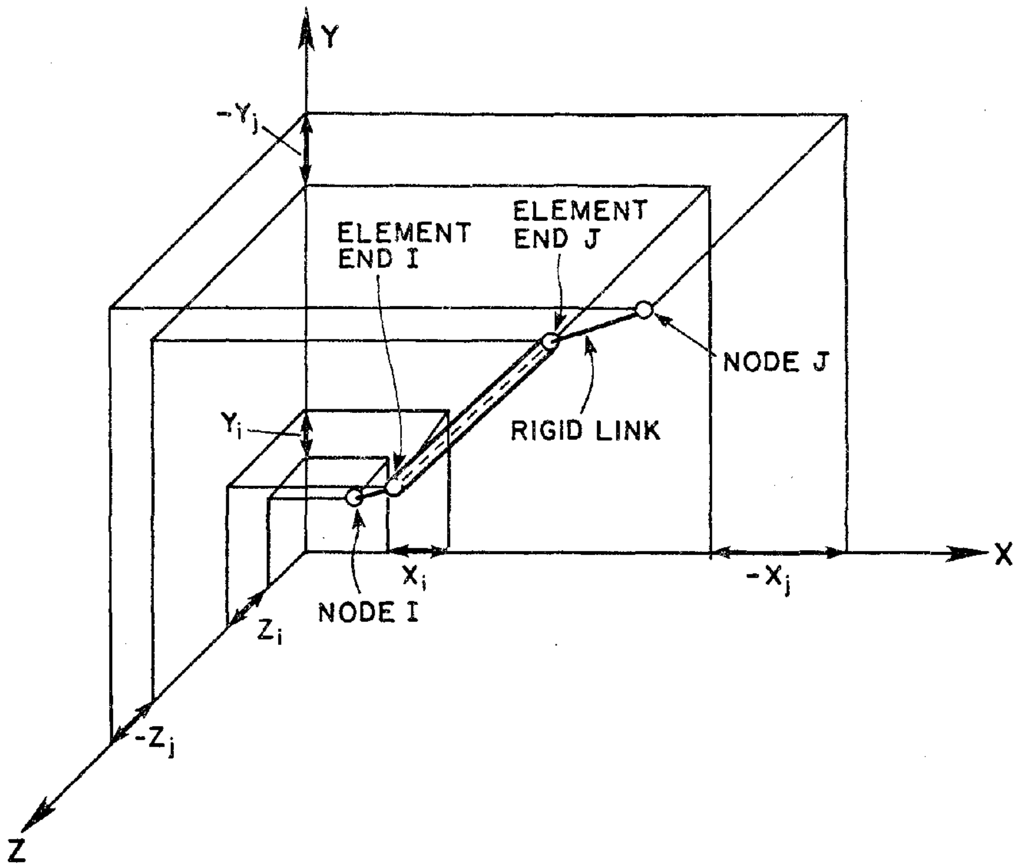

FIG. B2.7 END ECCENTRICITIES

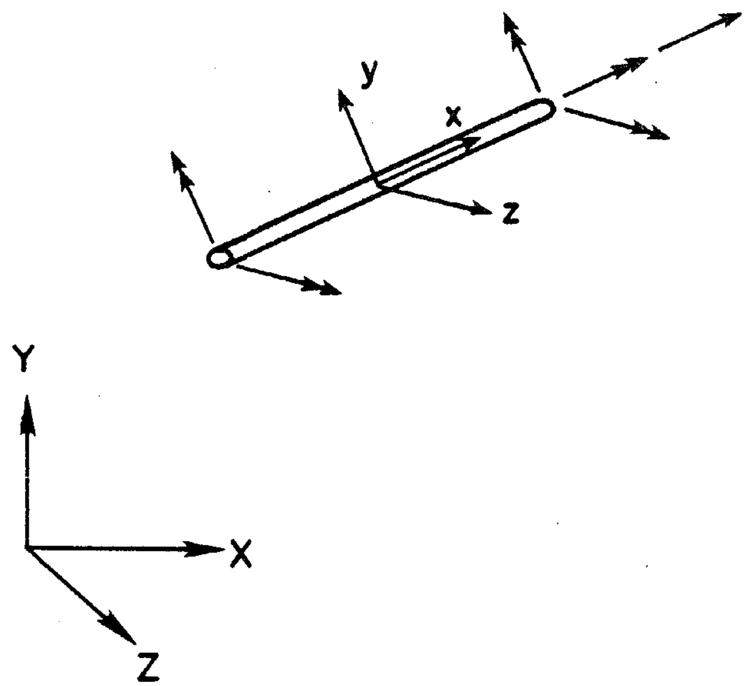

FIG. B2.8 POSITIVE DIRECTION OF
INITIAL ELEMENT ACTIONS

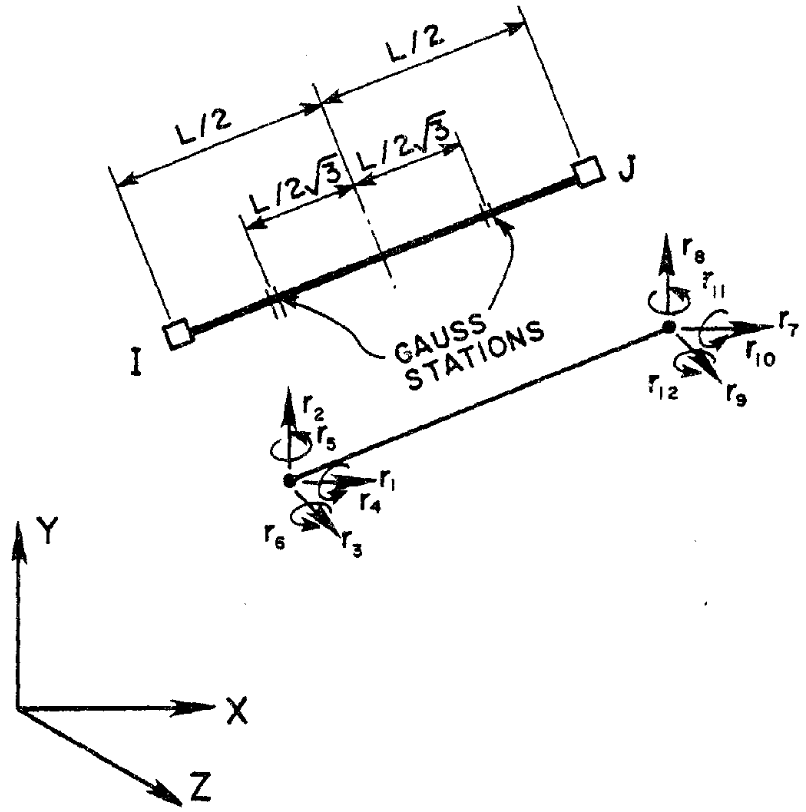

(a) GLOBAL DISPLACEMENTS

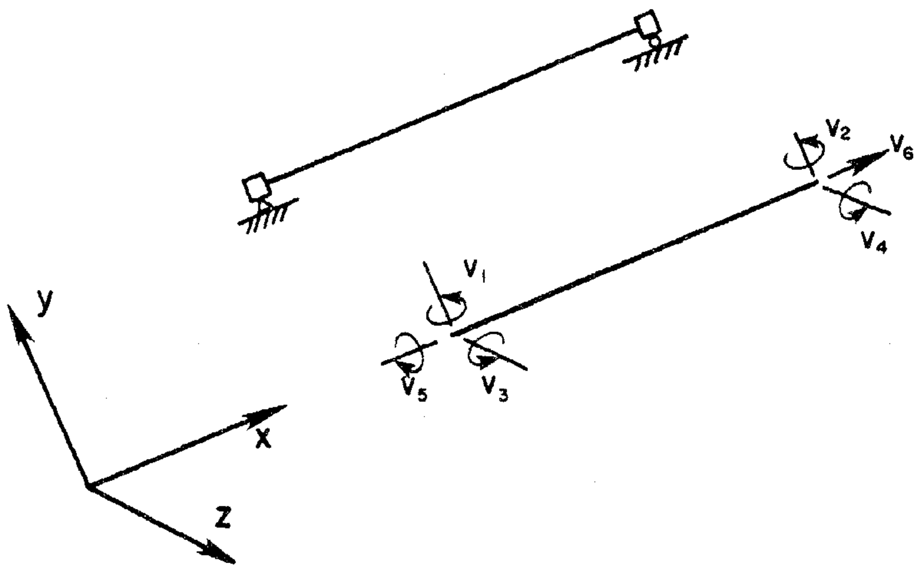

(b) LOCAL DISPLACEMENTS

FIG. B3.1 ELEMENT DEGREES OF FREEDOM

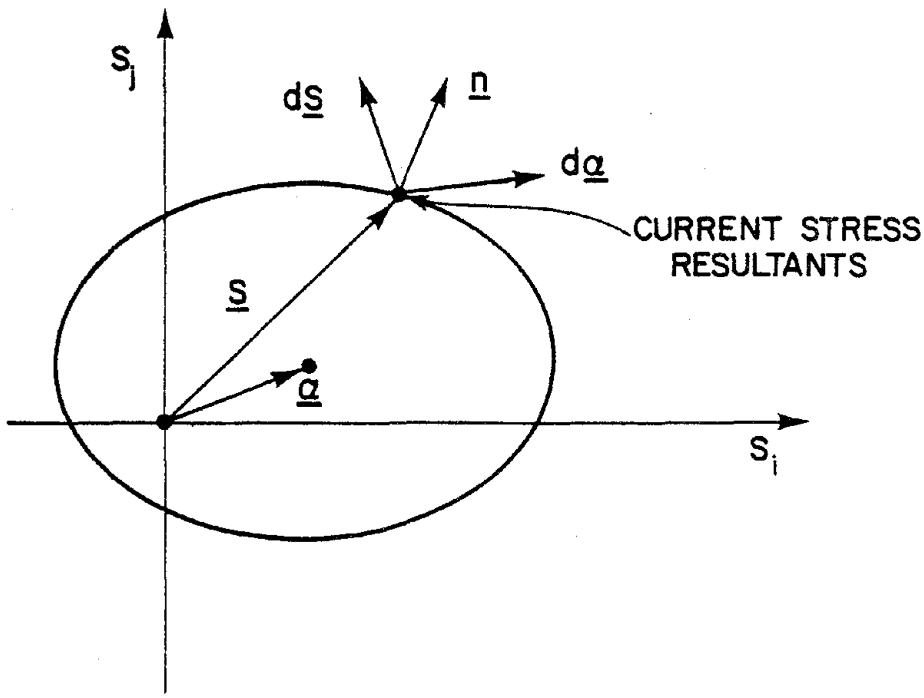

FIG. B3.2 INCREMENTS IN STRESS RESULTANTS AND YIELD SURFACE TRANSLATIONS

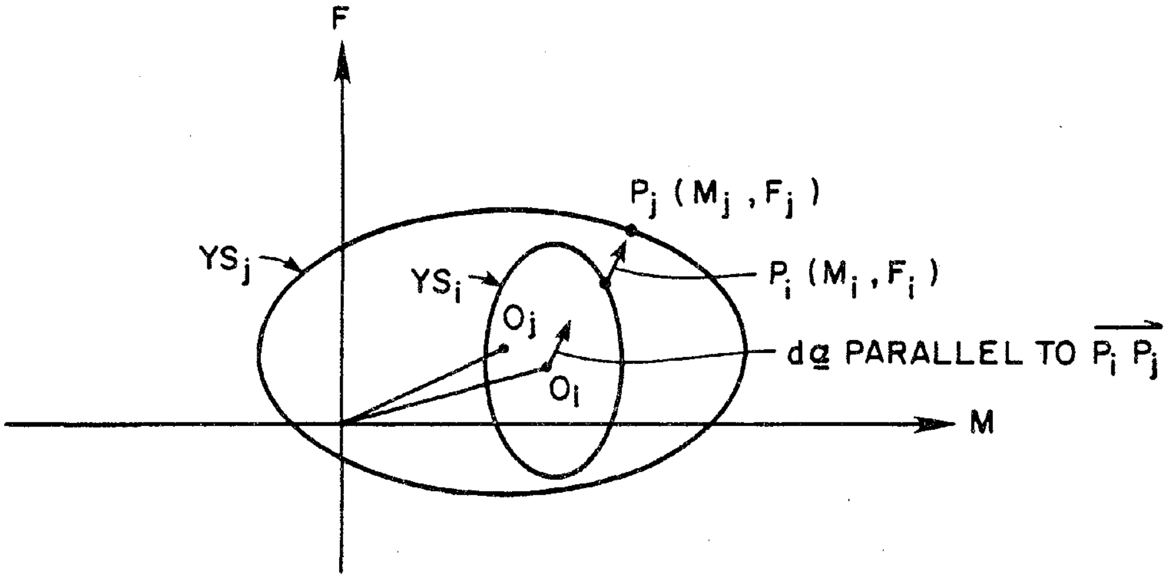

(a) YIELD SURFACES IN F-M SPACE

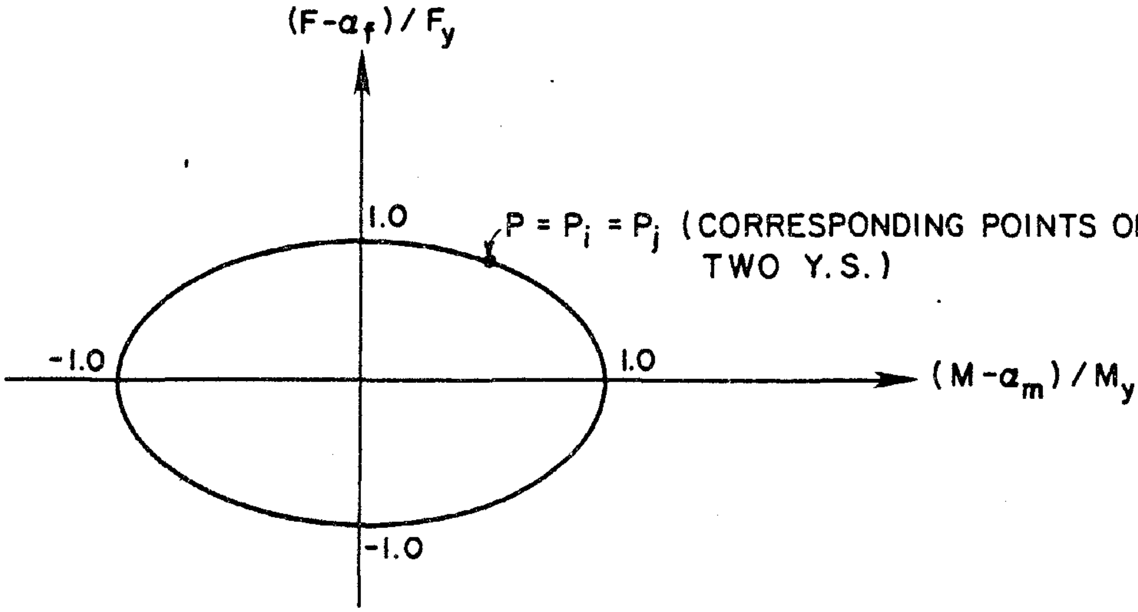

(b) YIELD SURFACES IN NORMALIZED SPACE

FIG. B3.3 MODIFIED MROZ HARDENING RULE

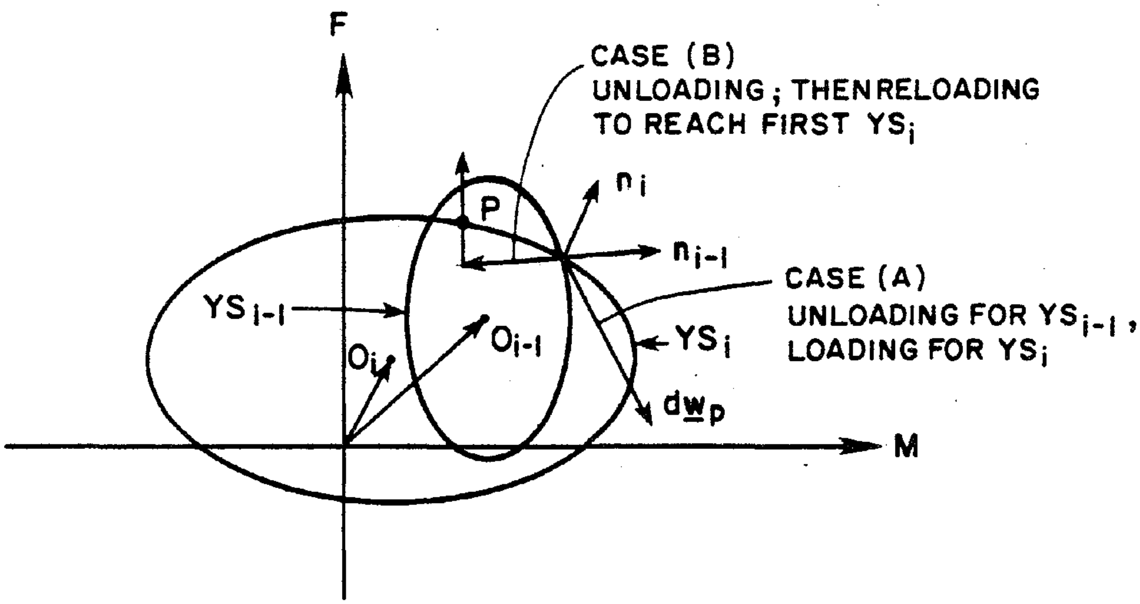

FIG. B3.4 LOADING/UNLOADING CRITERION

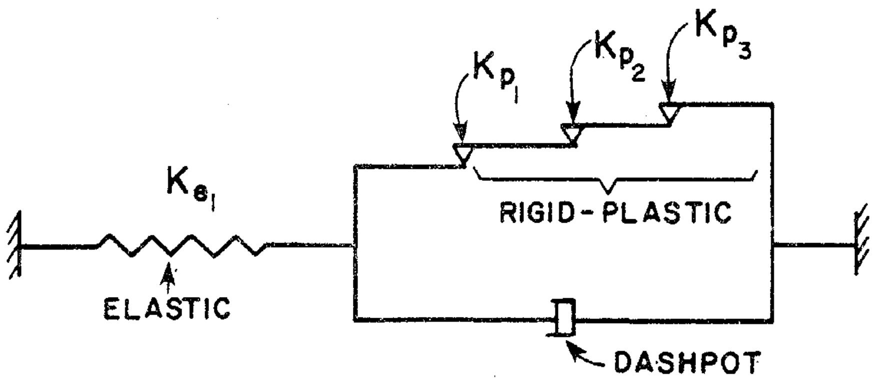

FIG. B4.1 1-D MODEL WITH STRAIN RATE EFFECTS

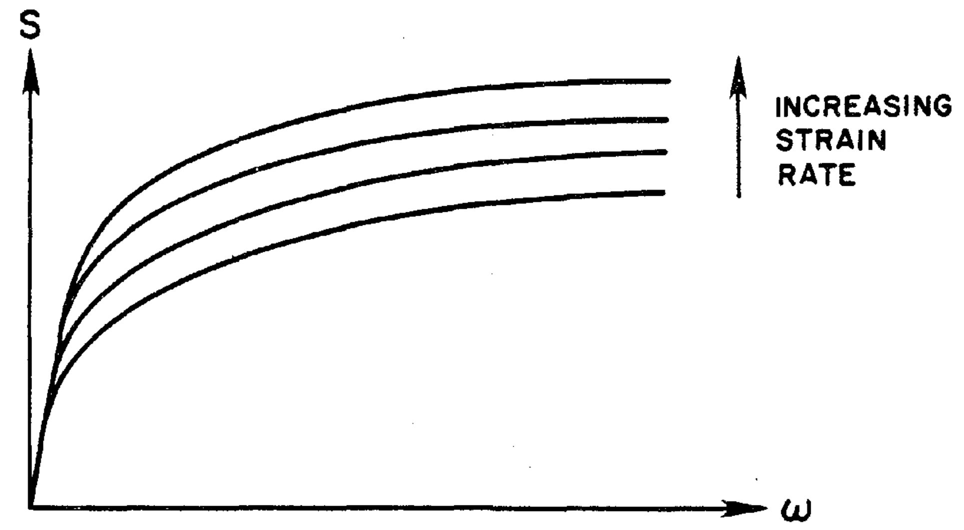

(a) FORCE-DEFORMATION RELATIONSHIP WITH DIFFERENT STRAIN RATES

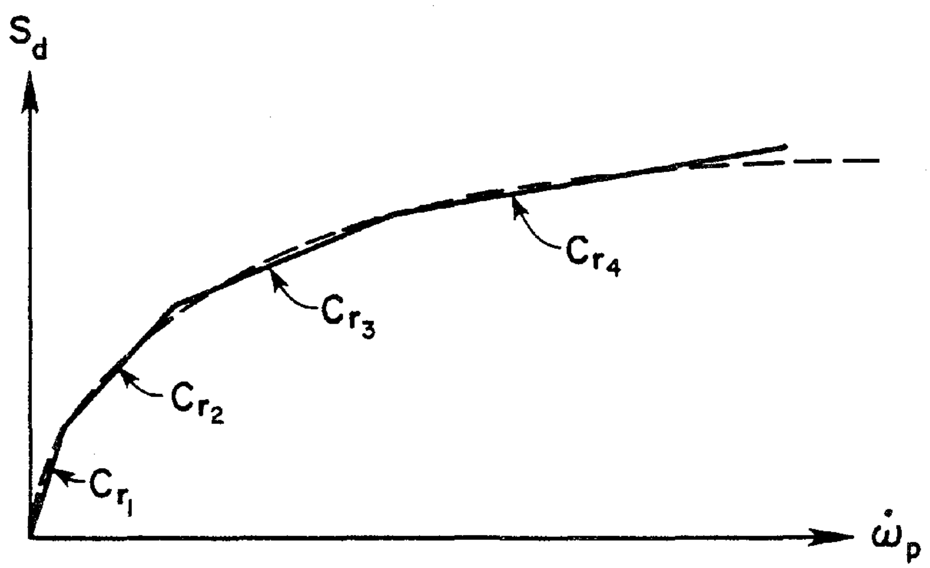

(b) STRENGTH INCREASE VS. PLASTIC DEFORMATION RATE

FIG. B4.2 DEFORMATION RATE EFFECT

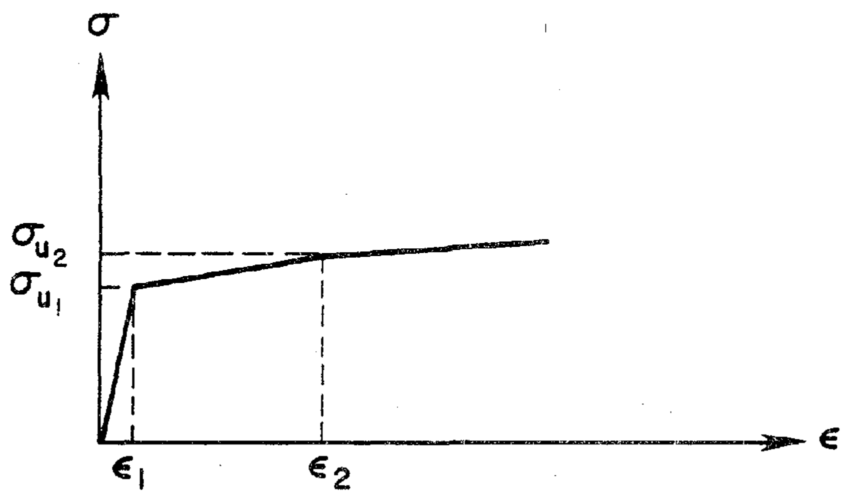

(a) STRESS VS. STRAIN

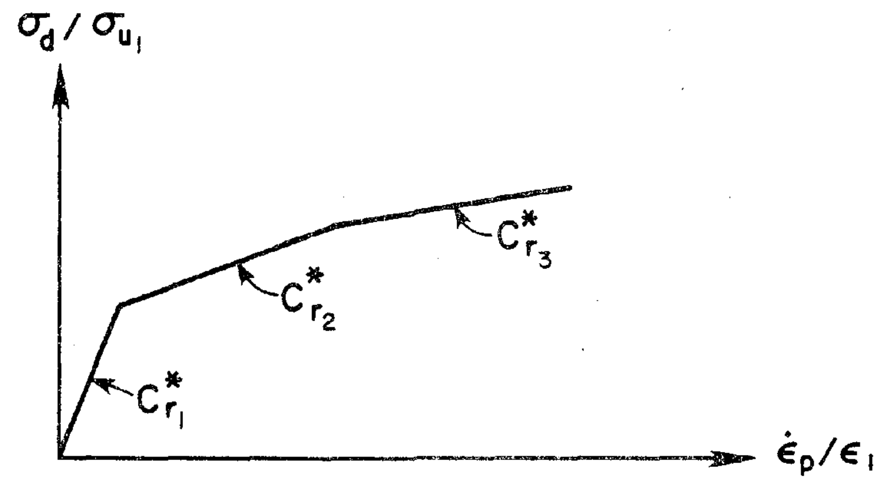

(b) DIMENSIONLESS STRESS VS. STRAIN RATE

FIG. B4.3 STRESS VS. STRAIN RATE FOR BEAM MATERIAL

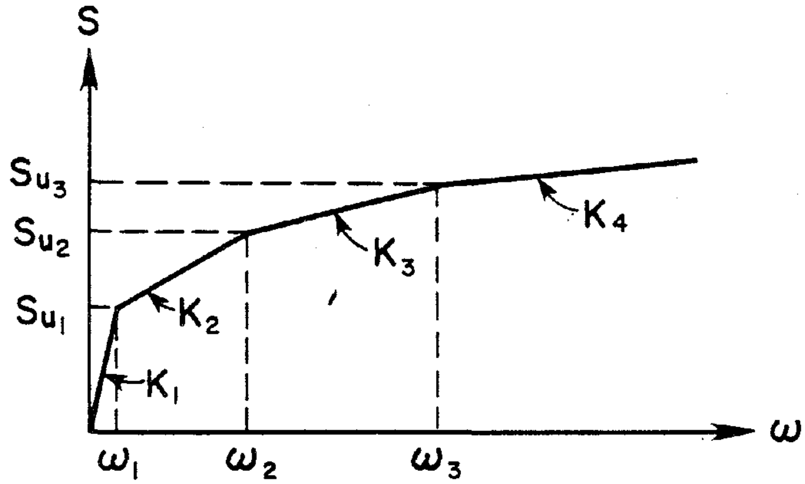

(a) ACTION VS. DEFORMATION

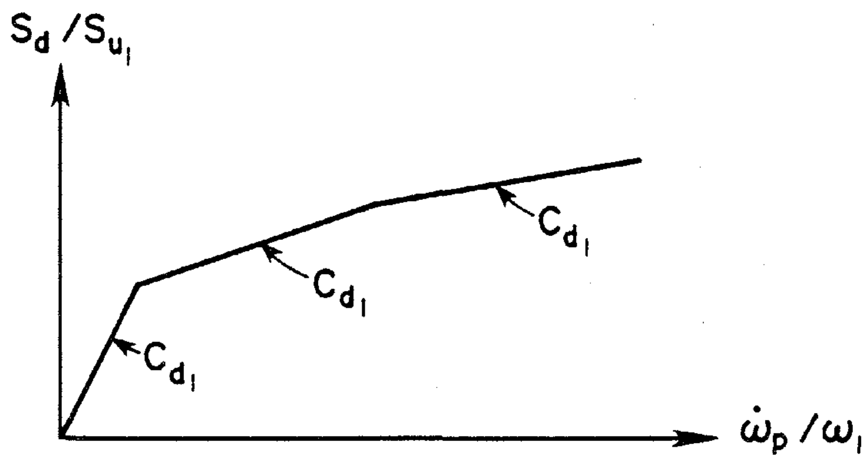

(b) DIMENSIONLESS ACTION VS. DEFORMATION RATE

FIG. B4.4 ACTION VS. DEFORMATION RATE FOR BEAM

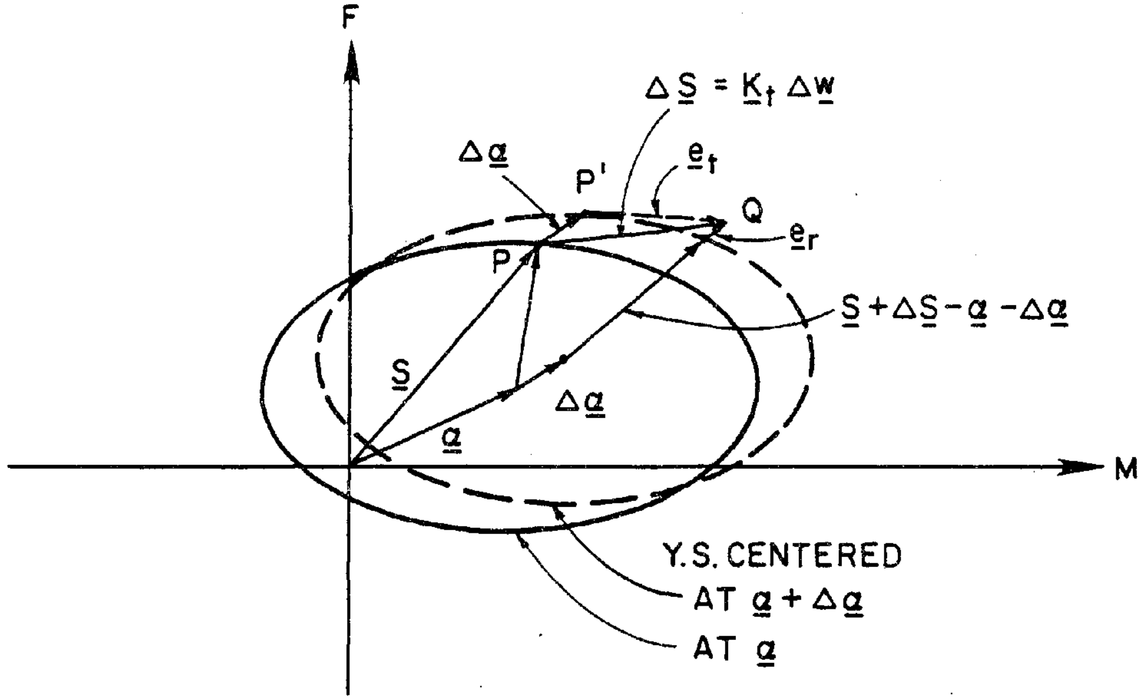

FIG. B5.1 ERROR CONTROL FOR STATE DETERMINATION

C. LUMPED PLASTICITY BEAM-COLUMN ELEMENT

C1. INTRODUCTION

The element described in this report is intended primarily for modeling inelastic effects in steel beams and columns for buildings, with particular emphasis on three-dimensional behavior. The element takes account of moment-force interaction for columns and of bending moment interaction for biaxial bending. Yielding is assumed to take place only in concentrated (i.e. zero length) plastic hinges located at the element ends. The part of the element between the hinges is assumed to remain linearly elastic.

Initial elastic stiffnesses must be specified for axial extension, torsional twist, and bending about two axes. Flexural shear deformations and the effects of eccentric end connections can be considered, if desired. The element strengths may be different at the two ends, and the elastic stiffnesses can include the effect of varying cross section along the element length.

The essential features of the element are as follows:

(1) The element may be arbitrarily oriented in space but must be straight.

(2) Inelastic behavior is confined to zero-length plastic hinges at the element ends.

(3) The hinges are assumed to have rigid-plastic-strain-hardening behavior. Strain hardening stiffnesses must be specified for the moment-rotation and force-extension relationships of the hinges. Multi-linear relationships (max. 4 segments) are assumed.

(4) Interaction between bending moments, torque, and axial force is considered by means of four-dimensional yield surfaces. A kinematic hardening rule (extended Mroz theory) is assumed for post-yield behavior (i.e., translation of yield surface without change of size or shape).

(5) Options are available for small displacements, second order (P- Δ) theory and full large displacement effects. Large displacements are considered using an "engineering" theory (i.e., not a consistent continuum mechanics approach).

Preceding page blank

(6) Eccentric end connections may be specified to model rigid joint regions, and rigid diaphragm slaving may be specified to model floor slabs.

A general description of the element properties is presented in Chapter C2. Theoretical details are presented in Chapter C3. Details of the computer logic are described in Chapter C4. An element user guide for the ANSR program is presented in Chapter C5.

C2. ELEMENT CHARACTERISTICS AND PROPERTIES

C2.1 GENERAL CHARACTERISTICS

The three-dimensional steel beam-column element is formulated to model steel beams and columns, which exhibit hysteretic behavior when subjected to cyclic loads. Elements may be arbitrarily oriented in the global XYZ coordinate system. The element properties are specified in a local xyz coordinate system. The orientations of the local axes are defined as shown in Fig. C2.1a. Node K, together with nodes I and J, defines the plane containing the local y axis.

Inelastic behavior of the element is governed by axial force, two flexural moments, and the torsional moment. Yielding may take place only in concentrated plastic hinges at the element ends. Strain hardening is approximated by assuming that the element consists of a linear elastic beam element with a nonlinear hinge at each end, as shown in Fig. C2.1b. For analysis, each hinge is subdivided into a series of subhinges. The action-deformation relationships for each subhinge are represented by bilinear functions. The bilinear action-deformation relationships for a series of subhinges combine to produce a multi-linear function for each complete hinge, and hence, also multi-linear relationships for the complete element.

The elastic beam properties are defined by an axial stiffness, two flexural stiffnesses, a torsional stiffness and two effective shear rigidities (if shear deformation is to be taken into account). Elements of variable cross section can be considered by specifying appropriate flexural stiffness and carry-over coefficients, and by using average cross section properties for the axial and torsional stiffnesses.

For each subhinge, bilinear relationships can be specified separately for moment-rotation about the element y and z axes, torque-twist, and force-axial extension. Different yield strengths can be specified at the hinges at each end, if desired.

Interaction among the two bending moments, torsional moment, and axial force at a hinge is taken into account for determining both initial yield and subsequent plastic flow. The force-deformation and interaction relationships will typically be based on observations of the behavior of steel members loaded by single actions and by multiple actions in combination.

Options are available for small displacements, second order (P-Δ) theory, and full large displacement effects. Large displacements are considered using an engineering theory (i.e., not a consistent continuum mechanics approach). Eccentric end connections and rigid diaphragm slaving may be specified. Initial element forces may be specified. These initial forces affect element yield but do not contribute to the nodal loads.

C2.2 AXES

Element properties and results are specified in the local coordinate system x,y,z, defined as shown in Fig. C2.1. If node K is not specified, its location is assumed as follows.

(a) If IJ is not vertical, node K is at $Y = +\infty$. The xy plane is then the vertical plane containing the element.

(b) If IJ is vertical, node K is at $X = +\infty$. The xy plane is then parallel to the XY plane.

C2.3 MODELING OF INELASTIC BEHAVIOR

C2.3.1 General

Yield is monitored at the potential hinges. Tangent stiffness relationships between the actions and deformations at a yielding hinge are established using a plasticity theory which is an extension of the Mroz theory for yield of metals. Each hinge is initially rigid, so that the initial stiffness of the complete element is the stiffness of the elastic beam. As the moments and forces at the element ends (the hinge actions) increase, the hinges can yield, causing a stiffness reduction in the element. Under increasing deformation, the hinges strain harden, following multi-linear action-deformation relationships. If the actions at a hinge decrease, the hinge becomes rigid again and the element unloads. The overall element behavior is thus multi-linearly inelastic, as illustrated in Fig. C2.2.

C2.3.2 Hinge Properties

The rigid-plastic-strain-hardening relationships between hinge actions and deformations must be defined for the two hinges. The relationships at the two hinges in any element may be different, if desired.

Relationships as shown in Fig. C2.3 must be defined for each of four action-deformation pairs, namely (1) bending moment, M_y, and corresponding rotation, θ_y; (2) bending moment, M_z, and corresponding rotation, θ_z; (3) torque, M_x, and corresponding twist, ϕ_x; and (4) axial force, F_x, and corresponding extension, δ_x. Each relationship is rigid-plastic-strain-hardening and may have up to three linear segments, as shown in Fig. C2.3. The relationships may be of different shape for each action. For material with an elastic-perfectly-plastic stress-strain relationship, the torque-twist and force-extension relationships will be rigid-perfectly-plastic, whereas the moment-rotation relationships will usually exhibit strain hardening behavior (Fig. C2.5). It is required that the deformations at changes in stiffness have the same ratios for all relationships, as indicated in Fig. C2.2. This restriction is necessary to avoid inconsistencies in the plasticity theory.

It may be noted that the assumption of a zero-length hinge implies infinitely high strains as a hinge deforms. This is inherent in any plastic hinge type of theory.

C2.3.3 Interaction Surfaces for First Yield

The actions M_y, M_z, M_x, and F_x interact with each other to produce initial yield of the hinge. The interaction effect is determined by a yield (interaction) surface. To allow for a variety of applications, provision is made in the theory for five different yield surfaces. These surfaces are all four-dimensional (i.e., M_y, M_z, M_x, and F_x), and hence, cannot be shown easily using diagrams. The surfaces differ, however, mainly in the way in which the axial force interacts with the three moments. Hence, the differences can be illustrated using the three-dimensional diagrams in Fig. C2.4. In these figures, the M_i and M_j axes indicate any two of the moments, and the F_x axis indicates axial force. The origin of the yield surface can be shifted along the axial force axis, if it is desired to have greater compressive capacity than tension capacity. The F-M interaction surface can then approximate that for a reinforced concrete column. The equations defining the yield surfaces are shown in the figure.

Surface 1 is elliptical and is the simplest mathematically. Surfaces 2, 3, and 4 allow more realistic modeling of moment-force interaction for cases in which axial force effects are substantial. For all of these four surfaces, the interaction among M_y, M_z, and M_x is elliptical and only the force-moment interaction changes. Surface 5 is of a different form than the other four and is included for greater generality in special cases.

C2.3.4 Interaction Surfaces for Subsequent Yield

For modeling a hinge with nonlinear material properties, it is assumed that the behavior is rigid-plastic-strain-hardening for each action individually, as shown in Fig. C2.3a. In one dimension, the rigid-plastic-strain-hardening behavior can be modeled using a series rigid-plastic subsprings, as shown in Fig. C2.3b. This model can be extended to the multi-dimensional case using a series of rigid-plastic "subsprings", with the yield of any subhinge governed by a yield surface. First yield occurs at the first subhinge and is governed by the initial yield surface. For each change of stiffness, there is a corresponding yield surface, each corresponding to a subhinge. These surfaces are assumed to have the same *basic* form as the surface for first yield. However, because the action-deformation relationships may be of different shape for each action, the surfaces for the first and subsequent subhinges will not have, in general, identical actual shapes. An example in 2D action space is illustrated in Fig. C2.6.

C2.3.5 Plastic Stiffnesses: Axial Force and Torque

The hinge yield strengths and the plastic stiffnesses of the hinge action-deformation relationships (K_{p1}, K_{p2}, and K_{p3} in Fig. C2.3) must be specified to provide appropriate post-yield stiffening of the complete element. The procedure is straight-forward for axial force and torque but more complex for bending.

Consider axial force, and let the force-extension relationship for the complete element be as shown in Fig. C2.7a. The steps are as follows.

(a) Elastic axial rigidity of beam $= EA = K_{F1} \cdot L$.

(b) Strength at first yield surface $= F_{y1}$.

(c) Plastic stiffness after first yield surface $= K_{p1} = \dfrac{K_{F1} \cdot K_{F2}}{K_{F1} - K_{F2}}$.

(d) Strength at yield surface i $= F_{yi}$.

(e) Plastic stiffness after yield surface i $= K_{pi} = \dfrac{K_{Fi} \cdot K_{F(i+1)}}{K_{Fi} - K_{F(i+1)}}$.

The same procedure applies for torque, as follows (Fig. C2.7c).

(a) Elastic torsional rigidity of beam $= GJ = K_{T1} \cdot L$.

(b) Strength at first yield surface $= T_{y1}$.

(c) Plastic stiffness after first yield surface $= K_{p1} = \dfrac{K_{T1} \cdot K_{T2}}{K_{T1} - K_{T2}}$.

(d) Strength of yield surface i $= T_{yi}$.

(e) Plastic stiffness after yield surface i $= K_{pi} = \dfrac{K_{Ti} \cdot K_{T(i+1)}}{K_{Ti} - K_{T(i+1)}}$.

C2.3.6 Plastic Stiffnesses: Bending

A complication in specifying the flexural plastic stiffnesses arises from the fact that moment-curvature nonlinearities are modeling using concentrated hinges. In an actual beam the moment typically varies along the length, and plastic deformations occur over finite regions. Consequently, the flexural stiffness depends on the moment variation along the beam. In a concentrated hinge model, it is not possible to account for all possible moment variations; and hence, assumptions must be made in specifying the hinge properties.

Three options are available in the computer program for assigning bending stiffness properties to the hinges. The first option is for a uniform beam with essentially constant moment along the element (Fig. C2.8a). This option is applicable, in general, only for a structure which is modeled using short beam-column elements, such that the bending moment does not vary greatly over a single element. The relationship between bending moment and end rotation for the initial loading of the element is as shown in Fig. C2.8b. The steps in establishing the hinge properties are as follows:

(a) Elastic flexural rigidity of beam = EI = $K_{M1} \cdot L/2$.

(b) Shear rigidity of beam assumed to be infinite (no shear deformations).

(c) Hinge strength at first yield = M_{y1}.

(d) Plastic stiffness after first yield surface = $K_{p1} = \dfrac{K_{M1} \cdot K_{M2}}{K_{M1} - K_{M2}}$.

(e) Strength at yield surface i = M_{yi}.

(f) Plastic stiffness after yield surface i = $K_{pi} = \dfrac{K_{Mi} \cdot K_{M(i+1)}}{K_{Mi} - K_{M(i+1)}}$.

The second option is applicable for a uniform beam in which a linear variation of bending moment can be assumed over the element length, with equal and opposite values at the ends (Fig. C2.9a). This option will typically apply for columns in an unbraced frame building. An equivalent cantilever for each half of the element is used, as shown in Fig. C2.9b. It is required that the relationship between the tip load and tip displacement of the cantilever be known (Fig. C2.9c). This relationship can then be used to obtain hinge stiffness as follows.

(a) Elastic flexural rigidity of beam = $EI = K_1 L^3/24$.

(b) Shear rigidity of beam assumed to be infinite (no shear deformations).

(c) Hinge strength at first yield = $P_{y1} \cdot L/2$.

(d) Plastic stiffness after first yield surface = $K_{p1} = \dfrac{K_1 \cdot K_2 \cdot L}{2(K_1 - K_2)}$.

(e) Strength at yield surface i = $P_{yi} \cdot L/2$.

(f) Plastic stiffness after yield surface i = $K_{pi} = \dfrac{K_i \cdot K_{i+1} \cdot L}{2(K_i - K_{i+1})}$.

For these first two options, the computer program calculates the K_p values, given the moment-rotation relationships (for Option 1) or load-deflection relationship (for Option 2). The third option provides the user with more flexibility by requiring that the EI/L and K_p values be specified directly. In addition, with this option it is not necessary for the element to be of uniform section. Flexural stiffness coefficients, K_{ii}, K_{jj}, and K_{ij}, which depend on the variation of the beam cross section, may be specified (for example, for a uniform element, $K_{ii} = K_{jj} = 4.0$ and $K_{ij} = 2.0$). Also, an effective shear stiffness (GA') can be specified.

C2.3.7 Plastic Flow

Interaction among the actions is considered as shown diagrammatically in Fig. C2.6. Yield begins when the yield surface of the first subhinge is reached. The surface then translates in action space, the motion being governed by the plastic flow of the first subhinge. Translation of the first surface continues until the second surface is reached. Both surfaces then translate together, governed by a combination of plastic flow on both yielded subhinges. For any subhinge, plastic flow is assumed to take place normal to the yield surface of that subhinge. If two or more subhinges are yielded, their yield surfaces move together, and the total plastic deformation is equal to the sum of the individual plastic deformations for each subhinge, directed along the normal directions of their respective yield surfaces at the action point. After some arbitrary amount of plastic deformation, the situation might be as illustrated in Fig. C2.6b.

On unloading, the elastic stiffness values, K_1, govern until the yield surface of the first subhinge is again reached (Fig. C2.6b). The surface then translates as before.

C2.3.8 Hardening Behavior

After first yield, the yield surfaces of the yielded subhinges are assumed to translate in action space, obeying a kinematic hardening rule (translation without change of shape or size). An extension of the Mroz theory of material plasticity is used to define the hardening behavior. Because the yield surfaces of the yielded subhinges are generally not exactly similar, overlapping of the surfaces can occur, as described in detail in Section C3.5. As a result, the hardening behavior is more complex than in the basic Mroz theory. For example, in Fig. C2.6b, the current action point, A, lies on yield surfaces YS_1, YS_2, and YS_3. Hence, all three subhinges (Fig. C2.3b) have yielded, and the direction of plastic flow is a combination of the normal vectors $\underline{n}_1$, $\underline{n}_2$, and $\underline{n}_3$. Details of the theory are given in Sections C3.2.5 and C3.2.6.

C2.4 END ECCENTRICITY

Plastic hinges in frames and coupled frame-shear wall structures will form near the faces of the joints rather than at the theoretical joint centerlines. This effect can be approximated by postulating rigid, infinitely strong connecting links between the nodes and the element ends, as shown in Fig. C3.5.

C2.5 RIGID FLOOR DIAPHRAGMS

A frequently made assumption in the analysis of tall buildings is that each floor diaphragm is rigid in its own plane. To introduce this assumption, a master node at the center of mass of each floor may be specified, as shown in Fig. C3.6. Each master node has only three degrees of freedom as shown, which are the displacements of the diaphragm horizontally as a rigid body. If any beam-column member is connected to these *master* displacements, its behavior depends partly on these displacements and partly on the displacements which are not affected by the rigid diaphragm assumption.

C2.6 INITIAL FORCES

For structures in which static analyses are carried out separately (i.e. outside the ANSR program), initial member forces may be specified. The sign convention for these forces is as shown in Fig. C2.10. These forces are not converted to loads on the nodes of the structure but are simply used to initialize the element end actions. For this reason, initial forces need not constitute a set of actions in equilibrium. The only effects they have on the behavior of the system are (a) to influence the onset of plasticity and (b) to affect the geometric stiffnesses.

C3. THEORY

C3.1 DEGREES OF FREEDOM

The element has two external nodes and two internal nodes, as shown in Fig. C3.1a. The external nodes connect to the complete structure and have six degrees of freedom each, namely X,Y,Z global translations and X,Y,Z, global rotations. After deletion of the six rigid body modes for the complete element and transformation to local element coordinates, the six deformation degrees of freedom shown in Fig. C3.1b remain. Each hinge has four deformations, namely an axial deformation plus rotations about each of the local x,y,z axes (i.e., shear deformations in the hinges are zero).

The transformation from global displacements to element deformations is:

$$\underline{v} = \underline{a}\,\underline{r} \tag{C3.1}$$

in which

$$\underline{v}^T = [v_1, v_2, \ldots, v_6] = \text{element deformations (Fig. C3.1b);}$$
$$\underline{r}^T = [r_1, r_2, \ldots, r_{12}] = \text{global displacements (Fig. C3.1a);}$$

and the transformation matrix $\underline{a}$ is well known.

The vector of degrees of freedom, $\underline{w}$, for the elastic element (Fig. C3.2a) is defined as:

$$\underline{w}^T = [w_1, w_2, \ldots, w_6]$$

The complete hinges at ends I and J have degrees of freedom defined by:

$$\underline{w}_{pI}^T = [(v_1 - w_1)\ \ (v_3 - w_3)\ \ (v_5 - w_5)'\ \ (v_6 - w_6)']$$

and

$$\underline{w}_{pJ}^T = [(v_2 - w_2)\ \ (v_4 - w_4)\ \ (v_5 - w_5)''\ \ (v_6 - w_6)'']$$

in which v_i, i=1,4 and w_i, i=1,4 are as shown in Fig. C3.1a and C3.2a, and in which:

$$(v_5 - w_5)' + (v_5 - w_5)'' = v_5 - w_5$$
$$(v_6 - w_6)' + (v_6 - w_6)'' = v_6 - w_6$$

That is, the torsional and axial hinge deformations are shared between the hinges at ends I and J. The proportions in which the deformations are shared are determined naturally during the numerical computation and do not need to be defined in advance. Each complete hinge is modeled as three subhinges in series (Fig. C3.2b). Each subhinge has four deformation degrees of freedom $\underline{w}_{sp}$, such that the sum of the $\underline{w}_{sp}$ deformation for the three subhinges gives the hinge deformation, $\underline{w}_p$. The proportions of any hinge deformation which are contributed by the separate subhinges are determined automatically during the computation.

C3.2 ELEMENT STIFFNESS

C3.2.1 Basic Procedure

The beam element connecting the internal nodes remains elastic, but the tangent stiffnesses of the hinges may change. For any state of the complete element, a 6 x 6 flexibility matrix is first formed for the elastic beam in terms of the degrees of freedom w_1 through w_6. This matrix is then modified by adding the flexibilities of the hinges to give a complete element flexibility matrix in terms of v_1 through v_6. This matrix is inverted to obtain a 6 x 6 element stiffness (computationally, the Sherman-Morrison formula is used, not direct inversion). Finally, this stiffness is transformed to the 12 x 12 global stiffness.

C3.2.2 Beam Element Elastic Flexibility

The local y,z axes are assumed to be the principal axes of the beam cross section. The local x axis is assumed to be both the centroidal axis and the axis of torsional twist.

The beam element stiffness relationships can be written as follows:

$$\begin{Bmatrix} dM_{yi} \\ dM_{yj} \end{Bmatrix} = \frac{EI_y}{L} \begin{bmatrix} K_{iiy} & K_{ijy} \\ K_{ijy} & K_{jjy} \end{bmatrix} \begin{Bmatrix} dw_1 \\ dw_2 \end{Bmatrix} \tag{C3.2a}$$

$$\begin{Bmatrix} dM_{zi} \\ dM_{zj} \end{Bmatrix} = \frac{EI_z}{L} \begin{bmatrix} K_{iiz} & K_{ijz} \\ K_{ijz} & K_{jjz} \end{bmatrix} \begin{Bmatrix} dw_3 \\ dw_4 \end{Bmatrix} \tag{C3.2b}$$

$$dM_x = \frac{GJ}{L} dw_5 \tag{C3.2c}$$

$$dF_x = \frac{EA}{L} dw_6 \tag{C3.2d}$$

in which

K_{ii}, K_{ij}, K_{jj} = flexural stiffness factors;
EI_y, EI_z = effective flexural rigidities;
M_y, M_z = bending moments;
i, j = element ends;
M_x = torsional moment;
F_x = axial force;
L = element length;
EA = effective axial rigidity; and,
GJ = effective torsional rigidity.

The flexural stiffness factors can be used to account for non-uniform elements. For a uniform element, $K_{ii} = K_{jj} = 4.0$ and $K_{ij} = 2.0$.

Equations C3.2a and C3.2b are inverted to obtain flexibilities and are modified, if necessary, to allow for shear deformations by adding the shear flexibility matrices, $\underline{f}_{sy}$ and $\underline{f}_{sz}$, where

$$\underline{f}_s = \frac{1}{GA'L} \begin{bmatrix} 1 & 1 \\ 1 & 1 \end{bmatrix} \tag{C3.3}$$

in which GA' = effective shear rigidity.

C3.2.3 Hinge Plastic Flexibility

The plastic deformation increment of a hinge is the sum of the deformations of its yielded subhinges. That is,

$$d\underline{w}_p = \sum_i d\underline{w}_{spi} \tag{C3.4}$$

in which

$d\underline{w}_{spi}$ = plastic deformations of each subhinge; and
$d\underline{w}_p$ = plastic deformation increments of complete hinge.

In multi-dimensional action space, each hinge has a 4 x 4 flexibility matrix in terms of its axial, torsional, y-flexural, and z-flexural deformations. The flexibility matrix before yield for any hinge is null (i.e. rigid hinge), and hence, has no effect on the complete element flexibility. After yield, the hinge flexibility is finite and contributes to the overall element flexibility. The hinge at end I affects degrees of freedom v_1, v_3, v_5, and v_6 of the complete element. The hinge flexibility coefficients are simply added to corresponding beam coefficients. Similarly, the hinge at end J affects degrees of freedom v_2, v_4, v_5, and v_6. Although the six deformation degrees of freedom are largely uncoupled for the elastic beam (Eqn. C3.2), this is not the case after yield. The complete element flexibility matrix will generally be full (except for zero values for f_{14} and f_{23}).

The hinge flexibility, in turn, is the sum of the flexibilities of the yielded subhinges. That is, a hinge flexibility relationship can be written as:

$$d\underline{w}_p = \underline{f}_p \, d\underline{S} = \sum_i \underline{f}_{spi} \, d\underline{S} \qquad \text{(C3.5)}$$

in which

$\underline{f}_{spi}$ = plastic flexibility of subhinge i;
$\underline{f}_p$ = flexibility matrix for the hinge; and
$d\underline{S}$ = action increment on the hinge.

The problem thus reduces to the determination of $\underline{f}_{spi}$ for each yielded subhinge.

C3.2.4 Yield Function

Each subhinge is effected by four actions (M_y, M_z, M_x, and F_x), with four corresponding deformations. The behavior is rigid-plastic-strain-hardening for each action individually. Different yield values and stiffnesses may be specified for each action component.

Yield of any subhinge is governed by a yield function (interaction relationship). Any one of five different yield functions may be specified, as considered in Section C2.2.3. After yield, each subhinge follows a kinematic hardening rule (that is, its yield surface translates in action space without change of shape or size). The hardening theory is a modification of the Mroz theory for plasticity in metals.

C3.2.5 Plastic Stiffness Matrix

A plastic stiffness matrix for a subhinge is defined as:

$$\underline{K}_{spi} = diag \; [K_{Myi} \, K_{Mzi} \, K_{Mxi} \, K_{Fxi}]$$

where K_{Myi}, K_{Mzi}, K_{Mxi}, and K_{Fxi} are the plastic stiffnesses after yield on surface i from Section C2.3.6.

C3.2.6 Plastic Flexibility for a Single Subhinge

Consider a single subhinge. Let $\underline{S}$ be the vector of actions, where

$$\underline{S}^T = [\, M_y \;\; M_z \;\; M_x \;\; F \,] \tag{C3.6}$$

Assume that the subhinge is *rigid-plastic,* and let $\underline{w}_{sp}$ be the vector of plastic subhinge deformations. That is, w_{sp1} = plastic flexural deformation about axis y; w_{sp2} = plastic flexural deformation about axis z; w_{sp3} = plastic rate of twist about axis x; and w_{sp4} = plastic rate of extension along axis x.

A flexibility relationship for the subhinge is required in the form:

$$d\underline{w}_{sp} = \underline{f}_{sp}\, d\underline{S} \tag{C3.7}$$

in which $\underline{f}_{sp}$ = subhinge flexibility matrix. The following assumptions are made:

(1) Let ϕ be the yield function, as considered in Section C3.2.4. The yield surface translates in action space. After some amount of hardening has taken place, the yield function is $\phi(\underline{S}-\underline{\alpha})$, where α = vector defining the new location of the yield surface origin. This is illustrated in Fig. C3.3 for a two-dimensional space.

(2) From any given plastic state (i.e. a point on the yield surface), any action increment ($d\underline{S}$) will produce increments of deformation ($d\underline{w}_{sp}$) and yield surface translation ($d\underline{\alpha}$). The direction of $d\underline{S}$ may be arbitrary. It is assumed that the direction of $d\underline{w}_{sp}$ is normal to the yield surface (i.e. an associated flow rule is assumed). The direction of $d\underline{\alpha}$ is determined by the hardening rule (as defined later) and is not necessarily parallel to either $d\underline{S}$ or $d\underline{w}_{sp}$. This is illustrated in Fig. C3.3 for a two-dimensional space.

(3) The direction of the outward normal to the yield surface is the gradient of the yield function. Define,

$$\underline{n} = \frac{\underline{\phi},_s}{(\underline{\phi},_s^T \cdot \underline{\phi},_s)^{1/2}} \tag{C3.8}$$

in which

$$\underline{\phi},_s^T = [\, \partial\phi/\partial M_y \;\; \partial\phi/\partial M_z \;\; \partial\phi/\partial M_x \;\; \partial\phi/\partial F \,] \tag{C3.9}$$

= yield function gradient; and

$\underline{n}$ = unit normal vector.

Hence, the deformation increment, $d\underline{w}_{sp}$, is given by:

$$d\underline{w}_{sp} = \underline{n} \cdot dw_{sp}^{*} \tag{C3.10}$$

in which dw_{sp}^{*} = scalar which defines the magnitude of the plastic deformation.

(4) Let the component of $d\underline{S}$ in the direction of $\underline{n}$ be $d\underline{S}_n$ (Fig. C3.3). Hence,

$$d\underline{S}_n = \underline{n} \cdot (\underline{n}^T \cdot d\underline{S}) \tag{C3.11}$$

(5) Assume that $d\underline{S}_n$ and $d\underline{w}_{sp}$ are related by:

$$d\underline{S}_n = \underline{K}_p \, d\underline{w}_{sp} \tag{C3.12}$$

in which

$$\underline{K}_{sp} = diag\, [K_{M_y}\, K_{M_z}\, K_{M_x}\, K_F] \tag{C3.13}$$

is a diagonal matrix of the *plastic* stiffnesses from the individual action-deformation relationships for the subhinge, as defined in Section C2.3.7.

(6) From the definition of $d\underline{S}_n$ (Eqn. C3.11), it follows that

$$\underline{n}^T d\underline{S} = \underline{n}^T d\underline{S}_n \tag{C3.14}$$

Substitute Eqns. C3.12 and C3.10 into Eqn. C3.14 to get:

$$\underline{n}^T \cdot d\underline{S} = \underline{n}^T \cdot \underline{K}_{sp} \cdot \underline{n} \cdot dw_{sp}^{*} \tag{C3.15}$$

(7) Solve for dw_{sp}^{*} as:

$$dw_{sp}^{*} = \frac{\underline{n}^T \cdot d\underline{S}}{\underline{n}^T \cdot \underline{K}_{sp} \cdot \underline{n}} \tag{C3.16}$$

(8) Hence, substitute Eqn. C3.16 into Eqn. C3.10 and use Eqn. C3.7 to get:

$$d\underline{w}_{sp} = \frac{\underline{n} \cdot \underline{n}^T}{\underline{n}^T \cdot \underline{K}_{sp} \cdot \underline{n}} \, d\underline{S} = \underline{f}_{sp} \, d\underline{S} \tag{C3.17}$$

Equation C3.17 is the required plastic flexibility relationship for any *active* subhinge.

C3.2.7 Plastic Flexibility for Complete Hinge

The 4 x 4 plastic flexibility of the complete hinge, $\underline{f}_s$, follows from Eqn. C3.5 as:

$$\underline{f}_p = \sum_i \underline{f}_{spi} \tag{C3.18}$$

where i = active subhinge. The flexibility for any active subhinge, as derived in Section C3.2.6, is given by:

$$\underline{f}_{spi} = \frac{\underline{n}_i \cdot \underline{n}_i^T}{\underline{n}_i^T \cdot \underline{K}_{spi} \cdot \underline{n}_i} \tag{C3.19}$$

in which

$\underline{n}_i$ = normal vector to the surface; and
$\underline{K}_{spi}$ = plastic stiffness matrix of the subhinge.

C3.2.8 Relationship to Basic Mroz Theory

In the special case where the action-deformation relationships for the four actions are all directly proportional to each other, the yield surfaces are all of the same shape and the plastic stiffnesses for each active yield surface are in the same proportion. The plastic stiffness matrix for each active subhinge can then be formed in terms of the elastic stiffness matrix. That is,

$$\underline{K}_{spi} = \alpha_i \underline{K}_e \tag{C3.20}$$

where α_i defines the plastic stiffness as a proportion of the elastic stiffness. The plastic flexibility of a complete hinge can then be written as:

$$\underline{f}_p = \sum_i \underline{f}_{spi} = \sum_i \left(\frac{1}{\alpha_i}\right) \frac{\underline{n}_i \cdot \underline{n}_i^T}{\underline{n}_i^T \cdot \underline{K}_e \cdot \underline{n}_i} \tag{C3.21}$$

Because all the yield surfaces are the same shape, the $\underline{n}_i$ are all the same. Hence, if $\underline{n}_i = \underline{n}$, Eqn. C3.21 can be written as:

$$\underline{f}_p = \frac{\underline{n} \cdot \underline{n}^T}{\underline{n}^T \cdot \left(\sum_i \alpha_i\right) \underline{K}_e \cdot \underline{n}} \tag{C3.22}$$

The flexibility given by this equation is the same as that from the basic Mroz material theory. This shows that the Mroz material theory is a special case of the extended theory derived here.

C3.3 ELEMENT STIFFNESS

For the complete element, a tangent action-deformation relationship is required in the form:

$$d\underline{S} = \underline{K}_t \, d\underline{v} \tag{C3.23}$$

in which $\underline{K}_t$ = 6 x 6 tangent stiffness matrix for the element.

From the preceding derivation, the procedure is to develop the tangent flexibility matrix and then invert to obtain the stiffness matrix. Computationally, the Sherman-Morrison formula rather than inversion is used, as follows.

The flexibility of any subhinge is given by:

$$\underline{f}_{spi} = \frac{\underline{n}_i \cdot \underline{n}_i^T}{\underline{n}_i^T \cdot \underline{K}_{pi} \cdot \underline{n}_i} \tag{C3.24}$$

in which

$\underline{n}_i$ = normal vector of active yield surface i;
$\underline{K}_{pi}$ = plastic stiffness matrix of active yield surface i; and
i = active subhinge number.

Define

$$\underline{g}_i = \frac{\underline{n}_i}{(\underline{n}_i^T \cdot \underline{K}_{pi} \cdot \underline{n}_i)^{1/2}} \tag{C3.25}$$

Expand $\underline{g}_i$ (4 x 1) to $\underline{u}_i$ (6 x 1) by adding two zero terms corresponding to the two flexural deformations of the hinge at the other end of the element. The tangent flexibility of the complete element can then be expressed as:

$$\underline{f}_t = \underline{f}_e + \sum_i \underline{u}_i \cdot \underline{u}_i^T \tag{C3.26}$$

in which $\underline{f}_e$ is the elastic element flexibility matrix.

The Sherman-Morrison formula states that:

$$[\underline{A} + \underline{u} \cdot \underline{u}^T]^{-1} = \underline{A}^{-1} - \frac{\underline{A}^{-1} \cdot \underline{u} \cdot \underline{u}^T \cdot \underline{A}^{-1}}{\underline{u}^T \cdot \underline{A}^{-1} \cdot \underline{u} + 1} \tag{C3.27}$$

Application of this formula to the inversion of $\underline{f}_t$, gives:

$$\underline{K}_t = \underline{K}_{t(l-1)} - \frac{\underline{K}_{t(l-1)} \cdot \underline{u}_l \cdot \underline{u}_l^T \cdot \underline{K}_{t(l-1)}}{\underline{u}_l^T \cdot \underline{K}_{t(l-1)} \cdot \underline{u}_l + 1} \tag{C3.28}$$

in which

l = the current highest active subhinge,

$\underline{K}_{t1} = \underline{f}_e^{-1} = \underline{K}_e$

and $\underline{K}_{ti}$ is obtained using the following recursion relationship.

$$\underline{K}_{ti} = \underline{K}_{t(i-1)} - \frac{\underline{K}_{t(i-1)} \cdot \underline{u}_i \cdot \underline{u}_i^T \underline{K}_{t(i-1)}}{\underline{u}_i^T \cdot \underline{K}_{t(i-1)} \cdot \underline{u}_i + 1} \tag{C3.29}$$

Equation C3.28 defines the tangent stiffness matrix for the complete beam element.

C3.4 EQUILIBRIUM NODAL LOADS

Nodal loads in equilibrium with the element actions in any given state are given by:

$$\underline{R} = \underline{a}^T \cdot \underline{S} \tag{C3.30}$$

in which

$\underline{S}^T = [S_1, S_2, ..., S_6]$; and

$\underline{a}$ = displacement transformation matrix relating element deformations to global displacements.

$\underline{R}$ = internal resisting forces for the element;

C3.5 HARDENING RULE

C3.5.1 Geometrical Interpretation

The relationship between any action and its corresponding deformation at a subhinge is multi-linear. The interaction among the actions (M_y, M_z, M_x, and F) is defined by the yield surface, as described earlier. After initial yield occurs, the behavior at a subhinge obeys a modification of the Mroz strain hardening rule for yield in metals [30].

C3.5.2 Modified Mroz Hardening Rule

For purposes of illustration, consider a two-dimensional M-F space, as shown in Fig. C3.3a. In this figure, it is assumed that the current state (point P_i) is on yield surface YS_i and that loading is taking place towards surface YS_j. It is necessary to define the direction in which surface YS_i translates.

As indicated in Fig. C3.3a, "corresponding" points P_i and P_j can be identified on YS_i and YS_j. The relationship between the actions at these two points ($\underline{S}_i$ at P_i and $\underline{S}_j$ at P_j) is obtained as follows.

Figure C3.3b shows a yield surface transformed into a normalized action space. In this space, surfaces YS_i and YS_j have identical shapes. Hence, points P_i and P_j coincide. The locations of P_i and P_j in Fig. C3.3a follow by transforming back to the natural action space. If the vector of actions at P_i is $\underline{S}_i$, it follows that the vector of actions at P_j is given by:

$$\underline{S}_j = \underline{S}_{uij} (\underline{S}_i - \underline{\alpha}_i) + \underline{\alpha}_j \qquad \text{(C3.31)}$$

in which

$\underline{S}_j$ = vector of actions at point P_j;

$\underline{\alpha}_i$ and $\underline{\alpha}_j$ = vectors defining the current origins, O_i and O_j, of yield surfaces YS_i and YS_j, respectively; and

$$\underline{S}_{uij} = diag \left[\frac{M_{yuj}}{M_{yui}} \;\; \frac{M_{zuj}}{M_{zui}} \;\; \frac{T_{uj}}{T_{ui}} \;\; \frac{F_{uj}}{F_{ui}} \right]$$

It is assumed that the direction of translation of yield surface YS_i is along the line connecting point P_i to point P_j, as shown in Fig. C3.3a. That is, the direction of motion of surface YS_i is defined by:

$$d\underline{\alpha}_i = (\underline{S}_j - \underline{S}_i)\, d\alpha^* \qquad \text{(C3.32)}$$

in which

$d\alpha^*$ = scalar which defines the amount of translation of yield surface YS_i; and

$d\underline{\alpha}_i$ = vector defining the direction of translation.

The magnitude of $d\alpha^*$ is determined as explained in the next section. For the hardening rule originally formulated by Mroz [30,33], all yield surfaces are geometrically similar in natural action space. The rule then ensures that the surfaces never overlap. For the modified Mroz rule, the yield surfaces are assumed to be geometrically similar only in normalized action space. As a result, overlapping of yield surfaces is allowed.

C3.5.3 Mathematical Formulation

Substitute Eqn. C3.31 into Eqn. C3.32 to get:

$$d\underline{\alpha}_i = \left[(\underline{S}_{uij} - \underline{I})\, \underline{S}_i - (\underline{S}_{uij}\, \underline{\alpha}_i - \underline{\alpha}_j) \right] d\alpha^{*} \tag{C3.33}$$

The yield surface is defined by:

$$\phi\, (\underline{S}_i - \underline{\alpha}_i) = 1 \tag{C3.34}$$

The requirement that the action point remain on the yield surface is:

$$d\phi = 0 = \underline{\phi},_s^T\, d\underline{S}_i - \underline{\phi},_s^T\, d\underline{\alpha}_i \tag{C3.35}$$

Substitute Eqns. C3.32 and C3.33 into Eqn. C3.35 to get:

$$d\alpha^{*} = \frac{\underline{\phi},_s^T\, d\underline{S}_i}{\underline{\phi},_s^T\, [(\underline{S}_{uij} - \underline{I})\, \underline{S}_i - (\underline{S}_{uij}\, \underline{\alpha}_i - \underline{\alpha}_j)]} \tag{C3.36}$$

Hence, substitute Eqn. C3.36 into Eqn. C3.32 to get $d\underline{\alpha}_i$ as:

$$d\underline{\alpha}_i = \frac{\left[(\underline{S}_{uij} - \underline{I})\, \underline{S}_i - (\underline{S}_{uij}\, \underline{\alpha}_i - \underline{\alpha}_j) \right] \underline{\phi},_s^T\, d\underline{S}_i}{\underline{\phi},_s^T \left[(\underline{S}_{uij} - \underline{I})\, \underline{S}_i - (\underline{S}_{uij}\, \underline{\alpha}_i - \underline{\alpha}_j) \right]} \tag{C3.37}$$

For any current state defined by $\underline{S}_i$, $\underline{\alpha}_i$, and $\underline{\alpha}_j$, Eqn. C3.37 defines, for an action increment $d\underline{S}_i$, the translation of yield surface YS_i for loading towards surface YS_j.

C3.5.4 Last Yield Surface

For the case when the action point lies on the largest yield surface, the hardening rule can be obtained by assuming that an additional infinitely large yield surface exists. The direction of translation for this case is then along the radial direction connecting the origin of the current yield surface to the current action point. This is exactly Ziegler's hardening rule [34]. It can be expressed as:

$$d\underline{\alpha}_n = (\underline{S}_n - \underline{\alpha}_n)\, d\alpha^{*} \tag{C3.38}$$

in which

n = number of largest yield surface;

$d\alpha^{*}$ = scalar which defines the amount of translation of the yield surface, as before;

$\underline{\alpha}_n$ = vector defining the yield surface origin; and

$d\underline{\alpha}_n$ = vector defining the direction of translation.

For this case, Eqn. C3.37 becomes:

$$d\underline{\alpha}_n = \frac{(\underline{S}_n - \underline{\alpha}_n)\,\underline{\phi},_s^T \cdot d\underline{S}_n}{\underline{\phi},_s^T(\underline{S}_n - \underline{\alpha}_n)} \qquad \text{(C3.39)}$$

C3.5.5 Overlapping of Yield Surfaces

In the original Mroz hardening rule, it is assumed that the yield surface YS_i is geometrically similar to the yield surface YS_j. This assumption is reasonable for metal plasticity in stress space because it is reasonable to assume an isotropic material. However, for dealing with stress resultants, each action-deformation relationship depends on the cross section shape in a different way, and the behavior is not isotropic in action space. That is, the yield surfaces will, in general, not be geometrically similar. The authors have considered a number of strategies in an attempt to obtain "correct" behavior while preventing yield surface overlap. None of these strategies proved satisfactory, and it was finally concluded that overlapping should be allowed.

C3.6 PLASTIC DEFORMATION

The flexibility relationship of the element can be written as:

$$d\underline{v} = \underline{f}_t\, d\underline{S} = \underline{f}_e\, d\underline{S} + d\underline{v}_p \tag{C3.40}$$

in which

$\underline{f}_e$ = the element elastic flexibility matrix; and

$d\underline{v}_p = \sum_i d\underline{v}_{pi}$ is the plastic deformation increment summed over all active subhinges.

Premultiply Eqn. C3.40 by $\underline{f}_p \cdot \underline{K}_e$ to get:

$$\underline{f}_p \cdot \underline{K}_e \cdot d\underline{v} = \underline{f}_p \cdot d\underline{S} + \underline{f}_p \cdot \underline{K}_e \cdot d\underline{v}_p \tag{C3.41}$$

in which

$\underline{K}_e$ = the element elastic stiffness matrix; and

$\underline{f}_p = \sum_i f_{pi}$ is the total plastic flexibility (the total of all the current active yield surfaces at both ends of the element), so that:

$$\underline{f}_p \cdot d\underline{S} = d\underline{v}_p \tag{C3.42}$$

Substitute Eqn. C3.42 into Eqn. C3.41 to get:

$$(I + \underline{f}_p \underline{K}_e)\, d\underline{v}_p = \underline{f}_p \cdot \underline{K}_e \cdot d\underline{v} \tag{C3.43}$$

Hence,

$$d\underline{v}_p = (I + \underline{f}_p \cdot \underline{K}_e)^{-1}\, \underline{f}_p \cdot \underline{K}_e \cdot d\underline{v} \tag{C3.44}$$

Equation C3.44 gives the plastic deformation increments of the complete element in terms of the total deformation increments.

C3.7 LOADING/UNLOADING CRITERION

The loading/unloading criterion enables continuous plastic flow at a subhinge to be distinguished from elastic unloading for any current plastic state and any specified deformation increment. Two procedures are of general applicability, as follows.

(1) Postulate that all subhinges have unloaded an infinitesimal amount, so that the current state lies just within the yield surface, and the element is elastic. Calculate the elastic action increments, $d\underline{S}_e$, corresponding to the specified deformation increments. If the state for any subhinge moves outside the yield surface, the assumed unloaded state is incorrect, indicating continuing plastic flow. If the state moves within the yield surface, the assumption is correct, indicating unloading.

(2) For the specified deformation increment, calculate the magnitude parameter for the plastic deformation increment of the subhinge. A positive magnitude indicates continuing plastic flow, and a negative magnitude indicates unloading.

By the first of these two procedures, continued loading of subhinge i is indicated if $d\underline{S}_e$ has a positive component along the outward normal, $\underline{n}_i$, of the yield surface. That is, continued loading occurs if

$$\underline{n}_i^T \cdot d\underline{S}_e \geqslant 0 \tag{C3.45}$$

To consider the second procedure, first assume that the current plastic flow directions of all active subhinges are the same (that is, $\underline{n}_i = \underline{n}$ for all i). Hence, the plastic deformation increment for a complete hinge is given by:

$$d\underline{v}_p = \underline{n} \cdot dv_p^* \tag{C3.46}$$

Premultiply Eqn. C3.40 by $\underline{n}^T \cdot \underline{f}_p \cdot \underline{K}_e$ to get:

$$dv_p^* = \frac{\underline{n}^T \underline{f}_p \cdot \underline{K}_e \, d\underline{v}}{1 + \underline{n}^T \cdot \underline{f}_p \cdot \underline{K}_e \cdot \underline{n}} \tag{C3.47}$$

Substitute Eqn. C3.19 into Eqn. C3.47 to get:

$$dv_p^* = \frac{r_2 \underline{n}^T d\underline{S}_e}{1 + r_1} \tag{C3.48}$$

in which r_1 and r_2 are scalars defined as follows:

$$r_1 = \sum_i \frac{\underline{n}^T \cdot \underline{K}_e \cdot \underline{n}}{\underline{n}^T \cdot \underline{K}_{spi} \cdot \underline{n}} \tag{C3.49}$$

$$r_2 = \sum_i \frac{1}{\underline{n}^T \cdot \underline{K}_{spi} \cdot \underline{n}} \tag{C3.50}$$

Because the matrices $\underline{K}_{spi}$ and $\underline{K}_e$ are always positive definite, the scalars r_1 and r_2 always exceed zero. Hence, the sign of dv_p^* is the same as the sign of $\underline{n}^T \cdot d\underline{S}_e$. This is the same criterion as Eqn. C3.45.

In general, the plastic flow directions for the active subhinges are not the same. Hence, it is possible for $\underline{n}_i^T \cdot d\underline{S}_e$ to be greater than zero for some subhinges and less than zero for others (i.e. continued loading on some, but unloading on others). This possibility is illustrated in Fig. C3.4. For computation, it is assumed that unloading is governed by the *highest active subhinge.* If unloading occurs on this subhinge, unloading is assumed to occur on all active subhinges. If the situation happens to be as shown in Case A of Fig. C3.4 (which is unlikely), reloading will immediately occur on one or more of the lower subhinges, and the analysis will continue.

Figure C3.4, Case B, illustrates another possible consequence of yield surface overlap. In this case, unloading occurs from both surfaces, but on reloading the higher yield surface is reached first. The solution algorithm recognizes this, so that yield occurs at point P, on the higher yield surface. The lower yield surface is then translated to pass through point P, and the analysis continues.

C3.8 END ECCENTRICITY

Plastic hinges in frames and coupled frame-shear wall structures will form near the faces of the joints rather than at the theoretical joint centerlines. This effect can be approximated by postulating rigid, infinitely strong connecting links between the nodes and the element ends, as shown in Fig. C3.5. The displacement transformation relating the increments of node displacements, $d\underline{r}_n$, to increments of displacement at the element ends is easily established, and can be written as:

$$d\underline{r} = \underline{a}_e \, d\underline{r}_n \tag{C3.51}$$

This transformation is used to modify the stiffness and state determination calculations to allow for end eccentricity effects.

C3.9 RIGID FLOOR DIAPHRAGMS

A frequently made assumption in the analysis of tall buildings is that each floor diaphragm is rigid in its own plane. To introduce this assumption, a "master" node at the center of mass of each floor may be specified, as shown in Fig. C3.6. Each master node has only three degrees of freedom, as shown, which are the displacements of the diaphragm horizontally as a rigid body. If any beam-column member is connected to these "master" displacements, its behavior depends partly on these displacements and partly on the displacements which are not affected by the rigid diaphragm assumption.

The displacement transformation relating the master (diaphragm) displacements, $d\underline{r}_d$, to the displacements at a "slaved" node is as follows.

$$\begin{Bmatrix} dr_{n1} \\ dr_{n3} \\ dr_{n5} \end{Bmatrix} = \begin{bmatrix} 1 & 0 & dz \\ 0 & 1 & -dx \\ 0 & 0 & 1 \end{bmatrix} \begin{Bmatrix} dr_x \\ dr_y \\ dr_\theta \end{Bmatrix} \tag{C3.52a}$$

or

$$d\underline{r}_{ns} = \underline{a}_d \, d\underline{r}_d \tag{C3.52b}$$

The "slaved" displacements at element ends i and j can thus be expressed in terms of the displacements at the master node (or nodes). The corresponding coefficients of the element stiffness matrix are transformed to account for the slaving. The resulting element stiffness matrix is assembled in terms of the three master degrees of freedom plus the three local degrees of freedom dr_{n2}, dr_{n4}, and dr_{n6} at each node, which are not affected by slaving.

C3.10 TOLERANCE FOR STIFFNESS REFORMULATION

Each time a new hinge yields or an existing hinge unloads, the element stiffness changes. Moreover, because the direction of plastic flow may change, the stiffness of a yielding element will generally change continuously. The change in stiffness results from differences in the directions of the normal to the yield surface as the actions at the hinge change. If the angle change is small, the change in stiffness will be small and can be neglected, to avoid recalculating the stiffness. In the computer program, an option is provided for the user to set a tolerance for the angle. If a nonzero tolerance is specified, the element stiffness is reformed only when the change in state is such that the angle between the current yield surface normal and that when the stiffness was last reformed exceeds the tolerance. A tolerance of about 0.1 radians is recommended.

C4. COMPUTER LOGIC

C4.1 STATE DETERMINATION

The state determination calculation for an inelastic element requires evaluation of the equation:

$$\Delta \underline{S} = \int_0^{\Delta v} \underline{K}_t \, d\underline{v} \qquad \text{(C4.1)}$$

in which

$\Delta \underline{S}$ = finite action increment for the element corresponding to the finite deformation increment $\Delta \underline{v}$; and

$\underline{K}_t$ = element tangent stiffness, which, in general, varies during the increment.

The computational procedure for state determination of the element is as follows.

(1) From the given nodal displacement increment, calculate the element deformation increment from:

$$\Delta \underline{v} = \underline{a} \cdot \Delta \underline{r} \qquad \text{(C4.2)}$$

in which

$\Delta \underline{r}$ = vector of nodal displacement increments;

$\Delta \underline{v}$ = vector of element deformation increments; and

$\underline{a}$ = displacement transformation matrix.

(2) Calculate linear action increments for the element from:

$$\Delta \underline{S} = \underline{K}_t \Delta \underline{v} \qquad \text{(C4.3)}$$

and hence determine hinge action increments as:

$$\Delta \underline{S}_h = \underline{b} \, \Delta \underline{S} \qquad \text{(C4.4)}$$

in which

Preceding page blank

$\Delta \underline{S}$ = linear action increment for element corresponding to the finite deformation increment $\Delta \underline{v}$;

$\underline{K}_t$ = element tangent stiffness matrix;

$\Delta \underline{S}_h$ = linear action increments for hinges; and

$\underline{b}$ = transformation matrix from $\Delta \underline{S}$ to $\Delta \underline{S}_h$, which is easily formed.

(3) Check for a nonlinear "event" in the current increment, and calculate the corresponding event factor for each complete hinge. The possible events are as follows:

(a) If the current state is elastic, calculate the proportion of the deformation increment required to reach the next yield surface. If this proportion is greater than 1.0, the state continues to be elastic and the event factor is 1.0. Otherwise, an event occurs and the event factor is set equal to the calculated proportion.

(b) If the current state is plastic, calculate $\underline{n}_i^T d\underline{S}_e$. If the value exceeds zero, continued loading is indicated. The event factor is then calculated for the next yield surface, allowing a tolerance as described in Section C4.2. Otherwise, unloading occurs. In this case the stiffness matrix is reformed as the elastic stiffness, and the calculation proceeds from Step 2.

(4) Calculate the element plastic deformation, $\Delta \underline{v}_p$, using Eqn. C3.44.

(5) Select the smallest event factor, FACM, from the event factors for the two complete hinges at the element ends.

(6) Use the event factor, FACM, to compute new hinge forces, new total plastic deformations, and new origins of all subhinges, as

$$\underline{S}_h = \underline{S}_h + FACM^* \Delta \underline{S}_h \qquad \text{(C4.5)}$$

$$\underline{\alpha}_i = \underline{\alpha}_i + FACM^* \Delta \underline{\alpha}_i \qquad \text{(C4.6)}$$

$$\underline{v}_p = \underline{v}_p + FACM^* \Delta \underline{v}_p \qquad \text{(C4.7)}$$

The new action point, $\underline{S}_h$, must lie on the yield surface if the subhinge is yielded. If the action point is not on the yield surface, scale the actions radially back to the yield surface.

(7) Calculate the complement of the event factor as:

$$SS = 1. - FACM \tag{C4.8}$$

(8) Reform the tangent stiffness matrix for the element if any event has occurred.

(9) If all of the displacement increment for the element has been used up, go to Step 11. Otherwise, continue to the next step.

(10) Calculate the remaining element displacement increment for the next cycle from:

$$\Delta \underline{v} = SS \cdot \Delta \underline{v} \tag{C4.9}$$

Then go to Step 2.

(11) Obtain the element actions, $\underline{S}$, using:

$$\underline{S} = \underline{b}^T \underline{S}_h \tag{C4.10}$$

(12) Calculate the internal resisting force for the element, $\underline{R}$, using:

$$\underline{R} = \underline{a}^T \cdot \underline{S} \tag{C4.11}$$

C4.2 YIELD SURFACE TOLERANCE

It is possible for the new action point, calculated assuming constant $\underline{K}_t$, to lie significantly outside the current yield surface. This will occur particularly when $\Delta\underline{S}$ and $\Delta\underline{\alpha}$ are distinctly nonparallel (Fig. C4.1). In this case, the calculation is assumed to be sufficiently accurate, provided the new action point lies within a tolerance zone (typically 2%-5% of the yield surface size). If not, $\Delta\underline{v}$ is scaled, $\underline{K}_t$ is reformed, and the calculation is repeated for the balance of $\Delta\underline{v}$.

The scale factor is conveniently determined by the procedure illustrated for M-F space in Fig. C4.1. In this figure, the current action point is P, and the new action point, obtained by applying Eqn. C4.3, is at Q. Hardening is affected only by the component of $\Delta\underline{S}$ parallel to the yield surface normal. Hence, the yield surface translates as shown. Point Q lies outside the new yield surface, the amount being defined by e_r, which is the length of the "radial" error vector, $\underline{e}_r$. This error must not exceed the allowable tolerance.

Computationally, it is convenient to consider the "tangential" error, $\underline{e}_t$, which is the length of vector P'Q. If the yield surface is assumed to be locally quadratic, then

$$e_r \doteq 0.5e_t^2 \tag{C4.12}$$

The value of e_r is calculated from this equation. If e_r is within the allowable tolerance, point Q is scaled to the new yield surface and the computation continues (this scaling introduces an error which is assumed to be acceptable). If e_r exceeds the allowable tolerance, it is assumed that e_t varies linearly with element deformation. A scale factor to set e_r equal to the tolerance is then calculated using Eqn. C4.12, the $\Delta\underline{S}$ and $\Delta\underline{\alpha}$ increments are scaled by this factor, and the new action point is scaled to the yield surface. The element stiffness is then reformed, and the process is repeated for the remainder of the deformation increment. If $\Delta\underline{S}$ is parallel to $\underline{S}-\underline{\alpha}$, no scaling will be required. If $\Delta\underline{S}$ makes a large angle with $\underline{S}-\underline{\alpha}$, the deformation increment may be subdivided into several subincrements, depending on the magnitude of $\Delta\underline{v}$ and the value specified for the error tolerance.

The deformation increment is also subdivided if a new yield surface is reached. In this case, the new action point is permitted to go beyond the yield surface by an amount equal to the allowable radial error. The proportion of the deformation increment required to reach this state is calculated; the new action point is scaled to the yield surface; the stiffness is reformed; and the calculation proceeds for the remainder of the deformation increment.

C5. ANSR USER GUIDE

3D STEEL BEAM COLUMN ELEMENT (TYPE 5)

C5.1 CONTROL INFORMATION - Two Cards

C5.1.1 First Card

Columns	Note	Name	Data
5(I)		NGR	Element group indicator (=5).
6-10(I)		NELS	Number of elements in group.
11-15(I)		MFST	Element number of first element in group. Default = 1.
16-25(F)		DKO	Initial stiffness damping factor, β_o.
26-35(F)		DKT	Tangent stiffness damping factor, β_T.
41-80(A)		GRHED	Optional group heading.

C5.1.2 Second Cards

Columns	Note	Name	Data
1-5(I)		NMBT	Number of different strength types (max. 20). Default = 1.
6-10(I)		NECC	Number of different end eccentricity types (max. 15). Default = zero.
11-15(I)		NPAT	Number of different initial force patterns (max. 30). Default = zero.

C5.2 STRENGTH TYPES

NMBT sets of cards.

C5.2.1 Strength Option

Columns	Note	Name	Data
1-5(I)			Strength type number, in sequence beginning with 1.

10(I)		INPT	Input options for element flexural stiffnesses, as follows. See Section C2.3.5. (a) INPT=1: Procedure assuming essentially uniform bending moment over element length. Leave rest of this card blank. (b) INPT=2: Procedure assuming double-cantilever behavior. Leave rest of this card blank. (c) INPT=3: General option. Complete rest of this card.
11-20(F)			Coefficient K_{ii} for bending about local y-axis. Default = 4.
21-30(F)			Coefficient K_{ij} for bending about local y-axis. Default = 2.
31-40(F)			Coefficient K_{jj} for bending about local y-axis. Default = 4.
41-50(F)			Coefficient K_{ii} for bending about local z-axis. Default = 4.
51-60(F)			Coefficient K_{ij} for bending about local z-axis. Default = 2.
61-70(F)			Coefficient K_{jj} for bending about local z-axis. Default = 4.

C5.2.2 Bending Properties About Local y-axis

(a) OPTN=1: Specify beam moment-rotation relationship. See Fig. C2.8. One card.

Columns	Note	Name	Data
1-10(F)			Stiffness K_{M1}.
11-20(F)			Stiffness K_{M2}.
21-30(F)			Stiffness K_{M3}.
31-40(F)			Stiffness K_{M4}.
41-50(F)			Yield moment M_{y1}.
51-60(F)			Yield moment M_{y2}.
61-70(F)			Yield moment M_{y3}.

(b) OPTN=2: Specify cantilever P-δ relationship. See Fig. C2.9. One card.

Columns	Note	Name	Data
1-10(F)			Stiffness K_1.
11-20(F)			Stiffness K_2.
21-30(F)			Stiffness K_3.
31-40(F)			Stiffness K_4.
41-50(F)			Yield force P_{y1}.
51-60(F)			Yield force P_{y2}.
61-70(F)			Yield force P_{y3}.

(c) OPTN=3: Specify beam elastic stiffness and hinge moment-rotation relationships. Two cards.

Columns	Note	Name	Data
Card 1			
1-10(F)			Elastic flexural stiffness, EI/L.
11-20(F)			Elastic shear rigidity, GA_z, along z-axis (i.e. shear associated with y-axis bending). If zero, shear deformation is neglected.
21-30(F)			Plastic stiffness K_{p1} of left-end hinge.
31-40(F)			Plastic stiffness K_{p2} of left-end hinge.
41-50(F)			Plastic stiffness K_{p3} of left-end hinge.
51-60(F)			Yield moment M_{y1} of left-end hinge.
61-70(F)			Yield moment M_{y2} of left-end hinge.
71-80(F)			Yield moment M_{y3} of left-end hinge.
Card 2			
1-10(F)			Plastic stiffness K_{p1} of right-end hinge.
11-20(F)			Plastic stiffness K_{p2} of right-end hinge.
21-30(F)			Plastic stiffness K_{p3} of right-end hinge.
31-40(F)			Yield moment M_{y1} of right-end hinge.
41-50(F)			Yield moment M_{y2} of right-end hinge.

51-60(F)			Yield moment M_{y3} of right-end hinge.

C5.2.3 Bending Properties About Local z-axis

As for Section C5.2.2, but specify z-axis properties.

C5.2.4 Torsional Properties

Columns	Note	Name	Data
1-10(F)			Torsional stiffness K_{T1}.
11-20(F)			Torsional stiffness K_{T2}.
21-30(F)			Torsional stiffness K_{T3}.
31-40(F)			Torsional stiffness K_{T4}.
41-50(F)			Torsional strength T_{y1}.
51-60(F)			Torsional strength T_{y2}.
61-70(F)			Torsional strength T_{y3}.

C5.2.5 Axial Properties

Columns	Note	Name	Data
1-10(F)			Axial stiffness K_{F1}.
11-20(F)			Axial stiffness K_{F2}.
21-30(F)			Axial stiffness K_{F3}.
31-40(F)			Axial stiffness K_{F4}.
41-50(F)			Axial strength F_{y1}.
51-60(F)			Axial strength F_{y2}.
61-70(F)			Axial strength F_{y3}.
71-80(F)	(1)		Axial strength F_{y4}. Input as a positive value. Default = F_{y1}.

C5.3 END ECCENTRICITY TYPES

NECC Cards. See Fig. C3.5

Columns	Note	Name	Data
1-5(I)	(2)		End eccentricity type number, in sequence beginning with 1.
11-20(F)			X_i = X eccentricity at end i.

21-30(F)			X_j = X eccentricity at end j.
31-40(F)			Y_i = Y eccentricity at end i.
41-50(F)			Y_j = Y eccentricity at end j.
51-60(F)			Z_i = Z eccentricity at end i.
61-70(F)			Z_j = Z eccentricity at end j.

C5.4 INITIAL ELEMENT FORCE PATTERNS

NPAT Cards.

Columns	Note	Name	Data
1-5(I)	(3)		Pattern number, in sequence beginning with 1.
11-20(F)			Initial moment M_{yy} at end i.
21-30(F)			Initial moment M_{zz} at end i.
31-40(F)			Initial moment M_{yy} at end j.
41-50(F)			Initial moment M_{zz} at end j.
51-60(F)			Initial axial force.
61-70(F)			Initial torque.

C5.5 ELEMENT DATA GENERATION

As many pairs of cards as needed to generate all elements in group.

Columns	Note	Name	Data
1-5(I)	(4)		Element number, or number of first element in a sequentially numbered series of elements to be generated by this card.
6-10(I)		NODI	Node Number I.
11-15(I)		NODJ	Node Number J.
16-20(I)		INC	Node number increment for element generation. Default = 1.
21-25(I)		NODK	Number of a third node, K, lying in the xy plane, for definition of the local y axis. Default = automatic orientation of y-axis.
26-30(I)		NSI	Number of node (diaphragm node) to which end I is slaved. If not slaved, leave blank.

31-35(I)		NSJ	Number of node to which end J is slaved. For a description of the slaving procedure, see Section C3.9.
36-40(I)		NSTR	Strength type number.
41-45(I)		IECC	End eccentricity type number. Default = no end eccentricity.
46-50(I)		NIT	Initial force pattern number. Default = no initial force.
51-55(I)		KTYP	Interaction surface type: (a) 1 = yield surface type 1 (b) 2 = yield surface type 2 (c) 3 = yield surface type 3 (d) 4 = yield surface type 4 (e) 5 = yield surface type 5
56-60(I)		KGEOM	Large displacement code: (a) 0 = small displacements (b) 1 = P-δ effect only (c) 2 = true large displacements
61-65(I)		KSD	Large displacement procedure code: (a) 0 = Euler procedure (b) 1 = Midpoint procedure The Euler procedure is recommended.
66-70(I)		KOUT	Time history output code: (a) 1 = output time history results (b) 0 = no output
71-80(F)	(5)		Stiffness reformulation angle tolerance (radians).

CARD 2

1-10(F)			Parameter, a_1, in interaction surface equation.

11-20(F)	Parameter, a_2, in interaction surface equation.
21-30(F)	Parameter, a_3, in interaction surface equation.
31-40(F)	Parameter, a_4, in interaction surface equation.

C5.6 NOTES

(1) The value of F_{y4}, as shown in Fig. C2.2, allows the origin of the yield surfaces to be shifted along the F-axis. The strengths in tension and compression are then different.

(2) All eccentricities are measured *from* the node *to* the element end (Fig. C3.5), positive in the positive coordinate directions.

(3) See Fig. C2.10 for the positive directions of initial element actions. Refer to Section C2.6 for a description of the effects of initial element actions.

(4) Cards must be input in order of increasing element number. Cards for the first and the last elements must be included (that is, data for these two elements cannot be generated). Cards may be provided for all elements, in which case each card specifies the data for one element, and the generation is not used. Alternatively, cards for a series of elements may be omitted, in which case data for the missing elements is generated as follows:

(a) All missing elements are assigned the same node "K" (NODK), slave nodes (NSI and NSJ), strength types, end eccentricity type, initial force pattern type, interaction surface type, codes for large displacements and response output, and stiffness reformulation angle tolerance, as those for the element preceding the missing series of elements.

(b) The node numbers I and J for each missing element are obtained by adding the increment (INC) to the node numbers of the preceding element. That is,

$$\text{NODI(N)} = \text{NODI(N-1)} + \text{INC}$$

$$\text{NODJ(N)} = \text{NODJ(N-1)} + \text{INC}$$

The node increment, INC, is the value specified with the element *preceding* the missing series of elements.

(5) Refer to Section C3.10 for a description of the stiffness reformulation tolerance.

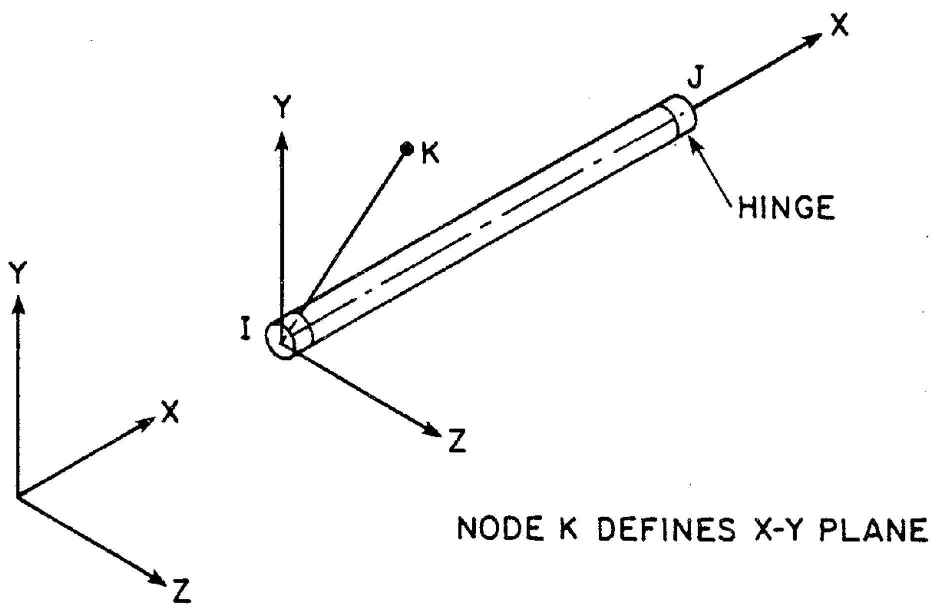

(a) ELEMENT AXES

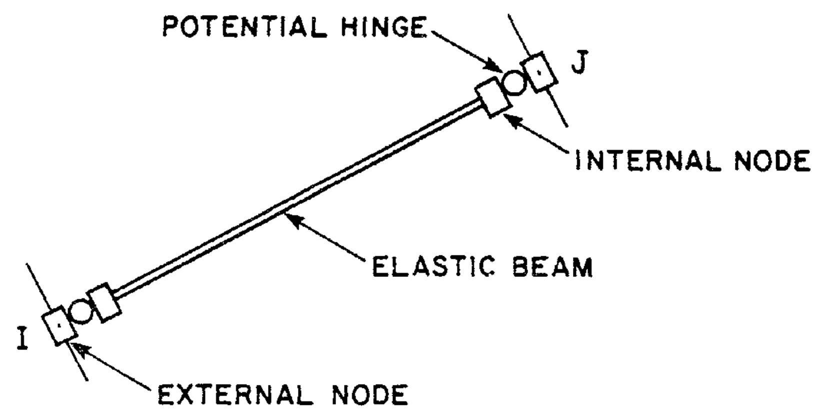

(b) ELEMENT IDEALIZATION

FIG. C2.1 ELEMENT AXES AND IDEALIZATION

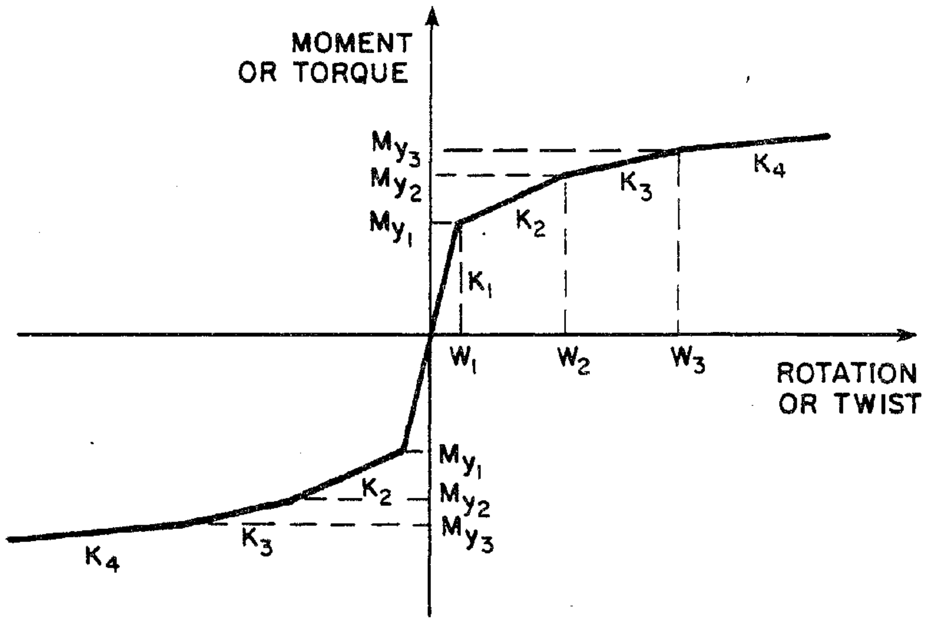

$W_1 : W_2 : W_3$ MUST BE SAME FOR ALL RELATIONSHIPS

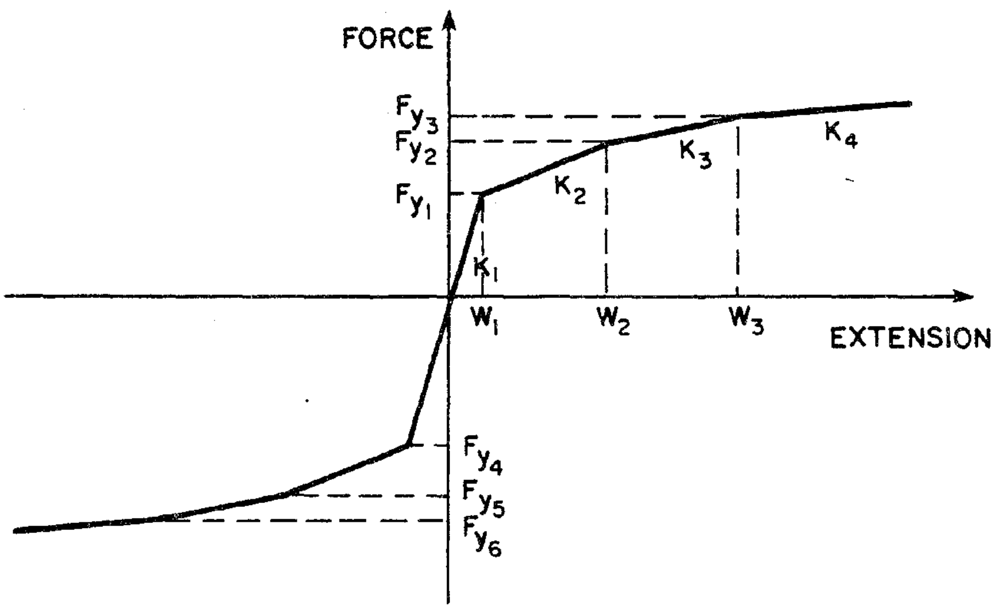

FIG. C2.2 ACTION VS. DEFORMATION FOR ELEMENT

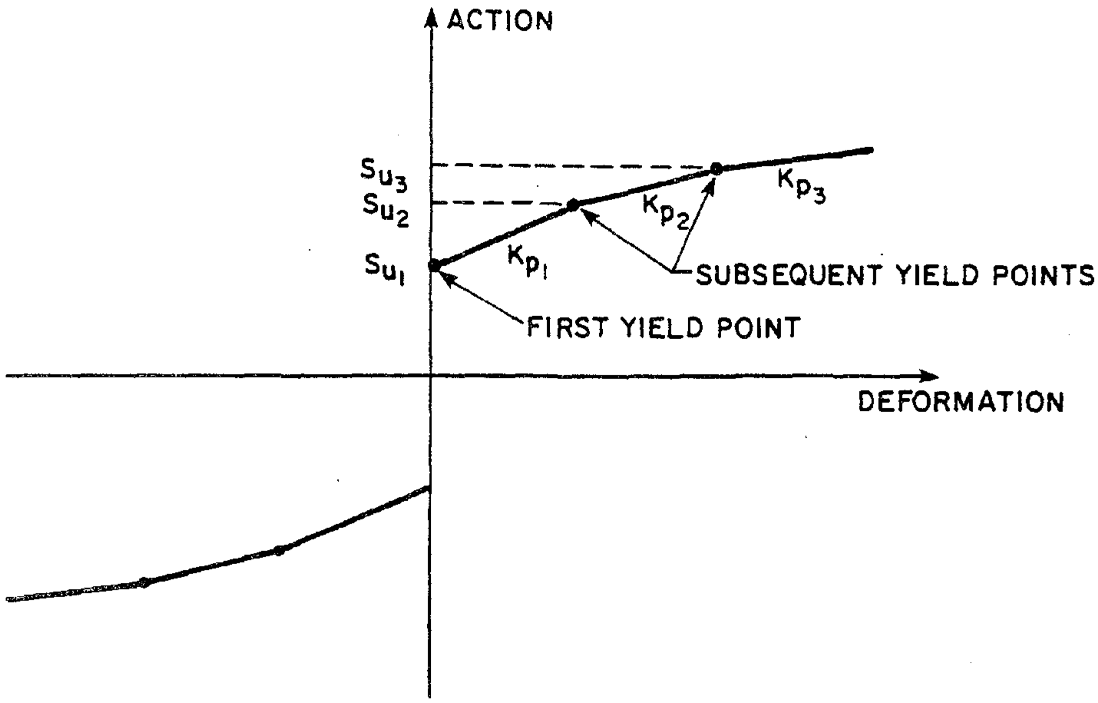

(a) ACTION VS. DEFORMATION RELATIONSHIP

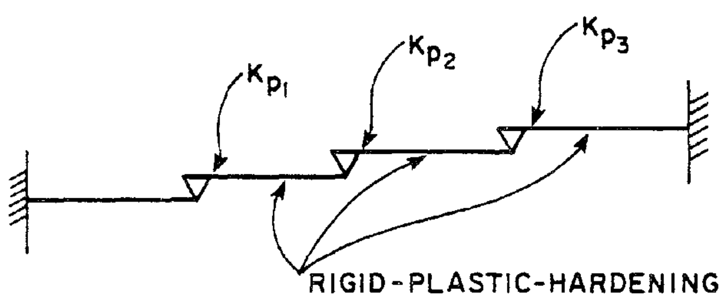

(b) 1-D MODEL

FIG. C2.3 1-D MODEL FOR A HINGE

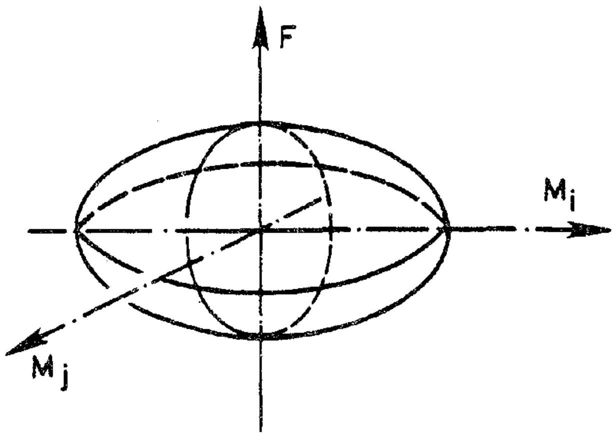

$$\phi = \left(\frac{M_y}{M_{yu}}\right)^2 + \left(\frac{M_z}{M_{zu}}\right)^2 + \left(\frac{M_x}{M_{xu}}\right)^2 + \left(\frac{F}{F_u}\right)^2 = 1$$

(A) SURFACE TYPE 1

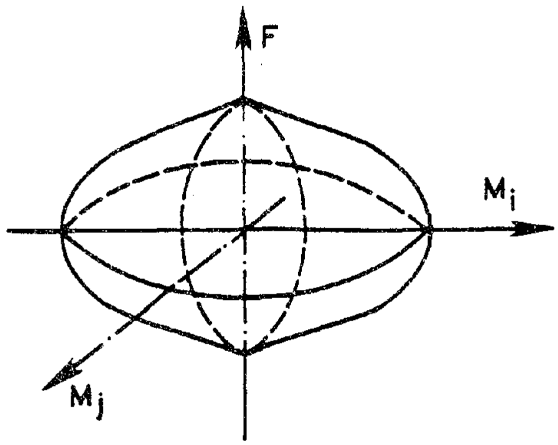

$$\phi = \left[\left(\frac{M_y}{M_{yu}}\right)^2 + \left(\frac{M_z}{M_{zu}}\right)^2 + \left(\frac{M_x}{M_{xu}}\right)^2\right]^{1/2} + \left(\frac{F}{F_u}\right)^2 = 1$$

(B) SURFACE TYPE 2

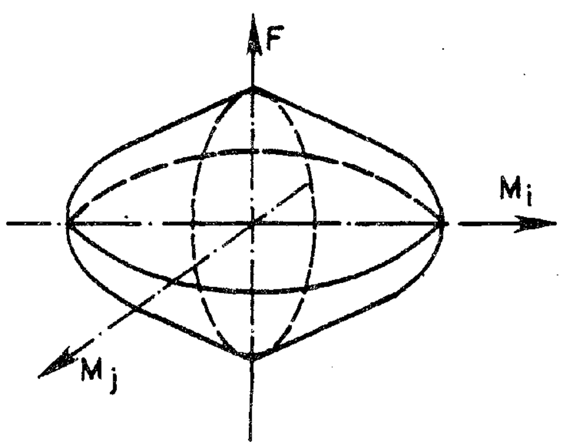

$$\phi = \left[\left(\frac{M_y}{M_{yu}}\right)^2 + \left(\frac{M_z}{M_{zu}}\right)^2 + \left(\frac{M_x}{M_{xu}}\right)^2\right]^{1/2} + \left(\frac{F}{F_u}\right)^{a_1} = 1$$

(C) SURFACE TYPE 3

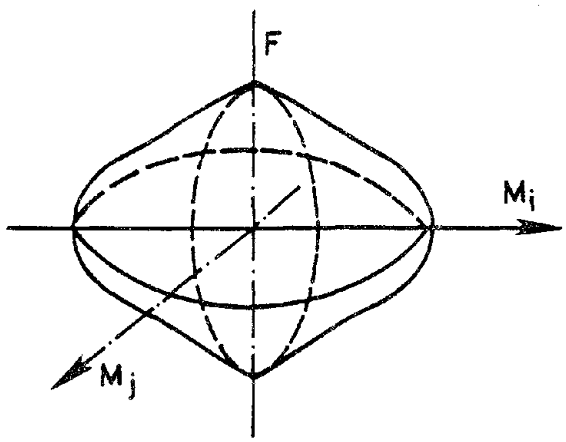

$$\phi = \left[\left(\frac{M_y}{M_{yu}}\right)^2 + \left(\frac{M_z}{M_{zu}}\right)^2 + \left(\frac{M_x}{M_{xu}}\right)^2\right]^{a_1} + \left(\frac{F}{F_u}\right)^{a_2} = 1$$

(D) SURFACE TYPE 4

FIG. C2.4 INTERACTION SURFACES

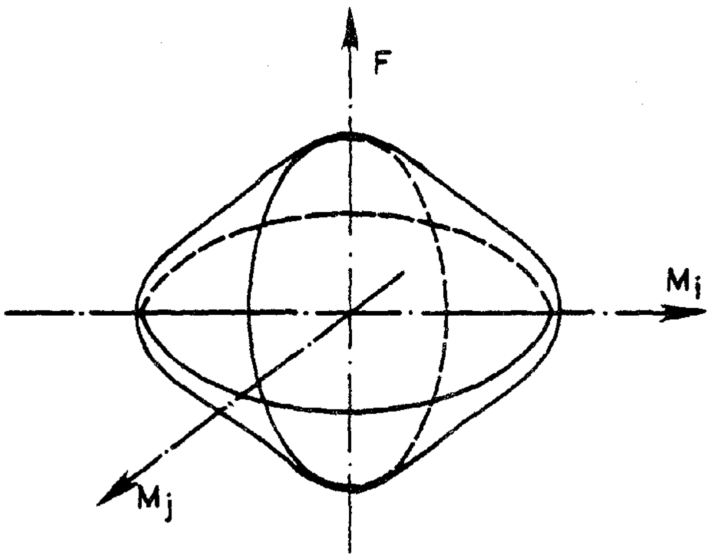

$$\phi = \left(\frac{M_y}{M_{yu}}\right)^{a_1} + \left(\frac{M_z}{M_{zu}}\right)^{a_2} + \left(\frac{T}{T_u}\right)^{a_3} + \left(\frac{F}{F_u}\right)^{a_4} = 1$$

(E) SURFACE TYPE 5

FIG. C2.4 INTERACTION SURFACES (CONT'D)

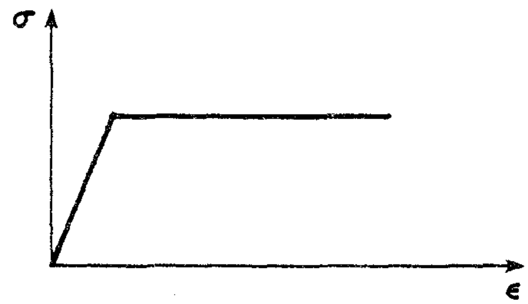

(a) ELASTIC-PLASTIC STRESS-STRAIN RELATIONSHIP

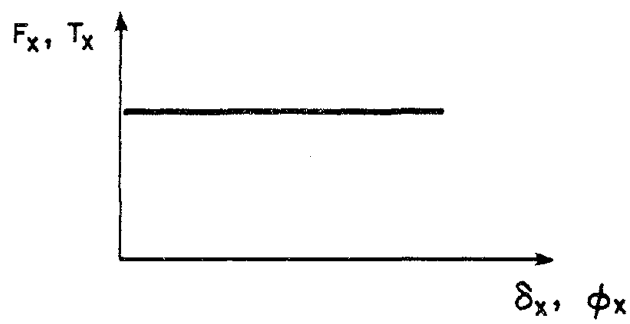

(b) FORCE-EXTENSION AND TORQUE-TWIST

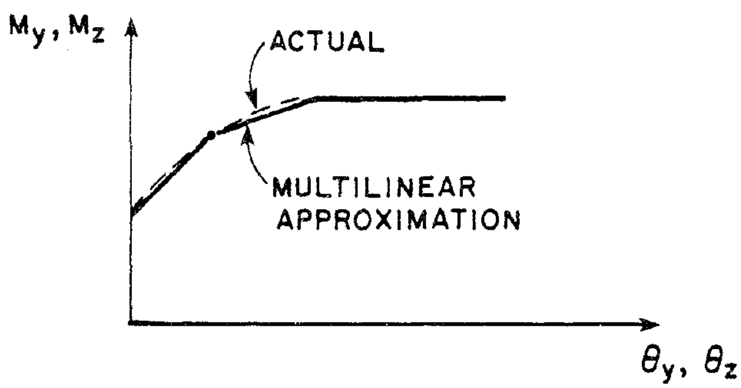

(c) MOMENT-CURVATURE

FIG. C2.5 DIFFERENCES IN SHAPES OF RELATIONSHIPS

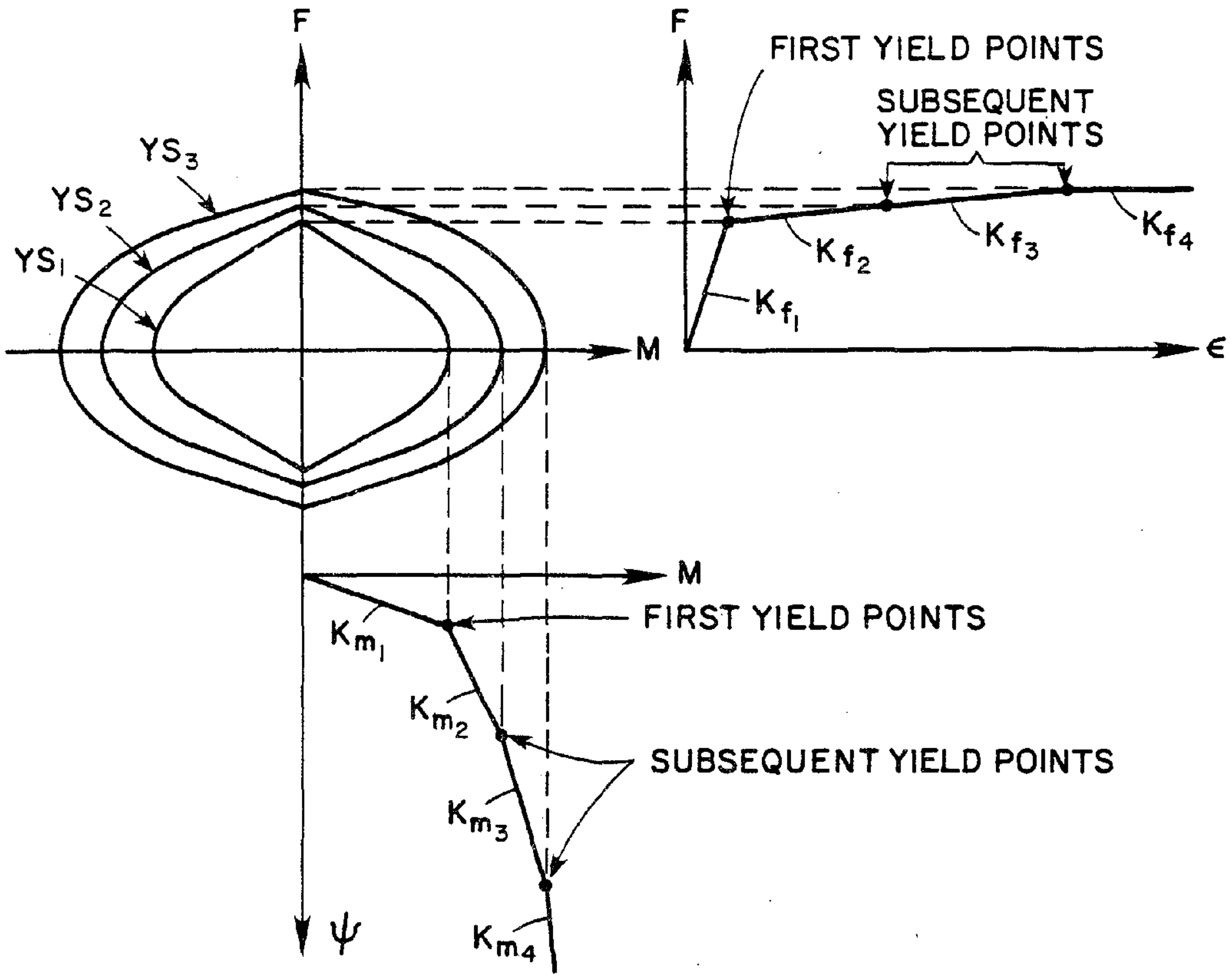

(a) INITIAL LOCATIONS OF SURFACES

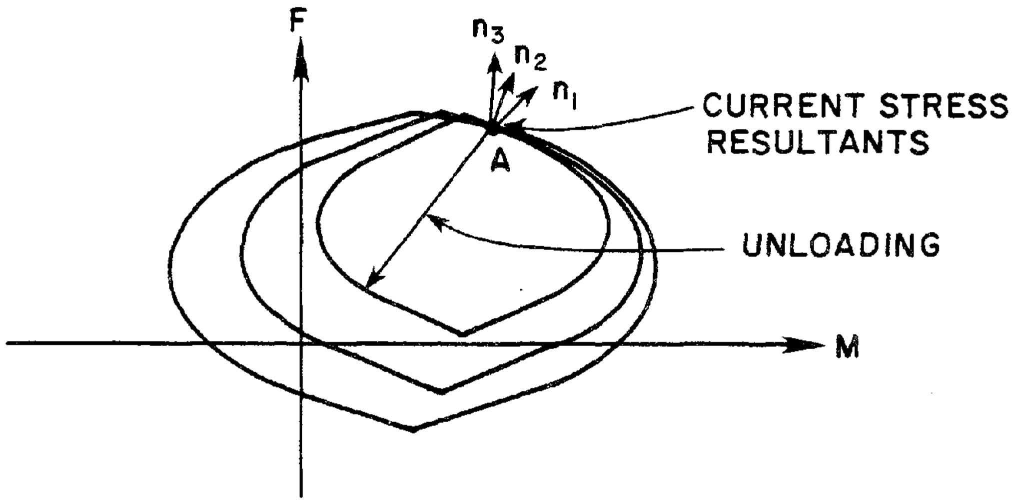

(b) DISPLACED SURFACES AFTER HARDENING

FIG. C2.6 STRAIN HARDENING BEHAVIOR

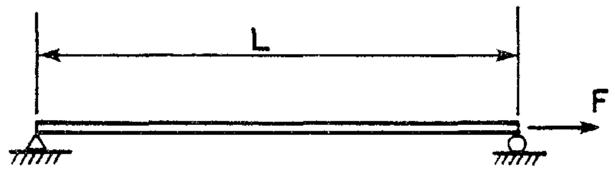

(a) BEAM UNDER AXIAL FORCE

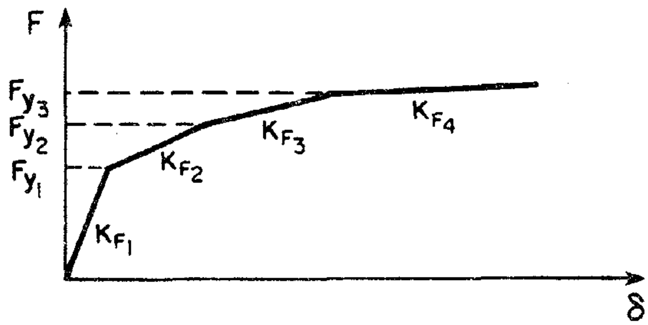

(b) F-δ RELATIONSHIP

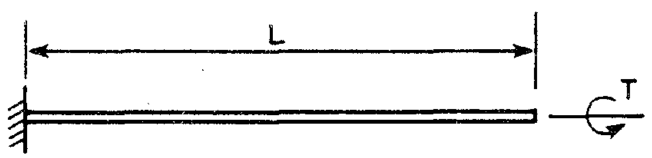

(c) BEAM UNDER TORQUE

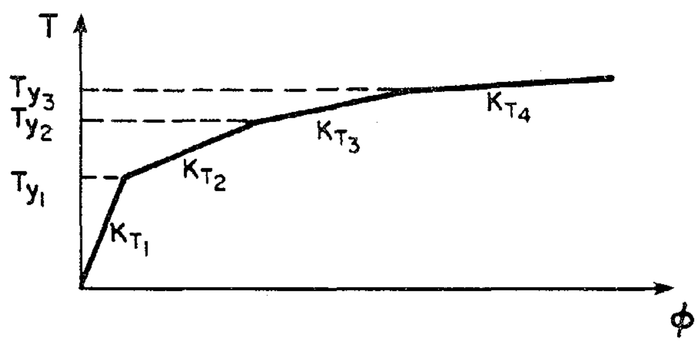

(d) T-ϕ RELATIONSHIP

FIG. C2.7 FORCE-EXTENSION AND TORQUE-TWIST RELATIONSHIPS

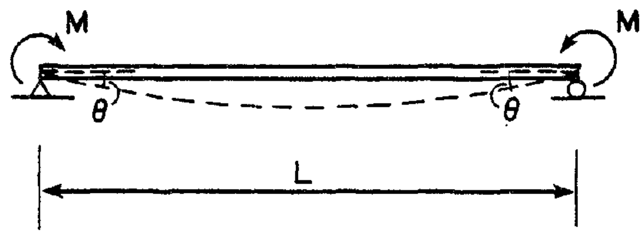

(a) BEAM WITH CONSTANT MOMENT

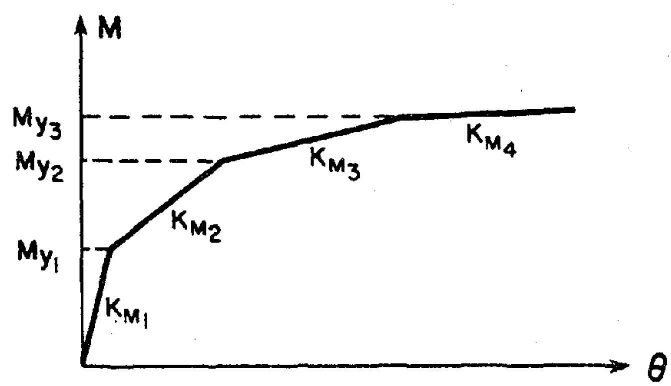

(b) MOMENT-ROTATION RELATIONSHIP

FIG. C2.8 MOMENT-ROTATION RELATIONSHIP

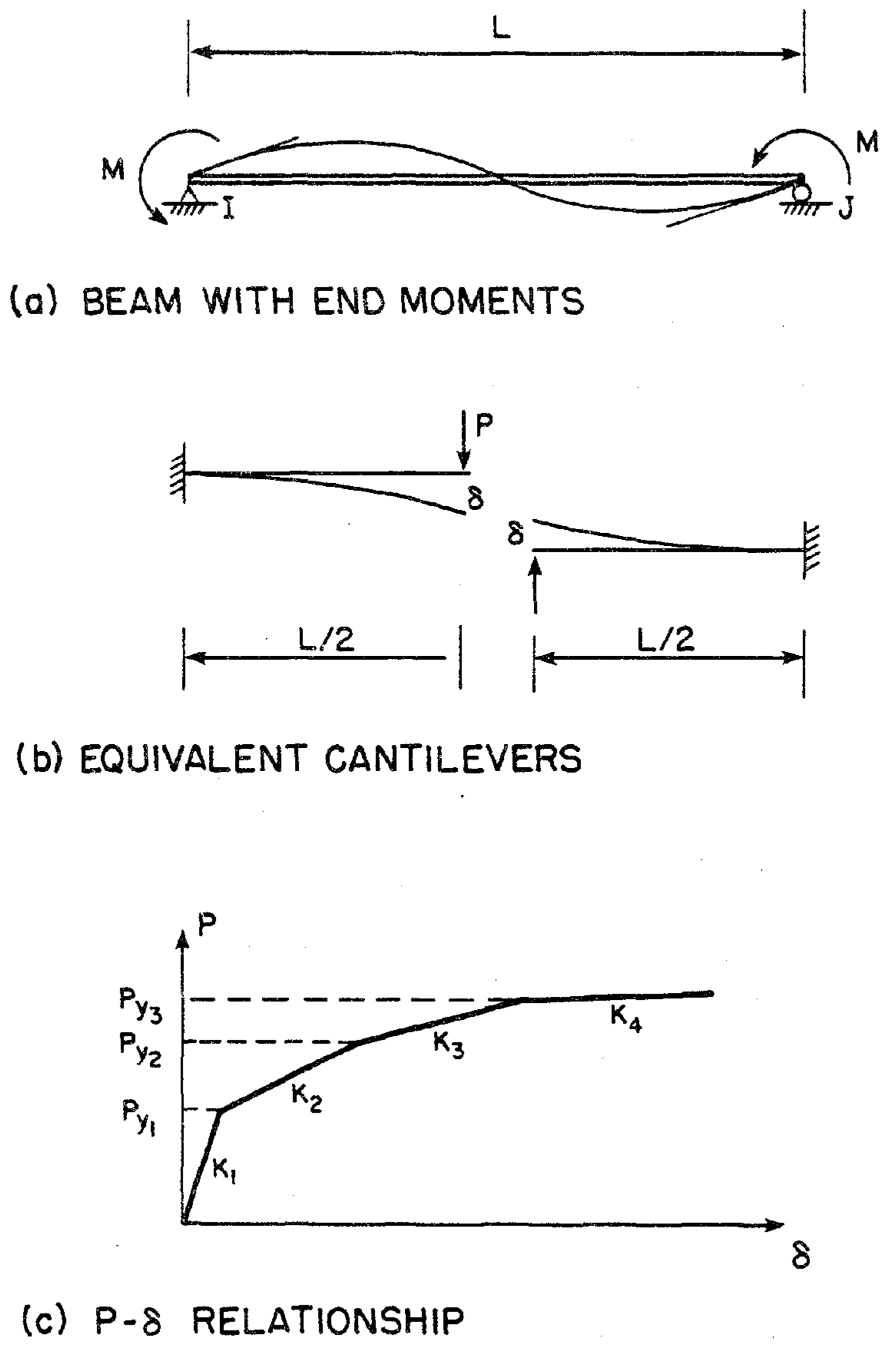

FIG. C2.9 REPRESENTATION OF CANTILEVER BEHAVIOR

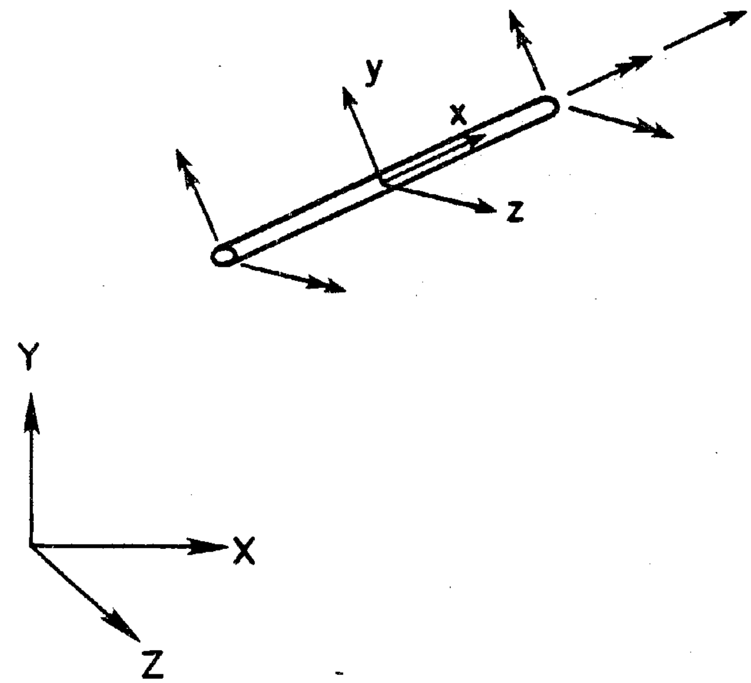

FIG. C2.10 POSITIVE DIRECTION OF INITIAL
ELEMENT ACTIONS

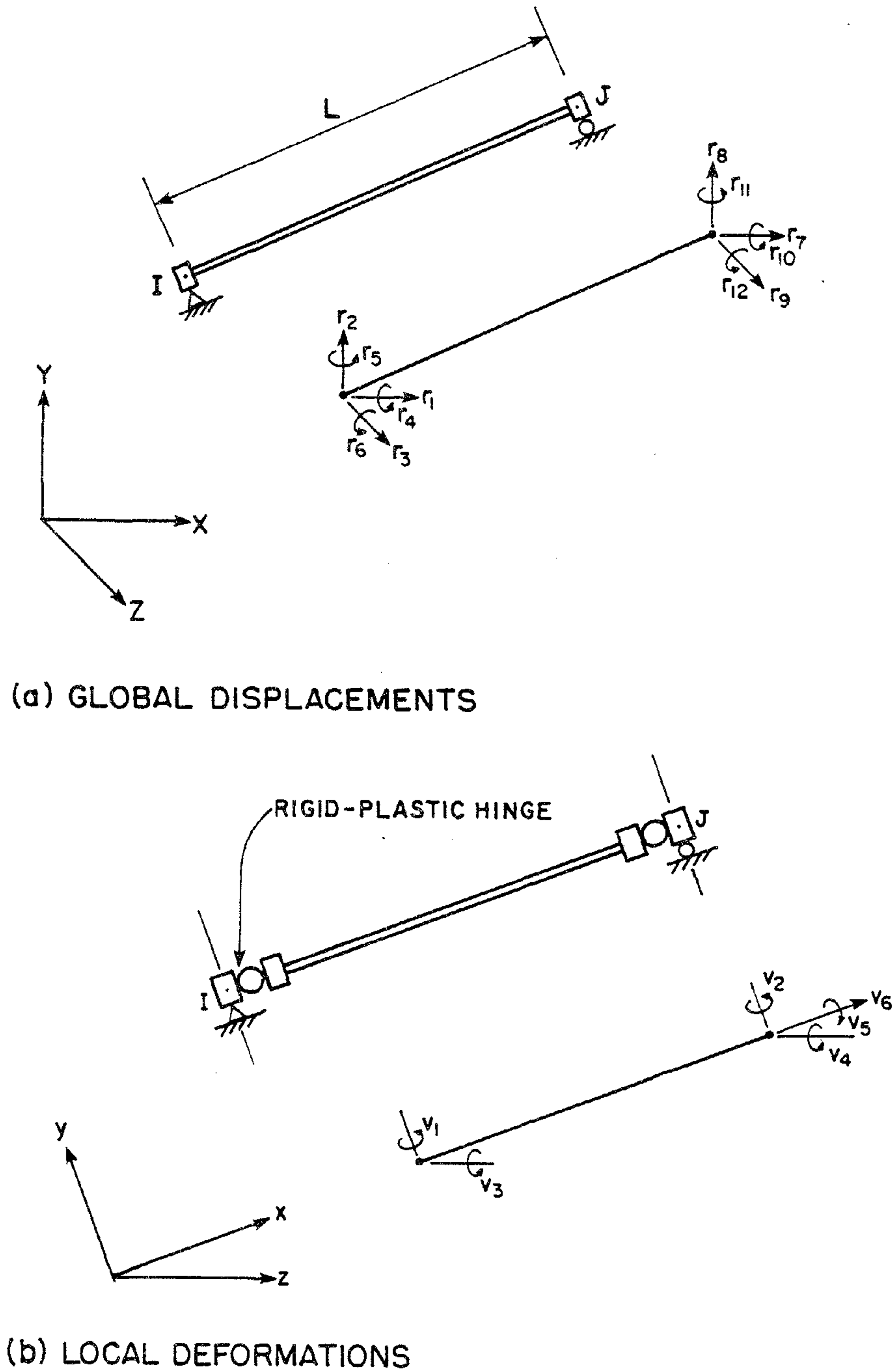

FIG. C3.1 ELEMENT DEGREES OF FREEDOM

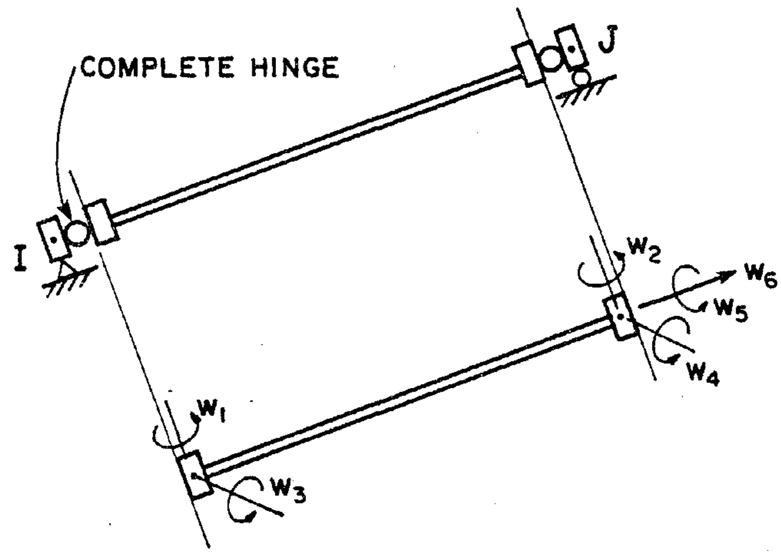

(a) INTERNAL DEGREES OF FREEDOM

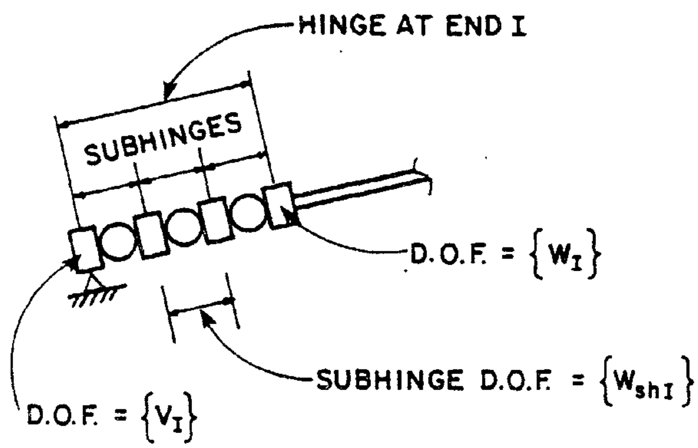

(b) HINGE AND SUBHINGES AT END I

FIG. C3.2 INTERNAL DEGREES OF FREEDOM

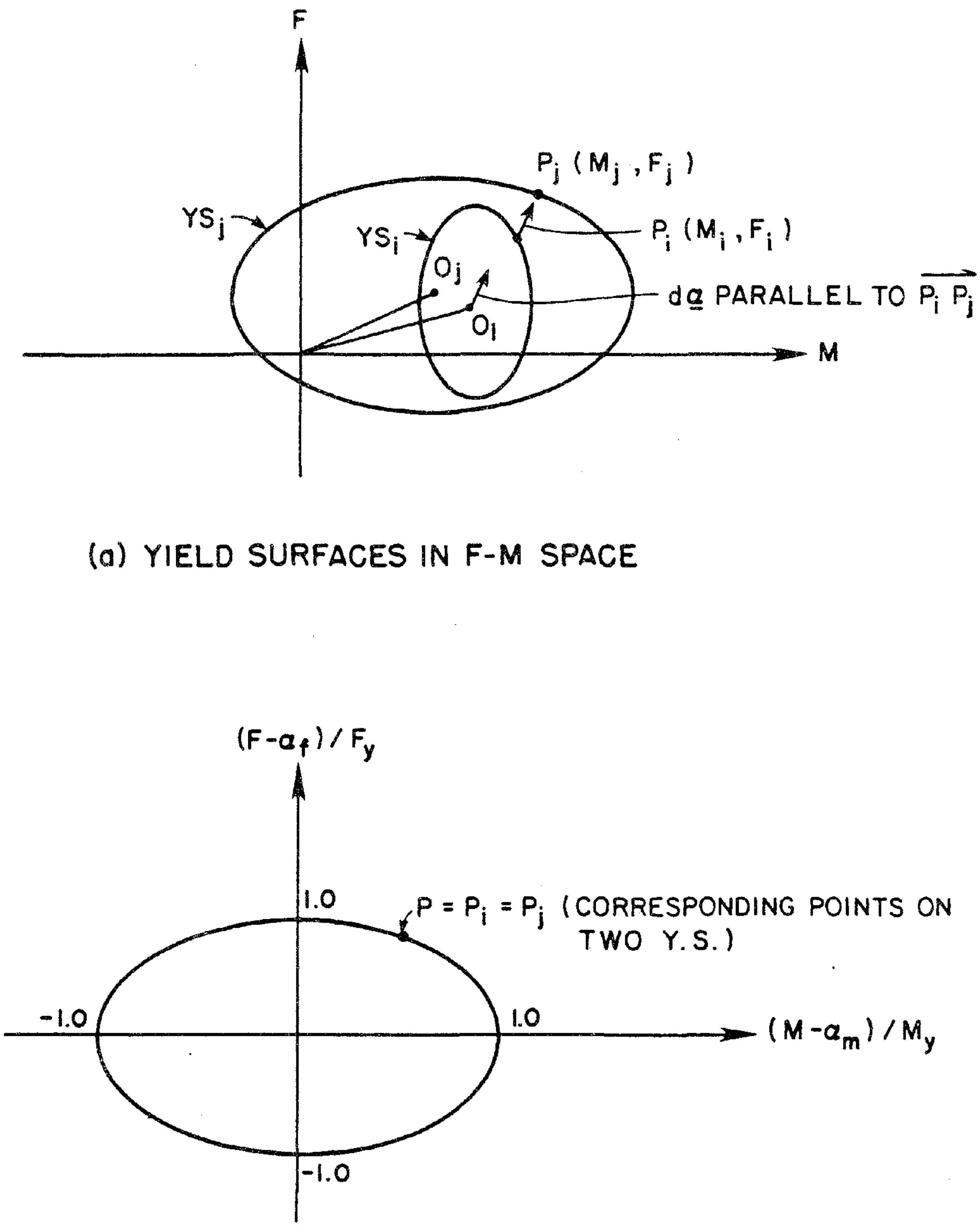

(a) YIELD SURFACES IN F-M SPACE

(b) YIELD SURFACES IN NORMALIZED SPACE

FIG. C3.3 MODIFIED MROZ HARDENING RULE

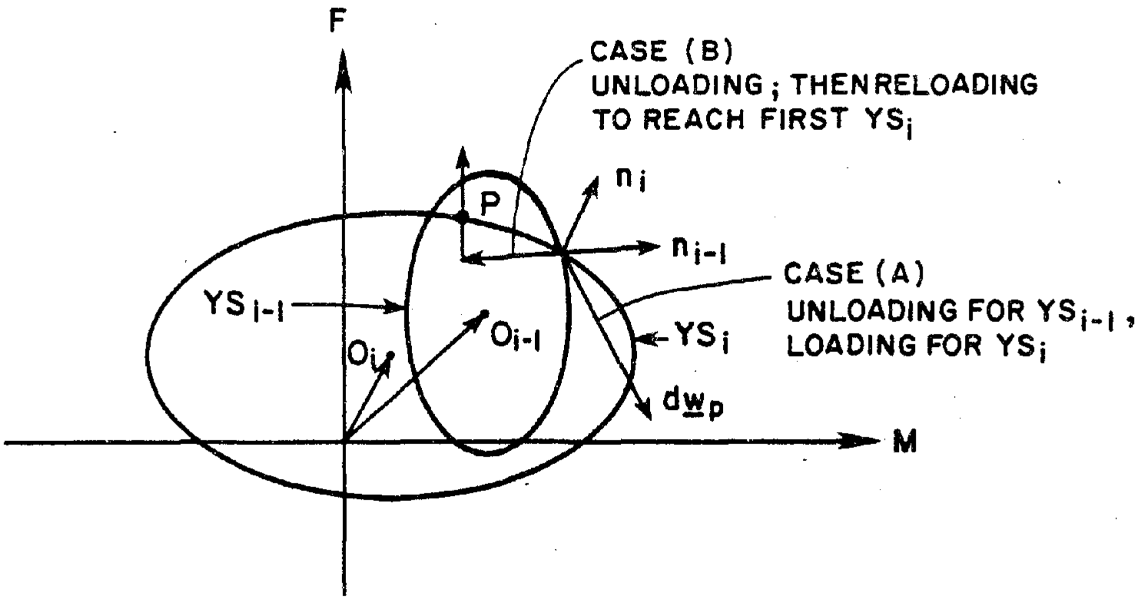

FIG. C3.4 LOADING/UNLOADING CRITERION

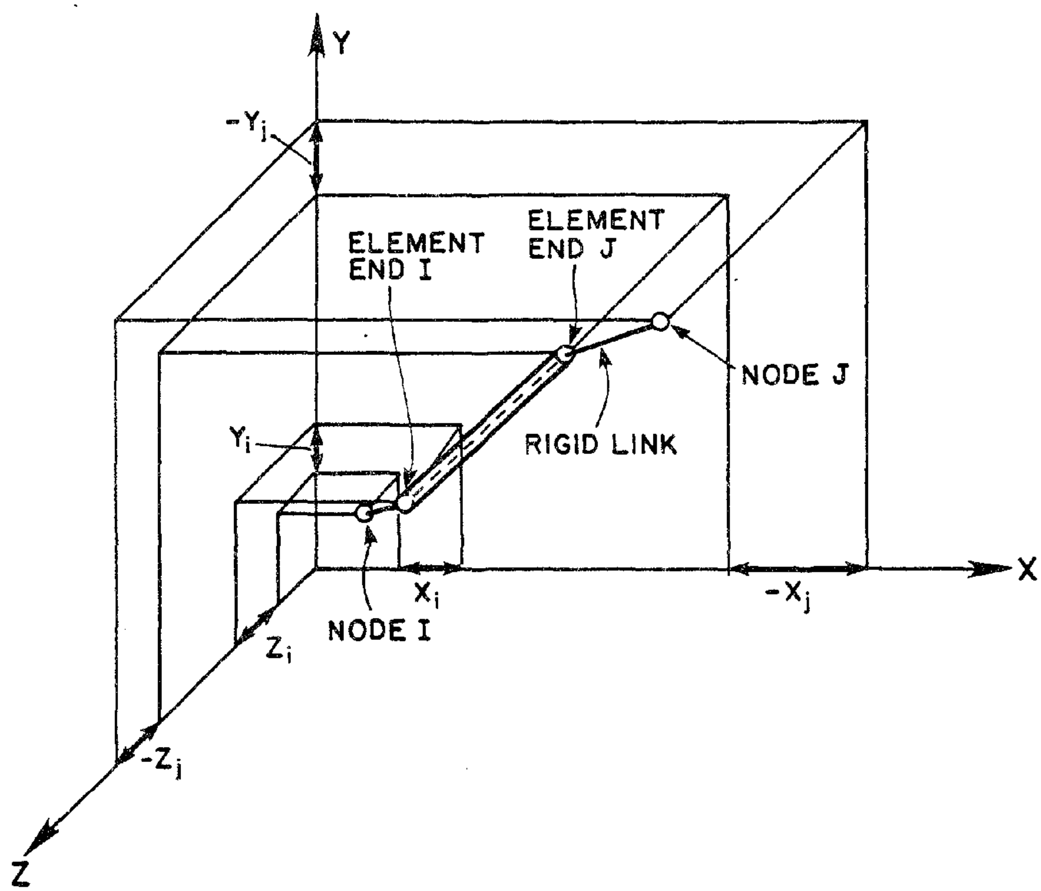

FIG. C3.5 END ECCENTRICITIES

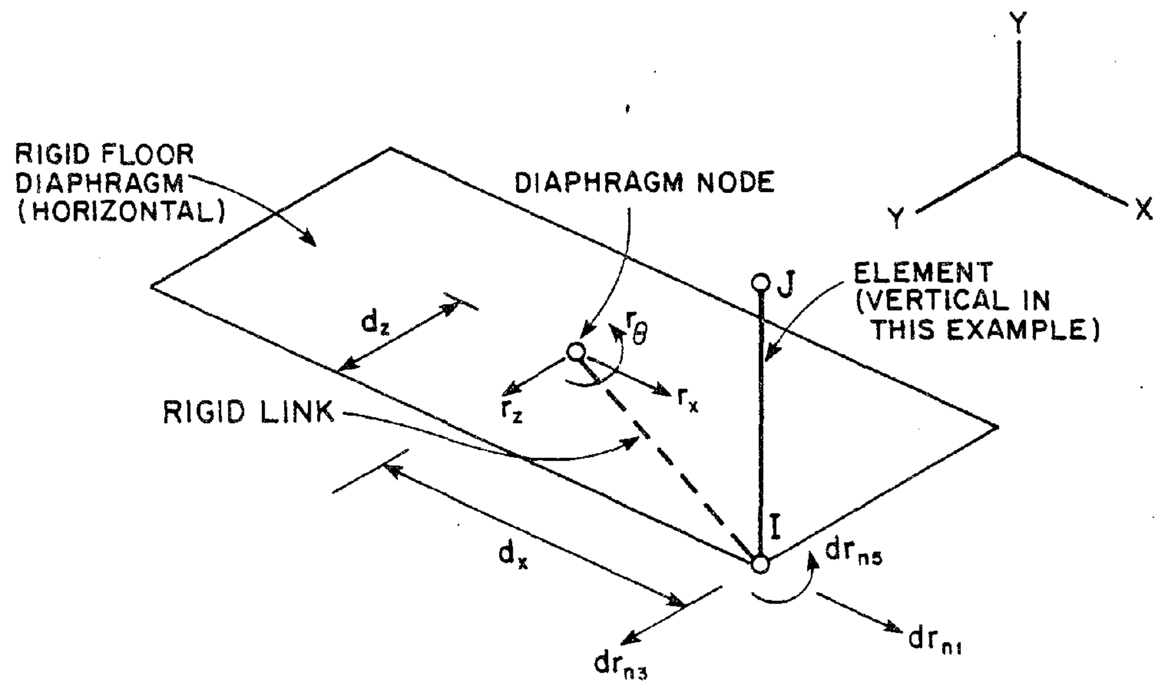

FIG. C3.6 RIGID FLOOR DIAPHRAGM

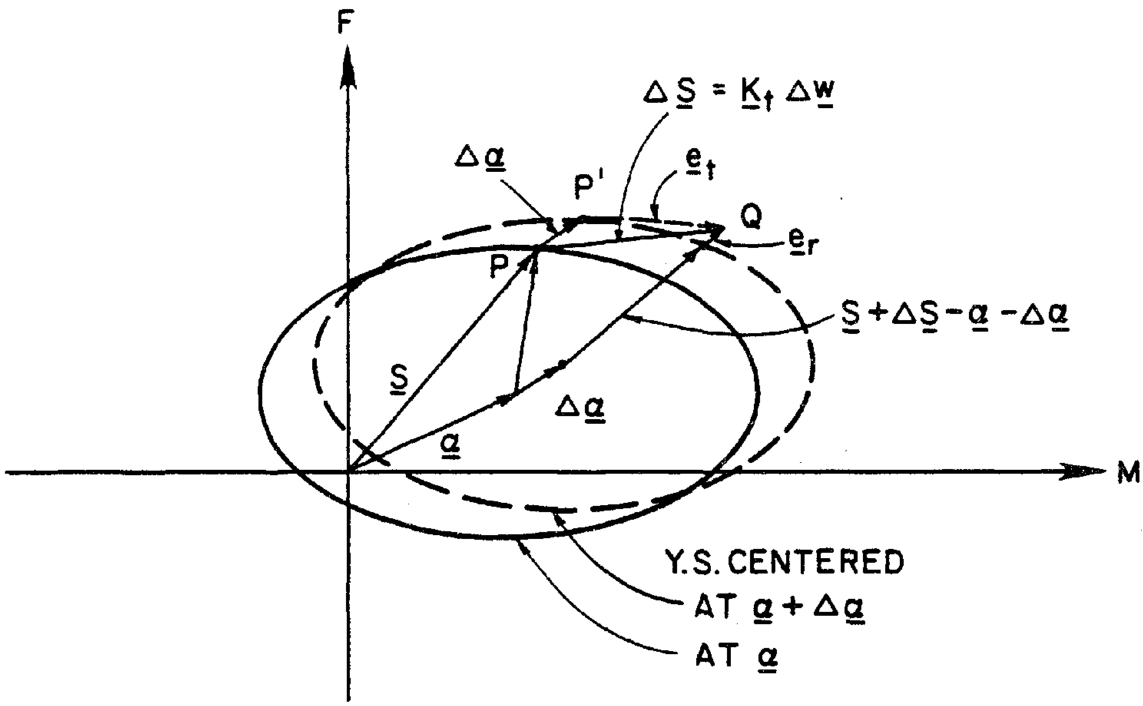

FIG. C4.1 ERROR CONTROL FOR STATE DETERMINATION

D. LUMPED PLASTICITY ELEMENT WITH STIFFNESS DEGRADATION

Preceding page blank

D1. INTRODUCTION

The element described in this report is intended for modeling inelastic effects in reinforced concrete beams and columns for buildings, with particular emphasis on three-dimensional behavior. The theory takes account of moment-force interaction, bending moment interaction for biaxial bending, and stiffness degradation under cyclic loading. Yielding is assumed to take place only in concentrated (i.e. zero length) plastic hinges located at the element ends. The part of the element between the hinges is assumed to remain linearly elastic.

Initial elastic stiffnesses must be specified for axial extension, torsional twist, and bending about two axes. Flexural shear deformations and the effects of eccentric end connections can be considered, if desired. The element strengths may be different at the two ends, and the elastic stiffnesses can include the effect of varying cross section along the element length.

The essential features of the element are as follows:

(1) The element may be arbitrarily oriented in space but must be straight.

(2) Inelastic behavior is confined to zero-length plastic hinges at the element ends.

(3) The hinges are assumed to have elastic-plastic-strain-hardening behavior. Strain hardening stiffnesses must be specified by moment-rotation and force-extension relationships for the hinges. Trilinear relationships are assumed.

(4) The stiffnesses of hinges may degrade when reversed loading is applied. The degradation is controlled by user specified coefficients.

(5) Interaction between bending moments, torque, and axial force is considered by means of four-dimensional yield surfaces. A kinematic hardening rule (extended Mroz theory) is assumed for post-yield behavior (translation of yield surface without change of size or shape).

(6) Options are available for small displacements and second order (P- Δ) theory.

(7) Eccentric end connections may be specified to model rigid joint regions, and rigid diaphragm slaving may be specified to model floor slabs.

A general description of the element characteristics and properties is presented in Section D2. Theoretical details are presented in Section D3. Details of the computer logic are described in Section D4. An element user's guide for the ANSR program is presented in Section D5.

D2. ELEMENT CHARACTERISTICS AND PROPERTIES

D2.1 GENERAL CHARACTERISTICS

The three-dimensional beam-column element with degrading stiffness is formulated to model reinforced concrete beams and columns, which characteristically exhibit degrading stiffness properties when subjected to cyclic loads. Elements may be arbitrarily oriented in the global XYZ coordinate system. The element properties are specified in a local x,y,z coordinate system. The orientations of the local axes are defined as shown in Fig. D2.1a. Node K, together with nodes I and J, defines the plane containing the local y axis.

Inelastic behavior of the element is governed by axial force, two flexural moments, and the torsional moment. Yielding may take place only in concentrated plastic hinges at the element ends. Strain hardening and stiffness degradation are approximated by assuming that the element consists of a linear elastic beam element with a nonlinear hinge at each end, as shown in Fig. D2.1b. All plastic deformation effects, including the effects of degrading stiffness, are introduced by means of the moment-rotation, torque-torsional twist, and force-axial extension relationships for the hinges.

For analysis, each hinge is subdivided into two subhinges which can be identified as "cracking" and "yielding" subhinges. The action-deformation relationships for each subhinge are represented by bilinear functions. The bilinear action-deformation relationships for the two subhinges combine to produce a trilinear function for each complete hinge, and hence, also trilinear relationships for the complete element.

The elastic beam is defined by an axial stiffness, two flexural stiffnesses, a torsional stiffness and an effective shear rigidity (if shear deformation is to be taken into account). Elements of variable cross section can be considered by specifying appropriate flexural stiffness coefficients, and by using average cross section properties for the axial and torsional stiffnesses.

For each subhinge, bilinear relationships can be specified separately for moment-rotation about the element y and z axes, torque-twist, and force-axial extension. Different yield strengths can be specified at the hinges at each end, if desired. Different strengths can also be specified for axial tension and axial compression.

Interaction among the two bending moments, torsional moment, and axial force at a hinge are taken into account for determining both initial yield and subsequent plastic flow. The force-deformation and interaction relationships will typically be based on observations of the behavior of reinforced concrete columns, considering loading by both single actions and by multiple actions in combination.

Element deformations are assumed to be small. A true large displacements option is not available, but P-Δ effects can be considered, if desired. Eccentric end connections and rigid diaphragm slaving may be specified. Initial element forces may be specified. These initial forces affect element yield but do not contribute to the nodal loads.

D2.2 AXES

Element properties and results are specified in the local coordinate system x,y,z, defined as shown in Fig. D2.1a. If node K is not specified, its location is assumed as follows.

(a) If IJ is not vertical, node K is at $Y = +\infty$. The xy plane is then the vertical plane containing the element.

(b) If IJ is vertical, node K is at $X = +\infty$. The xy plane is then parallel to the XY plane.

D2.3 MODELING OF INELASTIC BEHAVIOR

D2.3.1 General

Yield is monitored at the potential hinges at the element ends. Each hinge is initially rigid, so that the initial stiffness of the complete element is the stiffness of the elastic beam. As the moments and forces at the element ends (the hinge actions) increase, the hinges can yield, causing a stiffness reduction in the element. The overall element behavior is illustrated in Fig. D2.2. Under increasing deformation, the hinges strain harden, following trilinear action-deformation relationships. Tangent stiffness relationships between the actions and deformations at a yielding hinge are established using a plasticity theory which is an extension of the Mroz theory for yield of metals. If the actions at a hinge decrease, the hinge unloads, but does not become rigid again. Instead, an unloading hinge is assigned a finite stiffness based on the amount of plastic deformation in the hinge. Hence, under cyclic loading the stiffness of the element degrades. Details of the degrading procedure are described later.

D2.3.2 Hinge Properties

Rigid-plastic-strain-hardening relationships between hinge actions and deformations must be defined for initial loading of the hinges. The relationships at the two hinges in any element may be different, if desired.

Relationships as shown in Fig. D2.3 must be defined for each of four action-deformation pairs, namely (1) bending moment, M_y, and corresponding rotation, θ_y; (2) bending moment, M_z, and corresponding rotation, θ_z; (3) torque, M_x, and corresponding twist, ϕ_x; and (4) axial force, F_x, and corresponding extension, δ_x. The relationships may be of different shape for each action. For material with an elastic-perfectly-plastic stress-strain relationship, the torque-twist and force-extension relationships will be rigid-perfectly-plastic, whereas the moment-rotation relationships will usually exhibit strain hardening behavior (Fig. D2.5). It is required that the deformations at changes in stiffness have the same ratios for all relationships, as indicated in Fig. D2.2. This restriction is necessary to avoid inconsistencies in the plasticity theory.

It may be noted that the assumption of a zero-length hinge implies infinitely high strains as a hinge deforms. This is inherent in any plastic hinge type of theory.

D2.3.3 Interaction Surfaces for First Yield

The actions M_y, M_z, M_x, and F_x interact with each other to produce initial yield of the hinge. The interaction effect is determined by a yield (interaction) surface. To allow for a variety of applications, provision is made in the theory for five different yield surfaces. These surfaces are all four-dimensional (i.e., M_y, M_z, M_x, and F_x), and hence, cannot be shown easily using diagrams. The surfaces differ, however, mainly in the way in which the axial force interacts with the three moments. Hence, the differences can be illustrated using the three-dimensional diagrams in Fig. D2.4. In these figures, the M_i and M_j axes indicate any two of the moments, and the F_x axis indicates axial force. If desired, the origin of the yield surface can be shifted along the axial force axis. This permits an element to have greater compressive capacity than tension capacity, with a yield surface which approximates the F-M interaction surfaces for actual concrete columns. The equations defining the yield surfaces are shown in the figure.

Surface 1 is elliptical and is the simplest mathematically. Surfaces 2, 3, and 4 allow more realistic modeling of moment-force interaction for cases in which axial force effects are substantial. For all of these four surfaces, the interaction among M_y, M_z, and M_x is elliptical and only the force-moment interaction changes. Surface 5 is of a different form than the other four and is included for greater generality in special cases.

D2.3.4 Interaction Surfaces for Subsequent Yield

For modeling a hinge with nonlinear material properties, it is assumed that the behavior is initially rigid-plastic-strain-hardening for each action individually, as shown in Fig. D2.3a. In one dimension, the rigid-plastic-strain-hardening behavior can be modeled using two rigid-plastic "subsprings" in series, as shown in Fig. D2.3b. This model is extended to the multi-dimensional case. Each of the two subsprings becomes a "subhinge", with yield governed by a yield surface. First yield occurs at the cracking subhinge, which is governed by an initial yield surface. Second yield occurs at the yielding subhinge, which is governed by a larger yield surface. The second surface is assumed to have the same *basic* form as the surface for first yield. However, because the action-deformation relationships may be of different shape for each action, the two surfaces will not have, in general, identical actual shapes. An example in 2D action space is illustrated in Fig. D2.6.

D2.3.5 Plastic Stiffnesses: Axial Force and Torque

The yield strengths and the plastic stiffnesses of the hinge action-deformation relationships (K_{p1} and K_{p2} in Fig. D2.3) must be specified to provide appropriate post-yield stiffening of the complete element. The procedure is straight-forward for axial force and torque but more complex for bending.

Consider axial force, and let the force-extension relationship for the complete element be as shown in Fig. D2.7a. The steps are as follows.

(a) Elastic axial rigidity of beam $= EA = K_{F1} \cdot L$.

(b) Strength at first yield surface $= F_{y1}$.

(c) Plastic stiffness after first yield surface $= K_{p1} = \dfrac{K_{F1} \cdot K_{F2}}{K_{F1} - K_{F2}}$.

(d) Strength at second yield surface $= F_{y2}$.

(e) Plastic stiffness after second yield surface $= K_{p2} = \dfrac{K_{F2} \cdot K_{F3}}{K_{F2} - K_{F3}}$.

The same procedure applies for torque, as follows (Fig. D2.7c).

(a) Elastic torsional rigidity of beam $= GJ = K_{T1} \cdot L$.

(b) Strength at first yield surface $= T_{y1}$.

(c) Plastic stiffness after first yield surface $= K_{p1} = \dfrac{K_{T1} \cdot K_{T2}}{K_{T1} - K_{T2}}$.

(d) Strength at second yield surface $= T_{y2}$.

(e) Plastic stiffness after second yield surface $= K_{p2} = \dfrac{K_{T2} \cdot K_{T3}}{K_{T2} - K_{T3}}$.

D2.3.6 Plastic Stiffnesses: Bending

A complication in specifying the flexural plastic stiffnesses arises from the fact that moment-curvature nonlinearities are modeling using concentrated hinges. In an actual beam the moment typically varies along the length, and plastic deformations occur over finite regions. Consequently, the flexural stiffness depends on the moment variation along the beam. In a concentrated hinge model, it is not possible to account for all possible moment variations; and hence, assumptions must be made in specifying the hinge properties.

Three options are available in the computer program for assigning bending stiffness properties to the hinges. The first option is for a uniform beam with essentially constant moment along the element (Fig. D2.8a). This option is applicable, in general, only for a structure which is modeled using short beam-columns elements, such that the bending moment does not vary greatly over a single element. The relationship between bending moment and end rotation for the initial loading of the element is as shown in Fig. D2.8b. The steps in establishing the hinge properties are as follows:

(a) Elastic flexural rigidity of beam = EI = $K_{M1} \cdot L/2$.

(b) Shear rigidity of beam assumed to be infinite (no shear deformations).

(c) Hinge strength at first yield = M_{y1}.

(d) Plastic stiffness after first yield surface = $K_{p1} = \dfrac{K_{M1} \cdot K_{M2}}{K_{M1} - K_{M2}}$.

(e) Strength at second yield surface = M_{y2}.

(f) Plastic stiffness after second yield surface = $K_{p2} = \dfrac{K_{M2} \cdot K_{M3}}{K_{M2} - K_{M3}}$.

The second option is applicable for a uniform beam in which a linear variation of bending moment can be assumed over the element length, with equal and opposite values at the ends (Fig. D2.9a). This option will typically apply for columns in an unbraced frame building. An equivalent cantilever for each half of the element is used, as shown in Fig. D2.9b. It is required that the relationship between the tip load and tip displacement of the cantilever be known (Fig. D2.9c). This relationship can then be used to obtain hinge stiffness as follows.

(a) Elastic flexural rigidity of beam = $EI = K_1 L^3/24$.

(b) Shear rigidity of beam assumed to be infinite (no shear deformations).

(c) Hinge strength at first yield $= P_{y1} \cdot L/2$.

(d) Plastic stiffness after first yield surface $= K_{p1} = \dfrac{K_1 \cdot K_2 \cdot L}{2(K_1 - K_2)}$.

(e) Strength at second yield surface $= P_{y2} \cdot L/2$.

(f) Plastic stiffness after second yield surface $= K_{p2} = \dfrac{K_2 \cdot K_3 \cdot L}{2(K_2 - K_3)}$.

For these first two options, the computer program calculates the K_p values, given the moment-rotation relationships (for option 1) or load-deflection relationship (for option 2). The third option provides the user with more flexibility, by requiring that the EI/L and K_p values be specified directly. In addition, with this option it is not necessary for the element to be of uniform section. Flexural stiffness coefficients, K_{ii}, K_{jj}, and K_{ij}, which depend on the variation of the beam cross section, may be specified (for example, for a uniform element, $K_{ii} = K_{jj} = 4.0$ and $K_{ij} = 2.0$). Also, an effective shear stiffness (GA') can be specified.

D2.3.7 Plastic Flow

Interaction among the actions is considered as shown diagrammatically in Fig. D2.6. Yield begins when the first yield surface is reached. The surface then translates in action space, the motion being governed by the plastic flow of the cracking subhinge. Translation of the first surface continues until the second surface is reached. Both surfaces then translate together, governed by a combination of plastic flow on both the cracking and yielding subhinges. For any subhinge, plastic flow is assumed to take place normal to the yield surface of that subhinge. If both subhinges are yielded, their yield surfaces move together, and the total plastic deformation is equal to the sum of the individual plastic deformations for each subhinge, directed along the normal directions of their respective yield surfaces at the action point. After some arbitrary amount of plastic deformation, the situation might be as illustrated in Fig. D2.6b.

D2.3.8 Hardening Behavior

After first yield, the yield surfaces of any yielded subhinge is assumed to translate in action space, obeying a kinematic hardening rule (translation without change of shape or size).

An extension of the Mroz theory of material plasticity is used to define the hardening behavior. Because the yield surfaces for the two subhinges are generally not exactly similar, overlapping of the surfaces can occur and the hardening behavior is more complex than in the basic Mroz theory. For example, in Fig. D2.6b, the current action point, A, lies on yield surfaces YS_1 and YS_2. Hence, both subhinges have yielded, and the direction of plastic flow is a combination of the normal vectors $\underline{n}_1$ and $\underline{n}_2$. Details of the theory are given in Sections D3.2.5 and D3.2.6.

D2.4 STIFFNESS DEGRADATION

Stiffness degradation is introduced when reversed loading is applied. It is assumed that the stiffness degrades independently for each force component of each subhinge, in inverse proportion to the largest previous hinge deformation, as shown in Fig. D2.10. This figure also shows the reloading assumptions for both large and small cyclic deformations.

The unloading stiffnesses, K'_1 (for the cracking subhinge) and K'_2 (for the yielding subhinge), depend on the previous maximum positive and negative hinge deformations and are controlled by the input coefficients, α_1 and α_2 (for the cracking subhinge) and β_1 and β_2 (for the yielding subhinge). These coefficients control the unloading stiffnesses by locating the loading point, R^+, as shown in Fig. D2.10a. The reloading stiffnesses, K''_1 (cracking) and K''_2 (yielding), also depend on the previous maximum negative and positive hinge deformations and are governed by the same coefficients, α_i and β_i, as shown in Fig. D2.10b. The coefficients control the reloading stiffnesses by locating the point, R^-. Regardless of the values of α_i and β_i, the unloading or reloading slope is not allowed to be less than the strain hardening stiffnesses K_{p1} (cracking) or K_{p2} (yielding). That is, minimum stiffness coefficients ω_1 and ω_2 must be specified for each force component, either by the user or by default, to guarantee:

$$K_1 \leqslant \omega_1 K_{p1} \qquad \text{(D2.1a)}$$

$$K_2 \leqslant \omega_2 K_{p2} \qquad \text{(D2.1b)}$$

The behavior for small amplitude cycling, as illustrated in Fig. D2.10c, is based on the position X between R and A. The unloading or reloading stiffnesses are interpolated between K'_1 and K''_1 (for cracking subhinge) or K'_2 and K''_2 (for yielding subhinge), in the same proportion as X is positioned between R and A.

D2.5 P-DELTA EFFECT

Even for small displacements, changes in the shape of a structure can have a significant effect (the P-delta effect) on the equilibrium of the structure. This effect can be accounted for by adding a geometric stiffness to the element stiffness. The geometric stiffness assumed for the element is that for a truss bar in three dimensions, which depends on the axial force only. The geometric stiffness is changed each time the element stiffness changes, using the current axial force, but is otherwise assumed to remain constant. In addition, a modification is made to the internal resisting force for the element, to take account of the P-delta effect.

D2.6 END ECCENTRICITY

Plastic hinges in frames and coupled frame-shear wall structures will form near the faces of the joints rather than at the theoretical joint centerlines. This effect can be approximated by postulating rigid, infinitely strong connecting links between the nodes and the element ends, as shown in Fig. D3.5.

D2.7 RIGID FLOOR DIAPHRAGMS

A frequently made assumption in the analysis of tall buildings is that each floor diaphragm is rigid in its own plane. To introduce this assumption, a master node at the center of mass of each floor may be specified, as shown in Fig. D3.6. Each master node has only three degrees of freedom as shown, which are the displacements of the diaphragm horizontally as a rigid body. If any beam-column member is connected to these *master* displacements, its behavior depends partly on these displacements and partly on the displacements which are not affected by the rigid diaphragm assumption. The theory is described in Section D3.9.

D2.8 INITIAL FORCES

For structures in which static analyses are carried out separately (i.e. outside the ANSR program), initial member forces may be specified. The sign convention for these forces is as shown in Fig. D2.11. These forces are not converted to loads on the nodes of the structure but are simply used to initialize the element end actions. For this reason, initial forces need not constitute a set of actions in equilibrium. The only effects they have on the behavior of the system are (a) to influence the onset of plasticity and (b) to affect the geometric stiffnesses.

D3. THEORY

D3.1 DEGREES OF FREEDOM

The element has two external nodes and two internal nodes, as shown in Fig. D3.1a. The external nodes connect to the complete structure and have six degrees of freedom each, namely X,Y,Z global translations and X,Y,Z, global rotations. After deletion of the six rigid body modes for the complete element and transformation to local element coordinates, the six deformation degrees of freedom shown in Fig. D3.1b remain. Each hinge has four deformations, namely an axial deformation plus rotations about each of the local x,y,z axes (i.e., shear deformations in the hinges are zero).

The transformation from global displacements to element deformations is:

$$\underline{v} = \underline{a}\,\underline{r} \qquad \text{(D3.1)}$$

in which

$$\underline{v}^T = [v_1, v_2, ..., v_6] = \text{element deformations (Fig. D3.1b);}$$
$$\underline{r}^T = [r_1, r_2, ..., r_{12}] = \text{global displacements (Fig. D3.1a);}$$

and the transformation matrix $\underline{a}$ is well known.

The vector of degrees of freedom, $\underline{w}$, for the elastic element (Fig. D3.2a) is defined as:

$$\underline{w}^T = [w_1, w_2, ..., w_6]$$

The complete hinges at ends I and J have degrees of freedom defined by:

$$\underline{w}_{uI}^T = [(v_1 - w_1) \;\; (v_3 - w_3) \;\; (v_5 - w_5)' \;\; (v_6 - w_6)']$$

and

$$\underline{w}_{uJ}^T = [(v_2 - w_2) \;\; (v_4 - w_4) \;\; (v_5 - w_5)'' \;\; (v_6 - w_6)'']$$

in which v_i, i=1,4 and w_i, i=1,4 are as shown in Figs. D3.1a and D3.2a, and in which:

$$(v_5 - w_5)' + (v_5 - w_5)'' = v_5 - w_5$$
$$(v_6 - w_6)' + (v_6 - w_6)'' = v_6 - w_6$$

That is, the torsional and axial hinge deformations are shared between the hinges at ends I and J. The proportions in which the deformations are shared are determined naturally during the numerical computation and do not need to be defined in advance. Each complete hinge is modeled as two subhinges in series (Fig. D3.2b). Each subhinge has four deformation degrees of freedom, $\underline{w}_{su}$, such that the sum of the $\underline{w}_{su}$ deformations for the two subhinges gives the hinge deformation, $\underline{w}_u$. The proportions of any total hinge deformation which are contributed by the separate subhinges are determined automatically during the computation.

D3.2 ELEMENT STIFFNESS

D3.2.1 Basic Procedure

The beam element connecting the internal nodes remains elastic, but the tangent stiffnesses of the hinges may change. For any state of the complete element, a 6 x 6 flexibility matrix is first formed for the elastic beam in terms of the degrees of freedom w_1 through w_6. This matrix is then modified by adding the flexibilities of the hinges to give a complete element flexibility matrix in terms of v_1 through v_6. This matrix is inverted to obtain a 6 x 6 element stiffness. Finally, this stiffness is transformed to the 12 x 12 global stiffness.

D3.2.2 Beam Element Elastic Flexibility

The local y,z axes are assumed to be the principal axes of the beam cross section. The local x axis is assumed to be both the centroidal axis and the axis of torsional twist.

The beam element stiffness relationships can be written as follows:

$$\begin{Bmatrix} dM_{yi} \\ dM_{yj} \end{Bmatrix} = \frac{EI_y}{L} \begin{bmatrix} K_{iiy} & K_{ijy} \\ K_{ijy} & K_{jjy} \end{bmatrix} \begin{Bmatrix} dw_1 \\ dw_2 \end{Bmatrix} \tag{D3.2a}$$

$$\begin{Bmatrix} dM_{zi} \\ dM_{zj} \end{Bmatrix} = \frac{EI_z}{L} \begin{bmatrix} K_{iiz} & K_{ijz} \\ K_{ijz} & K_{jjz} \end{bmatrix} \begin{Bmatrix} dw_3 \\ dw_4 \end{Bmatrix} \tag{D3.2b}$$

$$dM_x = \frac{GJ}{L} dw_5 \tag{D3.2c}$$

$$dF_x = \frac{EA}{L} dw_6 \tag{D3.2d}$$

in which

K_{ii},K_{ij},K_{jj} = flexural stiffness factors;
EI_y,EI_z = effective flexural rigidities;
M_y,M_z = bending moments;
i,j = element ends;
M_x = torsional moment;
F_x = axial force;
L = element length;
EA = effective axial rigidity; and
GJ = effective torsional rigidity.

The flexural stiffness factors can be used to account for non-uniform elements. For a uniform element, $K_{ii} = K_{jj} = 4.0$ and $K_{ij} = 2.0$.

Equations D3.2a and D3.2b are inverted to obtain flexibilities and are modified, if necessary, to allow for shear deformations by adding the shear flexibility matrices, $\underline{f}_{sy}$ and $\underline{f}_{sz}$, where

$$\underline{f}_s = \frac{1}{GA'L}\begin{bmatrix}1 & 1\\ 1 & 1\end{bmatrix} \qquad \text{(D3.3)}$$

in which GA' = effective shear rigidity.

D3.2.3 Hinge Plastic Flexibility

The deformation increment of a hinge is the sum of the increments for the two subhinges. That is,

$$d\underline{w}_u = \sum_i d\underline{w}_{sui} \qquad \text{(D3.3a)}$$

in which

$d\underline{w}_{sui}$ = deformation increment of subhinge i; and
$d\underline{w}_u$ = deformation increment of complete hinge.

In multi-dimensional action space, each subhinge has a 4 x 4 flexibility matrix in terms of its axial, torsional, y-flexural, and z-flexural deformations. The flexibility matrix before yield for a subhinge is initially null (rigid subhinge). After yielding, or yielding followed by unloading, each subhinge has a finite 4 x 4 flexibility matrix. The hinge flexibility is the sum of the flexibilities of its two subhinges.

The hinge at end I affects degrees of freedom v_1, v_3, v_5, and v_6 of the complete element. The hinge flexibility coefficients are simply added to the corresponding beam coefficients. Similarly, the hinge at end J affects degrees of freedom v_2, v_4, v_5, and v_6. Although the six deformation degrees of freedom are largely uncoupled for the elastic beam (see Eqn. D3.2), this is not the case, in general, after yield. The complete element flexibility matrix will generally be full (except for zero values for f_{14} and f_{23}).

The hinge flexibility relationship can be written as:

$$d\underline{w}_u = \underline{f}_u \, d\underline{S} = \sum_i \underline{f}_{sui} \, d\underline{S} \tag{D3.5}$$

in which

$\underline{f}_{sui}$ = flexibility matrix of subhinge i;
$\underline{f}_u$ = flexibility matrix for the complete hinge; and
$d\underline{S}$ = action increments on the hinge.

The problem thus reduces to the determination of $\underline{f}_{sui}$ for each yielded hinge.

D3.2.4 Yield Function

Each subhinge is effected by four actions (M_y, M_z, M_x, and F_x), with four corresponding deformations. The behavior is initially rigid-plastic-strain-hardening for each action individually. Different yield values and stiffnesses may be specified for each action component.

Yield of any subhinge is governed by a yield function (interaction relationship). Any one of five different yield functions may be specified, as considered in Section D2.3.3. After yield, each subhinge follows a kinematic hardening rule (that is, its yield surface translates in action space without change of shape or size). The hardening theory is a modification of the Mroz theory for plasticity in metals.

D3.2.5 Subhinge Stiffness

A subhinge is initially rigid-plastic, so that its stiffness matrix is initially infinite. After reversed loading is applied, the stiffness degrades and becomes finite. An *elastic* stiffness matrix for each subhinge is defined as:

$$\underline{K}_{se} = diag\ [K'_{My}\ K'_{Mz}\ K'_{Mx}\ K'_F] \tag{D3.6}$$

where K'_{My}, K'_{Mz}, K'_{Mx}, and K'_F are elastic stiffness after unloading.

When a subhinge yields, a *plastic* stiffness matrix is defined as:

$$\underline{K}_{sp} = diag\ [K'_{Myp}\ K'_{Mzp}\ K'_{Mxp}\ K'_{Fp}] \tag{D3.7}$$

in which the plastic stiffnesses after yield are given by:

$$K'_p = \frac{K' \cdot K_p}{K' - K_p} \tag{D3.8}$$

and in which the stiffnesses K' are the current elastic stiffnesses; and the stiffnesses K_p are initial plastic stiffness before any degradation. For first yield, the K'_i values are infinite, and the K'_p values are identical to K_p.

D3.2.6 Plastic Flexibility for a Single Subhinge

Consider a single subhinge. Let $\underline{S}$ be the vector of actions, where

$$\underline{S}^T = [\ M_y\ \ M_z\ \ M_x\ \ F\ ] \tag{D3.9}$$

Assume that the subhinge is *elastic-plastic,* and let $\underline{w}_{su}$ be the vector of subhinge deformations. That is, w_{su1} = flexural rotation about axis y; w_{su2} = flexural rotation about axis z; w_{su3} = plastic twist about axis x; and w_{su4} = plastic extension along axis x.

A flexibility relationship for the subhinge is required in the form:

$$d\underline{w}_{su} = \underline{f}_{su}\ d\underline{S} \tag{D3.10}$$

in which $\underline{f}_{su}$ = subhinge flexibility matrix.

The flexibility of the yielded subhinge, $\underline{f}_{su}$, is the sum of its elastic and plastic flexibility matrices. That is,

$$\underline{f}_{su} = \underline{f}_{se} + \underline{f}_{sp} \tag{D3.11}$$

in which

$\underline{f}_{se}$ = elastic flexibility matrix of subhinge; and

$\underline{f}_{sp}$ = plastic flexibility matrix of subhinge.

The plastic flexibility matrix is derived as follows. The following assumptions are made:

(1) Let ϕ be the subhinge yield function. As the subhinge yields, the yield surface translates in action space. After some amount of hardening has taken place, the yield function is $\phi(\underline{S}-\underline{\alpha})$, where $\underline{\alpha}$ = vector defining the new location of the yield surface origin. This is illustrated in Fig. D3.3 for a two-dimensional space.

(2) From any given plastic state (i.e. a point on the yield surface), any action increment ($d\underline{S}$) will produce increments of deformation ($d\underline{w}_{sp}$) and yield surface translation ($d\underline{\alpha}$). The direction of $d\underline{S}$ may be arbitrary. It is assumed that the direction of $d\underline{w}_{sp}$ is normal to the yield surface (i.e. an associated flow rule is assumed). The direction of $d\underline{\alpha}$ is determined by the hardening rule (as defined later) and is not necessarily parallel to either $d\underline{S}$ or $d\underline{w}_{sp}$. This is illustrated in Fig. D3.3 for a two-dimensional space.

(3) The direction of the outward normal to the yield surface is the gradient of the yield function. Define:

$$\underline{n} = \frac{\underline{\phi},_s}{(\underline{\phi},_s^T \cdot \underline{\phi},_s)^{1/2}} \tag{D3.12}$$

in which

$$\underline{\phi},_s^T = [\ \partial\phi/\partial M_y \quad \partial\phi/\partial M_z \quad \partial\phi/\partial M_x \quad \partial\phi/\partial F\ ] \tag{D3.13}$$

= yield function gradient; and

$\underline{n}$ = unit normal vector.

Hence, the deformation increment, $d\underline{w}_p$, is given by:

$$d\underline{w}_{sp} = \underline{n} \cdot dw_{sp}^* \tag{D3.14}$$

in which dw_{sp}^* = scalar which defines the magnitude of the plastic deformation.

(4) Let the component of $d\underline{S}$ in the direction of $\underline{n}$ be $d\underline{S}_n$ (Fig. D3.3). Hence,

$$d\underline{S}_n = \underline{n} \cdot (\underline{n}^T \cdot d\underline{S}) \tag{D3.15}$$

(5) Assume that $d\underline{S}_n$ and $d\underline{w}_{sp}$ are related by:

$$d\underline{S}_n = \underline{K}_{sp}\, d\underline{w}_{sp} \tag{D3.16}$$

in which

$$\underline{K}_{sp} = diag\ [\,K'_{Myp}\ K'_{Mzp}\ K'_{Mxp}\ K'_{Fp}\,] \tag{D3.17}$$

is a diagonal matrix of the *plastic* stiffnesses from the individual action-deformation relationships for the subhinge, as defined in Section D2.3.5.

(6) From the definition of $d\underline{S}_n$ (Eqn. D3.15), it follows that

$$\underline{n}^T d\underline{S} = \underline{n}^T d\underline{S}_n \tag{D3.18}$$

Substitute Eqns. D3.16 and D3.14 into Eqn. D3.18 to get:

$$\underline{n}^T \cdot d\underline{S} = \underline{n}^T \cdot \underline{K}_{sp} \cdot \underline{n} \cdot dw^{*}_{sp} \tag{D3.19}$$

(7) Solve for dw^{*}_{sp} as:

$$dw^{*}_{sp} = \frac{\underline{n}^T \cdot d\underline{S}}{\underline{n}^T \cdot \underline{K}_{sp} \cdot \underline{n}} \tag{D3.20}$$

(8) Hence, substitute Eqn. D3.20 into Eqn. D3.14 to get:

$$d\underline{w}_{sp} = \frac{\underline{n} \cdot \underline{n}^T}{\underline{n}^T \cdot \underline{K}_{sp} \cdot \underline{n}} d\underline{S} = \underline{f}_{sp}\, d\underline{S} \tag{D3.21}$$

Equation D3.21 is the required plastic flexibility relationship for any *active* subhinge.

D3.2.7 Flexibility for Complete Hinge

The 4 x 4 plastic flexibility of the complete hinge, f_u, follows from Eqn. D3.5 as:

$$\underline{f}_u = \sum_i \underline{f}_{sui} \tag{D3.22}$$

where i = number of subhinge. The flexibility of any subhinge, as derived in Section D3.2.6, can be written as:

$$\underline{f}_{sui} = \underline{f}_{se} + \underline{f}_{spi} \quad \frac{\underline{n}_i \cdot \underline{n}_i^T}{\underline{n}_i^T \cdot \underline{K}_{spi} \cdot \underline{n}_i} \tag{D3.23}$$

in which

$$\underline{f}_{spi} = \frac{\underline{n}_i \cdot \underline{n}_i^T}{\underline{n}_i^T \cdot \underline{K}_{spi} \cdot \underline{n}_i} \tag{D3.24}$$

$\underline{n}_i$ = normal vector to the surface; and,

$\underline{K}_{spi}$ = plastic stiffness matrix of the subhinge.

D3.2.8 Relationship to Basic Mroz Theory

In the special case where the action-deformation relationships for the four actions are all directly proportional to each other, the yield surfaces are all of the same shape and the plastic stiffnesses for each active yield surface are in the same proportion. The plastic stiffness matrix for each subhinge can then be formed in terms of the elastic stiffness matrix. That is,

$$\underline{K}_{spi} = \alpha_i \underline{K}_e \tag{D3.25}$$

where α_i defines the plastic stiffness as a proportion of the elastic stiffness. The plastic flexibility of a complete hinge can then be written as:

$$\underline{f}_u = \sum_i \underline{f}_{spi} = \sum_i \left(\frac{1}{\alpha_i}\right) \frac{\underline{n}_i \cdot \underline{n}_i^T}{\underline{n}_i^T \cdot \underline{K}_e \cdot \underline{n}_i} \tag{D3.26}$$

Because all the yield surfaces are the same shape, the $\underline{n}_i$ are all the same. Hence, if $\underline{n}_i = \underline{n}$, Eqn. D3.26 can be written as:

$$\underline{f}_u = \frac{\underline{n} \cdot \underline{n}^T}{\underline{n}^T \cdot \left(\sum_i \alpha_i\right) \underline{K}_e \cdot \underline{n}} \tag{D3.27}$$

The flexibility given by this equation is the same as that from the basic Mroz material theory. This shows that the Mroz material theory is a special case of the extended theory derived here.

D3.3 ELEMENT STIFFNESS

For the complete element, a tangent action-deformation relationship is required in the form:

$$d\underline{S} = \underline{K}_t \, d\underline{v} \tag{D3.28}$$

in which $\underline{K}_t$ = tangent stiffness matrix for the element.

A 6 x 6 flexibility matrix $\underline{f}_e$ is first formed for the elastic beam, in terms of degrees of freedom w_1 through w_6. This matrix is then modified by adding the flexibilities of $\underline{f}_u$ of the two complete hinges at the ends, to give a complete element flexibility matrix $\underline{f}_t$ in terms of v_1 through v_6. This matrix is inverted to obtain a 6 x 6 element stiffness, $\underline{K}_t$.

D3.4 EQUILIBRIUM NODAL LOADS

Nodal loads in equilibrium with the hinge actions in any given state are given by:

$$\underline{R} = \underline{a}^T \cdot \underline{S} \tag{D3.29}$$

in which

$\underline{S}^T$ = $[S_1, S_2, ..., S_6]$;
$\underline{R}$ = internal resisting forces for the element; and
$\underline{a}$ = displacement transformation relating element deformation to global displacements.

D3.5 HARDENING RULE

D3.5.1 Geometrical Interpretation

The relationship between any action and its corresponding deformation at a subhinge is multi-linear. The interaction among the actions (M_y, M_z, M_x, and F) is defined by the yield surfaces, as described earlier. After initial yield occurs, the behavior at a subhinge obeys a modification of the Mroz strain hardening rule for yield in metals [30].

D3.5.2 Modified Mroz Hardening Rule

For purposes of illustration, consider a two-dimensional M-F space, as shown in Fig. D3.3a. In this figure, it is assumed that the current state (point P_1) is on yield surface YS_1 and that loading is taking place towards surface YS_2. It is necessary to define the direction in which surface YS_1 translates.

As indicated in Fig. D3.3a, corresponding points P_1 and P_2 can be identified on YS_1 and YS_2. The relationship between the actions at these two points ($\underline{S}_1$ at P_1 and $\underline{S}_2$ at P_2) is obtained as follows.

Figure D3.3b shows a yield surface transformed into a normalized action space. In this space, surfaces YS_1 and YS_2 have identical shapes. Hence, points P_1 and P_2 coincide. The locations of P_1 and P_2 in Fig. D3.3a follow by transforming back to the natural action space. If the vector of actions at P_1 is $\underline{S}_1$, it follows that the vector of actions at P_2 is given by:

$$\underline{S}_2 = \underline{S}_u (\underline{S}_1 - \underline{\alpha}_1) + \underline{\alpha}_2 \qquad \text{(D3.30)}$$

in which

$\underline{S}_2$ = vector of actions at point P_2;

$d\underline{\alpha}_1$ and $d\underline{\alpha}_2$ = vectors defining the current origins, O_1 and O_2, of yield surfaces YS_1 and YS_2, respectively;

$$\underline{S}_u = diag \left[\frac{M_{yu2}}{M_{yu1}} \;\; \frac{M_{zu2}}{M_{zu1}} \;\; \frac{T_{u2}}{T_{u1}} \;\; \frac{F_{u2}}{F_{u1}} \right]$$

It is assumed that the direction of translation of yield surface YS_1 is along the line connecting point P_1 to point P_2, as shown in Fig. D3.3a. That is, the direction of motion of surface YS_1 is defined by:

$$d\underline{\alpha}_1 = (\underline{S}_2 - \underline{S}_1)\, d\alpha^* \qquad \text{(D3.31)}$$

in which

$d\alpha^*$ = scalar which defines the amount of translation of yield surface YS_1; and

$d\underline{\alpha}_1$ = vector defining the direction of translation.

The magnitude of $d\alpha^*$ is determined as explained in the next section. For the hardening rule originally formulated by Mroz [30,33], all yield surfaces are geometrically similar in natural action space. The rule then ensures that the surfaces never overlap. For the modified Mroz rule, the yield surfaces are assumed to be geometrically similar only in normalized action space.

As a result, overlapping of yield surfaces is allowed.

D3.5.3 Mathematical Formulation

Substitute Eqn. D3.31 into Eqn. D3.32 to get:

$$d\underline{\alpha}_1 = \left[(\underline{S}_u - \underline{I})\, \underline{S}_1 - (\underline{S}_u \underline{\alpha}_1 - \underline{\alpha}_2) \right] d\alpha^* \tag{D3.32}$$

The yield surface is defined by:

$$\phi\,(\underline{S}_1 - \underline{\alpha}_1) = 1 \tag{D3.33}$$

The requirement that the action point remain on the yield surface is:

$$d\phi = 0 = \underline{\phi},_s^T d\underline{S}_1 - \underline{\phi},_s^T d\underline{\alpha}_1 \tag{D3.34}$$

Substitute Eqns. D3.32 and D3.33 into Eqn. D3.35 to get:

$$d\alpha^* = \frac{\underline{\phi},_s^T d\underline{S}_1}{\underline{\phi},_s^T [(\underline{S}_u - \underline{I})\, \underline{S}_1 - (\underline{S}_u \underline{\alpha}_1 - \underline{\alpha}_2)]} \tag{D3.35}$$

Hence, substitute Eqn. D3.36 into Eqn. D3.32 to get $d\underline{\alpha}_1$ as:

$$d\underline{\alpha}_1 = \frac{\left[(\underline{S}_u - \underline{I})\, \underline{S}_1 - (\underline{S}_u \underline{\alpha}_1 - \underline{\alpha}_2) \right] \underline{\phi},_s^T d\underline{S}_1}{\underline{\phi},_s^T \left[(\underline{S}_u - \underline{I})\, \underline{S}_1 - (\underline{S}_u \underline{\alpha}_1 - \underline{\alpha}_2) \right]} \tag{D3.36}$$

For any current state defined by $\underline{S}_1$, $\underline{\alpha}_1$, and $\underline{\alpha}_2$, Eqn. D3.37 defines, for an action increment $d\underline{S}_1$, the translation of yield surface YS_1 for loading towards surface YS_2.

D3.5.4 Second Yield Surface

For the case when the action point lies on the second yield surface, the hardening rule can be obtained by assuming that an additional infinitely large yield surface exists. The direction of translation for this case is then along the radial direction connecting the origin of the second yield surface to the current action point. This is exactly Ziegler's hardening rule [30]. It can be expressed as:

$$d\underline{\alpha}_2 = (\underline{S}_2 - \underline{\alpha}_2)\, d\alpha^* \tag{D3.37}$$

in which

$d\alpha^*$ = scalar which defines the amount of translation of the yield surface, as before;

$\underline{\alpha}_2$ = vector defining the yield surface origin; and

$d\underline{\alpha}_2$ = vector defining the direction of translation.

For this case, Eqn. D3.37 becomes:

$$d\underline{\alpha}_2 = \frac{(\underline{S}_2 - \underline{\alpha}_2)\,\underline{\phi},_s^T \cdot d\underline{S}_2}{\underline{\phi},_s^T(\underline{S}_2 - \underline{\alpha}_2)} \qquad \text{(D3.38)}$$

D3.5.5 Overlapping of Yield Surfaces

In the original Mroz hardening rule, it is assumed that the yield surface is geometrically similar to the yield surface YS_2. This assumption is reasonable for metal plasticity in stress space because it is reasonable to assume an isotropic material. However, for dealing with stress resultants, each action-deformation relationship depends on the cross section shape in a different way, and the behavior is not isotropic in action space. That is, the yield surfaces will, in general, not be geometrically similar. The authors have considered a number of strategies in an attempt to obtain "correct" behavior while preventing yield surface overlap. None of these strategies proved satisfactory, and it was finally concluded that overlapping should be allowed.

D3.6 PLASTIC DEFORMATION

The flexibility relationship of the element can be written as:

$$d\underline{v} = \underline{f}_t \, d\underline{S} = \underline{f}_e \, d\underline{S} + d\underline{v}_p \tag{D3.39}$$

in which

$d\underline{v}_p = \sum_i d\underline{v}_{spi}$ is the element plastic deformation increment; and

$\underline{f}_e$ = the element elastic flexibility matrix.

Premultiply Eqn. D3.39 by $\underline{f}_p \cdot \underline{K}_e$ to get:

$$\underline{f}_p \cdot \underline{K}_e \cdot d\underline{v} = \underline{f}_p \cdot d\underline{S} + \underline{f}_p \cdot \underline{K}_e \cdot d\underline{v}_p \tag{D3.40}$$

in which

$\underline{K}_e$ = the element elastic stiffness matrix;

$\underline{f}_p = \sum_i f_{pi}$ is the element total plastic flexibility.

$$\underline{f}_p \cdot d\underline{S} = d\underline{v}_p \tag{D3.41}$$

Substitute Eqn. D3.41 into Eqn. D3.40 to get:

$$(I + \underline{f}_p \underline{K}_e) \, d\underline{v}_p = \underline{f}_p \cdot \underline{K}_e \cdot d\underline{v} \tag{D3.42}$$

Hence,

$$d\underline{v}_p = (I + \underline{f}_p \cdot \underline{K}_e)^{-1} \, \underline{f}_p \cdot \underline{K}_e \cdot d\underline{v} \tag{D3.43}$$

Equation D3.43 gives the plastic deformation increments of the element in terms of the total deformation increments.

D3.7 LOADING/UNLOADING CRITERION

The loading/unloading criterion enables continuous plastic flow at a subhinge to be distinguished from elastic unloading for any current plastic state and any specified deformation increment. Two procedures are of general applicability, as follows.

(1) Postulate that the subhinge has unloaded an infinitesimal amount, so that the current state lies just within the yield surface. Calculate the elastic action increments, $d\underline{S}_e$, corresponding to the specified deformation increments. If the state moves outside the yield surface, the assumed elastic state is incorrect, indicating continuing plastic flow. If

the state moves within the yield surface, the elastic assumption is correct, indicating unloading.

(2) For the specified deformation increment, calculate the magnitude parameter for the plastic deformation increment. A positive magnitude indicates continuing plastic flow, and a negative magnitude indicates unloading.

By the first of these two procedures, continued loading of subhinge i is indicated if $d\underline{S}_e$ has a positive component along the outward normal, $\underline{n}_i$, of the yield surface. That is, continued loading occurs if

$$\underline{n}_i^T \cdot d\underline{S}_e \geqslant 0 \tag{D3.44}$$

To consider the second procedure, first assume that the current plastic flow directions of both active subhinges are the same. Hence, the plastic deformation increment for the subhinge is given by:

$$d\underline{v}_p = \underline{n} \cdot dv_p^* \tag{D3.45}$$

Premultiply Eqn. D3.39 by $\underline{n}^T \cdot \underline{f}^p \cdot \underline{K}_e$ to get:

$$dv_p^* = \frac{\underline{n}^T \underline{f}_p \cdot \underline{K}_e \, d\underline{w}}{1 + \underline{n}^T \cdot \underline{f}_p \cdot \underline{K}_e \cdot \underline{n}} \tag{D3.46}$$

Substitute Eqn. D3.24 into Eqn. D3.46 to get:

$$dv_p^* = \frac{r_2 \underline{n}^T d\underline{S}_e}{1 + r_1} \tag{D3.47}$$

in which r_1 and r_2 are scalars defined as follows:

$$r_1 = \sum_i \frac{\underline{n}^T \cdot \underline{K}_e \cdot \underline{n}}{\underline{n}^T \cdot \underline{K}_{spi} \cdot \underline{n}} \tag{D3.48}$$

$$r_2 = \sum_i \frac{1}{\underline{n}^T \cdot \underline{K}_{spi} \cdot \underline{n}} \tag{D3.49}$$

Because the matrices $\underline{K}_{spi}$ and $\underline{K}_e$ are always positive definite, the scalars r_1 and r_2 always exceed zero. Hence, the sign of dv_p^* is the same as the sign of $\underline{n}^T \cdot d\underline{S}_e$. This is the same criterion as Eqn. D3.44.

In general, the plastic flow directions for the yielded subhinges are not the same. Hence, it is possible for $\underline{n}_i^T \cdot d\underline{S}_e$ to be greater than zero for one subhinge and less than zero for the other (i.e. continued loading on one, but unloading on the other). This possibility is illustrated in Fig. D3.4. For computation, if both subhinges are yielded, it is assumed that unloading is governed by the *second subhinge.* If unloading occurs on this subhinge, unloading is assumed to occur on both subhinges. If the situation happens to be as shown in Case A of Fig. D3.4 (which is unlikely), reloading will immediately occur on the first subhinge, and the analysis will continue.

Figure D3.4, Case B, illustrates another possible consequence of yield surface overlap. In this case, unloading occurs from both surfaces, but on reloading the second yield surface is reached first. For this case, calculate the action on the second yield surface for reloading, then translate the first yield surface to attach the second yield surface at this action point, and the analysis continues.

D3.8 END ECCENTRICITY

Plastic hinges in frames and coupled frame-shear wall structures will form near the faces of the joints rather than at the theoretical joint centerlines. This effect can be approximated by postulating rigid, infinitely strong connecting links between the nodes and the element ends, as shown in Fig. D3.5. The displacement transformation relating the increments of node displacements, $d\underline{r}_u$, to increments of displacement at the element ends is easily established and can be written as:

$$d\underline{r} = \underline{a}_e \, d\underline{r}_u \tag{D3.50}$$

This transformation is used to modify the stiffness and state determination calculations to allow for end eccentricity effects.

D3.9 RIGID FLOOR DIAPHRAGMS

A frequently made assumption in the analysis of tall buildings is that each floor diaphragm is rigid in its own plane. To introduce this assumption, a "master node" at the center of mass of each floor may be specified, as shown in Fig. D3.6. Each master node has only three degrees of freedom, as shown, which are the displacements of the diaphragm horizontally as a rigid body. If any beam-column member is connected to these "master" displacements, its behavior depends partly on these displacements and partly on the displacements which are not affected by the rigid diaphragm assumption.

The displacement transformation relating the master (diaphragm) displacements, $d\underline{r}_d$, to the displacements at a "slaved" node is as follows.

$$\begin{Bmatrix} dr_{n1} \\ dr_{n3} \\ dr_{n5} \end{Bmatrix} = \begin{bmatrix} 1 & 0 & dz \\ 0 & 1 & -dx \\ 0 & 0 & 1 \end{bmatrix} \begin{Bmatrix} dr_x \\ dr_y \\ dr_\theta \end{Bmatrix} \tag{D3.51a}$$

or

$$d\underline{r}_{ns} = \underline{a}_d \, d\underline{r}_d \tag{D3.51b}$$

The "slaved" displacements at element ends i and j can, thus, be expressed in terms of the displacements at the "master" node (or nodes). The corresponding coefficients of the element stiffness matrix are transformed to account for the slaving. The resulting element stiffness matrix is assembled in terms of the three master degrees of freedom plus the three local degrees of freedom dr_{n2}, dr_{n4}, and dr_{n6} at each node, which are not affected by slaving.

D3.10 TOLERANCE FOR STIFFNESS REFORMULATION

Each time a new hinge yields or an existing hinge unloads, the element stiffness changes. Moreover, because the direction of plastic flow may change, the stiffness of a yielding element will generally change continuously. The change in stiffness results from differences in the directions of the normal to the yield surface as the actions at the hinge change. If the angle change is small, the change in stiffness will be small and can be neglected to avoid recalculating the stiffness. In the computer program, an option is provided for the user to set a tolerance for the angle. If a nonzero tolerance is specified, the element stiffness is reformed only when the change in state is such that the angle between the current yield surface normal and that when the stiffness was last reformed exceeds the tolerance. A tolerance of about 0.1 radians is recommended.

D4. COMPUTER LOGIC

D4.1 STATE DETERMINATION

The state determination calculation for an inelastic element requires evaluation of the equation:

$$\Delta \underline{S} = \int_0^{\Delta v} \underline{K}_t \, d\underline{v} \tag{D4.1}$$

in which

$\Delta \underline{S}$ = finite action increment for the element corresponding to the finite deformation increment $\Delta \underline{v}$; and

$\underline{K}_t$ = element tangent stiffness, which, in general, varies during the increment.

The computational procedure for state determination of the element is as follows.

(1) From the given nodal displacement increment, calculate the element deformation increment from:

$$\Delta \underline{v} = \underline{a} \cdot \Delta \underline{r} \tag{D4.2}$$

in which

$\Delta \underline{r}$ = vector of nodal displacement increments;

$\Delta \underline{v}$ = vector of element deformation increments; and

$\underline{a}$ = displacement transformation matrix.

(2) Calculate linear action increments for the element from:

$$\Delta \underline{S} = \underline{K}_t \Delta \underline{v} \tag{D4.3}$$

and hence determine hinge action increments as:

$$\Delta \underline{S}_h = \underline{b} \, \Delta \underline{S} \tag{D4.4}$$

in which

$\Delta \underline{S}$ = linear action increment for element corresponding to the finite deformation increment $\Delta \underline{v}$;

$\underline{K}_t$ = element tangent stiffness matrix;

$\Delta \underline{S}_h$ = linear action increment for hinges; and

$\underline{b}$ = transformation matrix from $\Delta \underline{S}$ to $\Delta \underline{S}_h$, which is easily formed.

(3) Check for a nonlinear "event" in the current increment, and calculate the corresponding event factor for each complete hinge. The possible events are as follows:

(a) If the current state is elastic, calculate the proportion of the deformation increment required to reach the next yield surface. If this proportion is greater than 1.0, the state continues to be elastic and the event factor is 1.0. Otherwise, an event occurs and the event factor is set equal to the calculated proportion.

(b) If the current state is plastic, calculate $\underline{n}^T d\underline{S}_e$. If the value exceeds zero, continued loading is indicated. The event factor is then calculated for the next yield surface, allowing a tolerance as described in Section D4.2. Otherwise, unloading occurs. In this case, the elastic degrading stiffness and the corresponding plastic stiffness matrix for each subhinge are calculated from the total plastic deformation. The stiffness matrix is then reformed as the elastic stiffness, and the calculation proceeds from Step 2.

(4) Calculate plastic deformation, $\Delta \underline{w}_{su}$, for each yielded subhinge by using Eqn. D3.44.

(5) Pick up the smallest event factor, FACM, from the event factors for the two complete hinges at the ends of the element.

(6) Use the event factor, FACM, to compute new hinge forces, new subhinge total plastic deformations, and new origins of all subhinges, as:

$$\underline{S}_h = \underline{S}_h + FACM^*\Delta \underline{S}_h \tag{D4.5}$$

$$\underline{\alpha}_i = \underline{\alpha}_i + FACM^*\Delta \underline{\alpha}_i \tag{D4.6}$$

$$\underline{w}_{su}^i = \underline{w}_{su}^i + FACM^*\Delta \underline{w}_{su}^i \tag{D4.7}$$

The new action point, $\underline{S}_h$, must lie on the yield surface if the subhinge is yielded. If the action point is not on the yield surface, scale the actions radially back to the yield surface.

(7) Calculate the complement of the event factor as:

$$SS = 1. - FACM \tag{D4.8}$$

(8) Reform the tangent stiffness matrix for the element if any event has occurred.

(9) If all of the displacement increments of the element have been used up (i.e. SS = 0), go to Step 11. Otherwise, continue to the next step.

(10) Calculate the remaining element displacement increment for the next cycle from:

$$\Delta \underline{v} = SS \cdot \Delta \underline{v} \tag{D4.9}$$

Then go to Step 2.

(11) Obtain the element actions, $\underline{S}$, using:

$$\underline{S} = \underline{b}^T \underline{S}_h \tag{D4.10}$$

(12) Calculate the internal resisting force for the element, $\underline{R}$, using:

$$\underline{R} = \underline{a}^T \cdot \underline{S} \tag{D4.11}$$

D4.2 YIELD SURFACE TOLERANCE

It is possible for the new action point, calculated assuming constant $\underline{K}_t$, to lie significantly outside the current yield surface. This will occur particularly when $\Delta\underline{S}$ and $\Delta\underline{\alpha}$ are distinctly nonparallel (Fig. D4.1). In this case, the calculation is assumed to be sufficiently accurate, provided the new action point lies within a tolerance zone (typically 2%-5% of the yield surface size). If not, $\Delta\underline{v}$ is scaled, $\underline{K}_t$ is reformed, and the calculation is repeated for the balance of $\Delta\underline{v}$.

The scale factor is conveniently determined by the procedure illustrated for M-F space in Fig. D4.1. In this figure, the current action point is P, and the new action point, obtained by applying Eqn. D4.3, is at Q. Hardening is affected only by the component of $\Delta\underline{S}$ parallel to the yield surface normal. Hence, the yield surface translates as shown. Point Q lies outside the new yield surface, the amount being defined by e_r, which is the length of the "radial" error vector, $\underline{e}_r$. This error must not exceed the allowable tolerance.

Computationally, it is convenient to consider the "tangential" error, $\underline{e}_t$, which is the length of vector P'Q. If the yield surface is assumed to be locally quadratic, then

$$e_r \doteq 0.5\, e_t^2 \qquad \text{(D4.12)}$$

The value of e_r is calculated from this equation. If e_r is within the allowable tolerance, point Q is scaled to the new yield surface and the computation continues (this scaling introduces an error which is assumed to be acceptable). If e_r exceeds the allowable tolerance, it is assumed that e_t varies linearly with element deformation. A scale factor to set e_r equal to the tolerance is then calculated using Eqn. D4.12, the $\Delta\underline{S}$ and $\Delta\underline{\alpha}$ increments are scaled by this factor; and the new action point is scaled to the yield surface. The element stiffness is then reformed, and the process is repeated for the remainder of the deformation increment. If $\Delta\underline{S}$ is parallel to $\underline{S}-\underline{\alpha}$, no scaling will be required. If $\Delta\underline{S}$ makes a large angle with $\underline{S}-\underline{\alpha}$, the deformation increment may be subdivided into several subincrements, depending on the magnitude of $\Delta\underline{v}$ and the value specified for the error tolerance.

The deformation increment is also subdivided if a new yield surface is reached. In this case, the new action point is permitted to go beyond the yield surface by an amount equal to the allowable radial error. The proportion of the deformation increment required to reach this state is calculated; the new action point is scaled to the yield surface; the stiffness is reformed; and the calculation proceeds for the remainder of the deformation increment.

D5. ANSR USER GUIDE

3D REINFORCED CONCRETE BEAM COLUMN ELEMENT

D5.1 CONTROL INFORMATION - Two Cards

D5.1.1 First Card

Columns	Note	Name	Data
5(I)		NGR	Element group indicator (=4).
6-10(I)		NELS	Number of elements in group.
11-15(I)		MFST	Element number of first element in group. Default = 1.
16-25(F)		DKO	Initial stiffness damping factor, β_o.
26-35(F)		DKT	Tangent stiffness damping factor, β_T.
41-80(A)		GRHED	Optional group heading.

D5.1.2 Second Card

Columns	Note	Name	Data
1-5(I)		NMBT	Number of different strength types (max. 20). Default = 1.
6-10(I)		NECC	Number of different end eccentricity types (max. 15). Default = zero.
11-15(I)		NPAT	Number of different initial force patterns (max. 30). Default = zero.

D5.2 STRENGTH TYPES

NMBT sets of cards.

D5.2.1 Strength Option

Columns	Note	Name	Data
1-5(I)			Strength type number, in sequence beginning with 1.

10(I)		INPT	Input options for element flexural stiffnesses, as follows. See Section D2.3.5. (a) INPT=1: Procedure assuming essentially uniform bending moment over element length. Leave rest of this card blank. (b) INPT=2: Procedure assuming double-cantilever behavior. Leave rest of this card blank. (c) INPT=3: General option. Complete rest of this card.
11-20(F)			Coefficient K_{ii} for bending about local y-axis. Default = 4.
21-30(F)			Coefficient K_{ij} for bending about local y-axis. Default = 2.
31-40(F)			Coefficient K_{jj} for bending about local y-axis. Default = 4.
41-50(F)			Coefficient K_{ii} for bending about local z-axis. Default = 4.
51-60(F)			Coefficient K_{ij} for bending about local z-axis. Default = 2.
61-70(F)			Coefficient K_{jj} for bending about local z-axis. Default = 4.
71-75(F)	(1)		Coefficient of stiffness degradation coupling parameter for first subhinge.
76-80(F)	(2)		Coefficient for second subhinge.

D5.2.2 Bending Properties About Local y-axis

(a) OPTN=1. Specify beam moment-rotation relationship. See Fig. D2.8. One card.

Columns	Note	Name	Data
1-10(F)			Stiffness K_{M1}.
11-20(F)			Stiffness K_{M2}.
21-30(F)			Stiffness K_{M3}.
31-40(F)			Yield moment M_{y1}.
41-50(F)			Yield moment M_{y2}.
51-55(F)			Degrading stiffness parameter, α_1.

56-60(F)			Degrading stiffness parameter, α_2.
61-65(F)			Degrading stiffness parameter, β_1.
66-70(F)			Degrading stiffness parameter, β_2.

(b) OPTN=2. Specify cantilever P-δ relationship. See Fig. D2.9. One card.

Columns	Note	Name	Data
1-10(F)			Stiffness K_1.
11-20(F)			Stiffness K_2.
21-30(F)			Stiffness K_3.
31-40(F)			Yield force P_{y1}.
41-50(F)			Yield force P_{y2}.
51-55(F)			Degrading stiffness parameter, α_1.
56-60(F)			Degrading stiffness parameter, α_2.
61-65(F)			Degrading stiffness parameter, β_1.
66-70(F)			Degrading stiffness parameter, β_2.

(c) OPTN=3. Specify beam elastic stiffness and hinge moment-rotation relationships. Two cards.

Columns	Note	Name	Data
Card 1			
1-10(F)			Elastic flexural stiffness, EI/L.
11-20(F)			Elastic shear rigidity (GA_z) along z-axis (i.e. shear associated with y-axis bending). If zero, shear deformation is neglected.
21-30(F)			Degrading stiffness parameter, α_1.
31-40(F)			Degrading stiffness parameter, α_2.
41-50(F)			Degrading stiffness parameter, β_1.
51-60(F)			Degrading stiffness parameter, β_2.
Card 2			
1-10(F)			Plastic stiffness K_{p1} of left-end hinge.
11-20(F)			Plastic stiffness K_{p2} of left-end hinge.

21-30(F)	Yield moment M_{y1} of left-end hinge.
31-40(F)	Yield moment M_{y2} of left-end hinge.
41-50(F)	Plastic stiffness K_{p1} of right-end hinge.
51-60(F)	Plastic stiffness K_{p2} of right-end hinge.
61-70(F)	Yield moment M_{y1} of right-end hinge.
71-80(F)	Yield moment M_{y2} of right-end hinge.

D5.2.3 Bending Properties About Local z-axis

As for Section D5.2.2, but specify z-axis properties.

D5.2.4 Torsional Properties

Columns	Note	Name	Data
1-10(F)			Torsional stiffness K_{T1}.
11-20(F)			Torsional stiffness K_{T2}.
21-30(F)			Torsional stiffness K_{T3}.
31-40(F)			Torsional strength T_{y1}.
41-50(F)			Torsional strength T_{y2}.
51-55(F)			Degrading stiffness parameter, α_1.
56-60(F)			Degrading stiffness parameter, α_2.
61-65(F)			Degrading stiffness parameter, β_1.
66-70(F)			Degrading stiffness parameter, β_2.

D5.2.5 Axial Properties

Columns	Note	Name	Data
1-10(F)			Axial stiffness K_{F1}.
11-20(F)			Axial stiffness K_{F2}.
21-30(F)			Axial stiffness K_{F3}.
31-40(F)			Axial strength F_{y1}.
41-50(F)			Axial strength F_{y2}.
51-55(F)			Degrading stiffness parameter, α_1.

56-60(F)			Degrading stiffness parameter, α_2.
61-65(F)			Degrading stiffness parameter, β_1.
66-70(F)			Degrading stiffness parameter, β_2.
71-80(F)	(3)		Axial strength F_{y4}. Input as a positive value. Default = F_{y1}.

D5.3 END ECCENTRICITY TYPES

NECC cards. See Fig. D3.5.

Columns	Note	Name	Data
1-5(I)	(4)		End eccentricity type number, in sequence beginning with 1.
11-20(F)			X_i = X eccentricity at end i.
21-30(F)			X_j = X eccentricity at end j.
31-40(F)			Y_i = Y eccentricity at end i.
41-50(F)			Y_j = Y eccentricity at end j.
51-60(F)			Z_i = Z eccentricity at end i.
61-70(F)			Z_j = Z eccentricity at end j.

D5.4 INTERNAL ELEMENT FORCE PATTERNS

NPAT cards.

Columns	Note	Name	Data
1-5(I)	I(5)		Pattern number, in sequence beginning with 1.
11-21(F)			Initial moment M_{yy} at end i.
21-30(F)			Initial moment M_{zz} at end i.
31-40(F)			Initial moment M_{yy} at end j.
41-50(F)			Initial moment M_{zz} at end j.
51-60(F)			Initial axial force.
61-70(F)			Initial torque.

D5.5 ELEMENT DATA GENERATION

As many pairs of cards as needed to generate all elements in group.

Columns	Note	Name	Data

Card 1

1-5(I)	(6)		Element number, or number of first element in a sequentially numbered series of elements to be generated by this card.
6-10(I)		NODI	Node number I.
11-15(I)		NODJ	Node number J.
16-20(I)		INC	Node number increment for element generation. Default = 1.
21-25(I)		NODK	Number of a third node, K, lying in the xy plane, for definition of the local y-axis. Default = automatic orientation of y-axis.
26-30(I)		NSI	Number of node (diaphragm node) to which end I is slaved. If not slaved, leave blank.
31-35(I)		NSJ	Number of node to which end J is slaved. If element generation is used, nodes NSI and NSJ are the same for all elements in the series. For a description of the slaving procedure, see Section D3.9.
36-40(I)		NSTR	Strength type number.
41-45(I)		IECC	End eccentricity type number. Default = no end eccentricity.
46-50(I)		NIT	Initial force pattern number. Default = no initial force.
51-55(I)		KTYP	Interaction surface type. (a) = 1 Y.S. type = 1 (b) = 2 Y.S. type = 2 (c) = 3 Y.S. type = 3 (d) = 4 Y.S. type = 4 (e) = 5 Y.S. type = 5
56-60(I)		KGEOM	Geometric stiffness code: (a) 0 = Geometric stiffness is not to be included. (b) 1 = Geometric stiffness is to be included.

61-65(I)	KOUT	Time history output code:
		(a) 1 = output time history results
		(b) 0 = no output
71-80(F) (7)		Stiffness reformulation angle tolerance, γ (radians). See Section D3.10 for explanation.
Card 2		
1-10(F)		Parameter a_1 in interaction surface equation.
11-20(F)		Parameter a_2 in interaction surface equation.
21-30(F)		Parameter a_3 in interaction surface equation.
31-40(F)		Parameter a_4 in interaction surface equation.

D5.6 NOTES

(1) Stiffness degradation coupling parameter is defined by input coefficient times the sum of degradation parameters for first subhinge (i.e. α_{12} = coefficient x $(\alpha_1 + \alpha_2)$).

(2) Stiffness degradation coupling parameter is defined by input coefficient times the sum of degradation parameters for second subhinge (i.e. β_{12} = coefficient x $(\beta_1 + \beta_2)$).

(3) The value of F_{y3}, as shown in Fig. D2.2, allows the origin of the yield surfaces to be shifted along the F-axis. The strengths in tension and compression are then different.

(4) All eccentricities are measured *from* the node *to* the element end (Fig. D3.5), positive in the positive coordinate directions.

(5) See Fig. D2.11 for the positive directions of initial element actions. Refer to Section D2.8 for a description of the effects of initial element actions.

(6) Cards must be input in order of increasing element number. Cards for the first and the last elements must be included (that is, data for these two elements cannot be generated). Cards may be provided for all elements, in which case each card specifies the data for one element, and the generation is not used. Alternatively, cards for a series of elements may be omitted, in which case data for the missing elements is generated as follows:

(a) All missing elements are assigned the same node "K" (NODK), slave nodes (NSI and NSJ), strength types, end eccentricity type, initial force pattern type, interaction surface type, codes for geometric stiffness and response output, and stiffness reformulation angle tolerance, as those for the element preceding the missing series of elements.

(b) The node numbers I and J for each missing element are obtained by adding the increment (INC) to the node numbers of the preceding element. That is,

NODI(N) = NODI(N-1)+INC

NODJ(N) = NODJ(N-1)+INC

The node increment, INC, is the value specified with the element *preceding* the missing series of elements.

(7) Refer to Section D3.10 for a description of the stiffness reformulation tolerance.

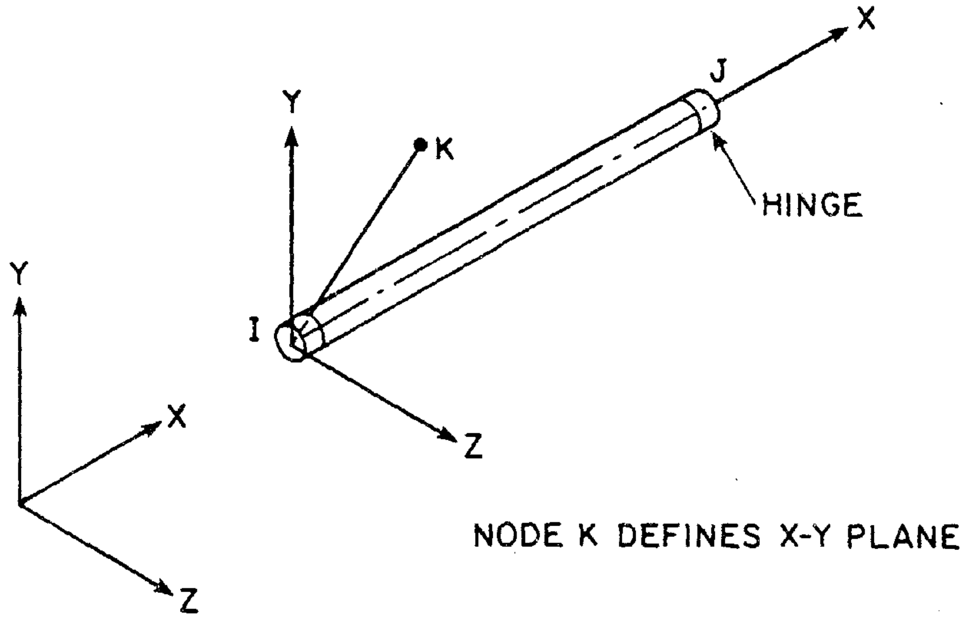

(a) ELEMENT AXES

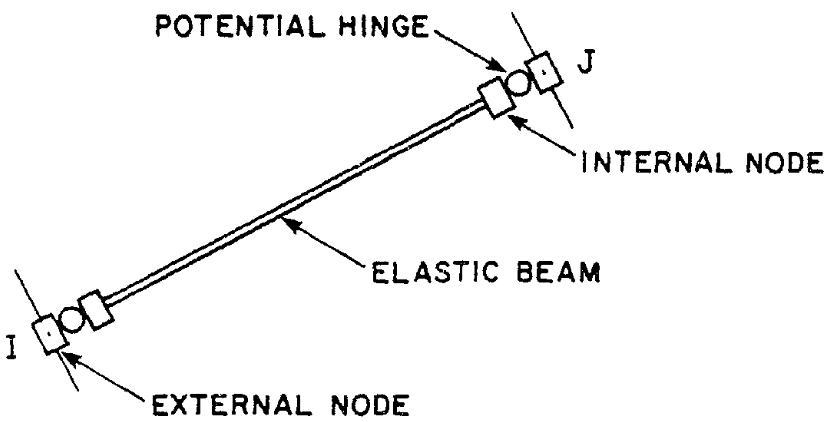

(b) ELEMENT IDEALIZATION

FIG. D2.1 ELEMENT AXES AND IDEALIZATION

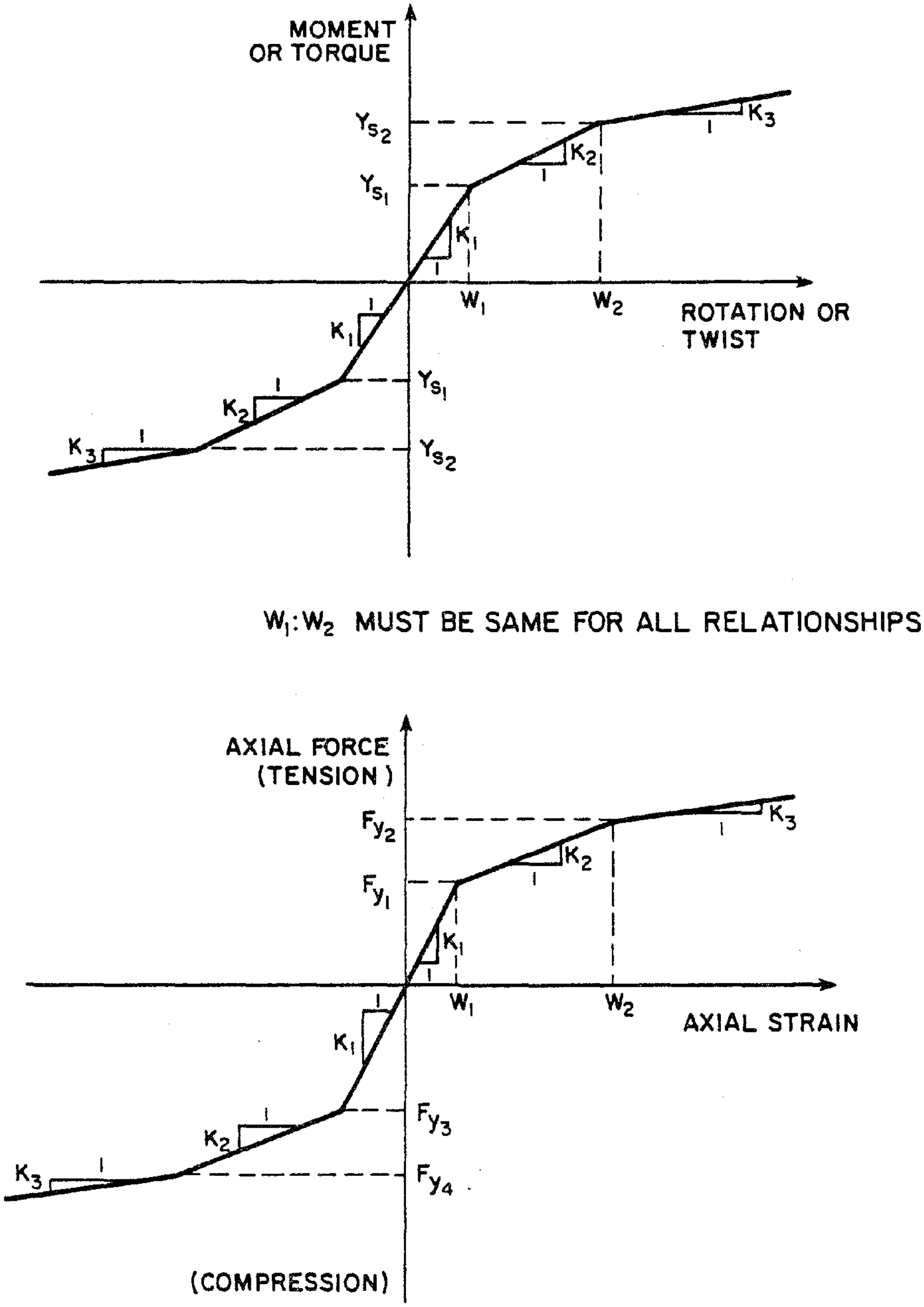

FIG. D2.2 ACTION VS. DEFORMATION FOR ELEMENT

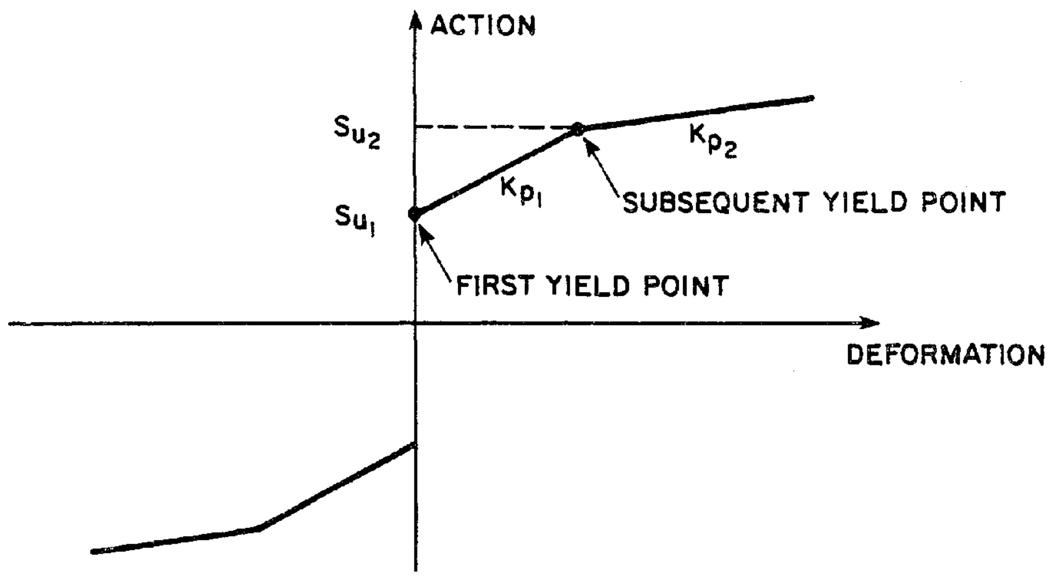

(a) ACTION VS. DEFORMATION RELATIONSHIP

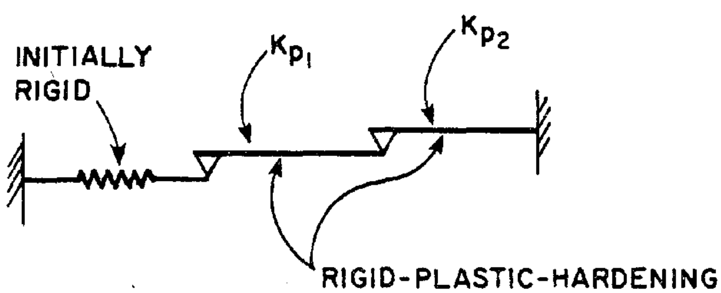

(b) 1-D MODEL

FIG. D2.3 1-D MODEL FOR A HINGE

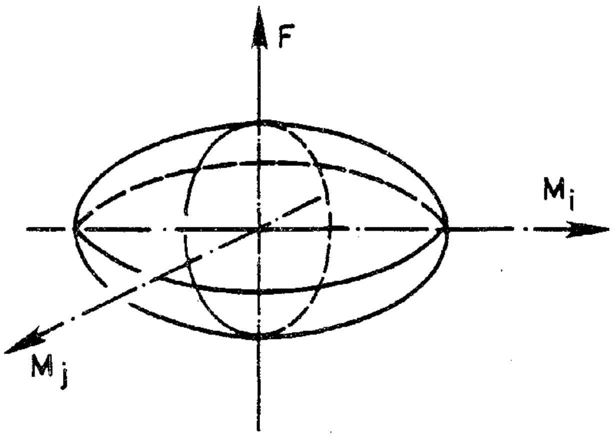

$$\phi = \left(\frac{M_y}{M_{yu}}\right)^2 + \left(\frac{M_z}{M_{zu}}\right)^2 + \left(\frac{M_x}{M_{xu}}\right)^2 + \left(\frac{F}{F_u}\right)^2$$
$$= 1$$

(A) SURFACE TYPE 1

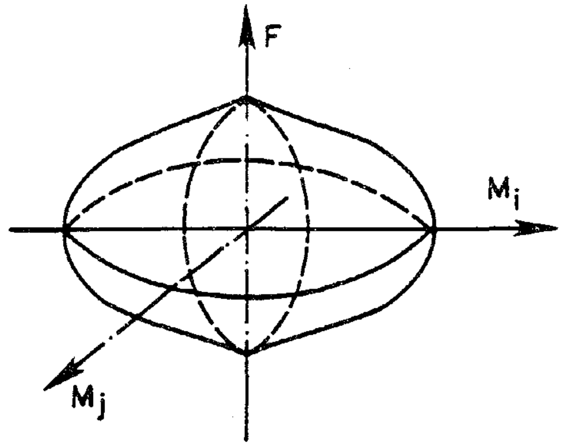

$$\phi = \left[\left(\frac{M_y}{M_{yu}}\right)^2 + \left(\frac{M_z}{M_{zu}}\right)^2 + \left(\frac{M_x}{M_{xu}}\right)^2\right]^{1/2} + \left(\frac{F}{F_u}\right)^2$$
$$= 1$$

(B) SURFACE TYPE 2

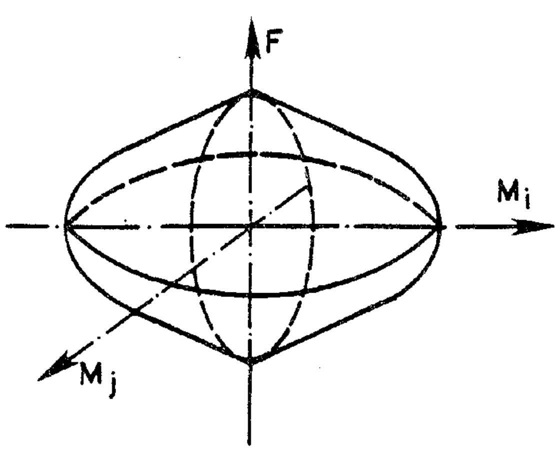

$$\phi = \left[\left(\frac{M_y}{M_{yu}}\right)^2 + \left(\frac{M_z}{M_{zu}}\right)^2 + \left(\frac{M_x}{M_{xu}}\right)^2\right]^{1/2} + \left(\frac{F}{F_u}\right)^{a_1}$$
$$= 1$$

(C) SURFACE TYPE 3

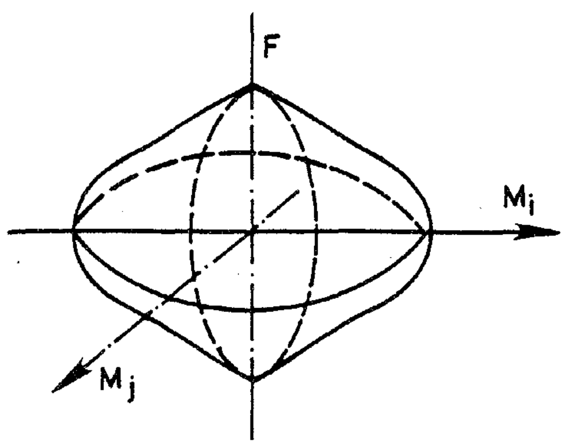

$$\phi = \left[\left(\frac{M_y}{M_{yu}}\right)^2 + \left(\frac{M_z}{M_{zu}}\right)^2 + \left(\frac{M_x}{M_{xu}}\right)^2\right]^{a_1} + \left(\frac{F}{F_u}\right)^{a_2}$$
$$= 1$$

(D) SURFACE TYPE 4

FIG. D2.4 INTERACTION SURFACES

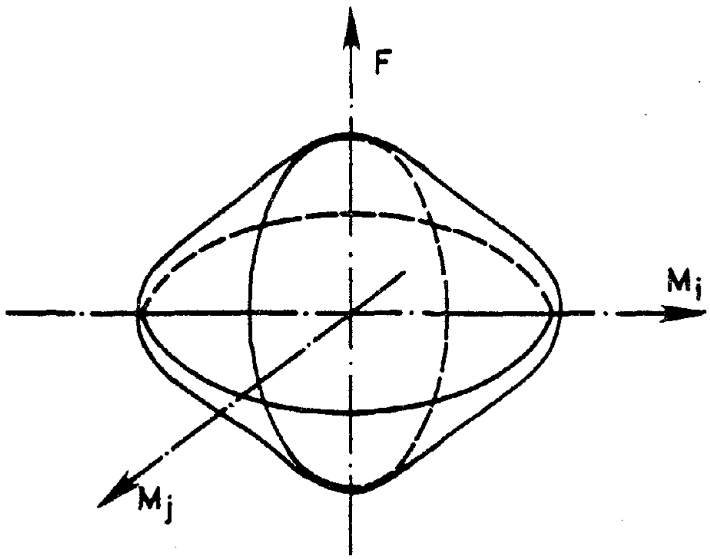

$$\phi = \left|\frac{M_y}{M_{yu}}\right|^{a_1} + \left|\frac{M_z}{M_{zu}}\right|^{a_2} + \left|\frac{T}{T_u}\right|^{a_3} + \left|\frac{F}{F_u}\right|^{a_4} = 1$$

(E) SURFACE TYPE 5

FIG. D2.4 INTERACTION SURFACES (CONT'D)

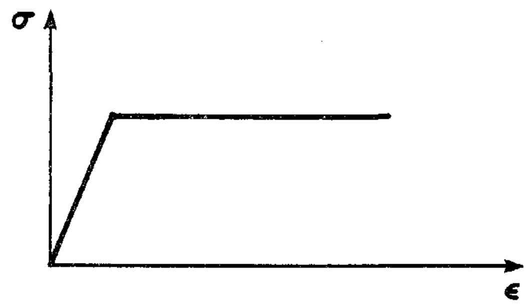

(a) ELASTIC-PLASTIC STRESS-STRAIN RELATIONSHIP

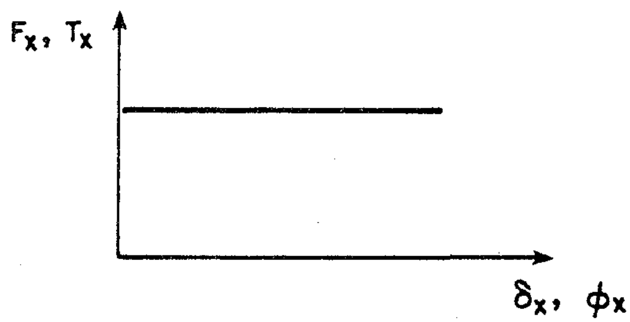

(b) FORCE-EXTENSION AND TORQUE-TWIST

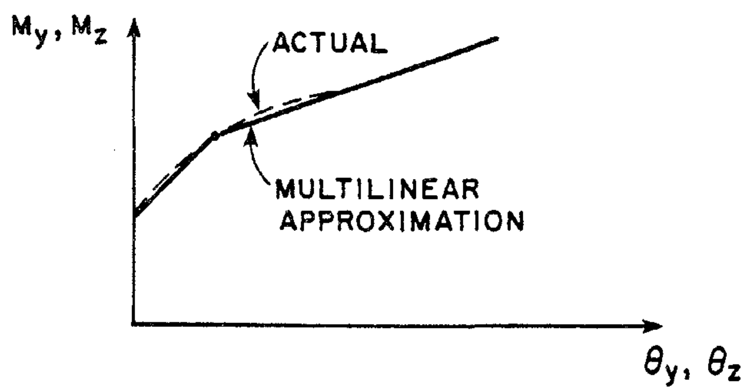

(c) MOMENT-CURVATURE

FIG. D2.5 DIFFERENCES IN SHAPES OF RELATIONSHIPS

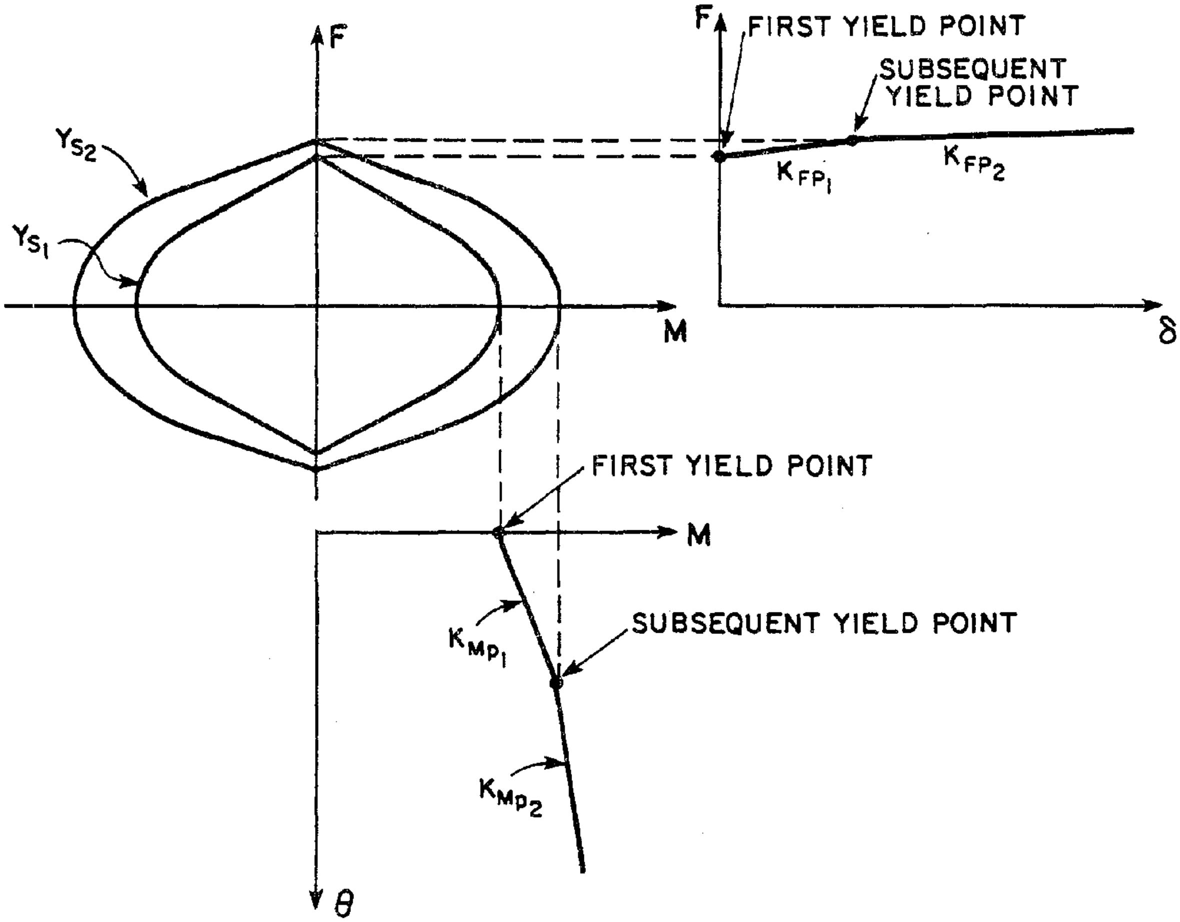

(a) INITIAL LOCATIONS OF SURFACES

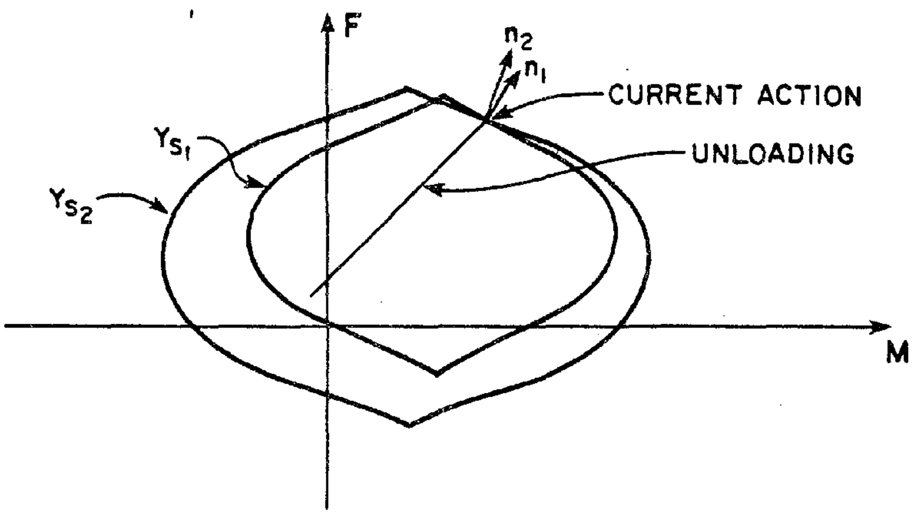

(b) DISPLACED SURFACES AFTER HARDENING

FIG. D2.6 STRAIN HARDENING BEHAVIOR

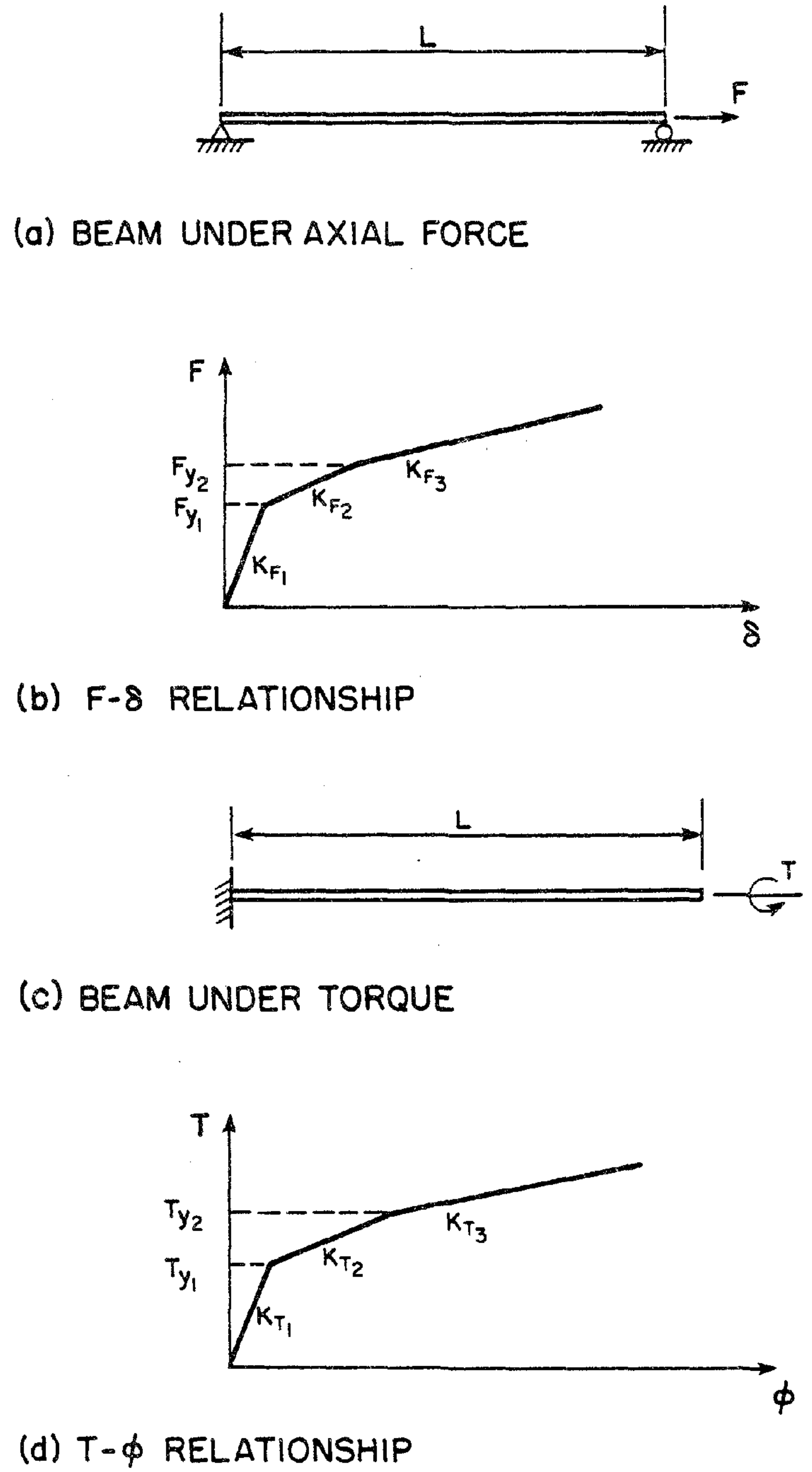

FIG. D2.7 FORCE-EXTENSION AND TORQUE-TWIST RELATIONSHIPS

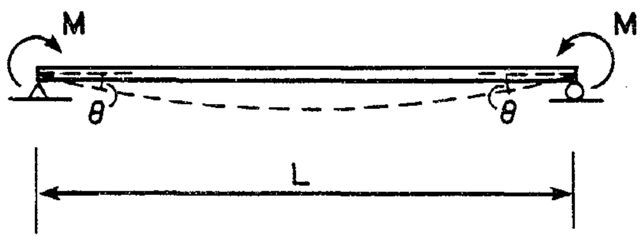

(a) BEAM WITH CONSTANT MOMENT

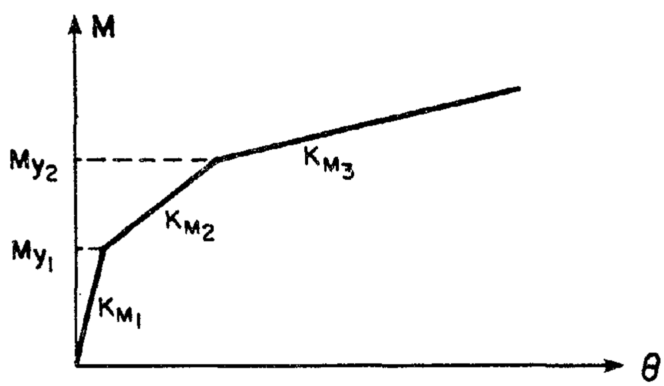

(b) MOMENT-ROTATION RELATIONSHIP

FIG. D2.8 MOMENT-ROTATION RELATIONSHIP

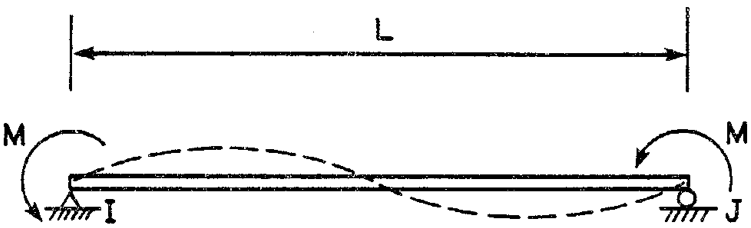

(a) BEAM WITH END MOMENTS

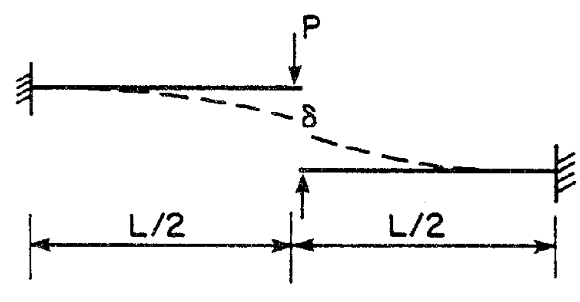

(b) EQUIVALENT CANTILEVERS

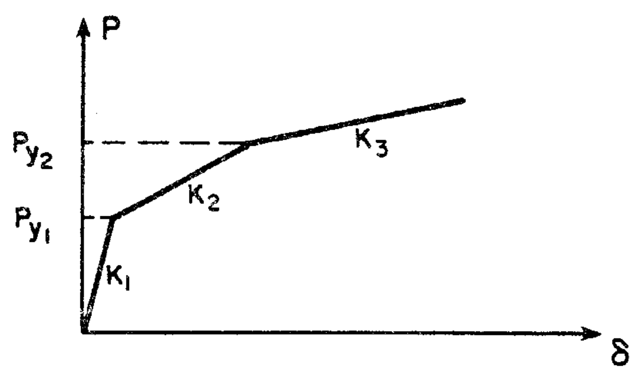

(c) P-δ RELATIONSHIP

FIG. D2.9 REPRESENTATION OF CANTILEVER BEHAVIOR

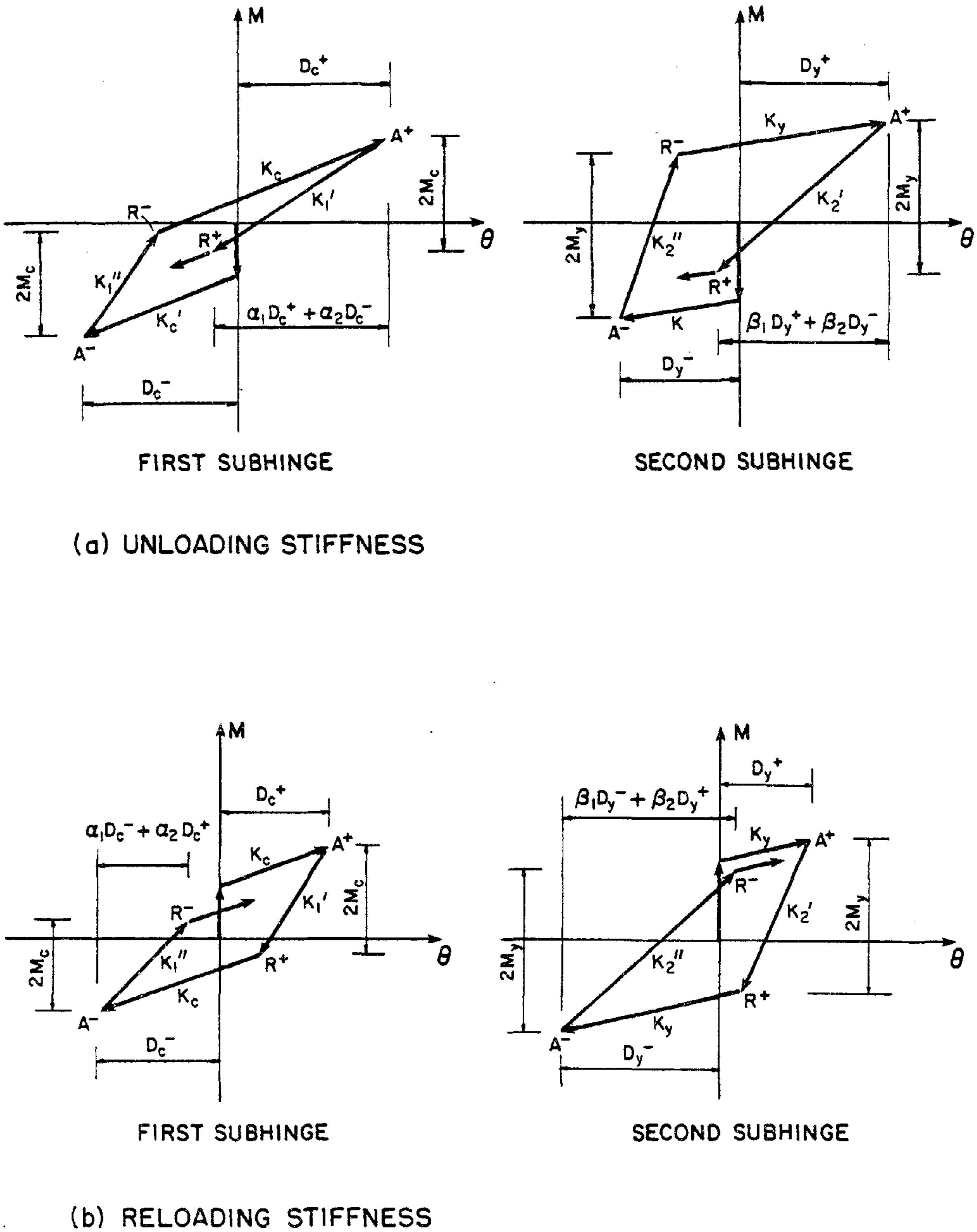

FIG. D2.10 SUBHINGE FORCE-DEFORMATION RELATIONSHIP

$K_1 = K_1' + \frac{x}{a}(K_1'' - K_1')$

$K_2 = K_2' + \frac{x}{a}(K_2'' - K_2')$

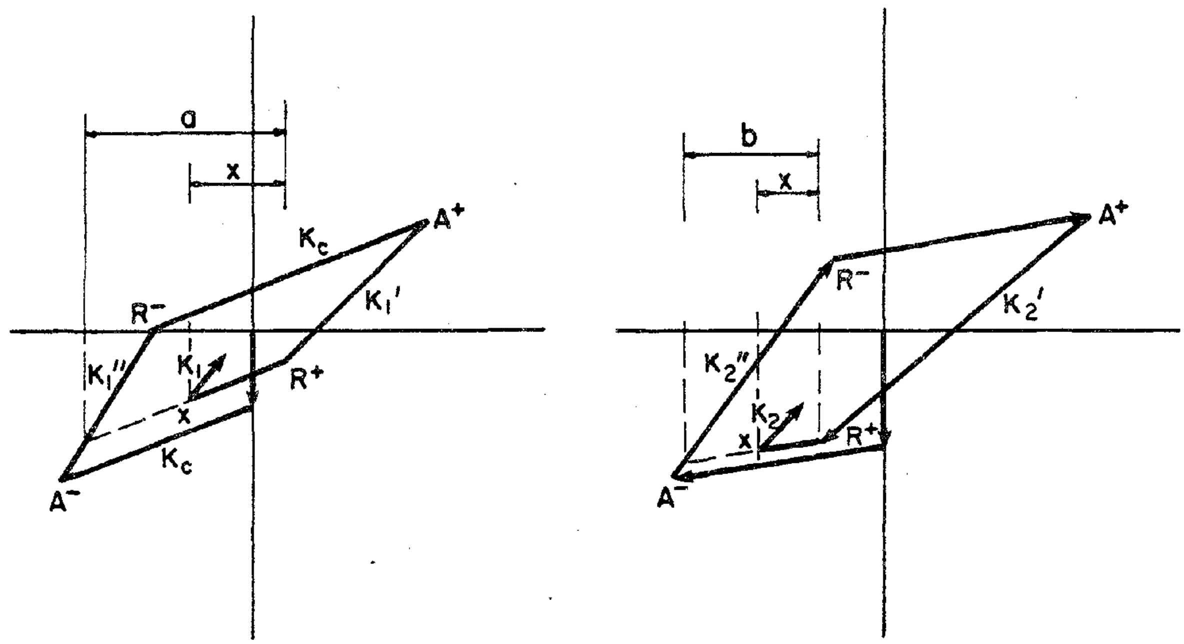

FIRST SUBHINGE

SECOND SUBHINGE

(c) RELOADING AFTER SMALL YIELD EXCURSION

FIG. D2.10 SUBHINGE FORCE-DEFORMATION RELATIONSHIP (CONT'D)

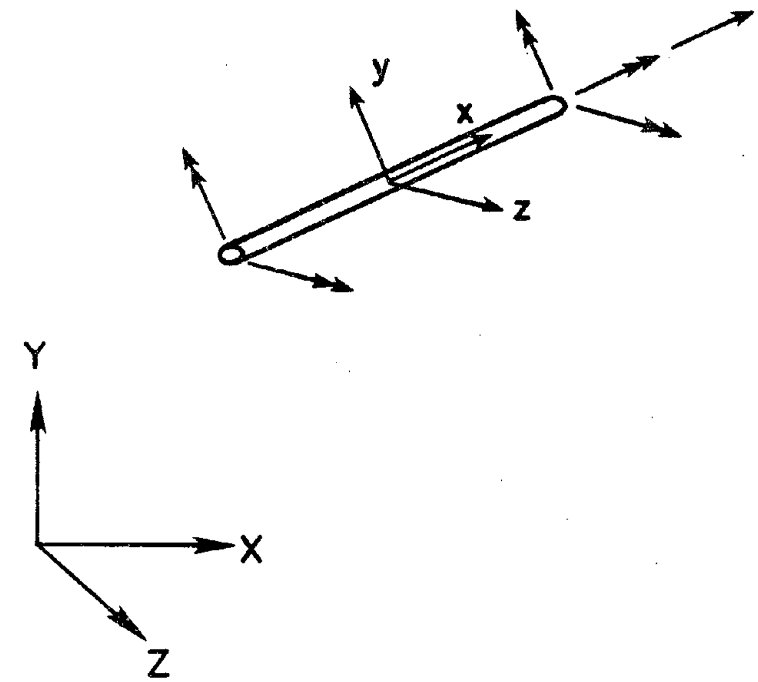

FIG. D2.11 POSITIVE DIRECTION OF INITIAL ELEMENT ACTIONS

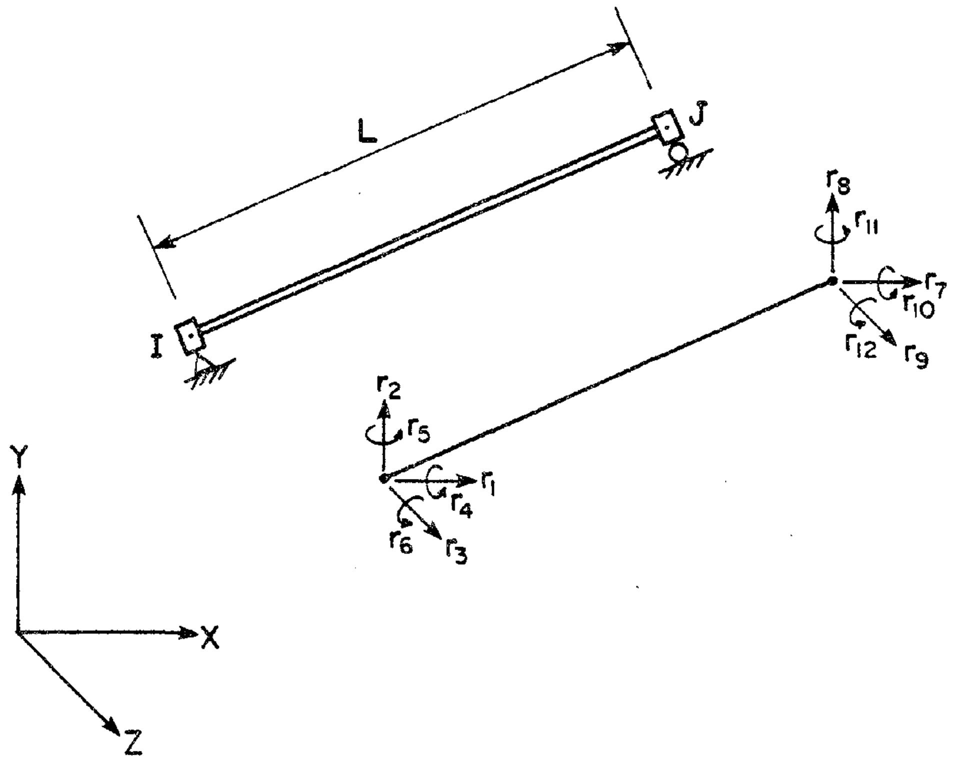

(a) GLOBAL DISPLACEMENTS

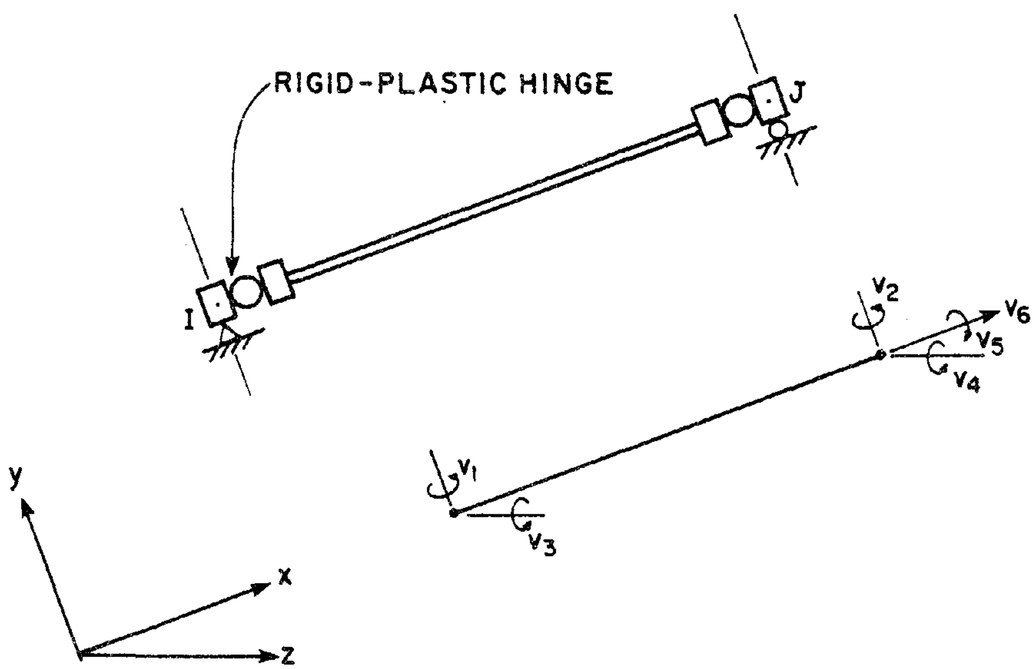

(b) LOCAL DEFORMATIONS

FIG. D3.1 ELEMENT DEGREES OF FREEDOM

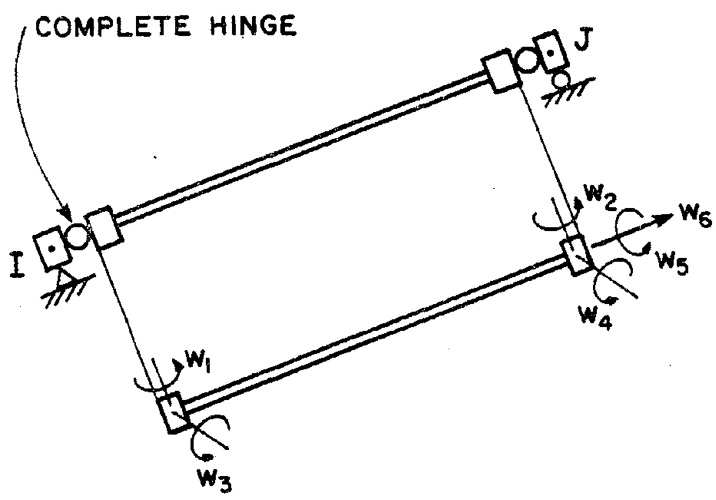

(a) INTERNAL DEGREES OF FREEDOM

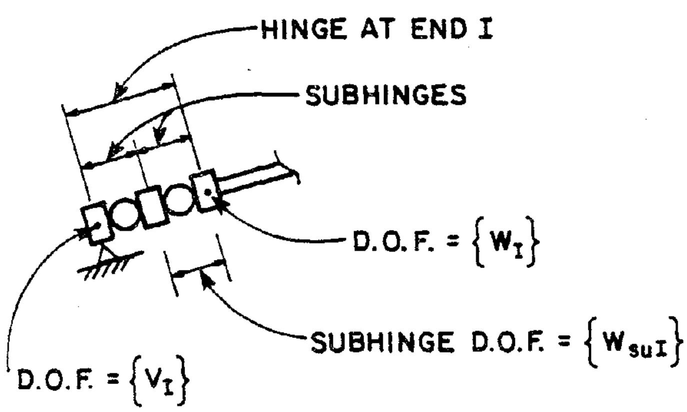

(b) HINGE AND SUBHINGES AT END I

FIG. D3.2 INTERNAL DEGREES OF FREEDOM

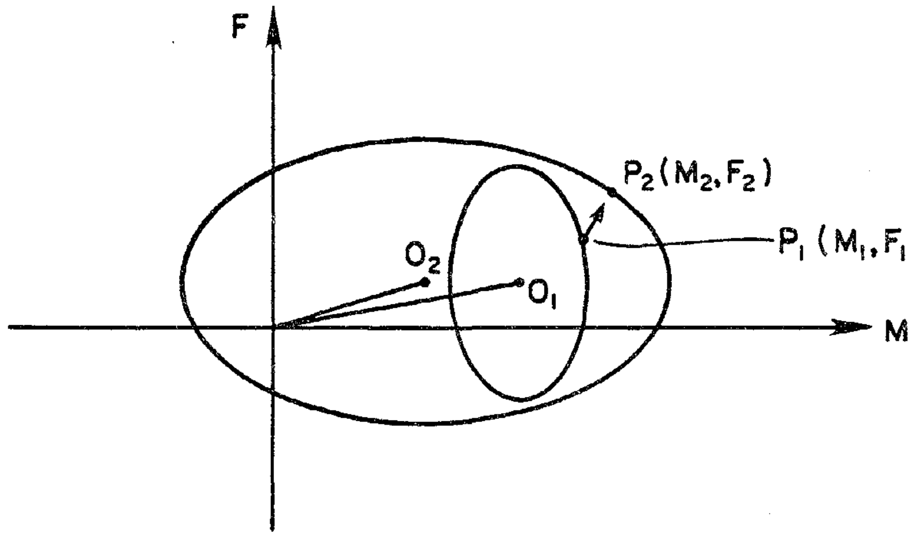

(a) YIELD SURFACES IN F-M SPACE

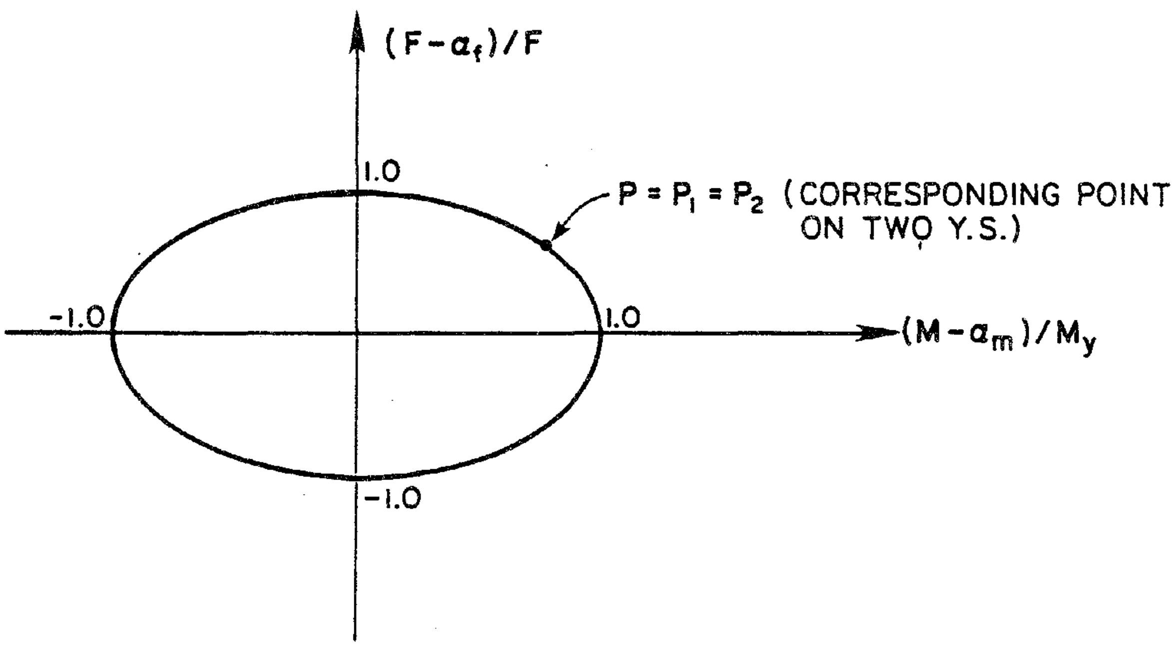

(b) YIELD SURFACES IN NORMALIZED SPACE

FIG. D3.3 MODIFIED MROZ HARDENING RULE

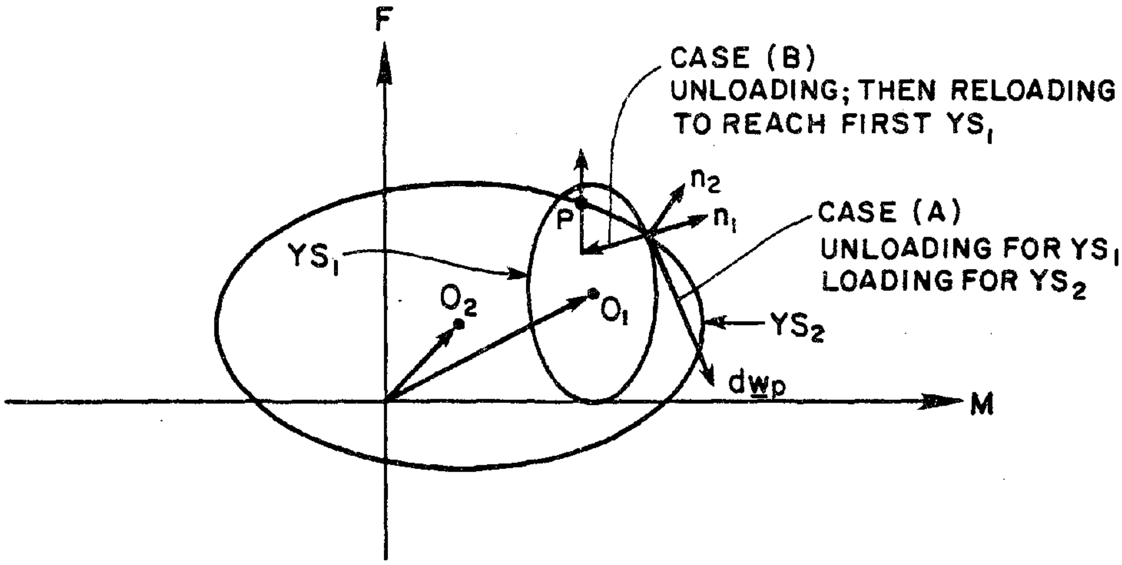

FIG. D3.4 LOADING/UNLOADING CRITERION

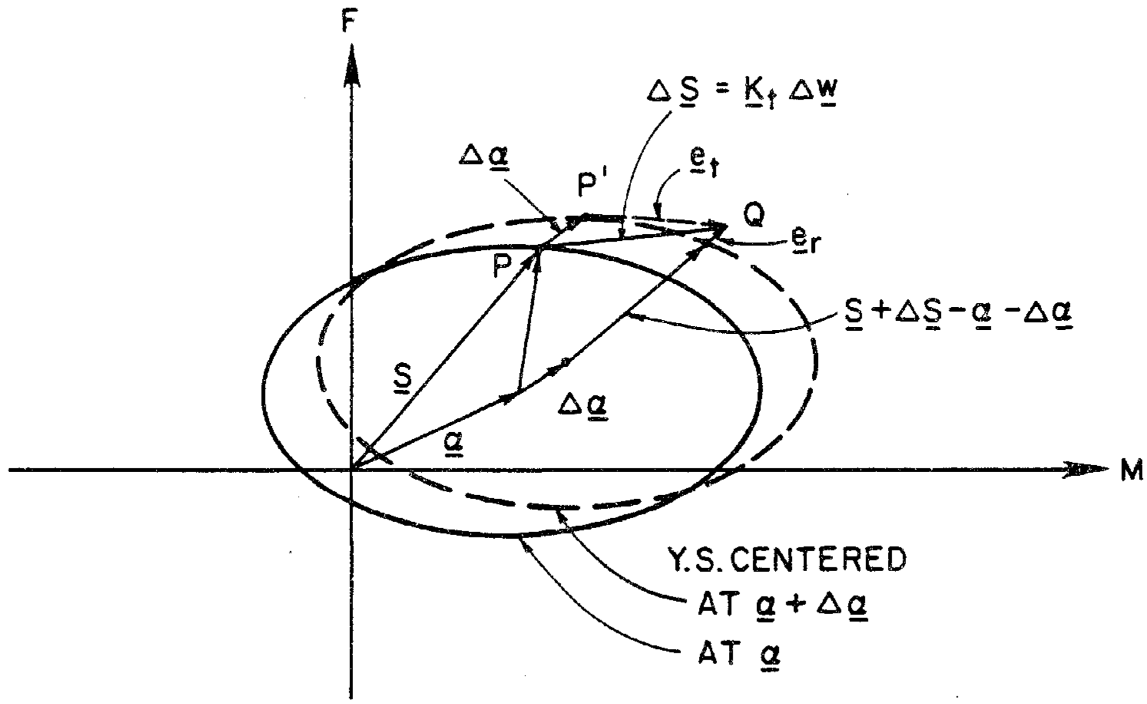

FIG. D4.1 ERROR CONTROL FOR STATE DETERMINATION

E. EXAMPLES

E1. TUBULAR STEEL BRACE AND BRACED FRAME

E1.1 PURPOSE OF ANALYSIS

A number of experimental and analytical studies on the inelastic behavior of diagonal braces and braced structures have been carried out over the past few years. Using the results of these studies in conjunction with advancements in nonlinear analysis techniques, analytical models for predicting the behavior of braces and braced frames in the inelastic range have been proposed and applied. The reliability of predictions of the overall structural behavior depends on the accuracy of the brace model used. An ideal brace model is one having the capability to describe axial force-deformation hysteresis loops accounting for the interaction between axial force and bending moment on a tubular section and accounting for loss of load capacity under repeated cyclic loading.

In this example, the element with distributed plasticity and nondegrading stiffness is used to determine whether it produces results in agreement with experimental results for the inelastic response of a single brace and a complete braced frame. The experimental studies were performed by Zayas, Mahin and Popov [19,20] at the University of California, using one-sixth scale models of elements typically found in X-braced tubular steel offshore platforms.

E1.2 INELASTIC BUCKLING OF TUBULAR STEEL BRACE

E1.2.1 Assumptions for Analysis

One-half of the tubular specimen (accounting for symmetry) was modeled using five elements. The experimental stress-strain curve [19] was used to calculate moment-curvature and force-strain relationships, which were then approximated by piecewise linear functions. The details of the analysis model are contained in Table E1.1, which is a listing of the ANSR-II input data for the analysis.

E1.2.2 Comparison of Analysis and Experiment

The response of the strut is shown in Figs. E1.1 and E1.2 for the experiment and analysis, respectively. The overall responses are similar, but the analysis predicts substantially less stiffness and strength degradation than the experiment. The area of a typical hysteresis loop on the analysis is approximately 16% more than in the experiment. That is, the analytical model tends to overestimate the energy dissipation by about 16%. A major weakness of the analytical model is that is does not predict progressive degradation of the buckling load with inelastic cycling. This is probably because the analytical model does not account adequately for the Bauschinger effect, and hence, overestimates the material tangent modulus. A second possible effect is that the model is unable to capture the effects of local buckling in the pipe wall which were noted in the tests for the later cycles.

E1.3 INELASTIC BEHAVIOR OF TUBULAR STEEL BRACED FRAME

E1.3.1 Test Configuration

Experimental results of one-sixth scale model of an X-braced tubular steel frame have been reported by Zayas, Mahin and Popov [20]. The test configuration is shown in Fig. E1.3. The frame was subjected to cyclic inelastic lateral displacements, simulating severe seismic motions. The frame was designed [20] so that failure would be controlled by yielding and buckling of the diagonal braces.

E1.3.2 Assumptions for Analysis

The analytical model is shown in Fig. E1.4. The ANSR-II input data is listed in Table E1.2. The diagonal braces were modeled using the distributed plasticity element, with nondegrading stiffness. The horizontal and vertical members were modeled using elastic beam-column elements because the frame was designed to limit the forces in these members to be below yield. Multi-linear approximations of the moment-curvature and force-strain relationships were deduced from the experimental stress-strain curves.

Cyclic displacements were imposed at the top level of the analytical model to match those imposed in the experiments. A step-by-step procedure, without iteration and with path dependent state determination, was used to analyze the frame.

E1.3.3 Comparison of Analytical and Experimental Results

The typical experimental and analytical results are shown in Figs. E1.5 and E1.6. The shapes of the hysteresis loops are basically similar for the analysis and experiment, but again the analysis shows less degradation and the loops for the analysis are significantly "fatter" than for the experiment. The analytical model thus tends to overestimate the energy dissipation.

E1.4 CONCLUSIONS

The reliability of analytical predictions of the inelastic structural behavior of braced offshore towers depends to a large extent on the accuracy which the brace hysteretic behavior can be modeled. The "section" type of model considered here is able to model certain important features of brace behavior, in particular compressive post-buckling strength loss and tensile yield. However, the model does not adequately account for stiffness and strength degradation, so that it tends to overestimate both the strength and the amount of energy absorption. The model must thus be improved to account for degradation effects before it can be used reliably for this type of structure.

E2. DEGRADATION COEFFICIENTS FOR REINFORCED CONCRETE

E2.1 GENERAL

In the beam-column element with degrading stiffness, the hinge stiffnesses are degraded when reversed loading is applied. The amount of degradation is controlled by the four degradation coefficients α_1, α_2, β_1, and β_2. To study the influence of these coefficients on element behavior, a study has been carried out using experimental data obtained by Takizawa and Aoyama [10] at the University of Tokyo.

The primary purpose of this study has been to devise a procedure for calculation of the degradation coefficients and to determine whether this procedure can be used to obtain accurate response predictions. For this purpose, it has been assumed that the stiffness for each separate action component degrades independently of the other stiffness (i.e. no interaction effects for stiffness degradation). A secondary purpose has been to perform a preliminary investigation of the effects of stiffness interaction, with a view to establishing a computational technique.

E2.2 SELECTION OF DEGRADATION COEFFICIENTS

A practical means of specifying the stiffness degradation coefficients is as follows. From an experiment involving only one of the element actions (e.g. a uniaxial bending test), obtain the action-deformation relationship for two or three loading cycles. From these results, sketch an idealized trilinear hysteresis loop that best fits the experimental results for each cycle. From this idealization, obtain the positive force P^+, the negative force P^-, stiffnesses K_1, K_2, and K_3, and degraded stiffnesses $t_{11}K_1$, $t_{12}K_2$, $t_{21}K_1$, and $t_{22}K_2$, as shown in Fig. E2.1.

The following equations express the relationships among the original stiffnesses, K_1, K_2, and K_3; the degrading stiffnesses, $t_{11}K_1$, $t_{12}K_2$, $t_{21}K_1$, and $t_{22}K_2$; the plastic stiffness K_c and degrading stiffnesses K'_1 and K''_1 of the cracking (first) subhinge; and the plastic stiffness K_y and degrading stiffnesses K'_2 and K''_2 of the yielding (second) subhinge:

$$\frac{1}{t_{11}K_1} = \frac{1}{K_1} + \frac{1}{K'_1} + \frac{1}{K'_2} \qquad \text{(E2.1a)}$$

Preceding page blank

$$\frac{1}{t_{12}K_2} = \frac{1}{K_1} + \frac{1}{K_c} + \frac{1}{K'_2} \qquad \text{(E2.1b)}$$

$$\frac{1}{t_{21}K_1} = \frac{1}{K_1} + \frac{1}{K''_1} + \frac{1}{K''_2} \qquad \text{(E2.1c)}$$

$$\frac{1}{t_{22}K_2} = \frac{1}{K_1} + \frac{1}{K_c} + \frac{1}{K''_2} \qquad \text{(E2.1d)}$$

The maximum positive plastic deformations, D_c^+ of the cracking subhinge and D_y^+ of the yielding subhinge, are related to: (a) the force p^+; (b) P_y and K_y of the yielding subhinge; and (c) the total plastic deformation D_t^+, as follows:

$$D_y^+ = \frac{p^+ - P_y}{K_y} \qquad \text{(E2.2a)}$$

$$D_c^+ = D_t^+ - D_y^+ \qquad \text{(E2.2b)}$$

The calculation of the degrading stiffness coefficients then proceeds as follows. From Fig. D2.10(a), for the initial unloading (i.e., $\alpha_2 = \beta_2 = 0$), the coefficients α_1 and β_1 are obtained as:

$$\alpha_1 = \frac{2P_c}{K'_1 D_c^+} \qquad \text{(E2.3a)}$$

$$\beta_1 = \frac{2P_y}{K'_2 D_y^+} \qquad \text{(E2.3b)}$$

Hence, from Eqns. E2.1b and E2.1a, the coefficients α_1 and β_1 follows as:

$$\alpha_1 = \frac{2P_c}{D_c^+}\left[\frac{1}{t_{11}K_1} + \frac{1}{K_c} + \frac{1}{t_{12}K_1}\right] \qquad \text{(E2.4a)}$$

$$\beta_1 = \frac{2P_y}{D_y^+}\left[\frac{1}{t_{12}K_2} - \frac{1}{K_1} - \frac{1}{K_c}\right] \qquad \text{(E2.4b)}$$

From Fig. E2.1, the maximum negative plastic deformations, D_c^- of the cracking hinge and D_y^- of the yielding hinge, are obtained as follows:

$$D_y^- = \frac{P^- - P_y}{K_y} \qquad \text{(E2.5a)}$$

$$D_c^- = D_t^- - D_y \qquad \text{(E2.5b)}$$

Hence, incorporating Fig. D2.10 with Eqns. E2.1c and E2.1d, the coefficients α_2 and β_2 are obtained from:

$$\alpha_2 = \frac{2P_c/K''_1 - \alpha_2 D_c^-}{D_c^+} \qquad \text{(E2.6a)}$$

$$\beta_2 = \frac{2P_y/K''_2 - \beta_1 D_y^-}{D_y^+} \tag{E2.6b}$$

and

$$\alpha_2 = \left[2P_c\left(\frac{1}{t_{21}K_1} + \frac{1}{K_c} - \frac{1}{t_{22}K_2}\right) - \alpha_1 D_c^-\right]/D_c^+ \tag{2.7a}$$

$$\beta_2 = \left[2P_y\left(\frac{1}{t_{22}K_2} - \frac{1}{K_1} - \frac{1}{K_c}\right) - \beta_1 D_y^-\right]/D_y^+ \tag{2.7b}$$

These calculations give values of α_i and β_i for each of the loops. The values for successive loops should not be greatly different from each other. Values for analysis are obtained by averaging the values for the individual loops.

E2.3 COMPARISON OF EXPERIMENT AND THEORY

A reinforced concrete cantilever under biaxial bending has been studied experimentally and theoretically by Takizawa and Aoyama [10]. Figure E2.2 shows the dimensions of the test specimen. Loading was imposed to produce predetermined displacement paths in the x and y directions at the cantilever tip. Five different paths were considered, as shown in Fig. E2.3.

E2.3.1 Calculation of Degradation Coefficients

Test specimen 1 of the experiment was subjected to uniaxial bending. The results of this test have been used to define values of the degradation coefficients α_i and β_i. These values have been then used for analysis of all five specimens. The calculation of the degrading stiffness coefficients proceeds as follows.

(a) An idealized trilinear hysteresis loop for the first loading cycle is shown in Fig. E2.1a. By measurement from the figure:

$D_t^+ = 0.85$ $\quad D_t^- = 0.83$ $\quad$ (centimeters)
$P_c = 3.0$ $\quad P_y = 4.5$ $\quad$ (metric tons)
$P^+ = 4.75$ $\quad P^- = 4.8$
$K_1 = 22.0$ $\quad K_2 = 7.0$ $\quad K_3 = 0.4$ $\quad$ (tons/cm.)
$t_{11}K_1 = 7.7$ $\quad t_{12}K_2 = 5.4$ $\quad t_{21}K_1 = 7.6$ $\quad t_{22}K_2 = 4.3$

Hence,

$$K_c = \frac{K_1 K_2}{K_1 - K_2} = \frac{22.0x7.0}{22.0-7.0} = 10.27$$

$$K_y = \frac{K_2 K_3}{K_2 - K_3} = \frac{7.0x0.4}{7.0-0.4} = 0.42$$

From Eqns. E2.2a and E2.2b:

$$D_y^+ = \frac{P^+ - P_y}{K_y} = \frac{4.75-4.5}{0.42} = 0.6$$

$$D_c^+ = D_t^+ - D_c^+ = 0.85 - 0.6 = 0.25$$

Then, from Eqns. E2.3:

$$\beta_1 = \frac{2P_y}{D_y^+}\left[\frac{1}{t_{12}K_2} - \frac{1}{K_1} - \frac{1}{K_c}\right] = \frac{9.0}{0.5}\left[\frac{1}{5.4} - \frac{1}{22.0} - \frac{1}{10.27}\right] = 0.76$$

$$\alpha_1 = \frac{2P_c}{D_c^+}\left[\frac{1}{t_{11}K_1} + \frac{1}{K_c} - \frac{1}{t_{12}K_2}\right] = \frac{6.0}{0.25}\left[\frac{1}{7.7} + \frac{1}{10.27} - \frac{1}{5.4}\right] = 1.0$$

From Eqns. E2.4:

$$D_y^- = \frac{P^- - P_y}{K_y} = \frac{4.8 - 4.5}{0.42} = 0.95$$

$$D_c^- = D_t^- - P_y^- = 0.83 - 0.95 = -0.12$$

Then, from Eqns. E2.6:

$$\beta_2 = \left[2P_y\left(\frac{1}{t_{22}K_2} - \frac{1}{K_1} - \frac{1}{K_c}\right) - \beta_1 D_y^-\right]/D_y^+$$

$$= \left[9.0 \times \left(\frac{1}{4.3} - \frac{1}{22.0} - \frac{1}{10.27}\right) - 0.76 \times 0.95\right]/0.6 = 0.14$$

$$\alpha_2 = \left[2P_c\left(\frac{1}{t_{21}K_1} + \frac{1}{K_c} - \frac{1}{t_{22}K_2}\right) - \alpha_1 D_c^-\right]/D_c^+$$

$$= \left[6.0 \times \left(\frac{1}{7.6} + \frac{1}{10.27} - \frac{1}{4.3}\right) + 0.12\right]/0.25 = 0.39$$

Thus,

$$\alpha_1 = 1.0, \quad \alpha_2 = 0.4, \quad \beta_1 = 0.75, \quad \text{and} \quad \beta_2 = 0.15$$

(b) An idealized loop for the second loading cycle is shown in Fig. E2.1b. By measurement from the sketch:

$$D_t^+ = 1.3 \qquad D_t^- = 1.05$$

$P_c = 3.0 \qquad P_y = 4.5$

$P^+ = 4.91 \qquad P^- = 5.06$

$t_{11}K_1 = 6.0 \qquad t_{12}K_2 = 4.73 \qquad t_{21}K_1 = 5.66 \qquad t_{22}K_2 = 3.64$

Hence, by the same procedure as for the first cycle, obtain:

$\alpha_1 = 1.0, \quad \alpha_2 = 0.4, \quad \beta_1 = 0.65, \quad$ and $\beta_2 = 0.45$

(c) Obtain values for analysis as the average values from the two loops. That is,

$\alpha_1 = 1.0, \quad \alpha_2 = 0.4, \quad \beta_1 = 0.7, \quad$ and $\beta_2 = 0.3$

E2.3.2 Lower Bound on Unloading Stiffness

Experience has shown that bounds are needed to prevent ridiculous results from being obtained. If results are available, lower bound values can be obtained from experimental results with large displacement cycling. In this example, judgement was required because the imposed displacements for test specimen 1 were not of large amplitude. Bounds as follows were specified for the cracking and yielding subhinges.

$$Min.\ K_c = 2 * K_{co} \tag{E2.8a}$$

$$Min.\ K_y = 2 * K_{yo} \tag{E2.8b}$$

in which

K_{co} = plastic stiffness before degradation of the cracking subhinge; and

K_{yo} = plastic stiffness before degradation of the yielding subhinge.

E2.3.3 Comparison of Experiment and Analysis

To compare the measured and calculated results, the deflection paths in the analysis were specified to correspond to the deflection paths observed in the experiments, as shown by the dashed lines in Fig. E2.3. Comparisons of the load-deflection curves for each case are shown in Figs. E2.4 through E2.11. In addition, comparisons of the force-path orbits for cases 3 and 4 are shown in Figs. E2.12 and E2.13.

The calculated and experimental results are encouragingly close, especially considering the complexity of the response. Nevertheless, there are substantial differences in the shapes of the response curves. The discrepancies are largest for specimens 3 and 4. The force-paths in Figs. E2.12 and E2.13 are substantially different, with the analysis following the circular form of the yield surface and the experiment following straighter lines. Also, the hysteresis loops from the analysis are too "fat" for specimen 3. It may be noted that the results are comparable in accuracy to the analytical results of Takizawa and Aoyama [10].

A possible reason for the discrepancies could be that degradation of stiffness in the x and y directions was assumed to be uncoupled. A further reason, as mentioned in Takizawa's report, could be that the loading in the experiment did not provide ideal deflection control. Fairly large deviations from the planned displacement paths occurred in the experiments.

E2.4 INVESTIGATION OF STIFFNESS COUPLING

As was noted in the preceding section, the hysteresis loops for specimen 3 were too fat in comparison with the experimental results. This discrepancy could result from ignoring coupling in stiffness degradation between the x and y directions. To investigate this phenomenon, a coupling option has been included in the computer program, and a preliminary study has been carried out.

For each hinge, it is assumed that the degrading stiffness is based not only on the maximum positive and negative plastic deformation in the direction of loading, but also on the maximum positive and negative plastic deformations in the direction at right angles. The procedure is as follows.

The diagonal flexibility matrix, $\underline{F}_d$, of a subhinge can be expressed in the following manner:

$$\underline{F}_d = diag\,[F_{d1} \;\; F_{d2} \;\; F_{d3} \;\; F_{d4}] \tag{E2.9}$$

in which

$$\begin{aligned}
F_{d1} &= (\alpha_{1y} D_y^+ + \alpha_{2y} D_y^- + \alpha_{12y}(D_z^+ + D_z^-))/2M_{yu} \\
F_{d2} &= (\alpha_{1z} D_z^+ + \alpha_{2z} D_z^- + \alpha_{12z}(D_y^+ + D_y^-))/2M_{zu} \\
F_{d3} &= (\alpha_{1T} D_T^+ + \alpha_{2T} D_T^-)/2T_u \\
F_{d4} &= (\alpha_{1F} D_F^+ + \alpha_{2F} D_F^-)/2F_u
\end{aligned}$$

and where

α_{1y}, α_{1y} = degradation coefficients α_1, α_2 for y bending;

α_{1z}, α_{2z} = coefficients for z bending;

α_{1T}, α_{2T} = coefficient for twist;

α_{1F}, α_{2F} = coefficient for axial deformation;

$\alpha_{ij} (i \neq j)$ = degradation coupling coefficient;

D_y^+, D_y^- = maximum positive and negative y plastic rotation;

D_z^+, D_z^- = z plastic rotation;

D_T^+, D_T^- = plastic torsional rotation; and

D_F^+, D_F^- = plastic axial deformation.

Hence, the degraded stiffness matrix, $\underline{K}_d$, is:

$$\underline{K}_d = diag\,[1/F_{d1} \;\; 1/F_{d2} \;\; 1/F_{d3} \;\; 1/F_{d4}] \tag{E2.10}$$

For analysis of the test specimens, the degradation coupling coefficients were arbitrarily assumed to be $\alpha_{12} = 1/10(\alpha_1 + \alpha_2)$ and $\beta_{12} = 1/10(\beta_1 + \beta_2)$. The results of analyses with these assumed values are shown in Figs. E2.14 to E2.16.

The analysis results show significantly better agreement with the experiment than those without stiffness degradation coupling. However, because of the complexity of the physical phenomena governing stiffness degradation coupling, there exists no obvious theory to aid in choosing the coupling coefficients, and substantial further study is needed.

The study suggests that the influence of stiffness degradation coupling is substantial. However, at present, experience and judgement provide the only means for choosing the coupling coefficients.

E3. 3D REINFORCED CONCRETE FRAME

E3.1 GENERAL

A simple 3D building frame of reinforced concrete has been studied experimentally and analytically by Oliva [21]. The frame has two stories, with one bay in each direction (Fig. E3.1). It was tested under uniaxial ground motion, but the frame was inclined in plan so that the motion produced biaxial response.

Several tests were performed, with progressively increasing ground motion intensity. Using the degrading stiffness element, analyses have been performed for two of these motions, namely a low amplitude motion ("T100" of [21], Fig. E3.2) and a high amplitude motion ("T1000" of [21], Fig. E3.3). Elastic behavior was assumed for the T100 motion, and inelastic behavior with degradation for the T1000 motion. The stiffness degradation coefficients were varied for the inelastic analyses to study their influence on the computed response.

E3.2 ASSUMPTIONS FOR ANALYSIS

The model used to analyze the frame is shown in Fig. E3.4. Nodes were placed at the points where the column centerlines intersect with the uncracked neutral axes of the beams. Short rigid connections were specified from the nodes to the beam and column faces to simulate rigid joint regions. Lumped masses were located at the centers of mass of the concrete blocks and connected to the beams by stiff truss members. Rotational inertia of the concrete blocks was not considered. The floor diaphragms were modeled using stiff truss members, and the pitching stiffness of the shaking table was modeled by a set of vertical springs.

For all analyses, uniaxial horizontal table motion was applied (Fig. E3.1a). Gravity load was ignored, and small displacements were assumed (no $P-\Delta$ effect).

E3.3 ELASTIC ANALYSIS

The analytical model for correlation of "elastic" response (i.e. small amplitude loading) was as shown in Fig. E3.4. The ANSR-II input data for the analysis is listed in Table E3.1.

Preceding page blank

Because the amplitude of motion during the test was small, the pitching motion of the shaking table was assumed to be negligible and the supporting springs were assumed to be rigid. The stiffness properties for the structural members were the same as those used by Oliva [21]. To ensure elastic behavior, the members were assigned very high strengths. Mass proportional and initial stiffness proportional damping (α M + β_o K_o) was used, assuming 4% critical damping at 3.5 Hz (first natural frequency as given by ref. [21]), and 3% at 8.5 Hz (second natural frequency). The imposed horizontal accelerogram is shown in Fig. E3.2. The integration time step was 0.02 seconds.

Figures E3.5 and E3.6 show time histories of the measured and computed horizontal displacements at the first floor. Close correlation was obtained for both the longitudinal and transverse directions. Previous experience has shown that if agreement between analysis and experiment is to be obtained for inelastic response, agreement must first be obtained for elastic response.

E3.4 INELASTIC ANALYSIS

E3.4.1 Analysis Model

For inelastic analysis, the analytical model was again as shown in Fig. E3.4. The supporting springs for modeling table pitching were assigned stiffnesses of 150 k/in. each, corresponding to a table rotational stiffness of 21640 in-k/rad. [21]. The action-deformation relationships for axial force and moment (monotonic loading) were obtained from cross section analyses performed by Oliva [21]. Insufficient experimental data was available for direct determination of the stiffness degradation coefficients. Hence, a limited parameter study has been carried out to determine the trend in the computed response as the degradation coefficients are changed.

E3.4.2 Parameter Study

Four cases were analyzed, as follows.

Case 1:

No degradation (coefficients α_1, α_2, β_1, and β_2 all zero), with viscous damping as for the elastic analysis.

Case 2:

No degradation, with increased viscous damping. Because the assumed viscous damping is based on the original stiffness, it is possible that the viscous energy absorption can be overestimated when the structure yields and/or degrades. To study this, the damping coefficients, α and β_o, were made ten times larger than for Case 1.

Case 3:

Large degradation coefficients, $\alpha_1 = 1.0$ and $\alpha_2 = 0.9$, were specified for the cracking hinges, and zero values for the yielding hinges. The experimental results [21] showed that the column actions never exceeded the assumed second yield point for column section, so that the values of β_1 and β_2 have no effect on the response. Viscous damping was the same as for Case 1.

Case 4:

Moderate degradation. The same values for coefficients α_1 and α_2 as those of Section E2 ($\alpha_1 = 1.0, \alpha_2 = 0.4$) were used for the cracking hinge, with zero values of β_1 and β_2 for the yielding hinge. Viscous damping was the same as for Case 1.

The solution strategy was step-by-step without iteration, using path dependent state determination and a constant integration time step of 0.005 seconds.

E3.4.3 Comparison of Analytical and Experimental Results

Comparisons of the results from analysis and experiment are shown in Figs. E3.7 and E3.8 for Case 1. The analytical results are not close to those obtained in the experiment, the former having smaller amplitudes and higher frequencies for both the x and y responses.

The results for Case 2 are shown in Figs. E3.9 and E3.10. The analytical results again deviate from the experimental results. The analytical results for Case 2 are very similar to those for Case 1, except that larger drifts are calculated towards the end of the response in Case 1. This result indicates that the effects of the assumed viscous damping are not large.

Figures E3.11 and E3.12 show the results for Case 3. It can be seen that the analysis predicts a larger amplitude response than was observed in the experiment, indicating that too much stiffness degradation was assumed in the analytical model. The analysis predicted substantial drift in the y component of response.

Figures E3.13 and E3.14 show the results for Case 4. The responses agree quite closely for the x direction response, both in period and amplitude. The y direction responses agree less well, but are nevertheless close considering the complexity of the problem. The agreement is significantly closer than that obtained by Oliva [21], which ignored the biaxial interaction effects.

E3.5 CONCLUSION

The analyses in this chapter, although limited in scope, suggest that the values of the degradation coefficients α_1 and α_2 should be approximately 1.0 and 0.4, respectively. In Chapter E2, these same values were found to give quite close agreement with the tests of Takizawa and Aoyama. For the analyses in this chapter, the coefficients β_1 and β_2 were not used, because the shaking was not intense enough to exceed the strength of the yielding hinges. If no better information is available, it is suggested that the values $\beta_1 = 0.7$ and $\beta_2 = 0.3$, as found in Chapter E2, be used for dynamic analyses.

E4. LARGE ROTATION PIPE WHIP STUDY

E4.1 GENERAL

The distributed plasticity element can be used to analyze the inelastic whipping motions of piping systems following hypothetical pipe rupture. Small displacement analyses can be used for piping confined by pipe whip restraints, whereas large displacements must be considered for unrestrained pipes. In this example, a high energy pipe system has been analyzed for an assumed break location which permits the piping to move a distance of over five diameters before impacting a very stiff wall. The purpose of the analysis is to predict the impact time and velocity, and to obtain an estimate of the impact force imposed on the wall. The analysis considers material yield, strain rate effects, material nonlinearity, large deflections, gap closure, and variable direction of the jet load (follower force). The analysis was performed using the distributed plasticity element in the computer program WIPS [31].

E4.2 ASSUMPTIONS FOR ANALYSIS

The idealized system is shown in Fig. E4.1. A configuration with similar properties has been analyzed by H. D. Hibbitt and B. I. Karlsson [28] and D. K. Vijay and M. J. Kozluk [38]. For the pipe elements, the stress-strain relationship shown in Fig. E4.2 was used. Force-strain and moment-curvature relationships as shown in Fig. E4.2 were obtained by determining "exact" relationships (using a small special purpose computer program) and constructing trilinear approximations. For the elbow elements, the straight pipe stiffnesses were divided 3.5 (the elbow flexibility factor) and the strengths were multiplied by 0.85 (chosen arbitrarily). Dimensionless damping action versus strain rate relationship was assumed as shown in Fig. 4.3, using yield stress versus strain rate relationship from J. M. Manjoine [32]. The jet force time history was as shown in Fig. E4.1. Because the rotation of the break is large, the blowdown thrust must be considered as a follower force acting along the pipe at all times rather than fixed in direction. Impact with the wall was allowed at nodes 2, 4, 6, and 8. The gaps between these nodes and the wall were modeled using gap elements [31]. The stiffness after gap closure was assumed to be 10000 K/in. This value was chosen arbitrarily to represent a very stiff wall. Because the impact force depends a great deal on the deformability of both the wall and the pipe, the calculated impact forces are unlikely to be accurate. However, the calculated motion of the pipe can be expected to correspond quite closely to the actual motion, both before and after impact. No experimental results are available.

E4.3 DISCUSSION OF ANALYSIS RESULTS

The WIPS analysis was carried out using the Hilber-Hughes-Taylor integration scheme [39] with a numerical damping factor, α, of -0.05. The calculated pipe shapes at three separate times are shown in Fig. E4.4. Figure E4.4 shows the time history of displacement at node 6 and the calculated impact force (the sum of the forces in the four gap elements). The results show a large initial impact force, followed by rebound and new contact. After the second contact, the force transmitted to the wall is of the order of magnitude as the blowdown force.

Analyses with and without strain rate effects were very similar. The calculated time for first contact with the wall was 95 milliseconds for the case with no strain rate effect and 98 milliseconds for the case with strain rate effects, as shown in Fig. E4.5. This result is quite similar to that obtained by H. D. Hibbitt and B. I. Karlsson [28].

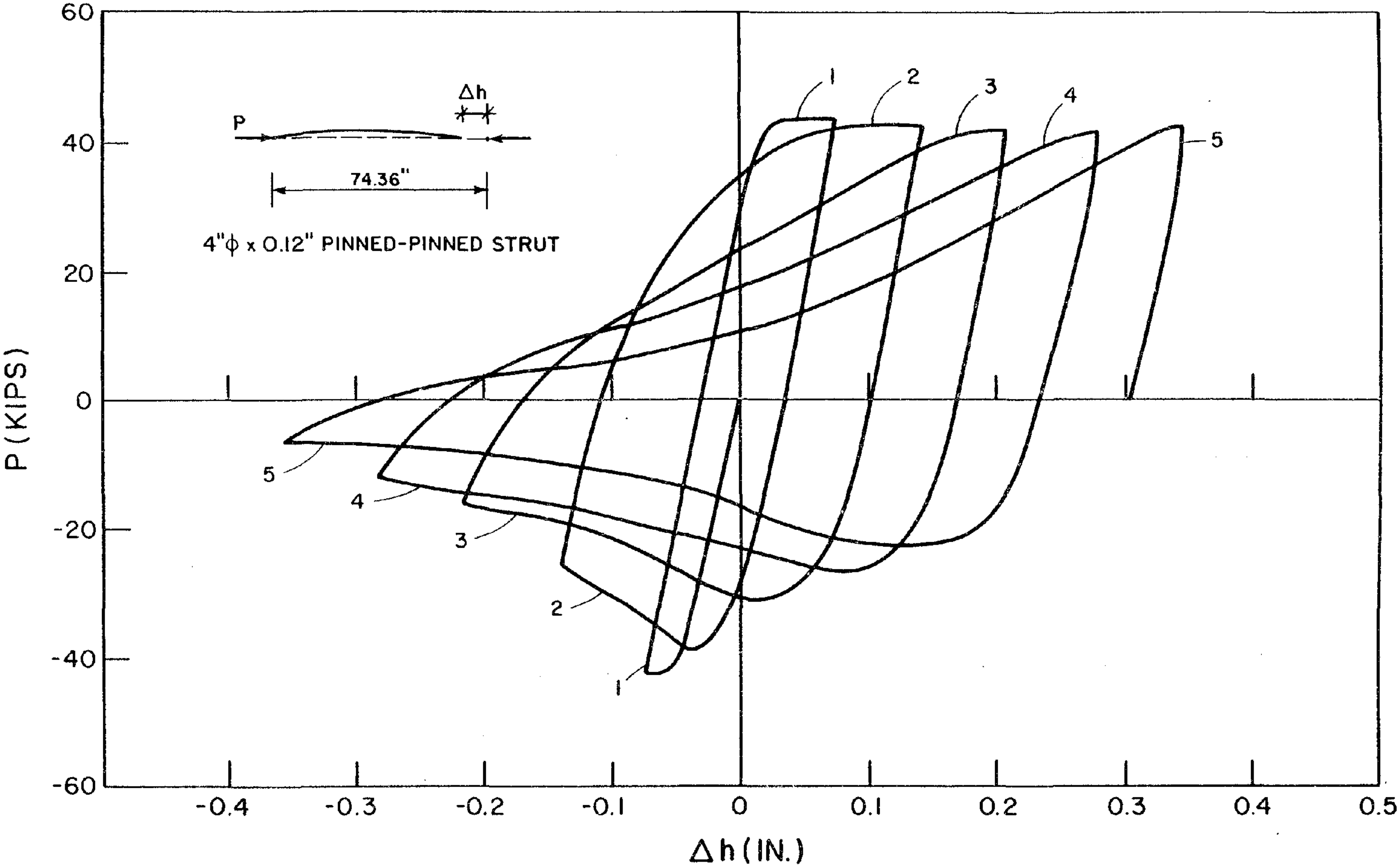

FIG. E1.1 AXIAL LOAD VS. AXIAL DISPLACEMENT. EXPERIMENT.

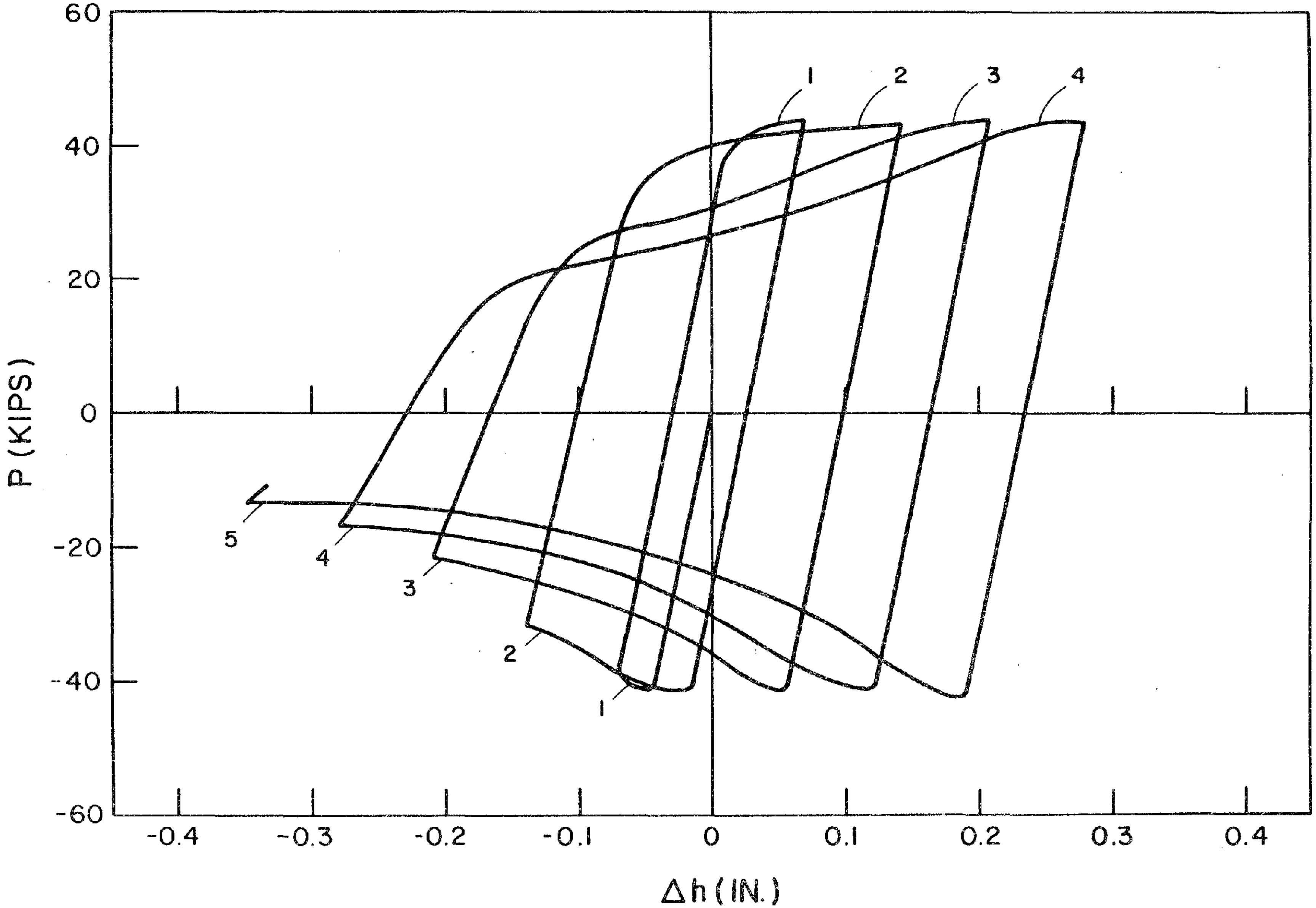

FIG. E1.2 AXIAL LOAD VS. AXIAL DISPLACEMENT. ANALYSIS.

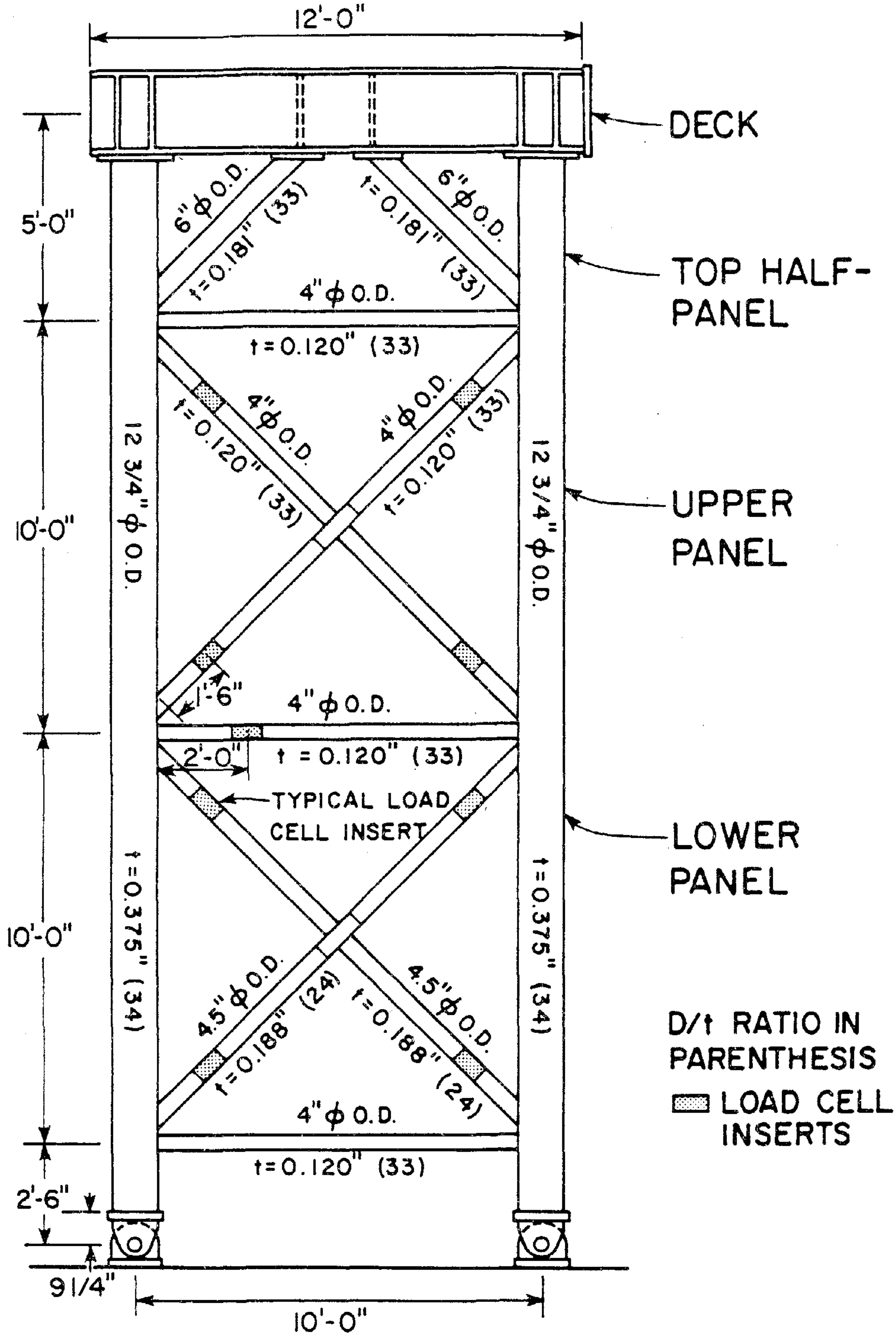

FIG. E1.3 TEST CONFIGURATION (FROM [20])

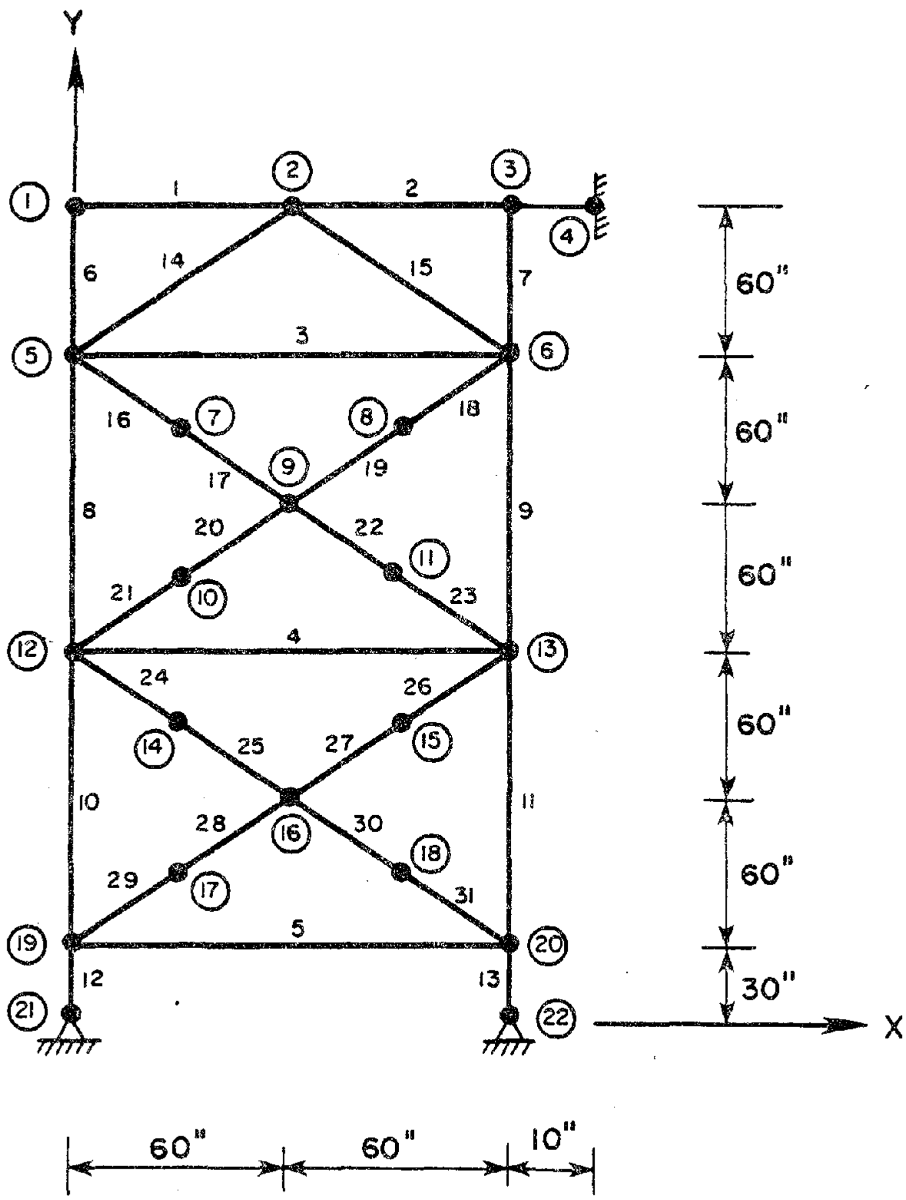

FIG. E1.4 ANALYTICAL MODEL

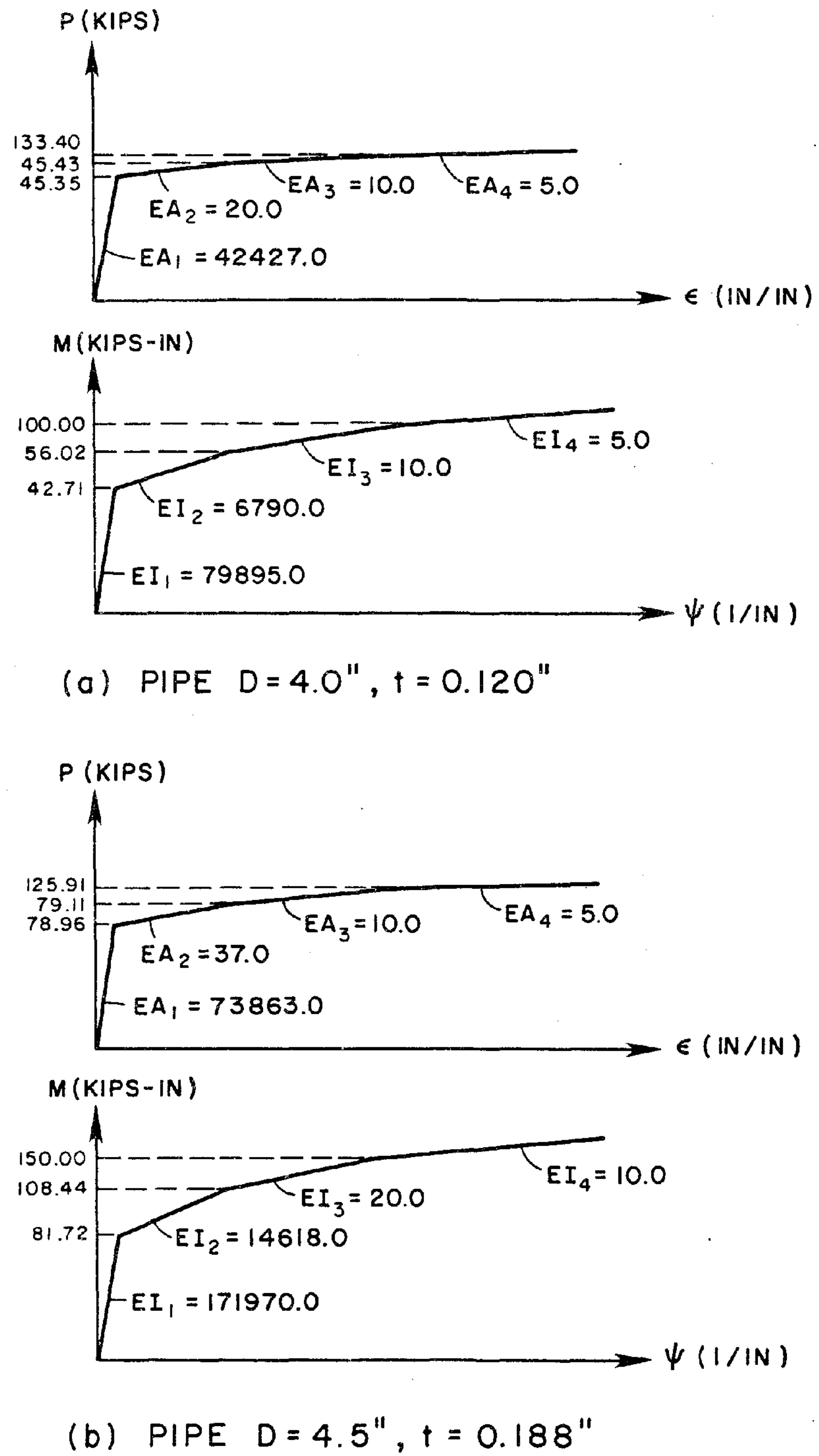

(a) PIPE D = 4.0", t = 0.120"

(b) PIPE D = 4.5", t = 0.188"

FIG. E1.5 ACTION-DEFORMATION RELATIONSHIPS USED FOR BRACED FRAME ANALYSIS

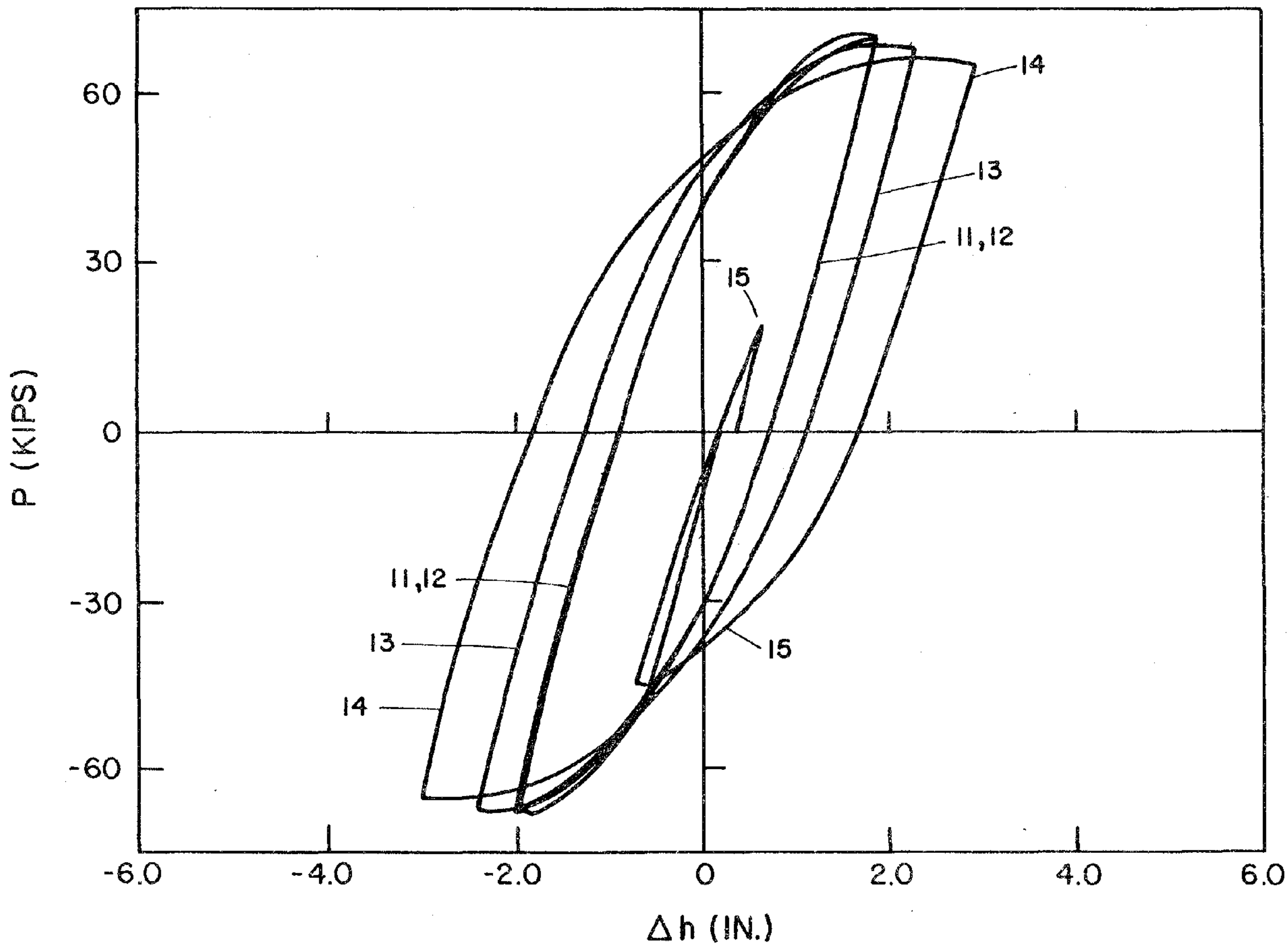

FIG. E1.6 FRAME LOAD VS. DECK DISPLACEMENT. EXPERIMENT.

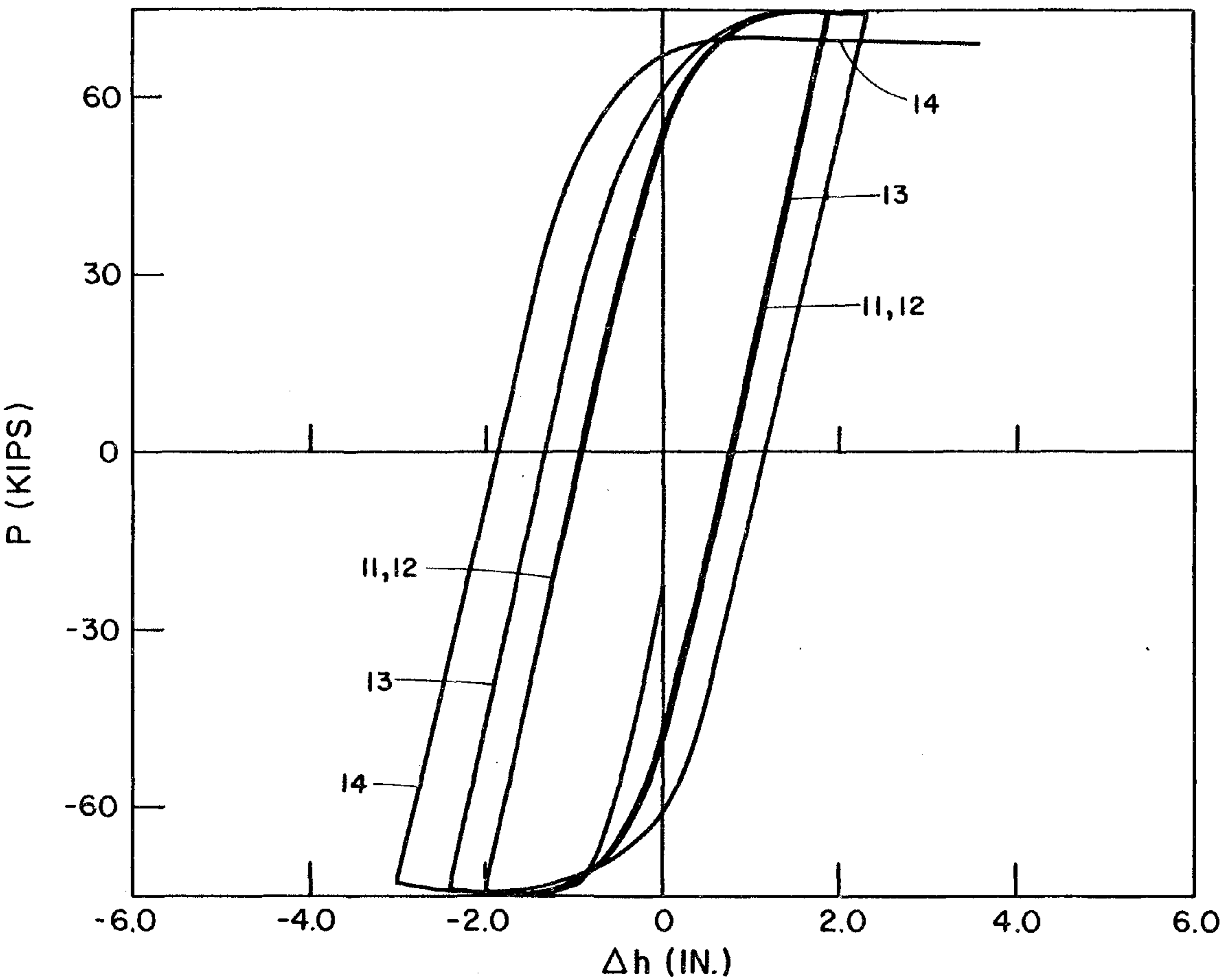

FIG. E1.7 FRAME LOAD VS. DECK DISPLACEMENT. ANALYSIS.

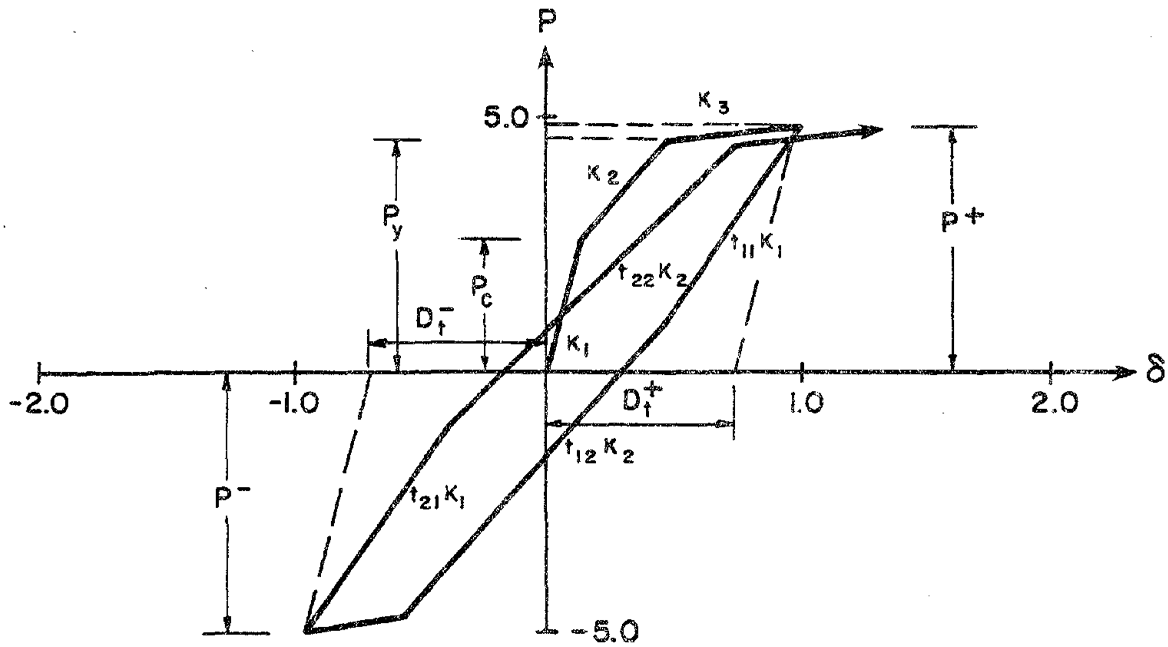

(a) 1 st. LOADING CYCLE

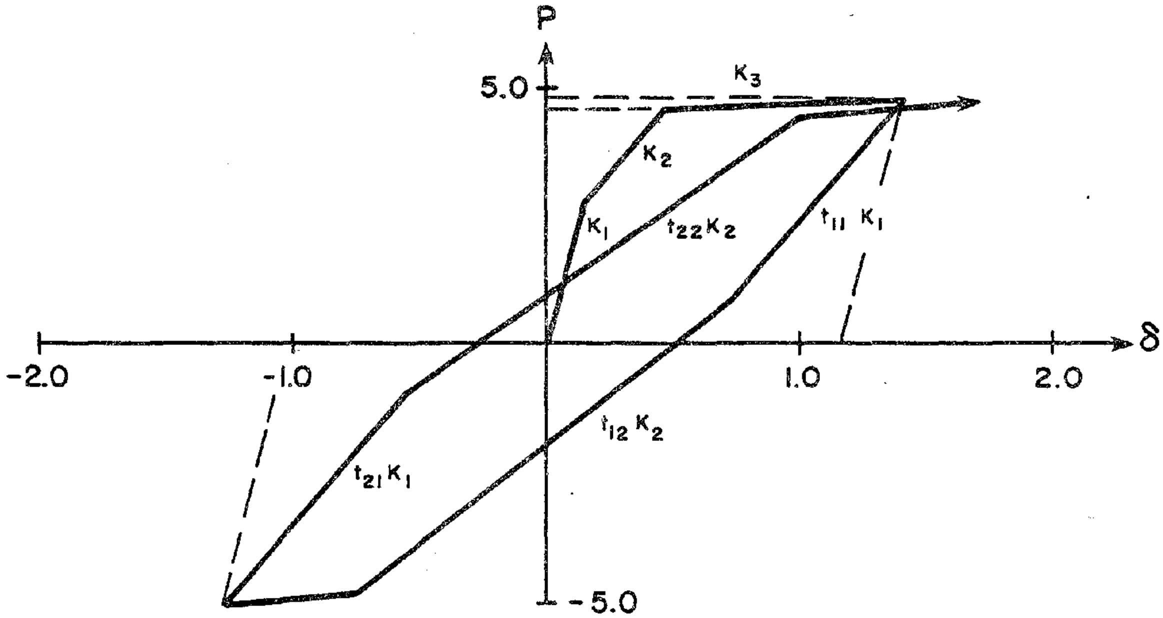

(b) 2 nd. LOADING CYCLE

FIG. E2.1 IDEALIZED TRILINEAR HYSTERESIS LOOP

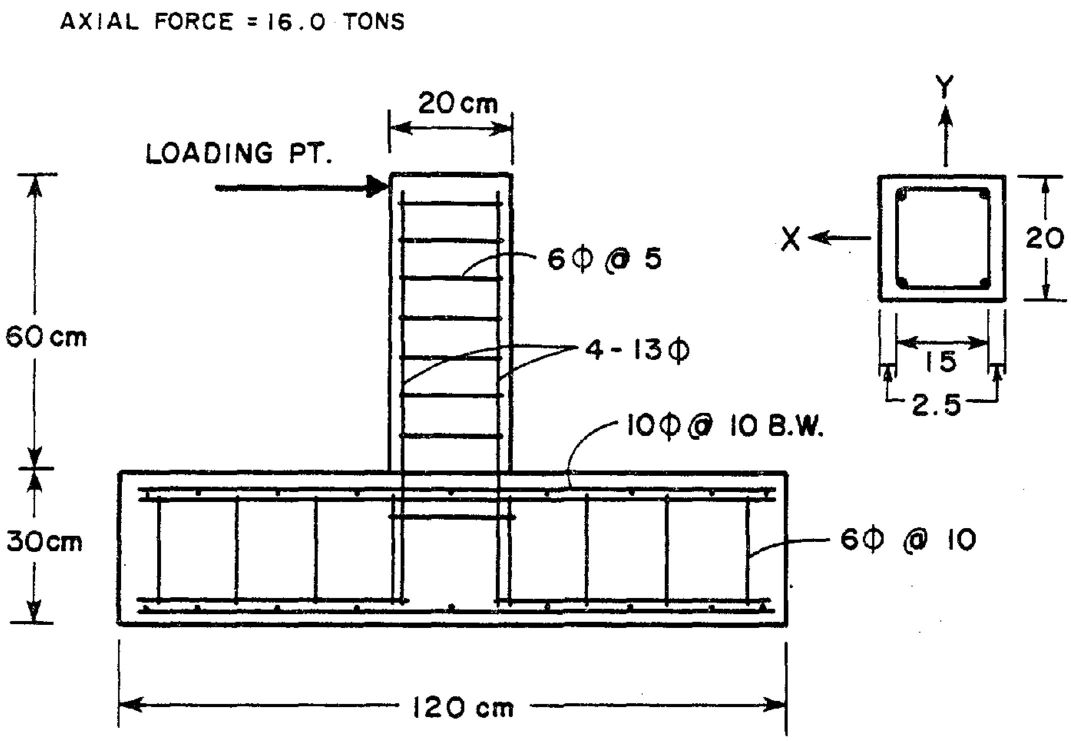

FIG. E2.2 DIMENSIONS OF TEST SPECIMEN

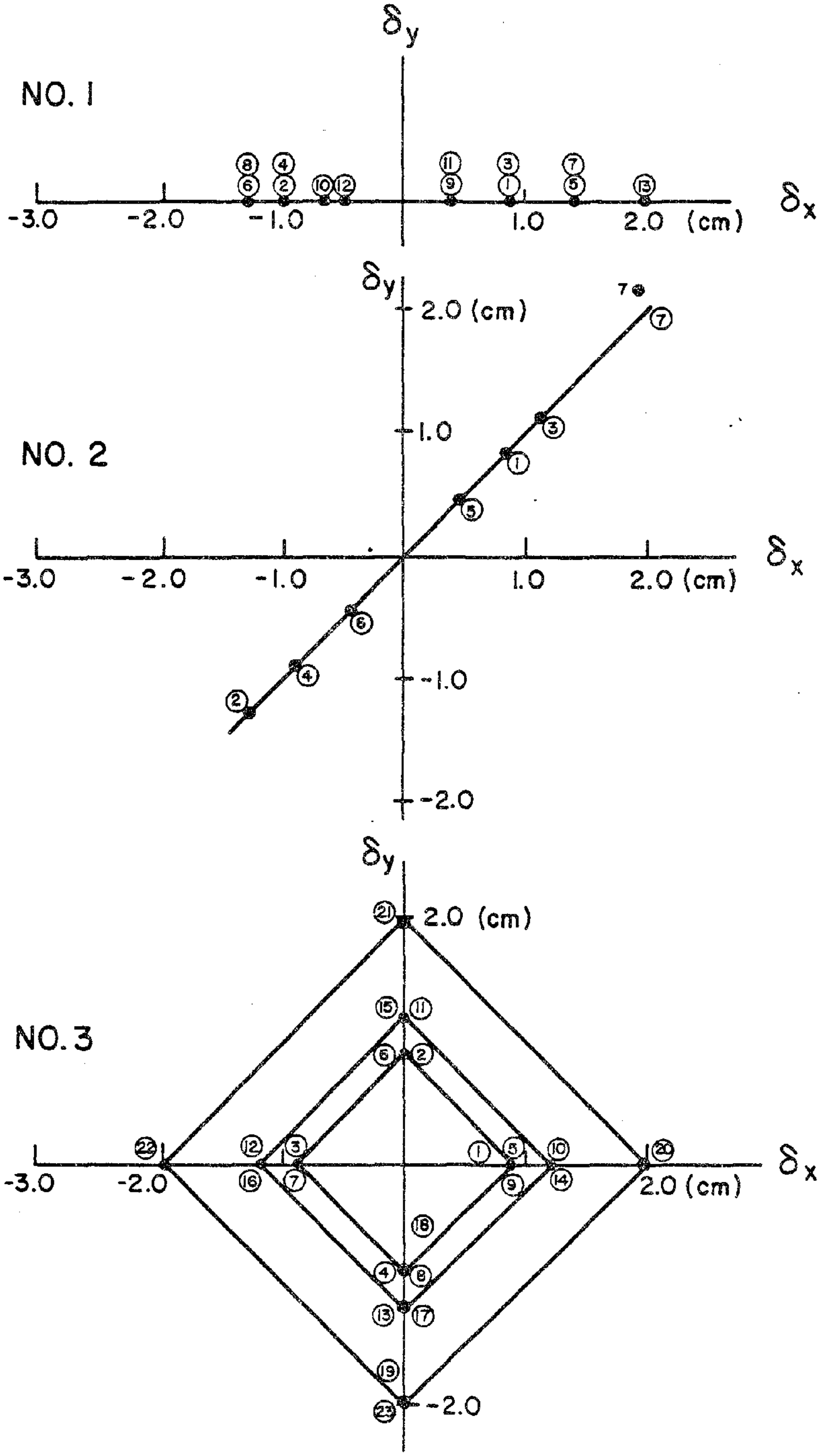

FIG. E2.3 IMPOSED DEFLECTION PATHS

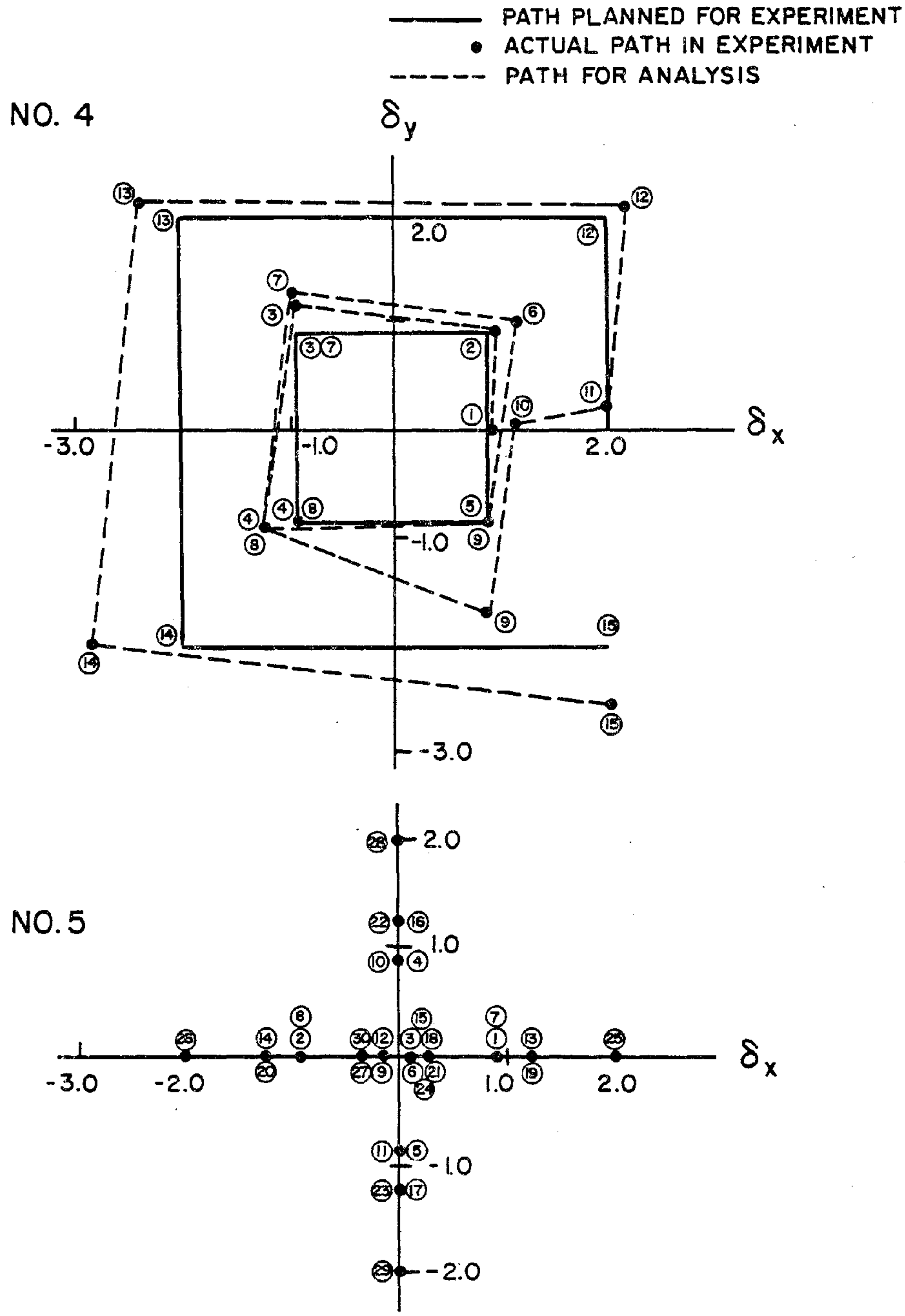

FIG. E2.3 IMPOSED DEFLECTION PATHS (CONT'D)

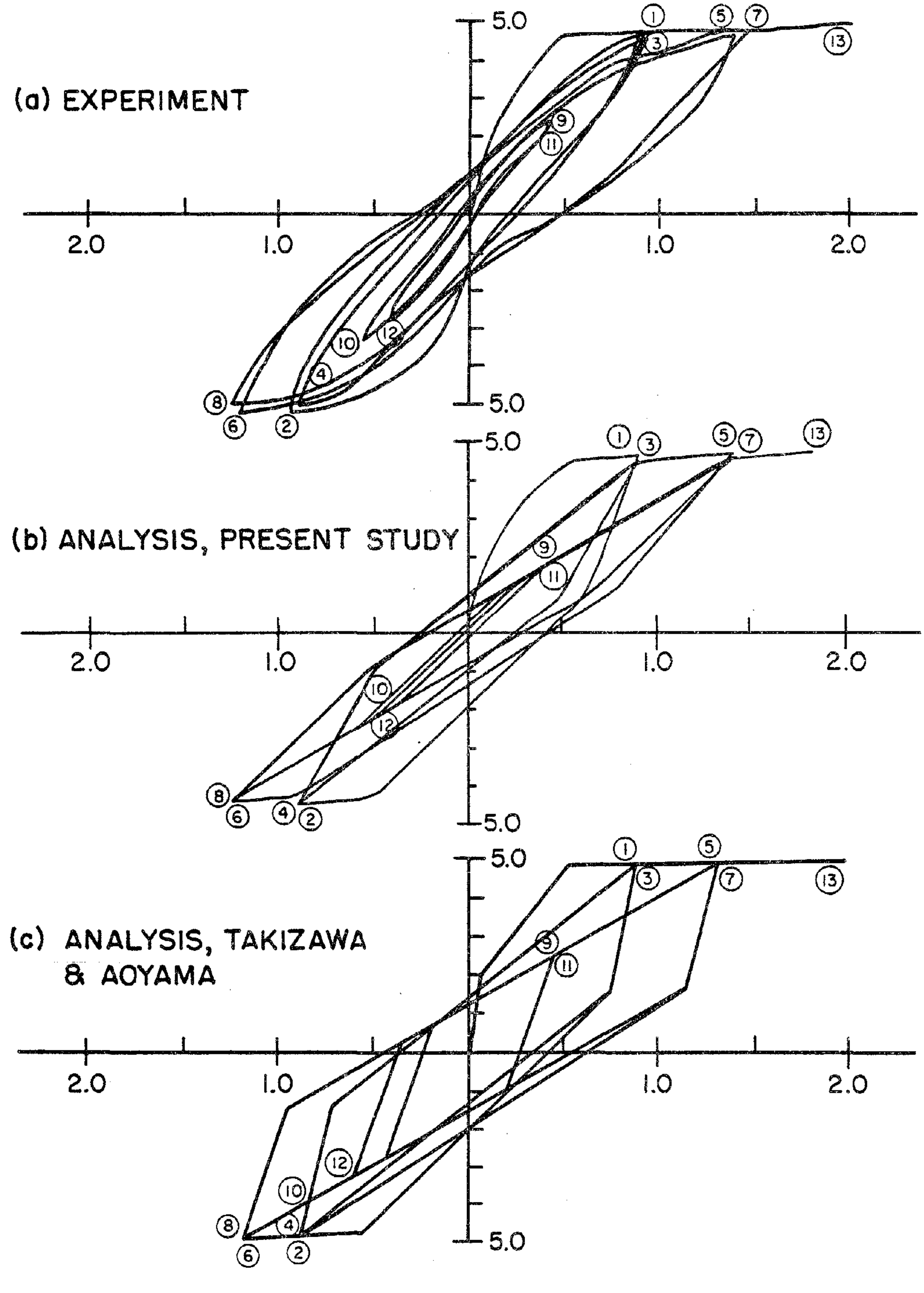

FIG. E2.4 TAKIZAWA-AOYAMA TESTS. LOAD SEQUENCE 1.
COMPARISON OF ANALYSIS AND EXPERIMENT.

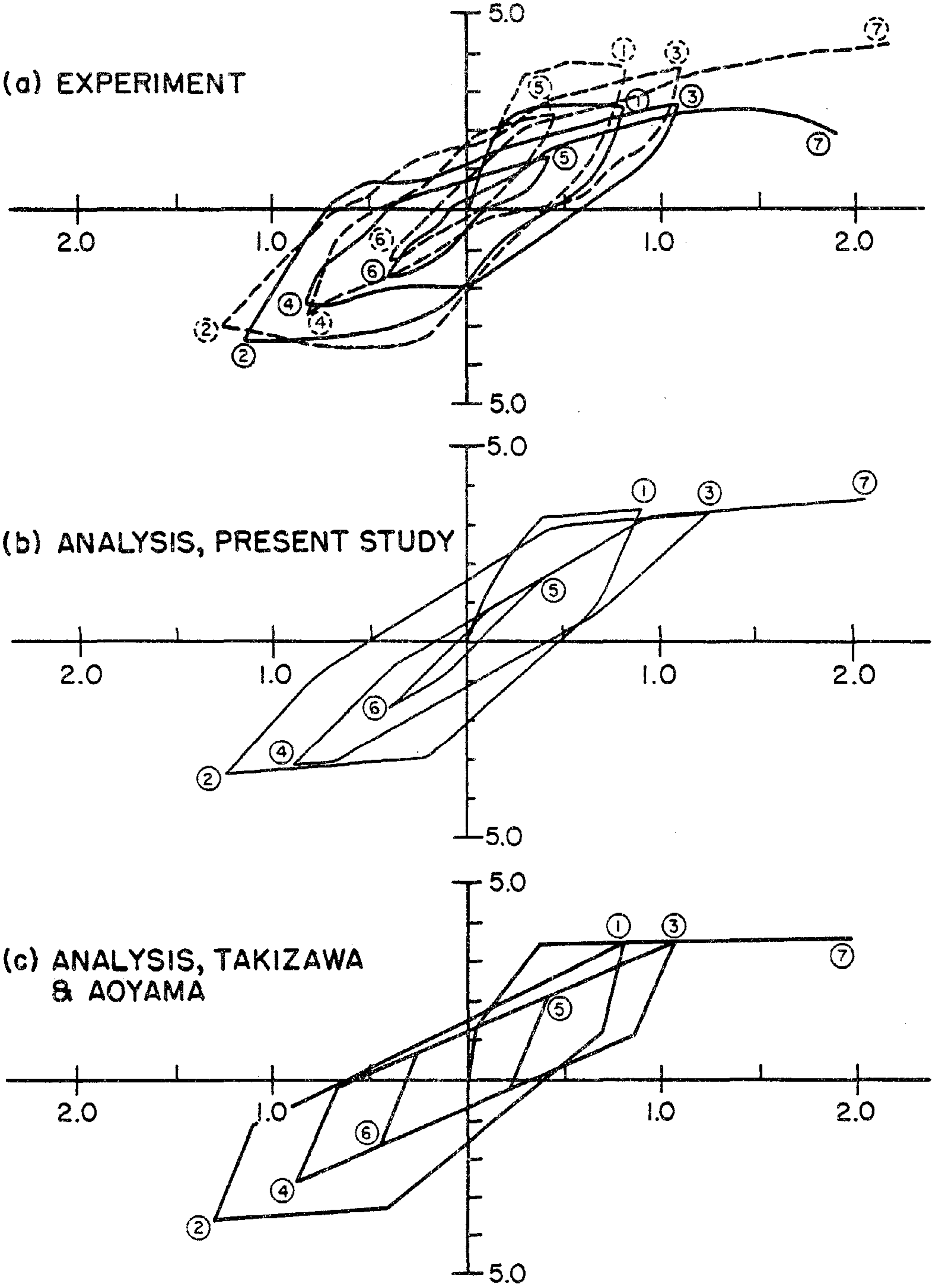

FIG. E2.5 TAKIZAWA-AOYAMA TESTS. LOAD SEQUENCE 2. COMPARISON OF ANALYSIS AND EXPERIMENT.

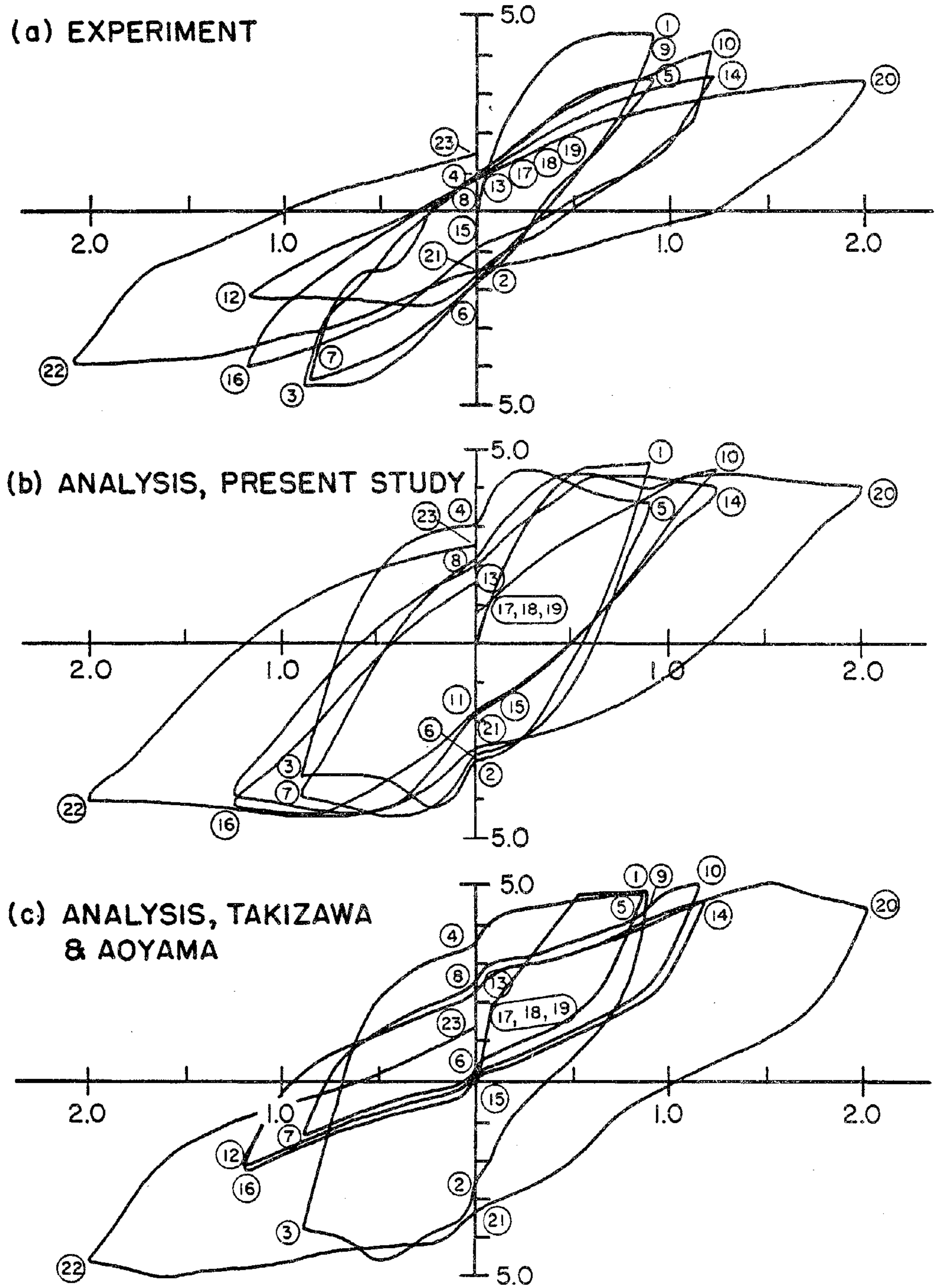

FIG. E2.6 LOAD SEQUENCE 3. X-COMPONENT.
COMPARISON OF ANALYSIS & EXPERIMENT.

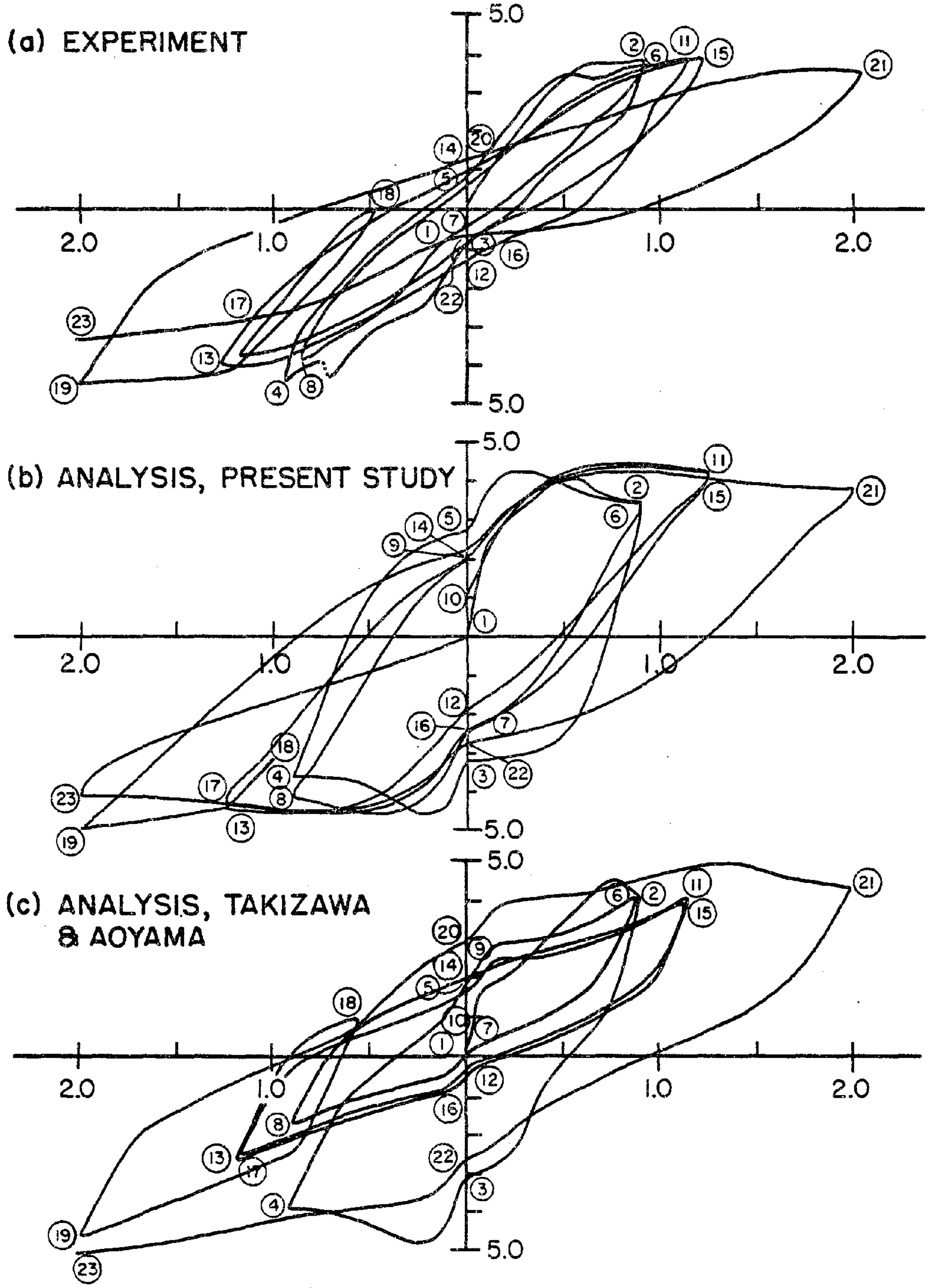

FIG. E2.7 LOAD SEQUENCE 3. Y-COMPONENT.
COMPARISON OF ANALYSIS & EXPERIMENT.

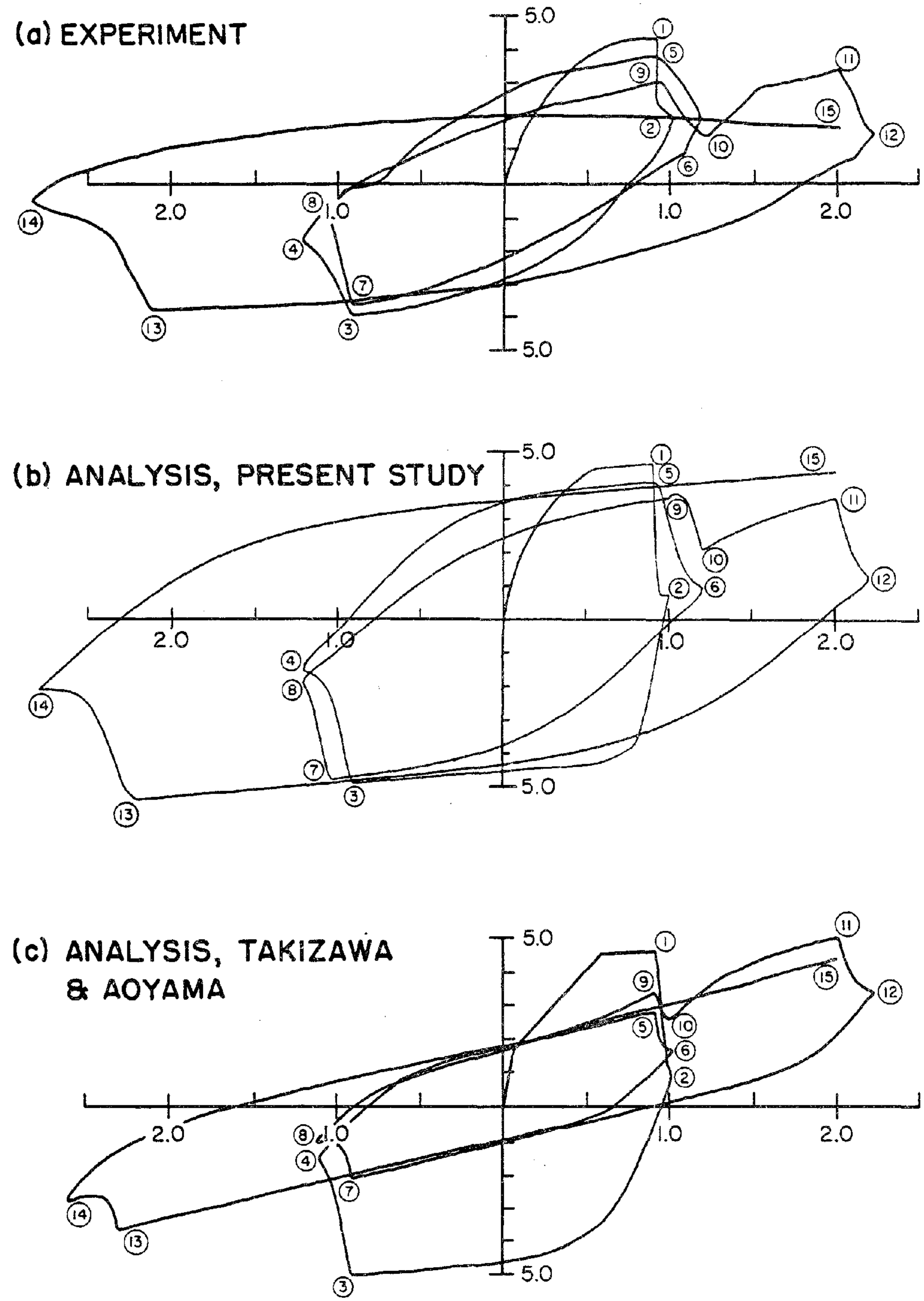

FIG. E2.8 LOAD SEQUENCE 4. X-COMPONENT.
COMPARISON OF ANALYSIS & EXPERIMENT.

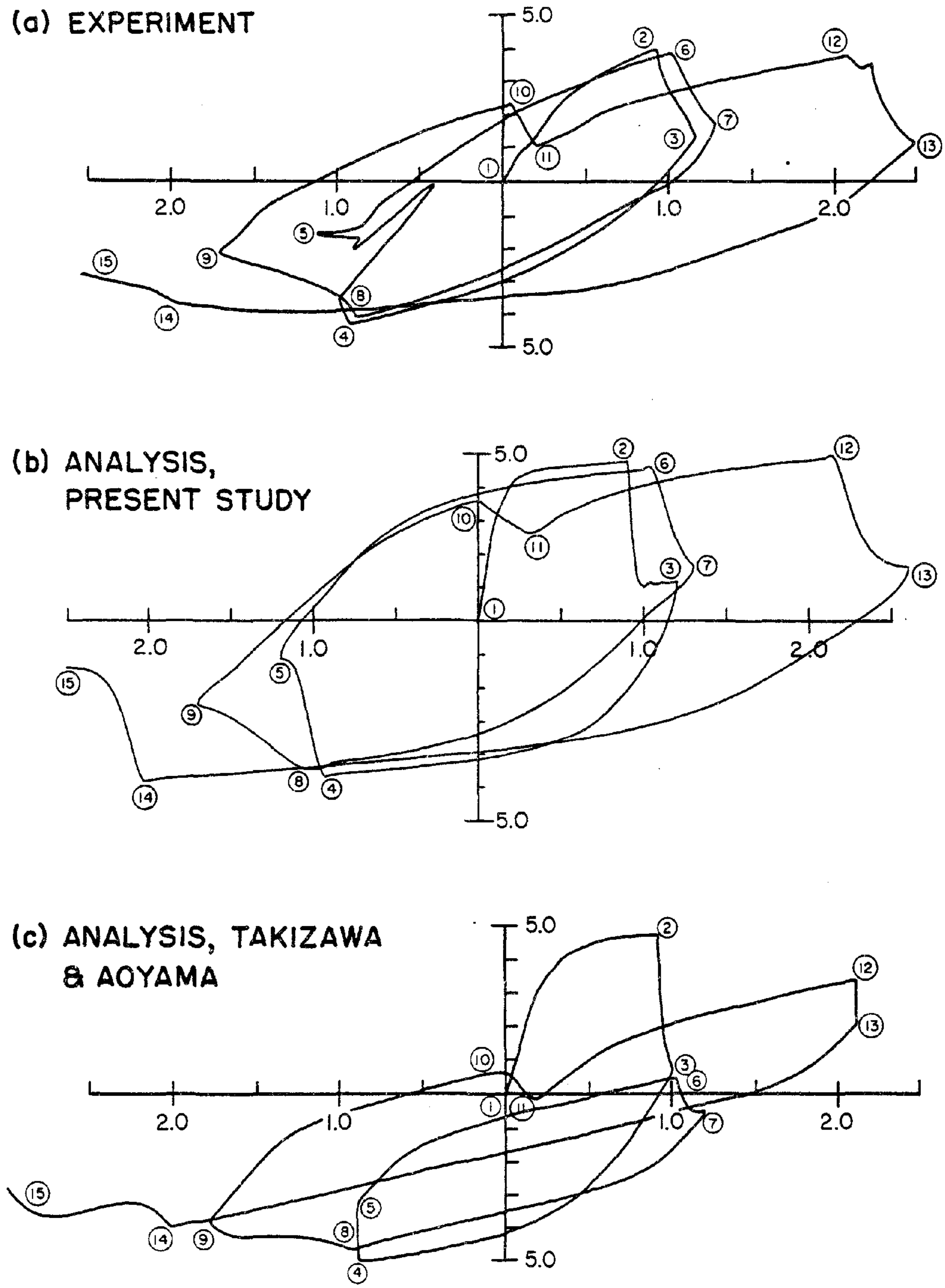

FIG. E2.9 LOAD SEQUENCE 4. Y-COMPONENT. COMPARISON OF ANALYSIS & EXPERIMENT.

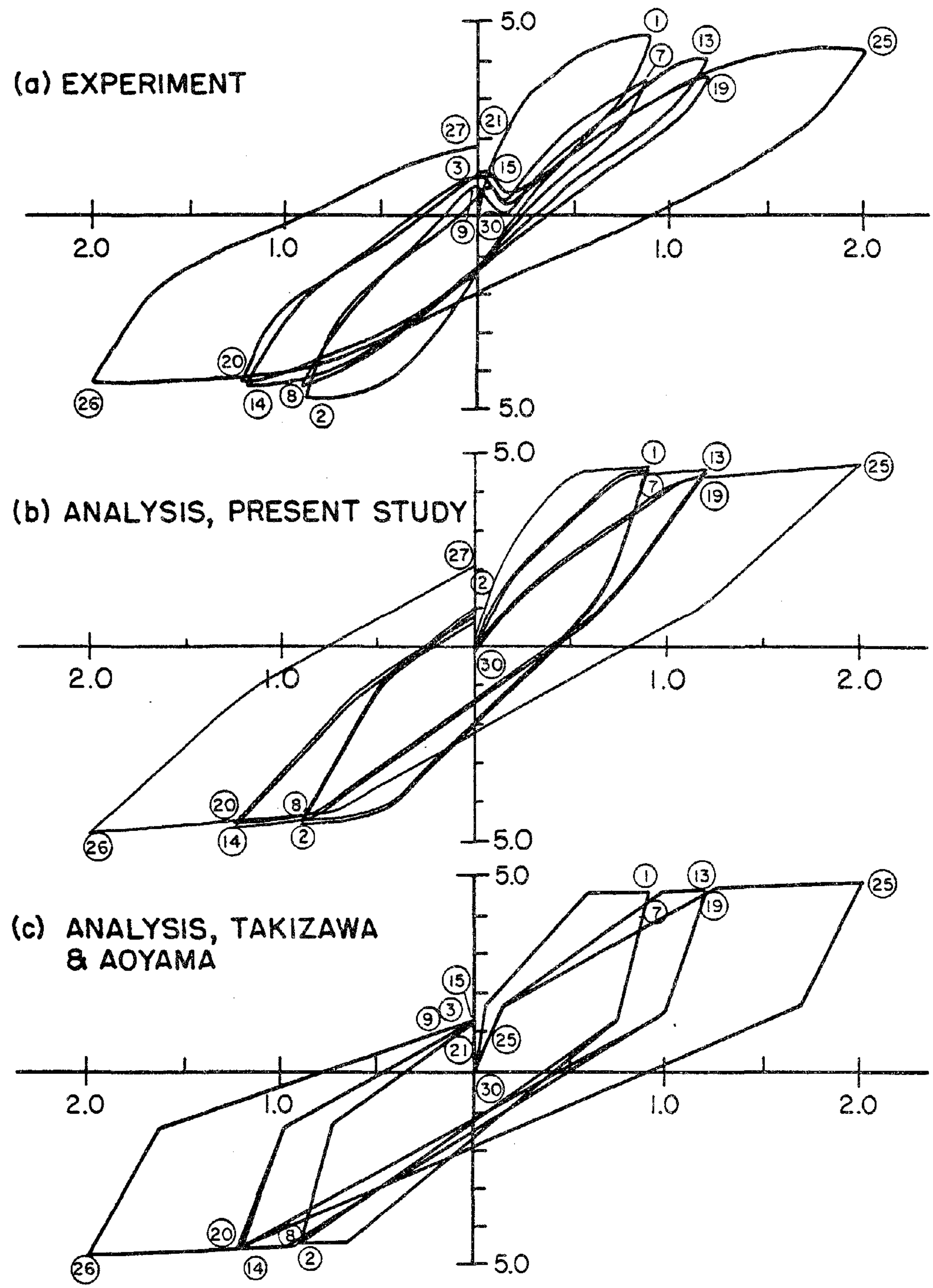

FIG. E2.10 LOAD SEQUENCE 5. X-COMPONENT.
COMPARISON OF ANALYSIS & EXPERIMENT.

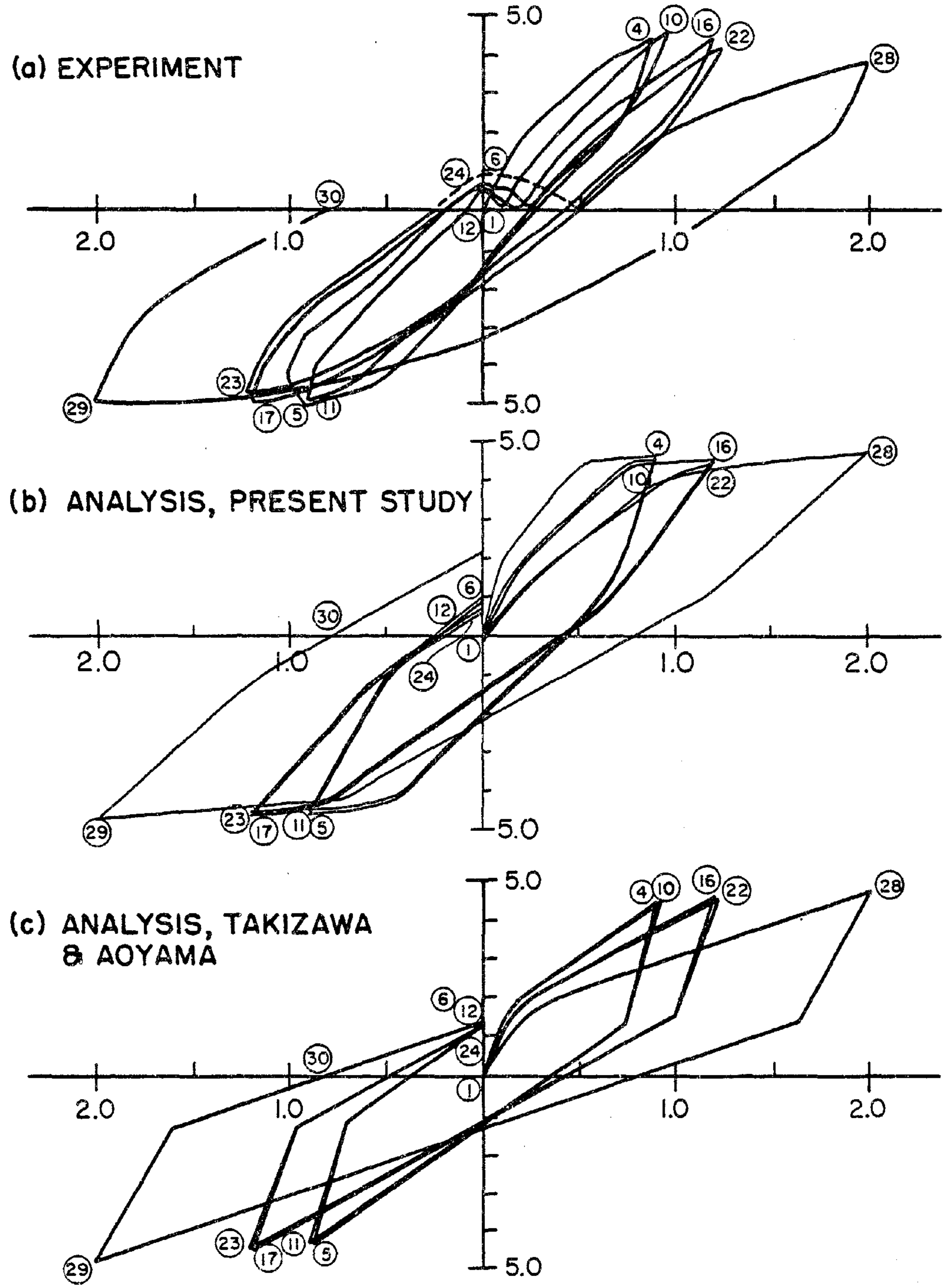

FIG. E2.11 LOAD SEQUENCE 5. Y-COMPONENT.
COMPARISON OF ANALYSIS & EXPERIMENT.

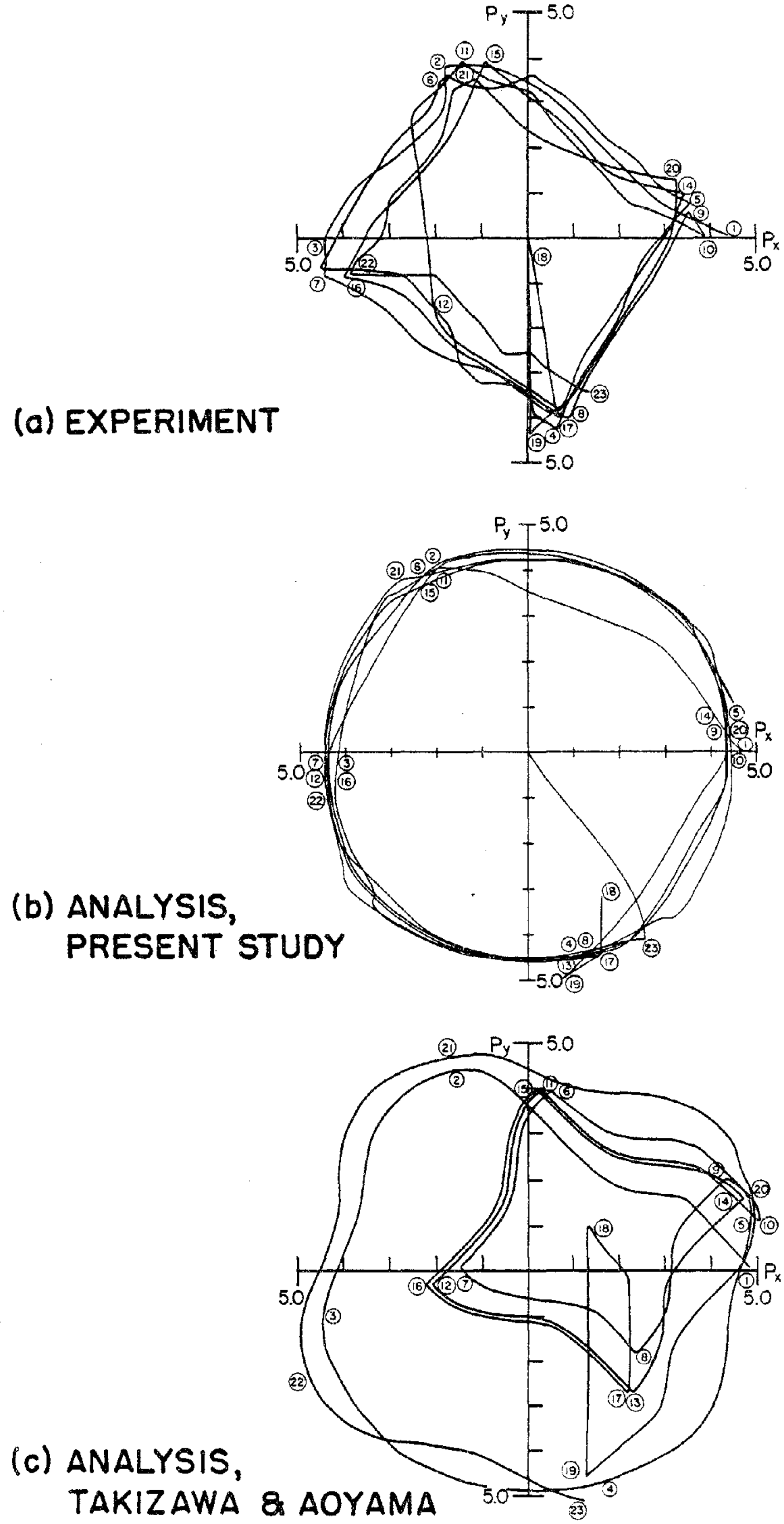

FIG. E2.12 FORCE ORBITS. LOAD SEQUENCE 3.
COMPARISON OF ANALYSIS & EXPERIMENT.

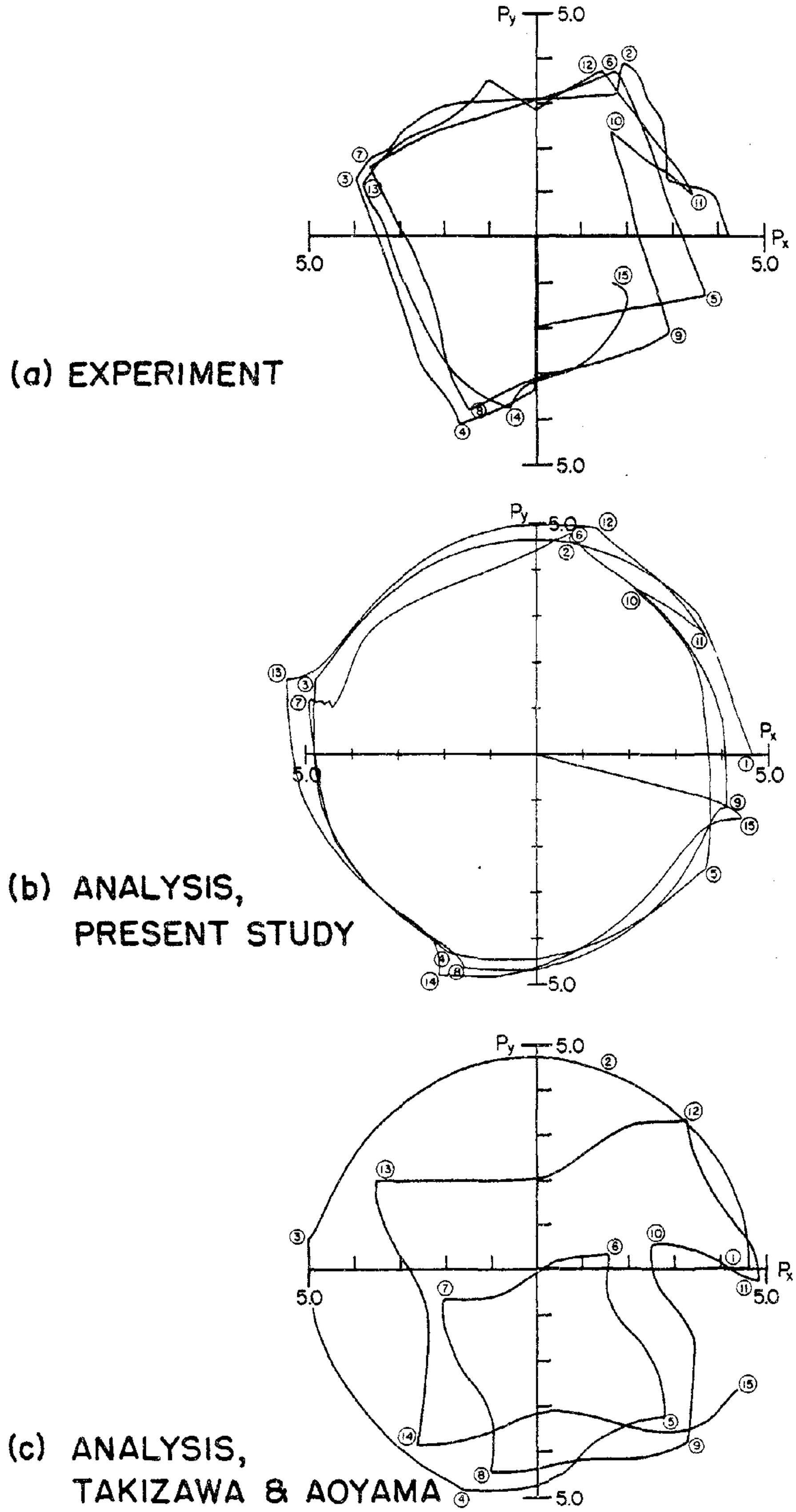

FIG. E2.13 FORCE ORBITS. LOAD SEQUENCE 4.
COMPARISON OF ANALYSIS & EXPERIMENT.

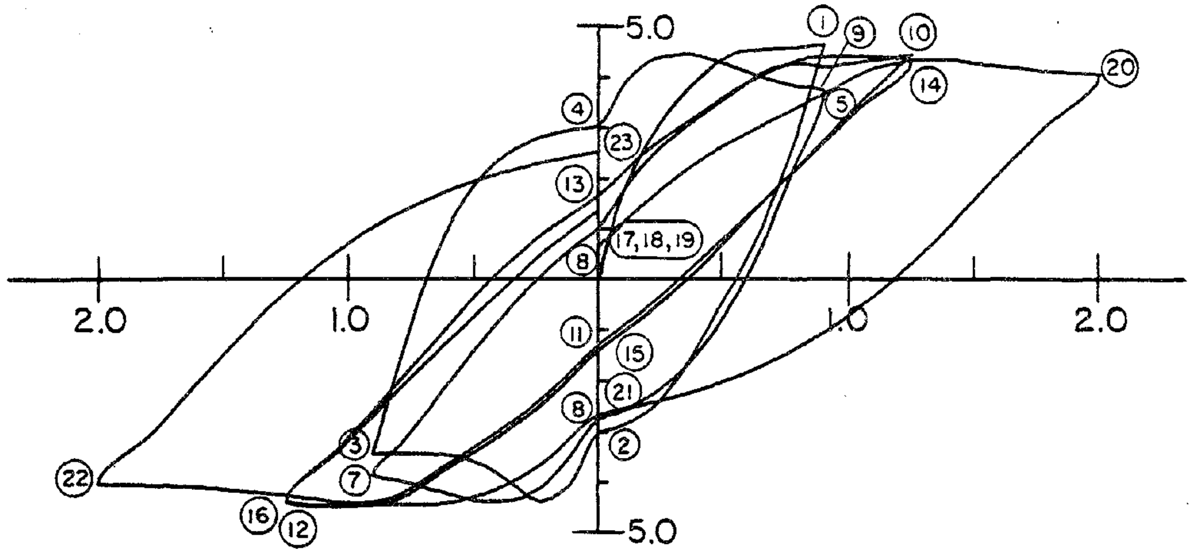

(a) X-COMPONENT

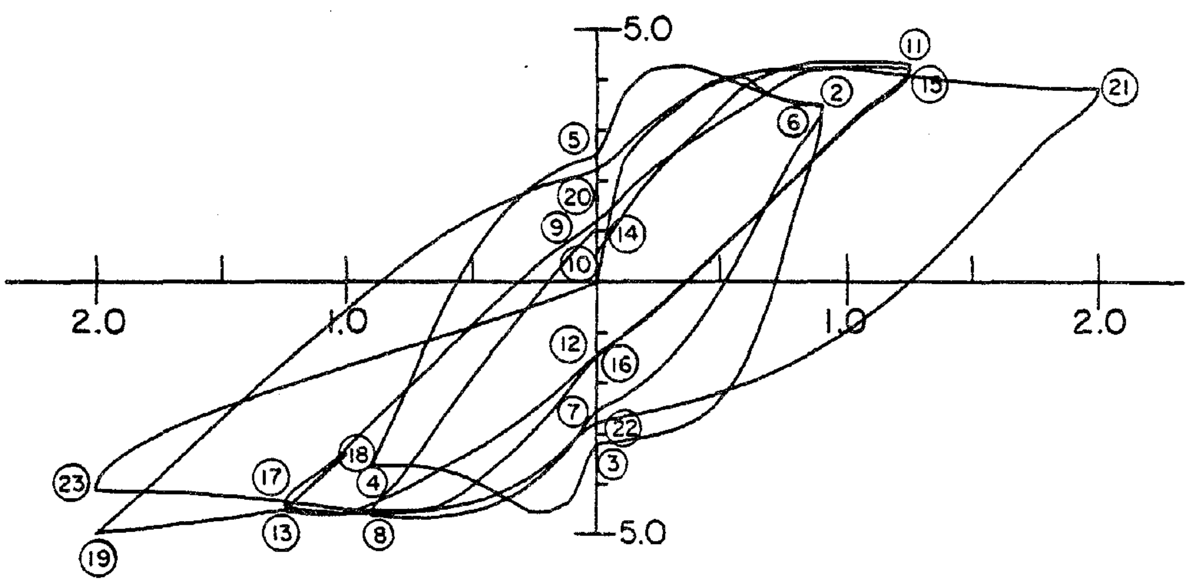

(b) Y-COMPONENT

FIG. E2.14 ANALYSIS WITH DEGRADING STIFFNESS COUPLING. LOAD SEQUENCE 3.

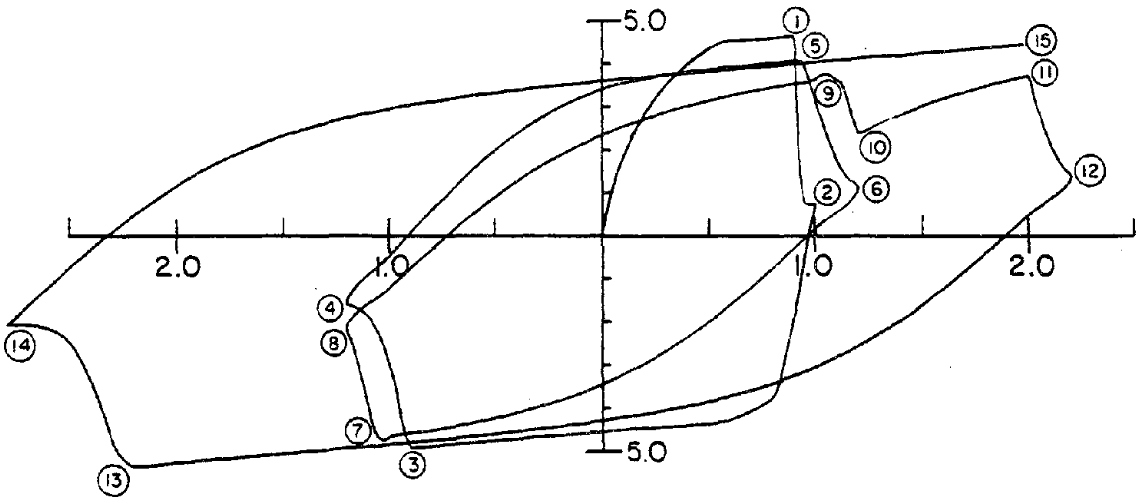

(a) X-COMPONENT

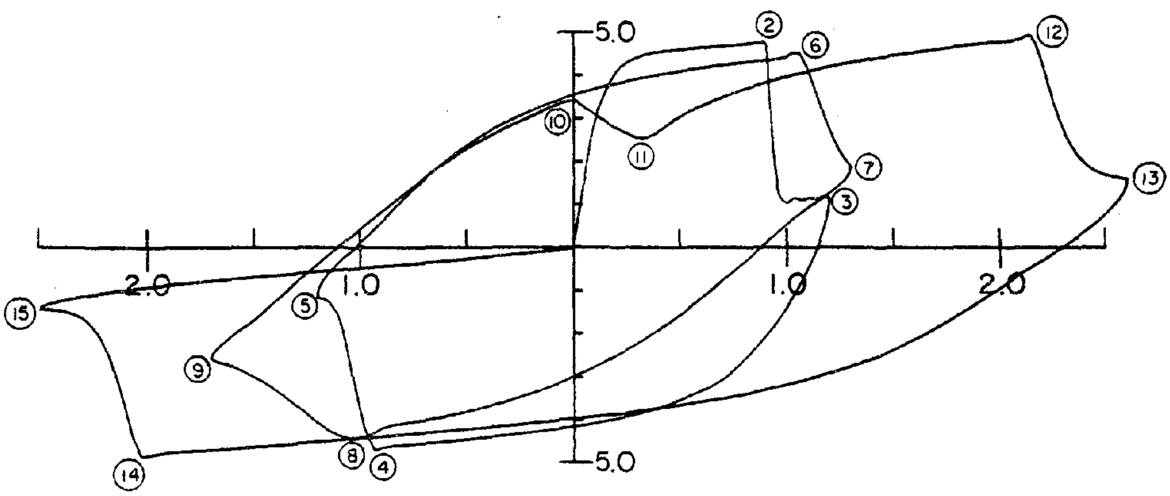

(b) Y-COMPONENT

FIG. E2.15 ANALYSIS WITH DEGRADING STIFFNESS COUPLING. LOAD SEQUENCE 4.

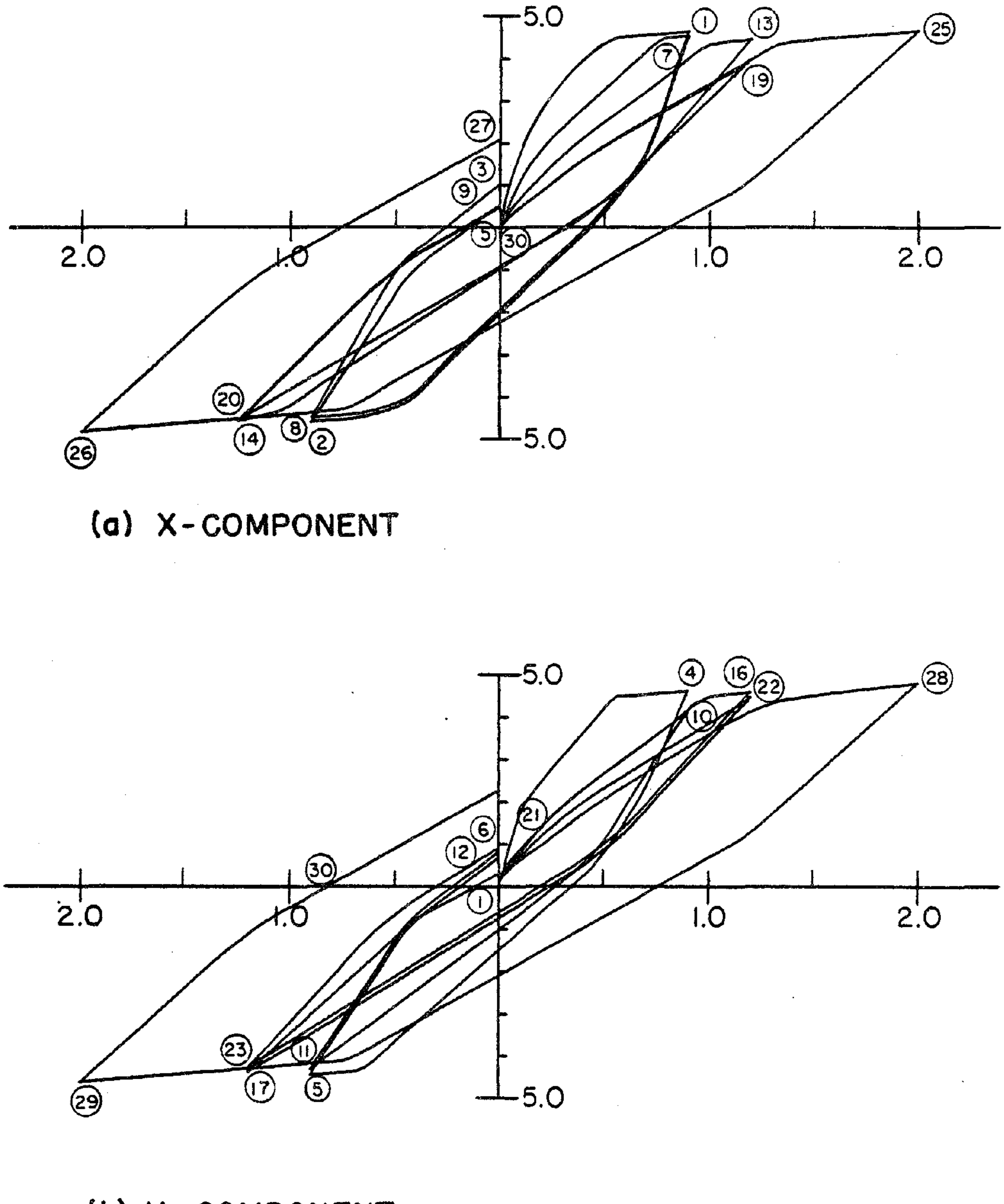

FIG. E2.16 ANALYSIS WITH DEGRADING STIFFNESS COUPLING.
LOAD SEQUENCE 5.

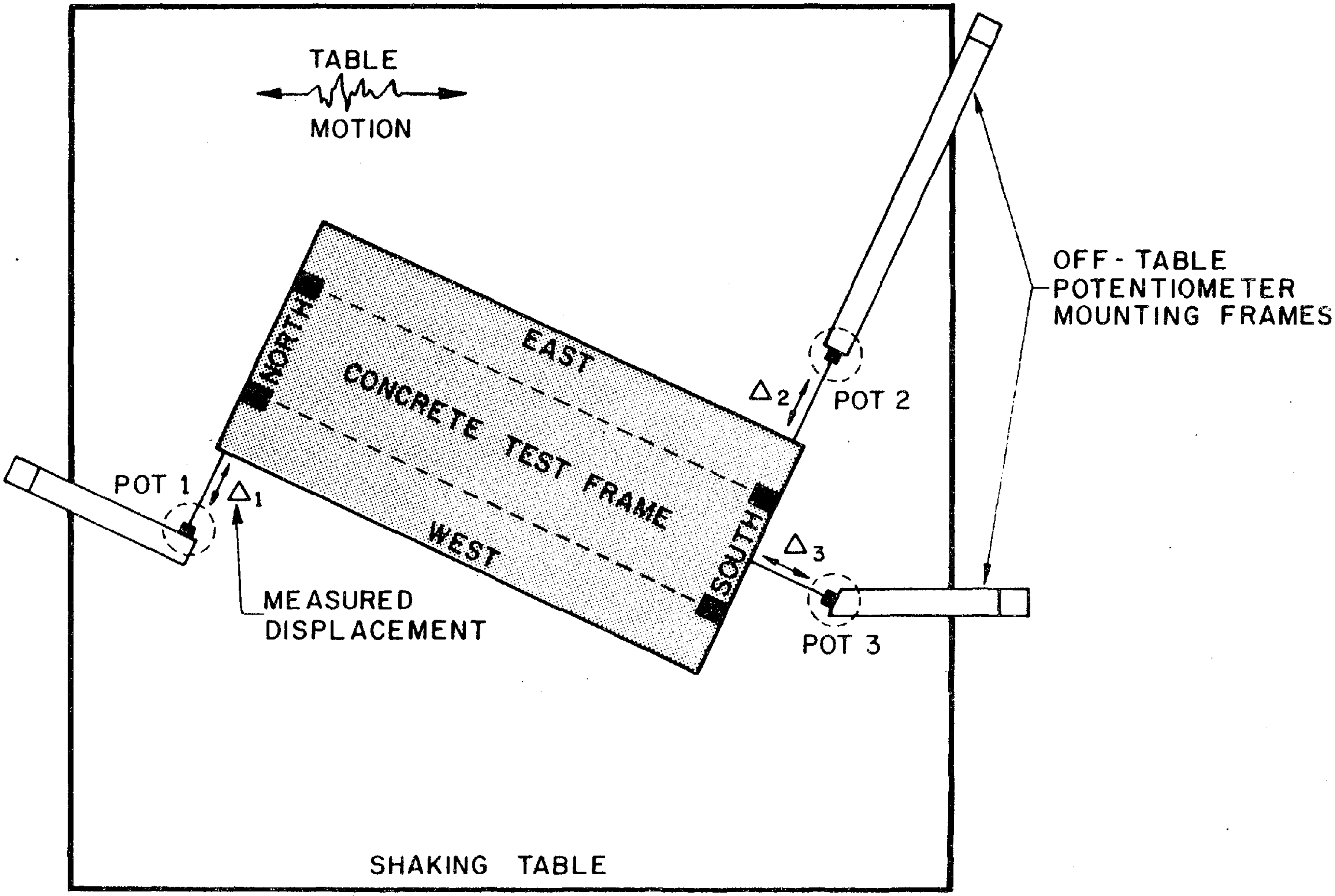

(A) PLAN OF TEST FRAME ON SHAKING TABLE (FROM [21])

FIG. E3.1 TEST CONFIGURATION OF 3-D R.C. FRAME

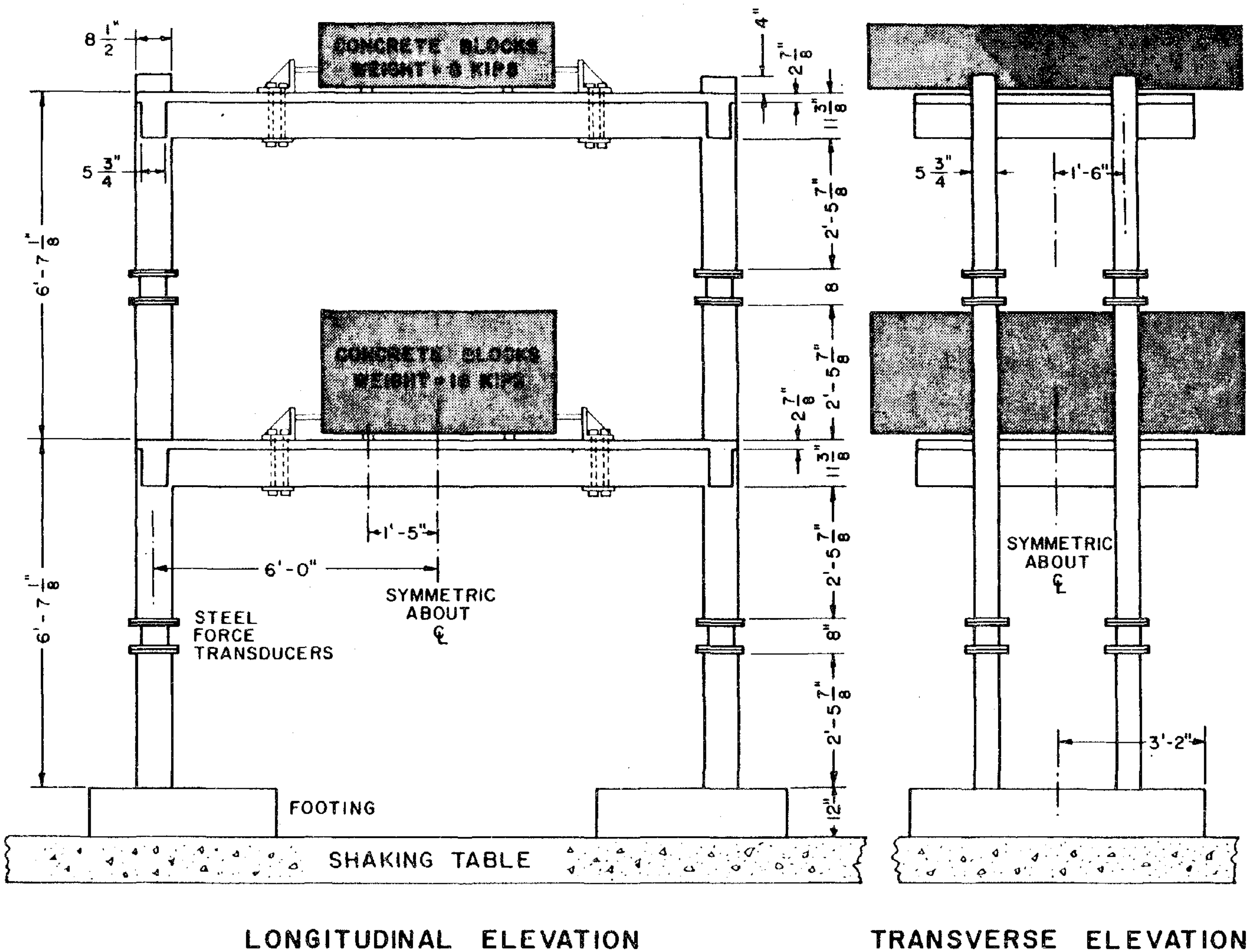

(B) OVERALL DIMENSIONS AND GEOMETRY OF TEST FRAME (FROM [21])

FIG. E3.1 TEST CONFIGURATION OF 3-D R.C. FRAME (CONT'D)

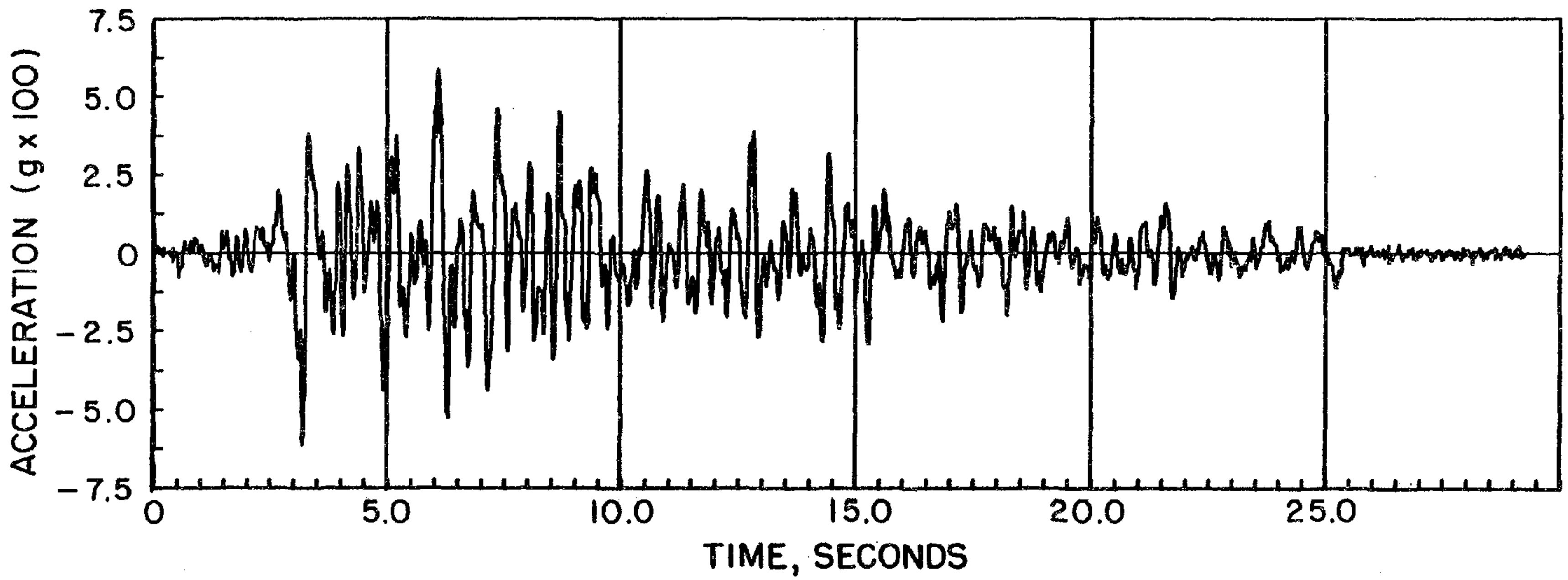

FIG. E3.2 LOW AMPLITUDE MOTION (T100)

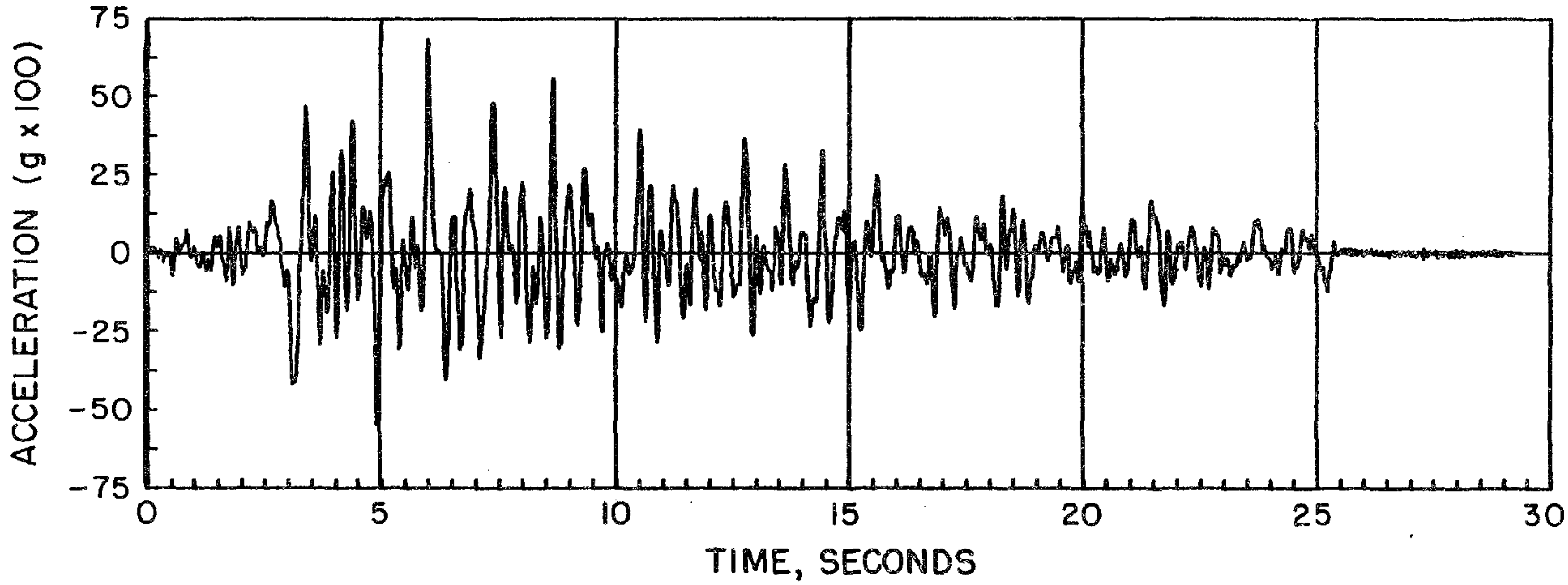

FIG. E3.3 HIGH AMPLITUDE MOTION (T1000)

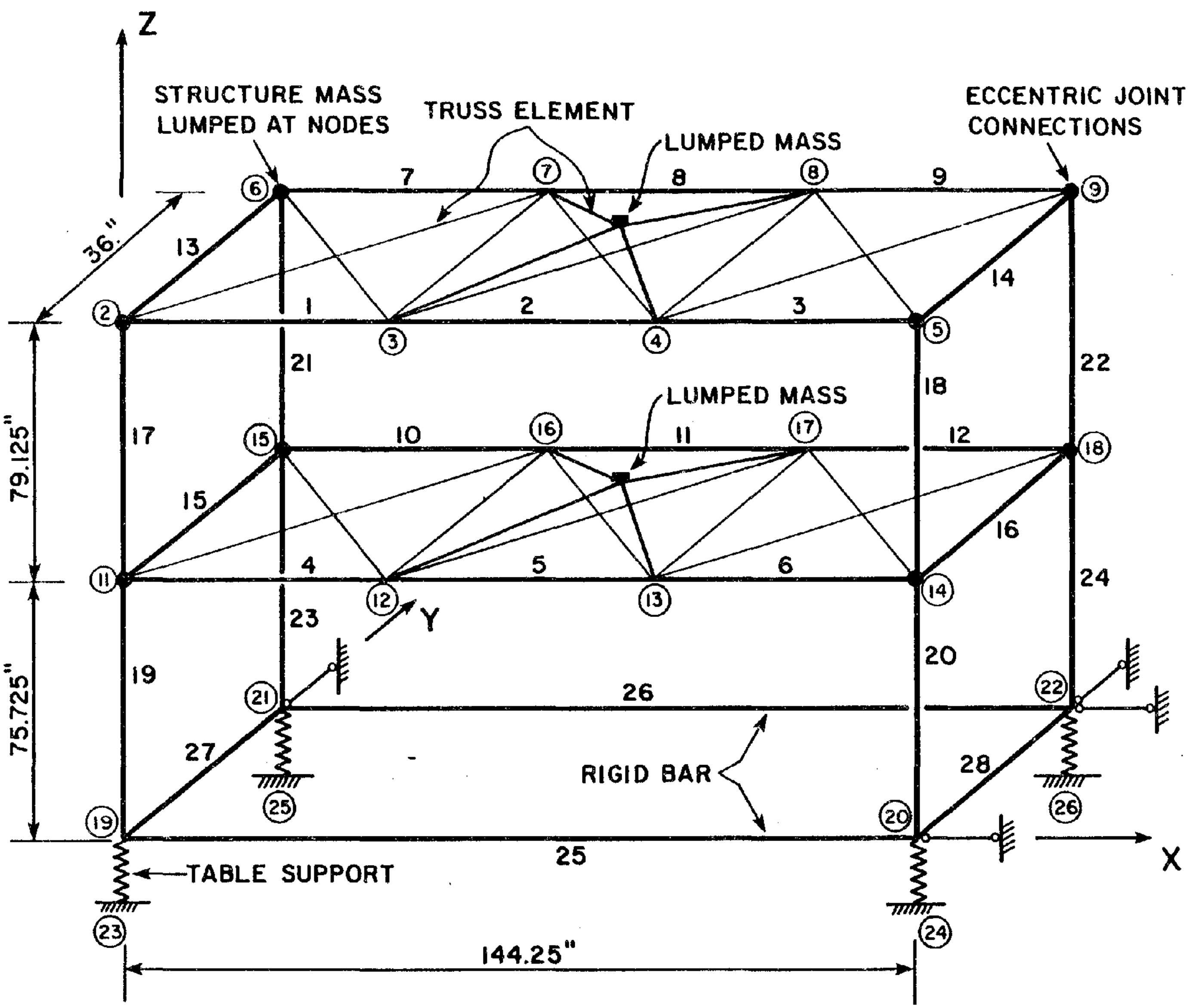

FIG. E3.4 ANALYTICAL MODEL OF 3-D R.C. FRAME

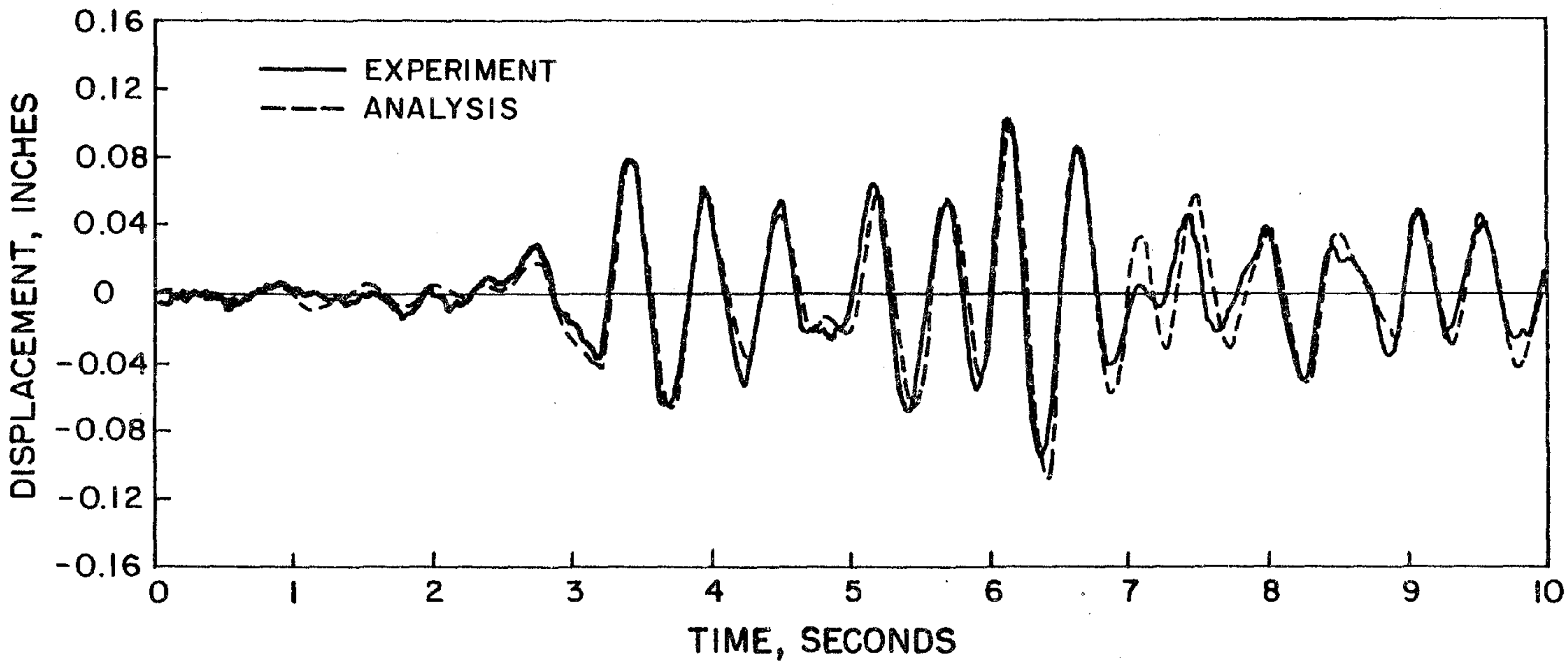

FIG. E3.5 COMPARISON OF ANALYSIS AND EXPERIMENT (T100)
X DISPLACEMENT AT FIRST FLOOR

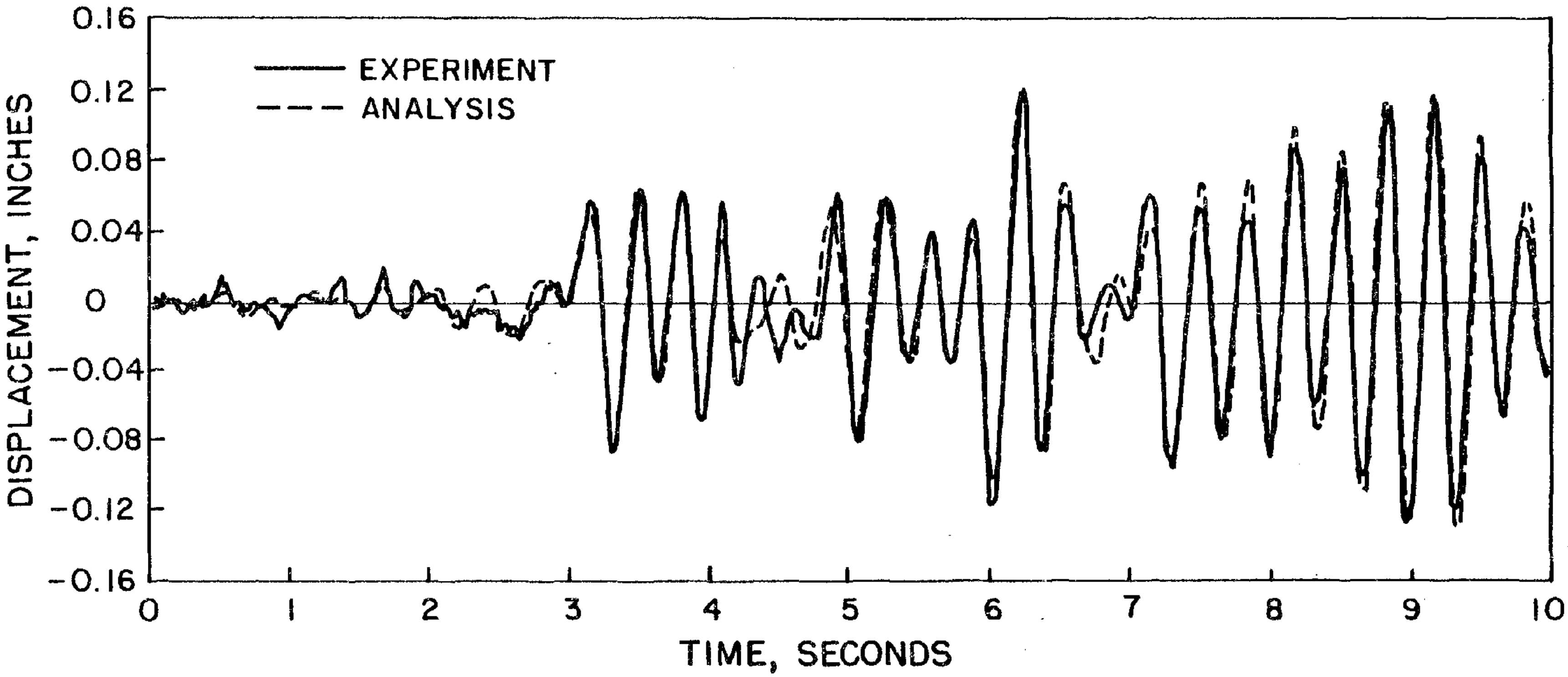

FIG. E3.6 COMPARISON OF ANALYSIS AND EXPERIMENT (T100)
Y DISPLACEMENT AT FIRST FLOOR

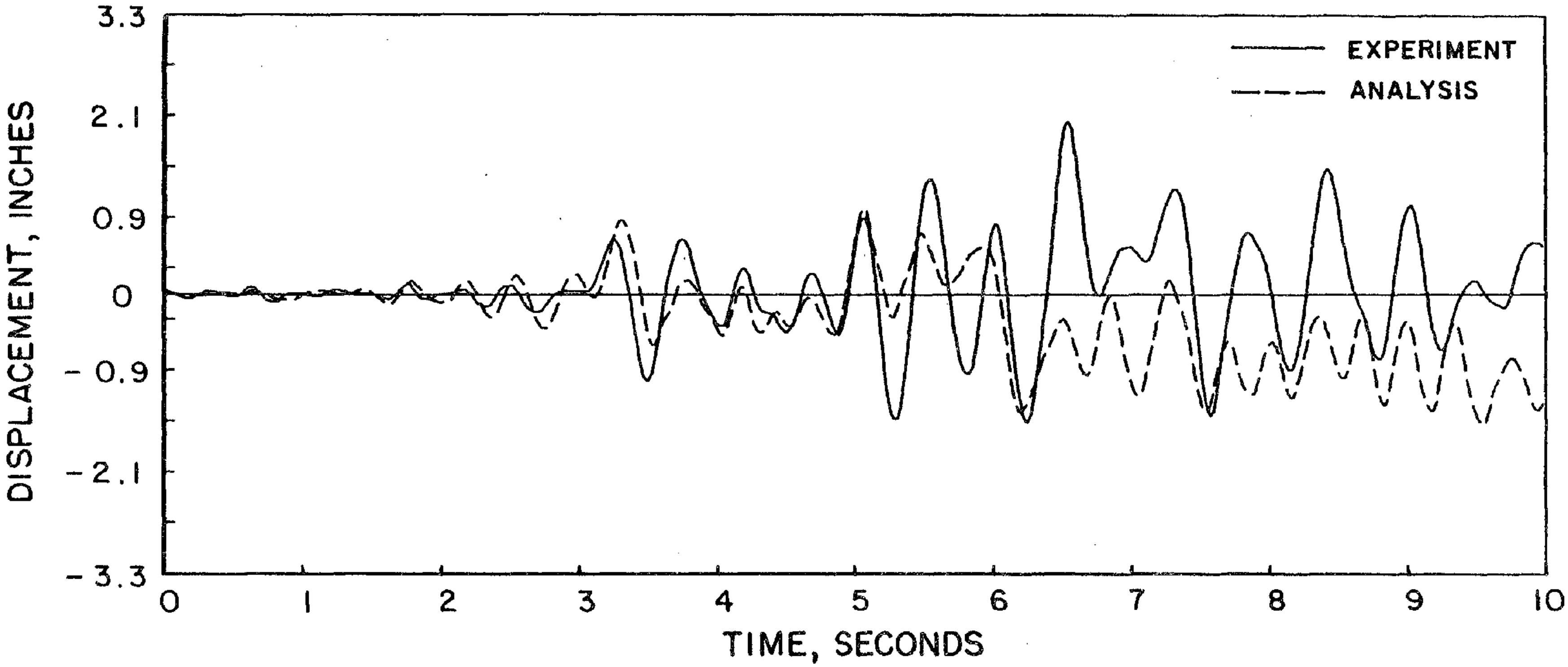

FIG. E3.7 COMPARISON OF ANALYSIS AND EXPERIMENT (T1000)
X DISPLACEMENT AT FIRST FLOOR
CASE 1: SMALL DAMPING, NO STIFFNESS DEGRADATION

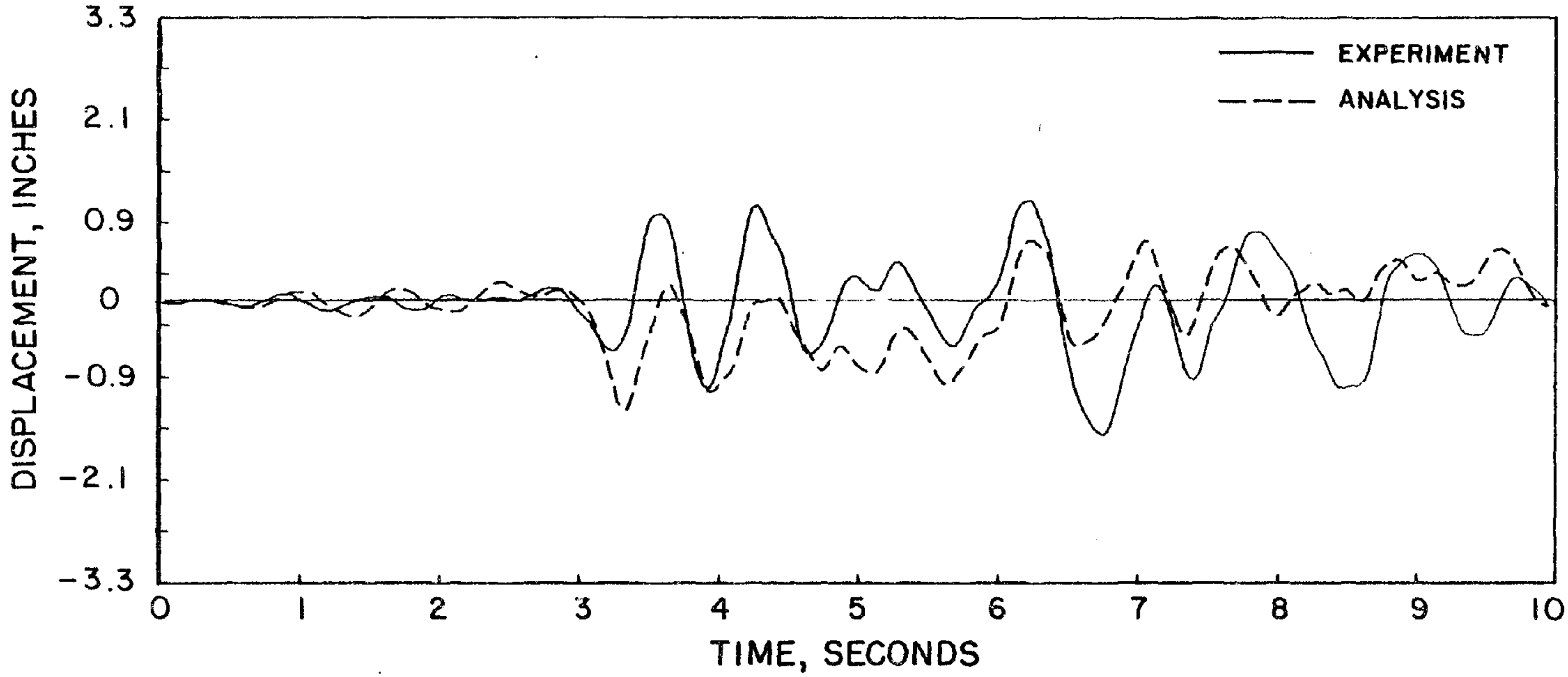

FIG. E3.8 COMPARISON OF ANALYSIS AND EXPERIMENT (T1000)
Y DISPLACEMENT AT FIRST FLOOR
CASE 1: SMALL DAMPING, NO STIFFNESS DEGRADATION

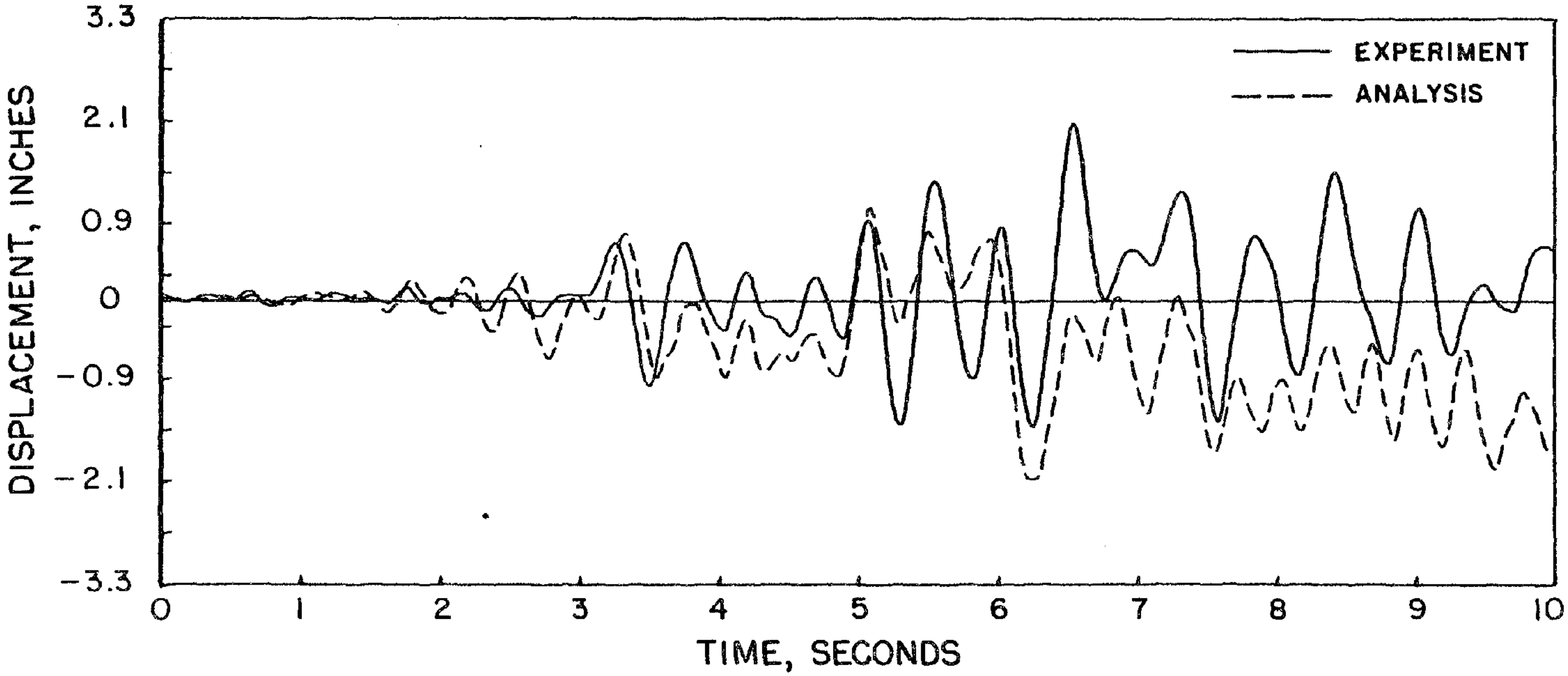

FIG. E3.9 COMPARISON OF ANALYSIS AND EXPERIMENT (T1000)
X DISPLACEMENT AT FIRST FLOOR
CASE 2: LARGE DAMPING, NO STIFFNESS DEGRADATION

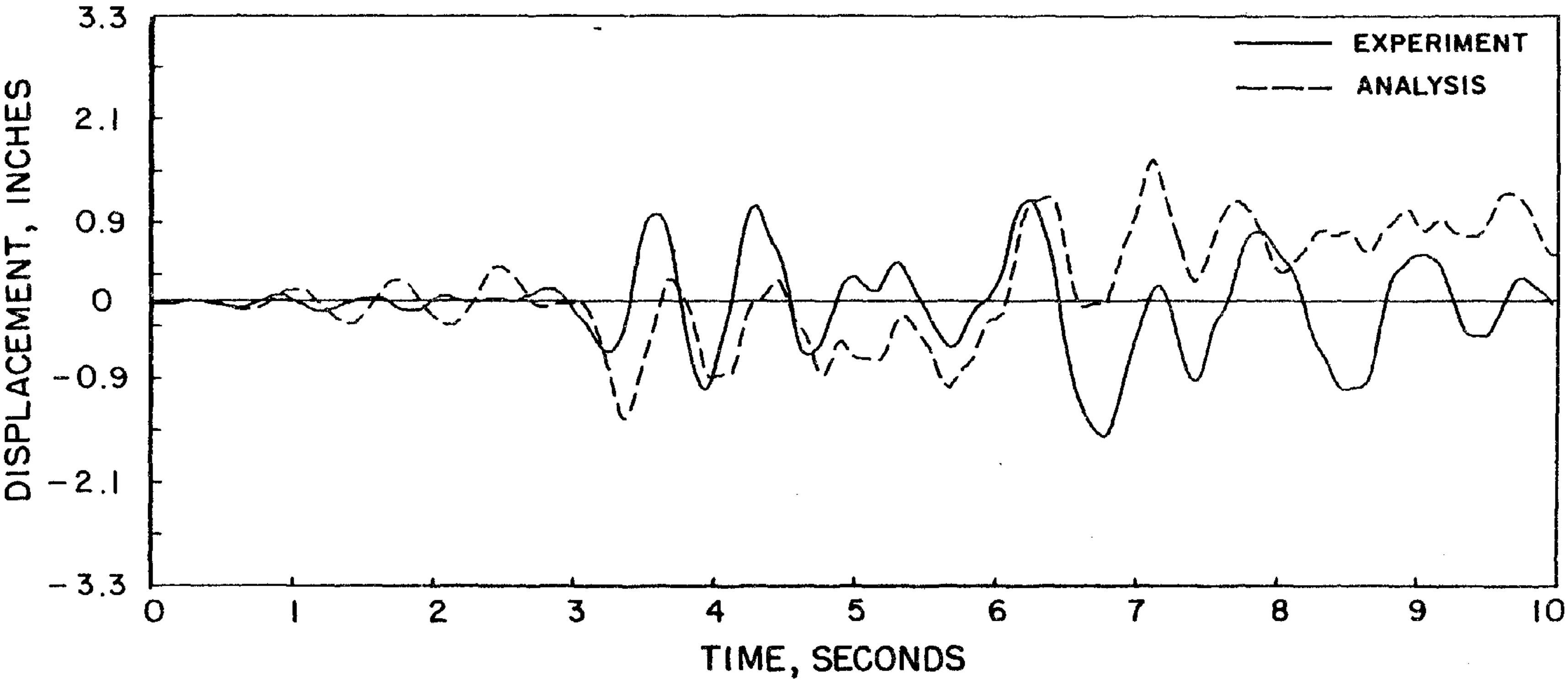

FIG. E3.10 COMPARISON OF ANALYSIS AND EXPERIMENT (T1000)
Y DISPLACEMENT AT FIRST FLOOR
CASE 2: LARGE DAMPING, NO STIFFNESS DEGRADATION

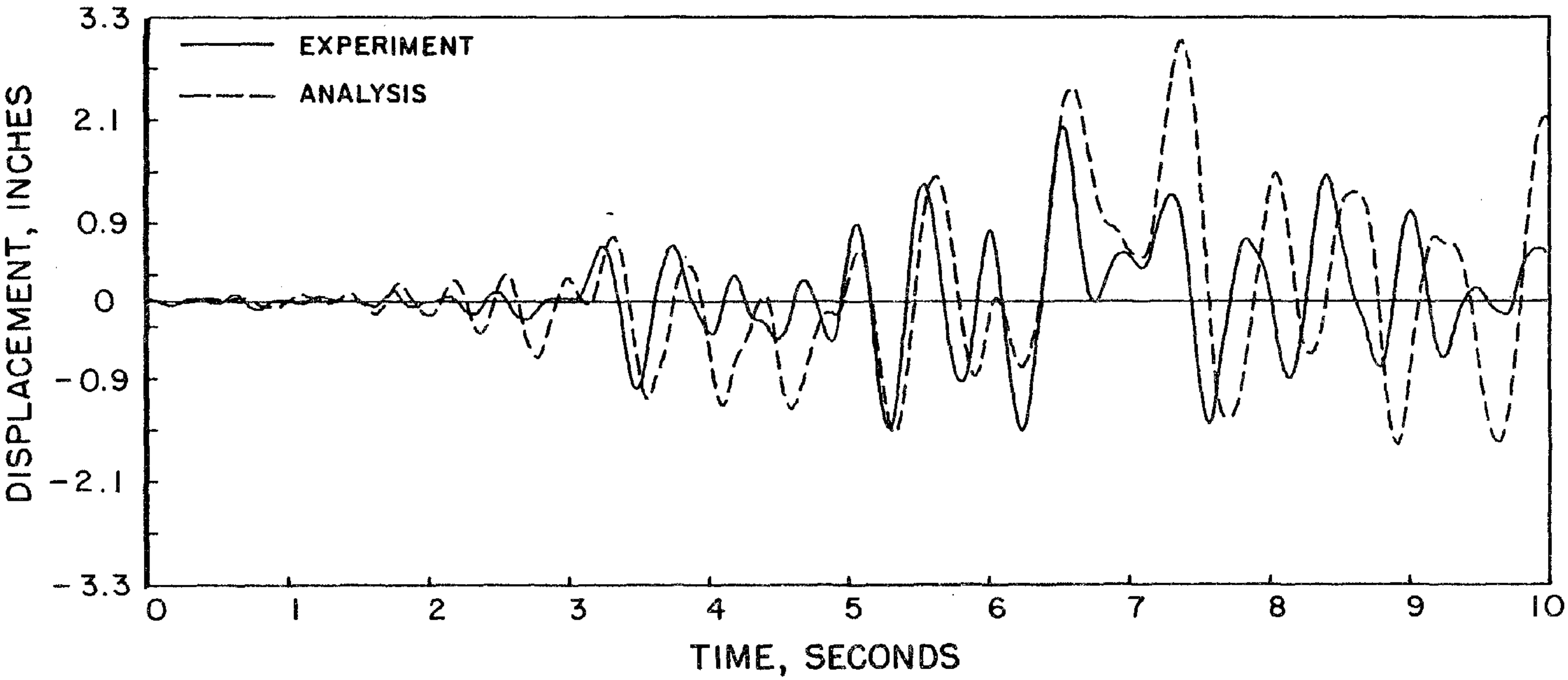

FIG. E3.11 COMPARISON OF ANALYSIS AND EXPERIMENT (T1000)
X DISPLACEMENT AT FIRST FLOOR
CASE 3: SMALL DAMPING, LARGE STIFFNESS DEGRADATION

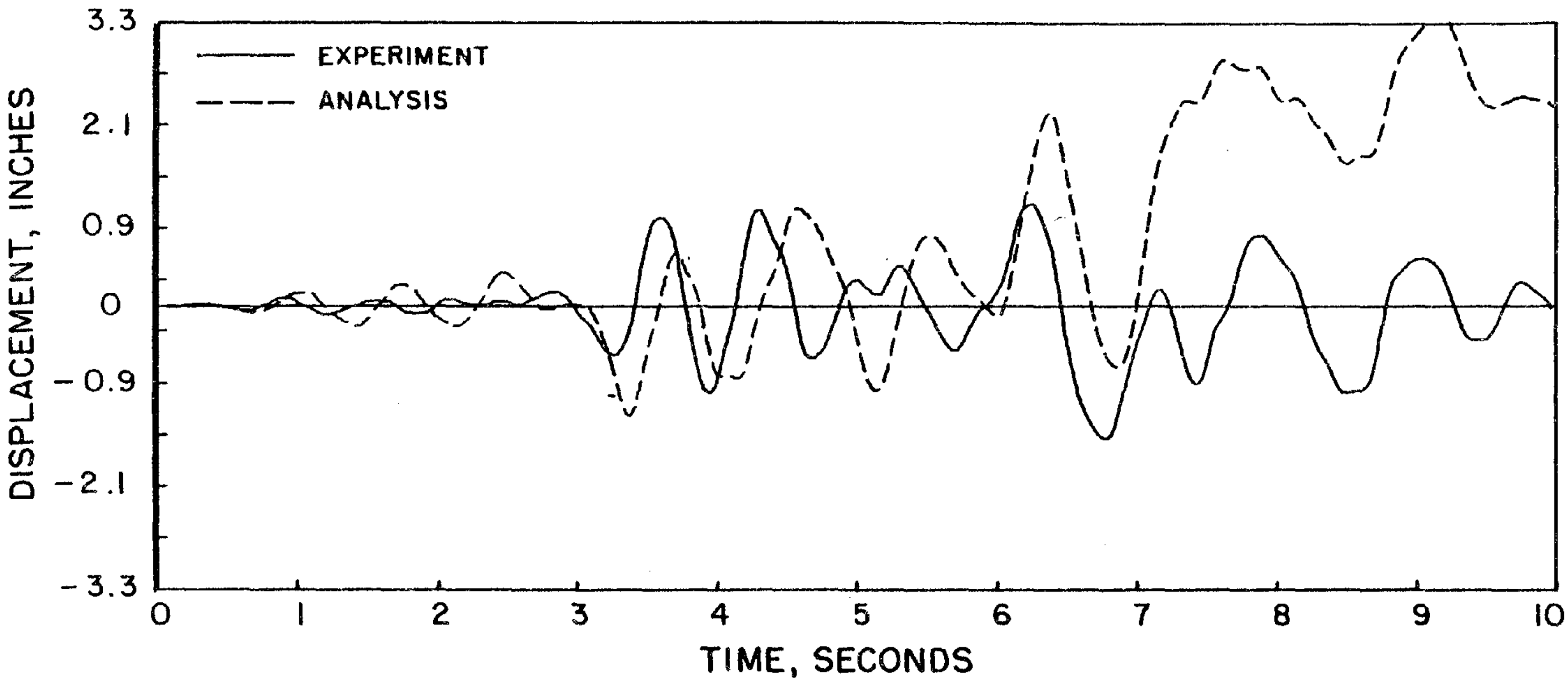

FIG. E3.12 COMPARISON OF ANALYSIS AND EXPERIMENT (T1000)
Y DISPLACEMENT AT FIRST FLOOR
CASE 3: SMALL DAMPING, LARGE STIFFNESS DEGRADATION

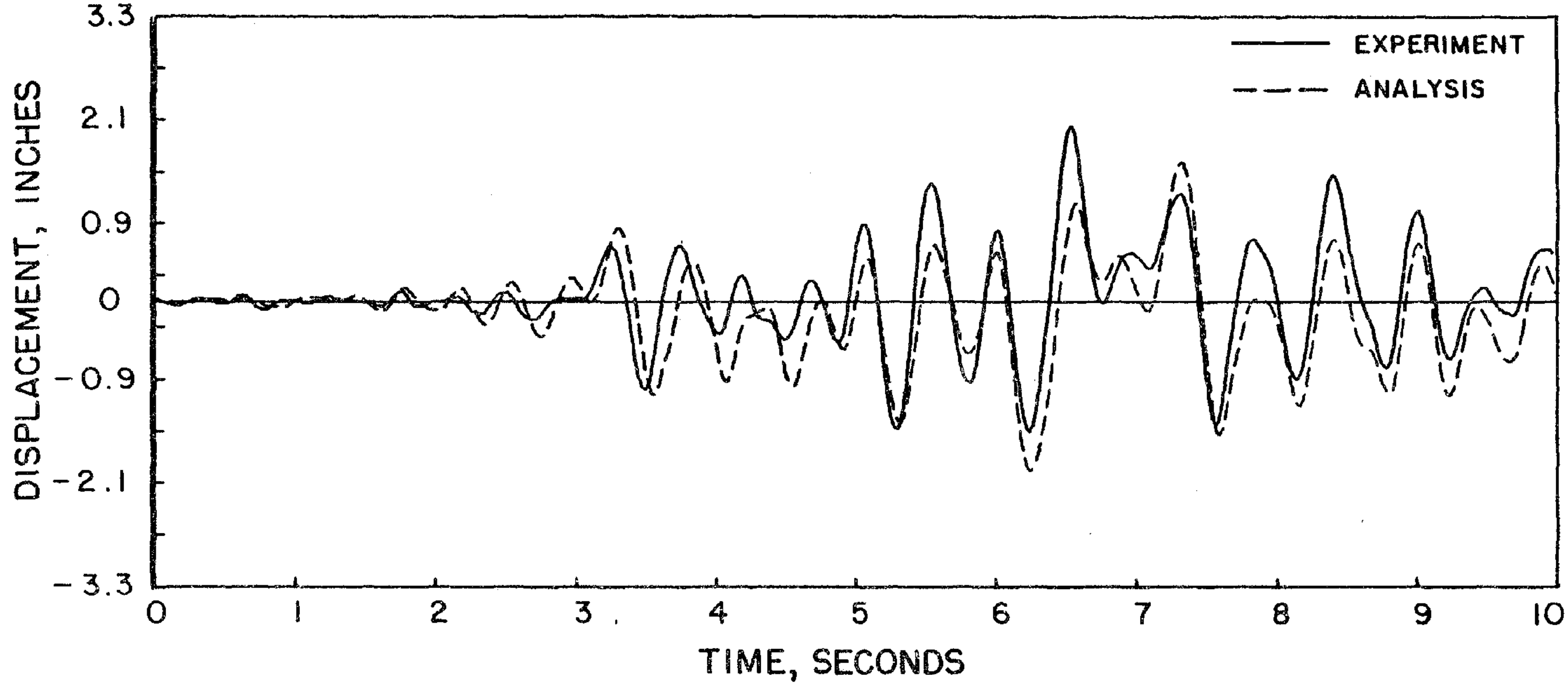

FIG. E3.13 COMPARISON OF ANALYSIS AND EXPERIMENT (T1000)
X DISPLACEMENT AT FIRST FLOOR
CASE 4: SMALL DAMPING, MODERATE STIFFNESS DEGRADATION

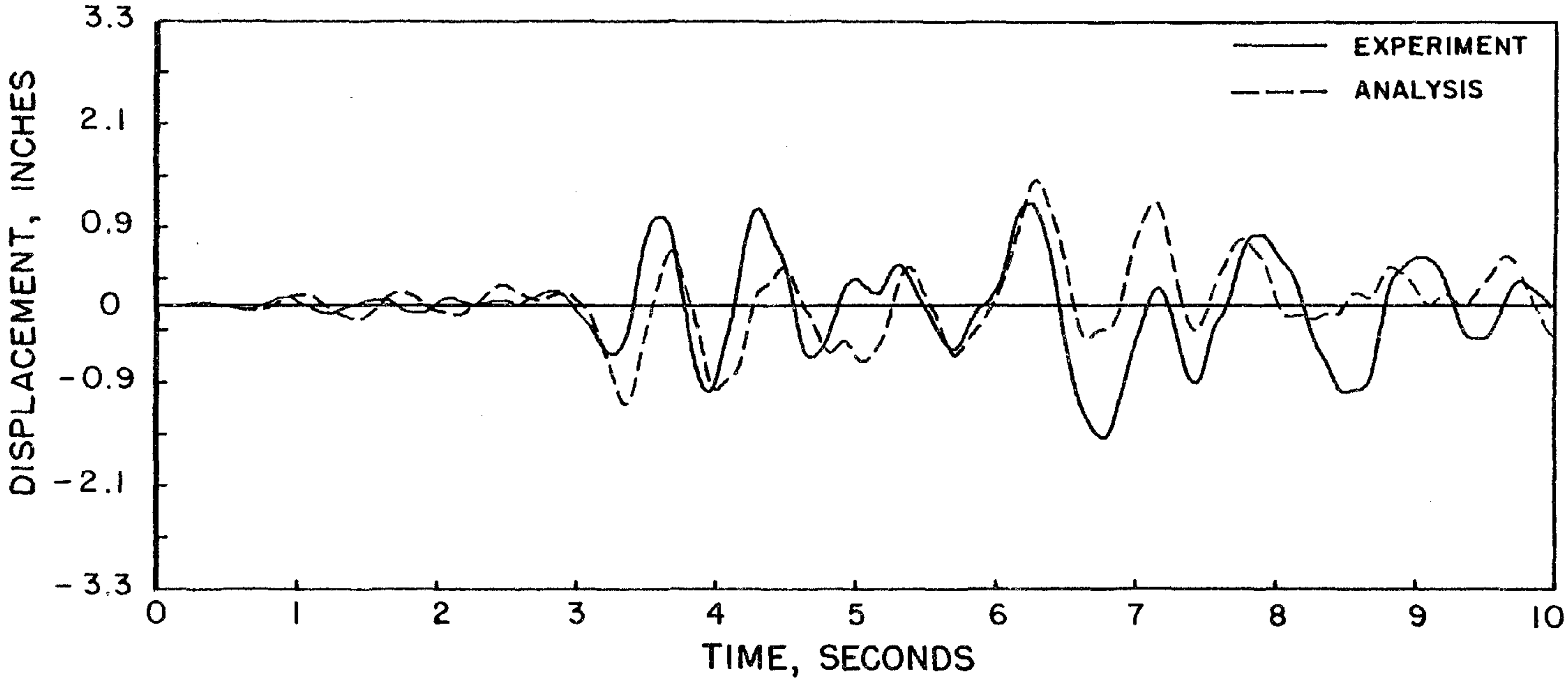

FIG. E3.14 COMPARISON OF ANALYSIS AND EXPERIMENT (T1000)
Y DISPLACEMENT AT FIRST FLOOR
CASE 4: SMALL DAMPING, MODERATE STIFFNESS DEGRADATION

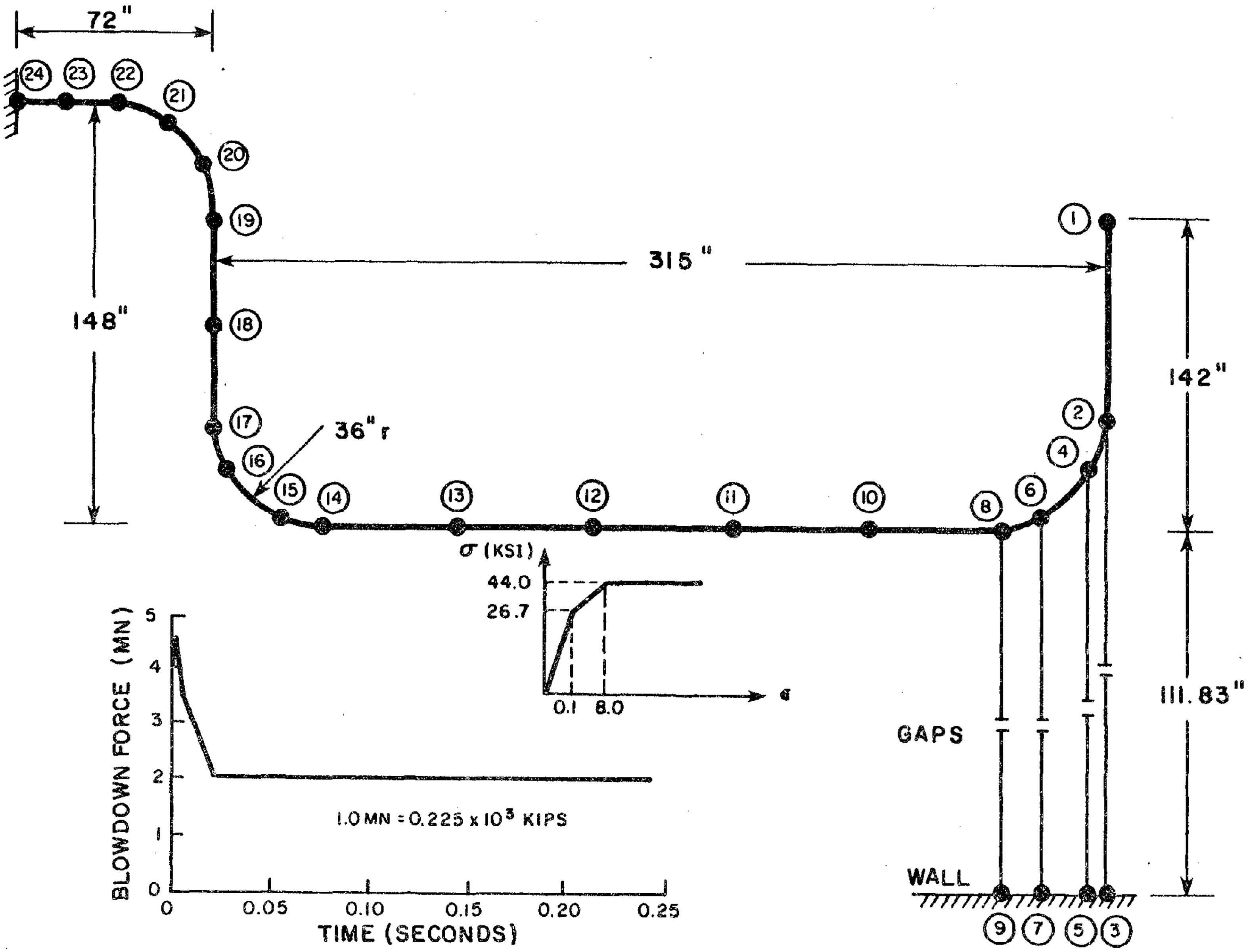

FIG. E4.1 IDEALIZATION OF PIPE WHIP PROBLEM

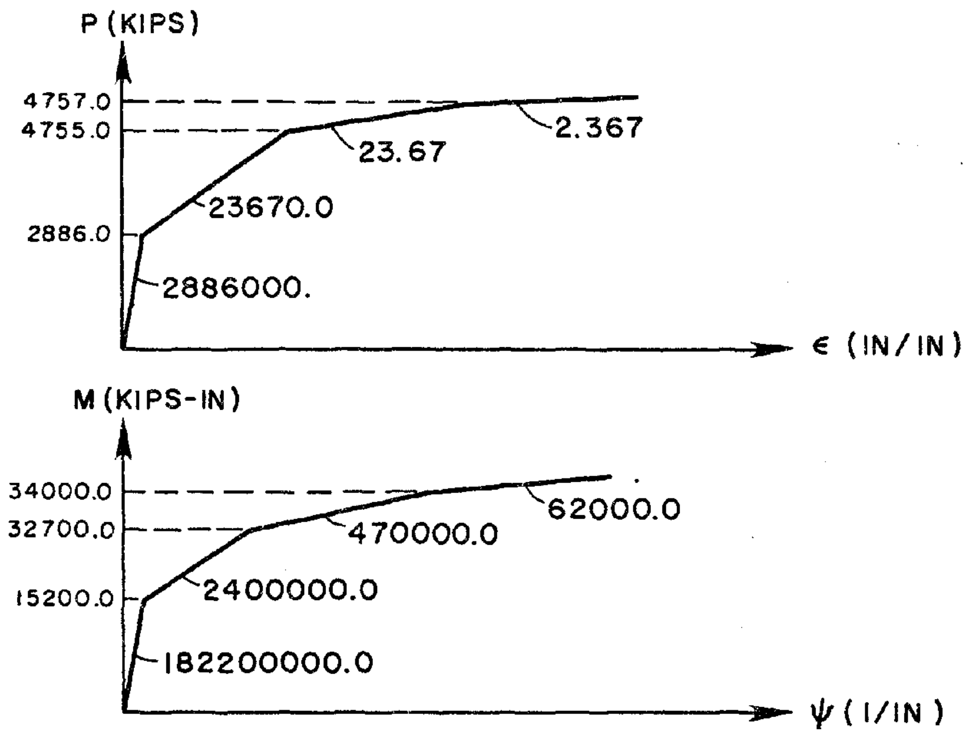

(a) STRAIGHT PIPE

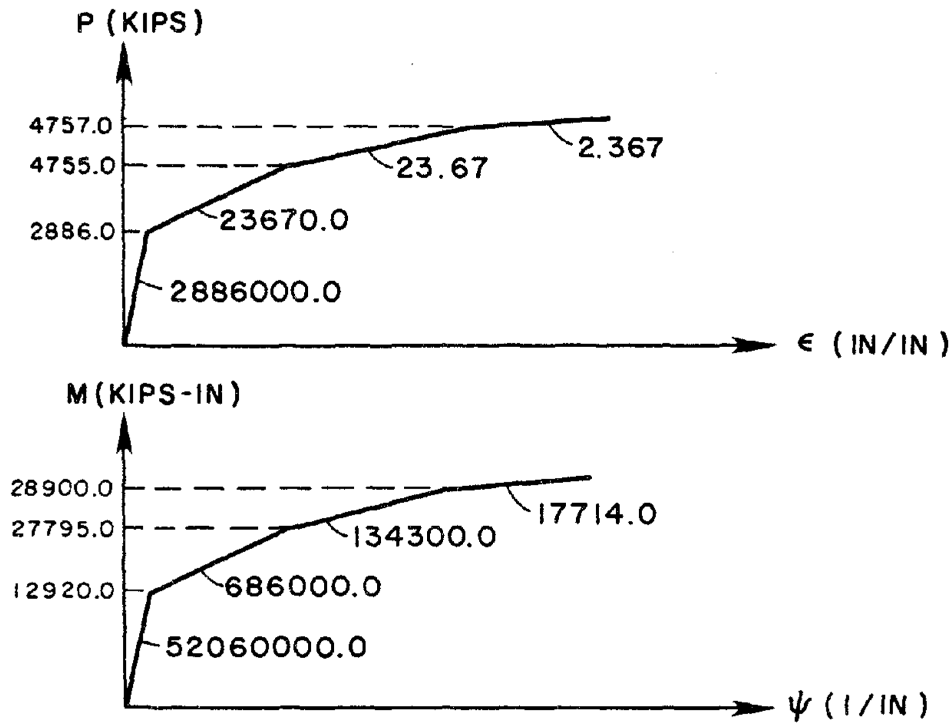

(b) ELBOW

FIG. E4.2 ACTION-DEFORMATION RELATIONSHIPS USED FOR PIPE WHIP ANALYSIS

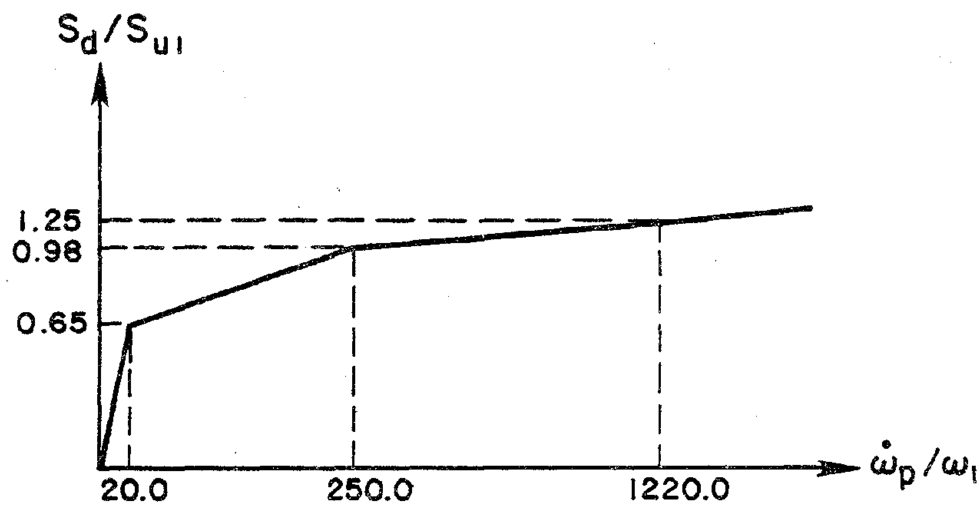

FIG. E4.3 DIMENSIONLESS ACTION VS. DEFORMATION RATE

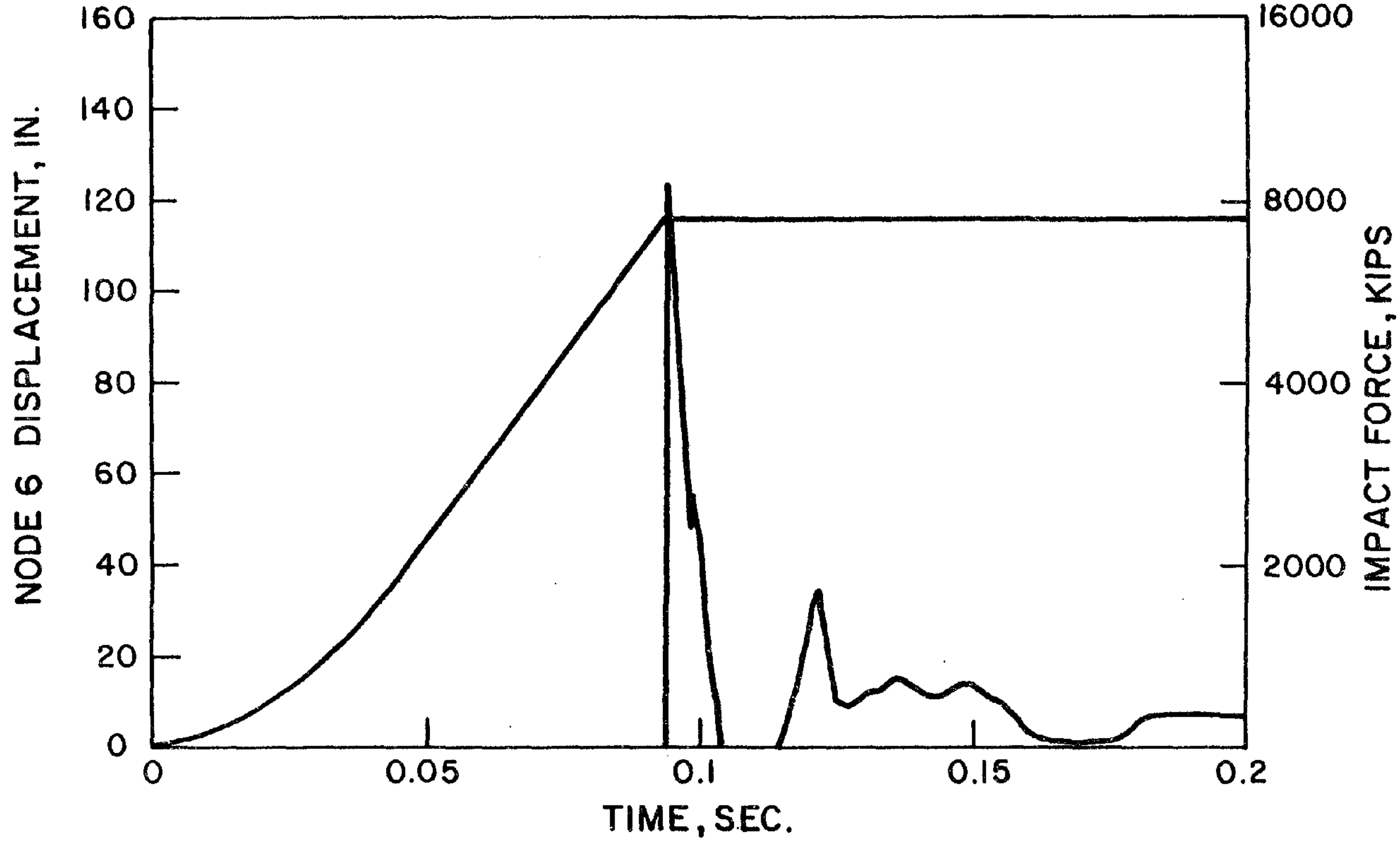

FIG. E4.4 DISPLACEMENT AND IMPACT FORCE HISTORIES

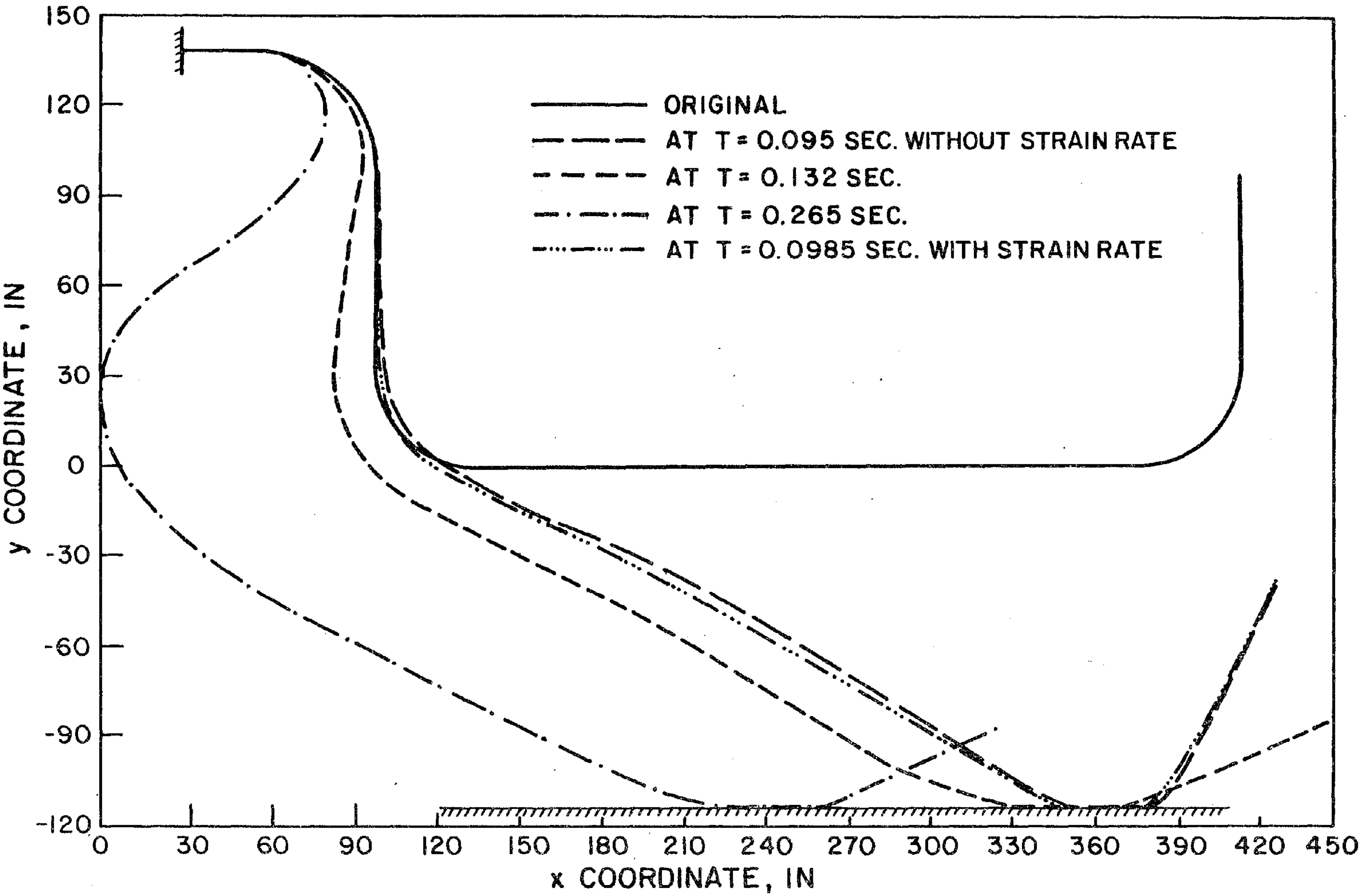

FIG. E4.5 LARGE DISPLACEMENT PIPE WHIP EXAMPLE

TABLE E1.1

```
start    popov-zayas strut example

    8    8    0    8    0    0    2
    1 38.18
    2 37.18
    3 27.69     0.012
    4 20.7675   0.024
    5 13.845    0.036
    6 6.9225    0.048
    7            .06
    8 -1.        .06
    1    111111
    2    001110
    3    001110
    4    001110
    5    001110
    6    001110
    7    001111
    8    111110
    1    1    1
    1
    1 53800.    .01        100000000.100000000.
    1    1    2    1 10000.                        1
    6    6    1 0.00000
    3
    1
101310.   8600.     20.       10.       47.       54.2      542.
101310.   8600.     20.       10.       47.       54.2      542.
101310.   8600.     20.       10.       47.       54.2      542.
53800.    27.4      10.       5.        43.5      43.54     880.52
    2
101310.   8600.     20.       10.       47000.    54200.    542000.
101310.   8600.     20.       10.       47000.    54200.    542000.
101310.   8600.     20.       10.       47000.    54200.    542000.
53800000. 27.4      10.       5.        43500.    43540.    880520.
    3
101310.   8600.     20.       10.       47000.    54200.    542000.
101310.   8600.     20.       10.       47000.    54200.    542000.
101310.   8600.     20.       10.       47000.    54200.    542000.
53800.    27.4      10.       5.        43500.    43540.    880520.
    1    2    3    0    0    2    2    0    0    2    1    0    1

    2    3    4    0    0    3    3    0    0    2    1    0    1

    3    4    5    0    0    3    3    0    0    2    1    0    1
```

```
    4    5    6    0    0    3    3    0    0    2    1    0    1

    5    6    7    0    0    1    1    0    0    2    1    0    1

    6    7    8    0    0    2    2    0    0    2    1    0    1

    0    0    0    1    0    1    0  2116000    0    0
0.0025    0.        0.        0.
     imposed force function                                      (8f10.0)
   21    0    0.   0.         16000     -1.
0.        0.        1.        18830000. 2.        0.        3.        -18830000.
4.        0.        5.        37660000. 6.        0.        7.        -37660000.
8.        0.        9.        56490000. 10.       0.        11.       -56490000.
12.       0.        13.       75320000. 14.       0.        15.       -75320000.
16.       0.        17.       94150000. 18.       0.        19.       -94150000.
20.       0.
    1    0    0    0    0    0
    2
dynm
 8000   -1    0    1    0    1    1
    1    1    0    1.        2
    0    1    1    1    1    1    1
100.      100.

stop
```

TABLE E1.2

```
start      popov-zayas bracing example
 newf

   22   22    0   12    0    0    2
    1     0.        330.      0.
    2     60.       330.      0.
    3     120.      330.      0.
    4     130.      330.      0.
    5     0.        270.      0.
    6     120.      270.      0.
    7     30.6      240.6     0.4242
    8     90.6      239.4     0.4242
    9     60.       210.      0.
   10     30.6      180.6     0.4242
   11     90.6      179.4     0.4242
   12     0.        150.      0.
   13     120.      150.      0.
   14     30.6      120.6     0.4242
   15     90.6      119.4     0.4242
   16     60.       90.       0.
   17     30.6      60.6      0.4242
   18     90.6      59.4      0.4242
   19     0.        30.       0.
   20     120.      30.       0.
   21     0.        0.        0.
   22     120.      0.        0.
    1   001000
    2   001000
    3   001000
    4   111111
    5   001000
    6   001000
   12   001000
   13   001000
   19   001000
   20   001000
   21   111000
   22   111000
    1    1    1
    1
    110000000. 0.001     100000000.100000000.
    1    3    4    1 1.                          1
    6   31    1 0.001
    4
    1
8100715.  10000.    1000.     100.      2059.54   10000.    100000.
8100715.  10000.    1000.     100.      2059.54   10000.    100000.
```

```
8100715.  10000.    1000.     100.      2059.54   10000.    100000.
422820.   100.      10.       5.        685.26    1000.     10000.
   2
406550.   10000.    1000.     100.      219.631   1000.     10000.
406550.   10000.    1000.     100.      219.631   1000.     10000.
406550.   10000.    1000.     100.      219.631   1000.     10000.
95960.    100.      10.       5.        155.52    1000.     10000.
   3
79895.    6790.     10.       5.        42.706    56.017    560.17
79895.    6790.     10.       5.        42.706    56.017    560.17
79895.    6790.     10.       5.        42.706    56.017    560.17
42427.    20.       10.       5.        45.35     45.43     1052.79
   4
171970.   14618.    20.       10.       81.716    108.438   1084.38
171970.   14618.    20.       10.       81.716    108.438   1084.38
171970.   14618.    20.       10.       81.716    108.438   1084.38
73863.    37.       10.       5.        78.96     79.11     1178.33
    1    1    2    0    0    1    1    0    0    1    1    0    0 0.01

    2    2    3    0    0    1    1    0    0    1    1    0    0 0.01

    3    5    6    0    0    3    3    0    0    1    1    0    0 0.01

    4   12   13    0    0    3    3    0    0    1    1    0    0 0.01

    5   19   20    0    0    3    3    0    0    1    1    0    0 0.01

    6    1    5    0    0    1    1    0    0    1    1    0    0 0.01

    7    3    6    0    0    1    1    0    0    1    1    0    0 0.01

    8    5   12    0    0    1    1    0    0    1    1    0    0 0.01

    9    6   13    0    0    1    1    0    0    1    1    0    0 0.01

   10   12   19    0    0    1    1    0    0    1    1    0    0 0.01

   11   13   20    0    0    1    1    0    0    1    1    0    0 0.01

   12   19   21    0    0    1    1    0    0    1    1    0    0 0.01

   13   20   22    0    0    1    1    0    0    1    1    0    0 0.01

   14    2    5    0    0    2    2    0    0    1    1    0    0 0.01

   15    2    6    0    0    2    2    0    0    1    1    0    0 0.01

   16    5    7    0    0    3    3    0    0    1    1    0    0 0.01

   17    7    9    0    0    3    3    0    0    1    1    0    0 0.01

   18    6    8    0    0    3    3    0    0    1    1    0    0 0.01

   19    8    9    0    0    3    3    0    0    1    1    0    0 0.01
```

```
   20    9   10     0     0     3     3     0     0     1     1     0     0 0.01
   21   10   12     0     0     3     3     0     0     1     1     0     0 0.01
   22    9   11     0     0     3     3     0     0     1     1     0     0 0.01
   23   11   13     0     0     3     3     0     0     1     1     0     0 0.01
   24   12   14     0     0     4     4     0     0     1     1     0     0 0.01
   25   14   16     0     0     4     4     0     0     1     1     0     0 0.01
   26   13   15     0     0     4     4     0     0     1     1     0     0 0.01
   27   15   16     0     0     4     4     0     0     1     1     0     0 0.01
   28   16   17     0     0     4     4     0     0     1     1     0     0 0.01
   29   17   19     0     0     4     4     0     0     1     1     0     0 0.01
   30   16   18     0     0     4     4     0     0     1     1     0     0 0.01
   31   18   20     0     0     4     4     0     0     1     1     0     0 0.01
    0    0    0    1    0    1    0   5811400    0    0
0.01      0.        0.        0.
   imposed force function                                        (8f10.0)
   58    0    0.        0.    11400     1.
0.        0.        1.        -460000.  2.        0.        3.        390000.
4.        0.        5.        -1080000. 6.        0.        7.        800000.
8.        0.        9.        -1060000. 10.       0.        11.       990000.
12.       0.        13.       -1250000. 14.       0.        15.       1140000.
16.       0.        17.       -1250000. 18.       0.        19.       1140000.
20.       0.        21.       -720000.  22.       0.        23.       640000.
24.       0.        25.       -1440000. 26.       0.        27.       1320000.
28.       0.        29.       -1630000. 30.       0.        31.       1510000.
32.       0.        33.       -2020000. 34.       0.        35.       1890000.
36.       0.        37.       -710000.  38.       0.        39.       640000.
40.       0.        41.       -2030000. 42.       0.        43.       1900000.
44.       0.        45.       -2030000. 46.       0.        47.       1890000.
48.       0.        49.       -2430000. 50.       0.        51.       2310000.
52.       0.        53.       -3020000. 54.       0.        55.       2430000.
56.       3570000.  57.       4000000.
   -1   -1   -1    0    0    0
dynm
 5700   -1    0    1    0   20   20
    1    1    0    1.        3
    0    1    1    1    1    1    1
100.      100.

stop
```

TABLE E3.1

```
start       oliva r.c. 3-d frame example
 newf

   22   22     0     4     0    10     2
    1 72.125    18.         168.5375
    2 0.        0.          154.85
    3 48.0833   0.          154.85
    4 96.1667   0.          154.85
    5 144.25    0.          154.85
    6 0.        36.         154.85
    7 48.0833   36.         154.85
    8 96.1667   36.         154.85
    9 144.25    36.         154.85
   10 72.125    18.         97.4125
   11 0.        0.          75.725
   12 48.0833   0.          75.725
   13 96.1667   0.          75.725
   14 144.25    0.          75.725
   15 0.        36.         75.725
   16 48.0833   36.         75.725
   17 96.1667   36.         75.725
   18 144.25    36.         75.725
   19 0.        0.          0.
   20 144.25    0.          0.
   21 0.        36.         0.
   22 144.25    36.         0.
   19     111111
   20     111111
   21     111111
   22     111111
    1 0.02802   0.02802
    2 0.00168750.0016875
    5 0.00168750.0016875
    6 0.00168750.0016875
    9 0.00168750.0016875
   10 0.04974   0.04974
   11 0.00198250.0019825
   14 0.00198250.0019825
   15 0.00198250.0019825
   18 0.00198250.0019825
    1    24     1
    1
    1100000000.0.001      100000000.100000000.
    1     1     3     1 100.
    2     1     4     1 100.
    3     1     7     1 100.
    4     1     8     1 100.
```

```
    5    2     7     1 100.
    6    3     6     1 100.
    7    3     7     1 100.
    8    3     8     1 100.
    9    4     7     1 100.
   10    4     8     1 100.
   11    4     9     1 100.
   12    5     8     1 100.
   13   10    12     1 100.
   14   10    13     1 100.
   15   10    16     1 100.
   16   10    17     1 100.
   17   11    16     1 100.
   18   12    15     1 100.
   19   12    16     1 100.
   20   12    17     1 100.
   21   13    16     1 100.
   22   13    17     1 100.
   23   13    18     1 100.
   24   14    17     1 100.
    4   24     1 0.0006
    5    5
    1    3     4.        2.        4.        4.        2.        4.
23317.87  0.        0.        0.        0.        0.
233.2     23.32     1000.     4000.     233.2     23.32     1000.     4000.
23317.87  0.        0.        0.        0.        0.
233.2     23.32     1000.     4000.     233.2     23.32     1000.     4000.
23317.87  233.17    23.32     1000.     4000.     0.   0.   0.   0.
9676.92   96.77     9.677     1000.     4000.     0.   0.   0.   0.
    2    3     4.        2.        4.        4.        2.        4.
32645.    0.        0.        0.        0.        0.
326.45    32.645    1000.     4000.     326.45    32.645    1000.     4000.
32645.    0.        0.        0.        0.        0.
326.45    32.645    1000.     4000.     326.45    32.645    1000.     4000.
32645.    326.45    32.645    1000.     4000.     0.   0.   0.   0.
9851.8    98.52     9.852     1000.     4000.     0.   0.   0.   0.
    3    3     4.        2.        4.        4.        2.        4.
26472.78  0.        0.        0.        0.        0.
264.73    26.473    1000.     4000.     264.73    26.473    1000.     4000.
26472.78  0.        0.        0.        0.        0.
264.73    26.473    1000.     4000.     264.73    26.473    1000.     4000.
26472.78  264.73    26.473    1000.     4000.     0.   0.   0.   0.
8019.7    80.2      8.02      1000.     4000.     0.   0.   0.   0.
    4    3     4.        2.        4.        4.        2.        4.
1771.25   0.        0.        0.        0.        0.
17.713    1.77      1000.     4000.     17.713    1.77      1000.     4000.
9919.     0.        0.        0.        0.        0.
99.19     9.92      1000.     4000.     99.19     9.92      1000.     4000.
1594.12   15.9412   1.594     1000.     4000.     0.   0.   0.   0.
2054.65   20.5465   2.05465   1000.     4000.     0.   0.   0.   0.
    5    3     4.        2.        4.        4.        2.        4.
1665.7    0.        0.        0.        0.        0.
16.66     1.666     1000.     4000.     16.66     1.666     1000.     4000.
5552.33   0.        0.        0.        0.        0.
```

```
55.52      5.552      1000.      4000.      55.52      5.552      1000.      4000.
1665.7     16.66      1.666      1000.      4000.      0.    0.    0.    0.
2146.9     21.47      2.147      1000.      4000.      0.    0.    0.    0.
   1 4.25
   2          -4.25
   3 0.        0.        2.875      -2.875
   4 0.        0.        0.          0.        -5.6875   5.6875
   5 0.        0.        0.          0.        -5.6875    0.
```

1	2	3	1	20	0	0	1	1	0	2	0	0	0.01
2	3	4	1	20	0	0	1	0	0	2	0	0	0.01
3	4	5	1	20	0	0	1	2	0	2	0	0	0.01
4	11	12	1	20	0	0	2	1	0	2	0	0	0.01
5	12	13	1	20	0	0	2	0	0	2	0	0	0.01
6	13	14	1	20	0	0	2	2	0	2	0	0	0.01
7	6	7	1	22	0	0	1	1	0	2	0	0	0.01
8	7	8	1	22	0	0	1	0	0	2	0	0	0.01
9	8	9	1	22	0	0	1	2	0	2	0	0	0.01
10	15	16	1	22	0	0	2	1	0	2	0	0	0.01
11	16	17	1	22	0	0	2	0	0	2	0	0	0.01
12	17	18	1	22	0	0	2	2	0	2	0	0	0.01
13	2	6	1	21	0	0	3	3	0	2	0	0	0.01
14	5	9	1	22	0	0	3	3	0	2	0	0	0.01
15	11	15	1	21	0	0	3	3	0	2	0	0	0.01
16	14	18	1	21	0	0	3	3	0	2	0	0	0.01
17	2	11	1	21	0	0	4	4	0	2	0	0	0.01
18	5	14	1	22	0	0	4	4	0	2	0	0	0.01
19	11	19	1	21	0	0	5	5	0	2	0	0	0.01
20	14	20	1	22	0	0	5	5	0	2	0	0	0.01
21	6	15	1	19	0	0	4	4	0	2	0	0	0.01
22	9	14	1	20	0	0	4	4	0	2	0	0	0.01
23	15	21	1	19	0	0	5	5	0	2	0	0	0.01

```
  24   18   22    1   20    0    0    5    5    0    2    0    0     0.01

   0    0    1    0    0    0    0 1500 2600    0
0.01952   0.        0.        1.5
   t 100(2) ground accel.                                   (8f10.8)
 1500     0 0.01952  0.        2600      386.4
-.00108555 .00065332-.00058873 .00264060 .00139855 .00065332 .00214378 .00214378
 .00139855-.00058873 .00115014-.00133396 .00189537-.00034032-.00009191 .00015650
 .00015650 .00065332-.00034032-.00083714-.00009191 .00189537-.00282442-.00009191
-.00009191 .00040491-.00133396-.00356965-.00804103-.00555693-.00481170-.00456329
 .00015650 .00090173 .00363424 .00413106 .00139855 .00040491 .00115014 .00040491
 .00115014 .00338583 .00413106 .00288901 .00090173 .00313742 .00512470 .00413106
 .00462788 .00189537-.00034032 .00040491 .00239219 .00288901 .00015650-.00083714
-.00257601-.00431488-.00356965-.00158237-.00406647-.00083714-.00034032-.00108555
-.00158237-.00282442-.00580534-.00332124-.00506011-.00356965-.00381806-.00406647
-.00630216-.00282442 .00139855 .00437947 .00711198 .00115014 .00239219 .00288901
 .00487629 .00736039 .00363424-.00232760 .00015650-.00232760-.00729580-.00779262
-.00679898-.00356965 .00115014 .00512470 .00562152 .00040491-.00356965-.00506011
-.00655057-.00456329-.00257601 .00164696 .00785721 .00760880 .00611834 .00288901
-.00257601-.00456329-.00307283-.00555693-.00605375-.00481170-.00307283 .00338583
 .00611834 .00860244 .00860244 .00810562 .00785721 .00512470 .00413106 .00686357
 .00810562 .00512470 .00239219 .00338583 .00239219 .00040491 .00338583-.00282442
 .00065332 .00189537 .00239219 .00586993 .00909926 .00909926 .00860244 .01307382
 .01282541 .01779361 .02027771 .01903566 .01406746 .01009290 .00512470 .00586993
 .00437947 .00512470 .00686357-.00133396-.00555693-.00729580-.01176718-.01524492
-.01474810-.00257601 .00040491-.00257601-.00928308-.01996471-.02865906-.03313045
-.03437249-.02816225-.02418768-.05027074-.06144919-.05151279-.04728982-.03163999
-.00009191 .02301022 .03766641 .03841164 .03567913 .03071093 .02301022 .02375545
 .02524591 .02027771 .02052612 .00835403 .00562152-.00034032-.00133396-.00207919
 .00363424 .00711198 .00462788-.00083714-.00828944-.01921948-.01897107-.01474810
-.01027672-.00481170-.00754421-.01300923-.01623856-.02542973-.02617496-.01772902
-.00977990 .00413106 .01580633 .02276181 .02027771 .01257700-.00108555-.01822585
-.02667179-.02393927-.01027672 .00885085 .02201658 .02847524 .02673637 .01878725
 .01133495 .00264060-.00655057-.01325764-.01499651-.01400288-.00630216 .00214378
 .01481269 .03046252 .03369185 .02599114 .02151976 .01878725 .00512470-.00729580
-.01300923-.00903467-.00257601-.00009191 .00313742 .00711198 .01307382 .01679997
 .01456428 .00562152 .00338583 .00537311 .00984449 .01232859 .01679997 .01058972
 .00214378-.01127036-.02319405-.03660819-.04406049-.03909229-.02443609-.03909229
-.03760183-.02095835-.00356965 .00959608 .02474909 .03095934 .02673637 .02201658
 .01878725 .01953248 .02773001 .03791482 .02822683 .01307382-.00555693-.01723220
-.01748061-.01176718-.01102195-.01226400-.02244882-.02692020-.01648697-.02021312
-.01599015-.00406647 .00661516 .00586993 .00065332-.00754421-.00953149-.01002831
-.00828944-.00058873 .00413106 .00785721 .01034131 .00686357 .00015650-.00456329
-.00406647 .00115014 .00437947-.00183078-.01375446-.02220040-.02493291-.01797743
-.00605375 .00760880 .02027771 .03418867 .04511872 .04586394 .03692118 .05530352
 .05902965 .05753922 .04934169 .04015052 .02946888 .01158336-.00853785-.02145517
-.03039793-.04704141-.05200961-.05275484-.03660819-.01797743-.00356965-.00356965
-.00555693-.01499651-.02393927-.01971630-.00828944 .00288901 .00264060 .00636675
 .01108654 .00984449 .00785721 .00512470-.00630216-.01524492-.02418768-.01822585
-.02766543-.03635978-.03337885-.01946789 .00015650 .01431587 .02002930 .01953248
 .01481269 .00959608 .01158336 .00984449 .00860244 .00810562 .00760880 .00909926
 .00413106 .00239219-.00009191-.00804103-.01350605-.03288204-.04306684-.04406049
-.03511773-.03313045-.02791384-.02269723-.01201559 .00065332 .01481269 .03021411
 .04487031 .04660917 .03443708 .02450068 .02201658 .02524591 .02375545 .01878725
```

.01978089	.01729679	.00189537	-.01599015	-.03139158	-.02344246	-.00530852	-.00183078
.00686357	.01406746	.01406746	.01381905	.01580633	.00934767	.01034131	.00512470
.00611834	.00562152	.00239219	-.00257601	-.01102195	-.01897107	-.01772902	-.00953149
-.00108555	.00835403	.01406746	.02127135	.02872365	.02847524	.02176817	.00537311
-.01276082	-.02816225	-.02443609	-.02294564	-.01897107	-.01300923	-.01102195	-.01127036
-.01176718	-.01151877	-.02046153	-.02617496	-.02145517	-.01300923	.00090173	.01506110
.01903566	.01878725	.01034131	-.00183078	-.01052513	-.02642337	-.03412408	-.03238522
-.02170358	-.01127036	.00562152	.02350704	.03890846	.04536712	.03369185	.01456428
.01108654	.01058972	.00860244	-.00481170	-.01599015	-.01797743	-.02393927	-.02791384
-.01872267	-.01052513	-.00754421	.00264060	.01034131	.01729679	.02176817	.02077453
.01829043	.01406746	.01655156	.02325863	.02077453	.00611834	-.01276082	-.02195199
-.02220040	-.01648697	-.01599015	-.02418768	-.02319405	-.00356965	.01481269	.02648796
.02723319	.01903566	.01953248	.02549432	.02549432	.01953248	.01853884	.01729679
.01679997	.00810562	-.00307283	-.00779262	-.01077354	-.00928308	-.00356965	-.00332124
-.00853785	-.01772902	-.02443609	-.01921948	-.00828944	.00437947	.00413106	.00562152
.00040491	-.00058873	-.00456329	-.00729580	-.00729580	-.00828944	-.00878626	-.00555693
-.00232760	-.00406647	-.00530852	-.00332124	-.00804103	-.00903467	-.01002831	-.01400288
-.01698379	-.01698379	-.01325764	-.00853785	-.00754421	-.00530852	.00115014	-.00431488
-.00506011	-.01176718	-.01027672	-.00506011	.00164696	-.00083714	.00040491	.00413106
.00860244	.01406746	.01729679	.02176817	.02623955	.02648796	.01829043	.01530951
.01406746	-.00009191	-.01425128	-.01772902	-.01052513	.00040491	.00736039	.01332223
.01704838	.01878725	.01481269	.00562152	-.00605375	-.01698379	-.02195199	-.02021312
-.01474810	-.00605375	-.00307283	-.00158237	.00313742	.00313742	.00264060	.00139855
.00040491	-.00207919	-.00232760	-.00530852	-.00903467	-.01127036	-.00779262	.00239219
.01257700	.01630315	.00909926	.01580633	.02176817	.02226499	.01704838	.00909926
.00015650	-.00779262	-.01400288	-.01648697	-.01599015	-.01449969	-.01176718	-.00754421
-.00853785	-.01027672	-.01425128	-.01946789	-.01673538	-.01077354	.00388265	.01307382
.01779361	.02002930	.01953248	.00736039	.00661516	.00984449	.00512470	.00189537
.01009290	.00611834	.00015650	-.00853785	-.01499651	-.01648697	-.01027672	-.00183078
.00288901	.00537311	.00537311	.00810562	.00636675	-.00083714	-.00630216	-.00655057
-.00679898	-.01052513	-.00530852	-.01027672	-.01996471	-.02070994	-.01400288	-.00282442
.00413106	.01034131	.01406746	.01381905	.01058972	.01183177	.00785721	.00413106
.00661516	.00562152	.00313742	-.00704739	-.00953149	-.00903467	-.01276082	-.01748061
-.01698379	-.02095835	-.01599015	-.00878626	.00661516	.02499750	.03518231	.03120775
.02151976	.03418867	.03915687	.03120775	.01232859	-.00232760	-.02021312	-.02692020
-.02592655	-.01797743	-.01151877	-.00580534	-.00133396	-.00083714	-.00431488	-.00580534
-.01077354	-.00356965	-.00431488	.00040491	.00413106	.00040491	.00040491	-.00332124
-.00555693	-.00580534	-.00456329	-.00729580	-.01151877	-.01499651	-.01375446	-.00878626
.00264060	.00810562	.01034131	.00711198	.00686357	.00462788	.00115014	-.00431488
-.00779262	-.00555693	-.00009191	.01431587	.02077453	.01530951	.01232859	.01853884
.01928407	.01058972	.00288901	-.00605375	-.00481170	-.00729580	-.00282442	-.00034032
-.00332124	-.00406647	-.00506011	-.00555693	-.00506011	.00139855	.00363424	.00810562
.00537311	.00562152	.00413106	.00214378	-.00282442	-.00853785	-.01474810	-.01723220
-.01549333	-.01027672	-.00977990	-.02046153	-.02716861	-.02841066	-.02468450	-.01549333
-.00207919	.00760880	.01878725	.02872365	.03195298	.02648796	.01704838	.01506110
.00934767	.00909926	-.00083714	-.00878626	-.01797743	-.01300923	-.01797743	-.02418768
-.02070994	-.01549333	-.00630216	.00065332	.00512470	.01133495	.01530951	.01530951
.01605474	.01034131	.01009290	.00760880	.00487629	.00885085	.01083813	.00736039
-.00108555	-.01077354	-.01425128	-.00828944	-.00232760	-.00058873	.00040491	.00040491
.00413106	.00115014	-.00009191	-.00481170	-.01449969	-.02046153	-.02766543	-.02915588
-.02592655	-.01872267	-.00580534	-.00034032	.00736039	.01530951	.01530951	.00512470
.00040491	.00040491	.00313742	.00437947	.00711198	.00835403	.01108654	.01506110
.02052612	.01903566	.01530951	.00711198	.01208018	.00984449	.00115014	-.00133396
.00015650	-.00207919	-.00406647	-.00406647	-.00655057	-.00804103	-.00804103	-.00729580

```
-.00456329-.00555693-.00779262-.00381806 .00015650 .00338583 .00636675 .00835403
 .00959608 .00711198 .01083813 .01133495 .00413106-.00034032-.00034032-.00630216
-.00779262-.00481170-.00083714 .00288901 .00711198 .00413106 .00686357 .00860244
 .00487629 .00288901 .00363424 .00388265 .00487629 .00736039 .00313742 .00164696
-.00108555-.00704739-.01002831-.01151877-.00878626-.00853785-.00679898-.01002831
-.00928308-.00356965-.00332124 .00065332-.00133396-.00481170-.01102195-.01872267
-.02195199-.01797743-.00779262 .00115014 .00711198 .00984449 .01083813 .01357064
 .00959608 .00785721 .00760880 .00984449 .00959608 .01058972 .01232859 .01605474
 .01108654 .00512470-.00332124-.00953149-.01648697-.01897107-.01623856-.00530852
-.00356965-.00381806-.00009191-.00158237 .00040491 .00363424 .00736039 .00363424
-.00133396-.00381806-.00506011-.00555693-.00406647-.00605375-.00779262-.00903467
-.01077354-.00853785-.00530852 .00164696 .00736039 .00959608 .00860244 .00860244
 .00760880 .00611834 .00413106 .00413106 .00388265 .00413106 .00860244 .00760880
 .00462788 .00189537 .00139855 .00090173 .00512470 .00512470-.00083714-.00108555
-.00679898-.00828944-.01027672-.01127036-.01027672-.01151877-.01996471-.01623856
-.00754421 .00264060 .01133495 .01530951 .01083813 .00338583 .00040491-.00133396
-.00009191 .00388265 .00562152 .00760880 .00711198 .00661516 .01108654 .01332323
 .00686357 .00040491-.00903467-.01176718-.00853785-.00481170-.00083714 .00338583
 .00661516 .00835403 .00711198 .00462788 .00115014-.00605375-.00977990-.01052513
-.00754421-.00580534-.01077354-.01251241-.00903467-.00605375-.00183078-.00108555
 .00015650 .00214378 .00388265 .00636675 .00338583 .00413106 .00661516 .00413106
 .00586993 .00363424-.00183078-.00133396-.00108555-.00332124-.00083714 .00214378
 .00413106 .00214378 .00164696 .00512470 .00636675 .00835403 .00934767 .01158336
 .00785721 .00363424-.00009191-.00282442-.00481170-.00431488-.00183078-.00232760
 .00164696 .00189537 .00164696-.00108555-.00555693-.01002831-.00828944-.00729580
-.00555693-.00332124-.00332124-.00356965-.00481170-.00506011-.00828944-.00605375
-.00207919 .00164696 .00835403 .01009290 .00760880 .00338583 .00810562 .01058972
 .01183177 .00885085 .00661516 .00686357 .00189537-.00183078-.00655057-.00704739
-.00456329-.00356965-.00555693-.00828944-.00853785-.00704739-.00530852-.00257601
 .00139855 .00388265 .00586993 .00636675 .00164696-.00207919-.00481170-.00431488
-.00679898-.00555693-.00158237-.00282442-.00679898-.00630216-.00704739-.00655057
-.00381806-.00332124 .00040491 .00512470 .00487629 .00214378 .00040491-.00356965
-.00580534-.00630216-.01151877-.00928308-.00679898-.00356965 .00139855 .00785721
 .00885085 .00934767 .00934767 .01009290 .00785721 .00388265 .00164696-.00133396
 .00115014-.00058873 .00090173-.00058873-.00183078-.00580534-.00977990-.01027672
-.00754421-.00332124 .00090173 .00661516 .00760880 .01208018 .01133495 .00860244
 .00810562 .01332223 .01530951 .01605474 .01456428 .01232859 .00885085 .00115014
-.00630216-.01276082-.01474810-.01375446-.01276082-.00779262-.00257601 .00214378
 .00189537 .00040491-.00108555-.00307283-.00754421-.00630216-.00506011-.00332124
-.00133396-.00058873-.00183078-.00108555-.00009191-.00058873 .00214378 .00239219
 .00065332-.00207919-.00083714-.00183078 .00139855-.00034032 .00214378 .00437947
 .00512470 .00512470 .00686357 .00388265 .00388265 .00214378-.00083714-.00232760
-.00058873-.00406647-.00679898-.00481170-.00655057-.00530852 .00015650-.00207919
-.00058873-.00207919-.00356965-.00431488-.00729580-.00853785-.00605375-.00083714
 .00214378 .00885085 .00760880 .00562152 .00686357 .00586993-.00009191 .00388265
 .00363424-.00108555-.00257601-.00431488-.00158237-.00307283 .00040491-.00158237
-.00257601-.00356965-.00456329-.00704739-.00779262-.00655057-.00406647-.00506011
-.00481170-.00332124-.00555693-.00207919-.00207919-.00133396-.00083714 .00040491
-.00257601 .00239219 .00537311 .00214378 .00065332-.00307283-.00481170-.00307283
-.00133396-.00183078 .00214378 .00214378 .00214378 .00413106 .00760880 .00984449
 .00909926 .00785721 .00760880 .01058972 .00586993 .00388265 .00586993 .00512470
 .00388265 .00313742 .00313742 .00139855 .00040491-.00232760 .00040491-.00108555
-.00605375-.00356965-.00381806-.00530852-.00506011-.00307283-.00257601-.00108555
-.00356965-.00530852-.00282442-.00133396-.00158237 .00115014 .00015650-.00282442
```

```
-.00034032 .00214378 .00562152 .00860244 .00487629 .00562152 .00860244 .00611834
 .00214378 .00065332-.00183078-.00356965-.00356965-.00506011-.00456329-.00232760
-.00183078 .00139855 .00090173 .00363424 .00388265 .00437947 .00736039 .00661516
 .00711198 .00636675 .00363424 .00562152 .00611834 .00586993 .00313742-.00034032
-.00083714-.00183078-.00034032-.00058873-.00083714-.00356965-.00257601-.00332124
-.00332124-.00456329-.00655057-.00804103-.00928308-.01127036-.00953149-.01102195
-.00555693-.00754421-.00729580-.00332124 .00139855 .00189537 .00115014 .00065332
 .00139855 .00090173 .00189537 .00015650-.00083714-.00034032-.00034032-.00058873
 .00015650-.00034032 .00040491 .00214378-.00058873 .00189537 .00115014 .00115014
-.00158237 .00189537-.00108555-.00406647-.00083714-.00009191 .00065332-.00034032
 .00065332 .00090173 .00239219 .00090173 .00239219-.00009191-.00083714-.00058873
 .00040491-.00034032 .00090173 .00065332-.00133396-.00058873 .00015650-.00009191
 .00090173 .00139855-.00158237 .00015650-.00058873 .00015650 .00264060-.00307283
 .00015650-.00034032-.00108555-.00183078-.00009191 .00015650-.00009191 .00065332
 .00015650 .00164696 .00313742 .00090173 .00040491-.00158237-.00232760-.00108555
-.00083714-.00133396-.00009191-.00083714 .00040491 .00139855 .00040491 .00015650
 .00164696-.00009191-.00158237 .00040491-.00207919-.00183078 .00090173-.00083714
-.00083714-.00083714 .00139855 .00065332 .00065332 .00090173 .00015650 .00115014
 .00115014 .00015650-.00034032-.00108555-.00232760-.00083714-.00207919-.00034032
-.00009191-.00133396 .00090173 .00065332 .00115014 .00040491 .00115014-.00009191
 .00065332-.00207919-.00183078-.00083714-.00009191 .00065332-.00058873 .00040491
 .00065332 .00115014-.00083714 .00115014-.00009191 .00015650-.00183078 .00065332
-.00133396 .00040491 .00065332-.00158237-.00034032-.00232760-.00058873-.00108555
 .00189537-.00083714-.00058873 .00139855-.00034032 .00115014 .00065332-.00083714
-.00108555-.00009191-.00356965 .00090173-.00083714-.00108555 .00090173 .00015650
 .00090173 .00115014 .00189537-.00083714 .00065332-.00207919 .00040491-.00083714
-.00133396 .00015650-.00108555 .00090173 .00040491 .00090173 .00115014 .00115014
 .00040491 .00189537-.00183078 .00139855-.00058873-.00108555-.00034032-.00058873
-.00158237-.00009191-.00058873 .00090173 .00164696-.00034032 .00239219-.00009191
 .00115014-.00133396 .00139855-.00108555-.00133396-.00108555-.00058873-.00108555
 .00015650 .00164696-.00058873 .00164696-.00133396 .00239219-.00133396 .00040491
-.00009191-.00133396-.00009191-.00058873
   -1    -1     0     0     0     0
dynm
  512    -1     1     0     0     1     1
    1     0 0.906308      1     0 0.422518      1     0 0.
    0     1     1     1     1     1     1
100.       100.

stop
```

REFERENCES

1. Kanaan, A. and Powell, G., "DRAIN-2D - A General Purpose Computer Program for Dynamic Analysis of Inelastic Plane Structures," Earthq. Engng. Res. Ctr., *Report No. EERC 73-22,* University of California, Berkeley, 1973.

2. Otani, S. and Sozen, M. A., "Behavior of Multistory Reinforced Concrete Frames During Earthquakes," Civil Engineering Studies, *Structural Research Series No. 392,* University of Illinois, Urbana, November 1972.

3. Hidalgo, P. and Clough, R. W., "Earthquake Simulator Study of a Reinforced Concrete Journal," Earthq. Engng. Res. Ctr., *Report No. EERC 74-13,* University of California, Berkeley, 1974.

4. Takeda, T., Sozen, M., and Neilson, N., "Reinforced Concrete Response to Simulated Earthquakes," *J. Struc. Div., ASCE,* V. 96, ST-12, December 1970.

5. Litton, R. W., "A Contribution to the Analysis of Concrete Structures under Cyclic Loading," *Ph.D. Dissertation,* Department of Civil Engineering, University of California, Berkeley, 1975.

6. Otani, S. and Sozen, M. A., "Behavior of Multistory Reinforced Concrete Frames During Earthquakes," Civil Engineering Studies, *Structural Research Series No. 392,* University of Illinois, Urbana, November 1972.

7. Riahi, A., Powell, G. H., and Mondkar, D. P., "3D Beam-Column Element (Type 2-Parallel Element Theory) for the ANSR-II Program," Earthq. Engng. Res. Ctr., *Report No. EERC 79-31,* University of California, Berkeley, 1979.

8. Mondkar, D. P. and Powell, G. H., "ANSR-I - A General Purpose Computer Program for Analysis of Nonlinear Structural Response," Earthq. Engng. Res. Ctr., *Report No. EERC 75-37,* University of California, Berkeley, 1975.

9. Mondkar, D. P. and Powell, G. H., "ANSR-II - Analysis of Nonlinear Structural Response, Users Manual," Earthq. Engng. Res. Ctr., *Report No. EERC 79-17,* University of California, Berkeley, 1979.

10. Takizawa, H. and Aoyama, H., "Biaxial Effects in Modelling Earthquake Response of R/C Structures," *Int. J. Earthq. Engng. Struc. Dyn.,* V. 4, 1976.

11. Morris, N. F., "Dynamic Analysis of Elasto-Plastic Space Structures," *Proceedings,* International Symposium on Earthq. Struct. Engng., St. Louis, Missouri, U.S.A., 1976.

12. Tebedge, N. and Chen, W. F., "Design Criteria for H Columns under Biaxial Loading," *J. Struct. Div., ASCE,* 100, 579-598, 1974.

13. Uzgider, E. A., "Inelastic Response of Space Frames to Dynamic Loads," *Computers and Structures,* Vol. 11, pp. 97-112, Pergammon Press Ltd., Great Britain, 1980.

14. Aktan, A. E., Pecknold, D.A.W., and Sozen, M. A., "Effects of Two-Dimensional Earthquake Motion on a Reinforced Concrete Column," Civil Engineering Studies, *Structural Research Series No. 399,* University of Illinois, Urbana, 1973.

15. Aktan, A. E., Pecknold, D.A.W., and Sozen, M. A., "R/C Column Earthquake Response in Two Dimensions," *J. Struct. Div., ASCE,* 100, 1999-2015, 1974.

16. Pecknold, D.A.W. and Sozen, M. A., "Calculated Inelastic Structural Response to Uniaxial and Biaxial Earthquake Motion," *Proceedings,* 5th Conference on Earthquake Engineering, Rome, Italy, 2, 1792-1795, 1973.

17. Pecknold, D. A., "Inelastic Structural Response to 2D Ground Motion," *J. Engng. Mech. Div., ASCE,* 100, 949-963, 1974.

18. Selna, L. G., Morrill, K. B., and Ersoy, O. K., "Earthquake Response Analysis of the Olive View Hospital Psychiatric Day Clinic," *Int. J. Earthq. Engng. Struct. Dyn.*, 3, 15-32, 1974.

19. Zayas, V. A., Popov, E. P. and Mahin, S. A., "Cyclic Inelastic Buckling of Tubular Steel Braces," Earthq. Engng. Res. Ctr., *Report No. EERC 80/16,* University of California, Berkeley, 1980.

20. Zayas, V. A., Mahin, S. A., and Popov, E. P., "Cyclic Inelastic Behavior of Steel Offshore Structures," Earthq. Engng. Res. Ctr., *Report No. EERC 80/28,* University of California, Berkeley, 1980.

21. Oliva, M. G., "Shaking Table Testing of a Reinforced Concrete Frame with Biaxial Response," Earthq. Engng. Res. Ctr., *Report No. EERC 80/28,* University of California, Berkeley, 1980.

22. Hughes, T.J.R., Taylor, R. L., Sackman, J. L., Curnier, A., and Kanoknukulchai, W., "A Finite Element Method for a Class of Contact-Impact Problems," *Computer Meth. in Appl. Mech. & Engng.,* Vol. 8, 249-276, 1976.

23. Hughes, T.J.R., Taylor, R. L., and Sackman, J. L., "Finite Element Formulation and Solution of Contact-Impact Problems in Continuum Mechanics," *SESM Report No. 74-8,* Department of Civil Engineering, University of California, Berkeley, 1974.

24. Nickell, R. E., "Direct Integration Methods in Structural Dynamics," *J. Engng. Mech. Div., ASCE,* Vol. 99, No. EM2, 303-317, 1973.

25. Hilber, H. H. and Hughes, T.J.R., "Collocation Dissipation and 'Overshoot' for Time Integration Schemes in Structural Dynamics," *Earthq. Engng. & Struct. Dyn.,* Vol. 6, 99-117, 1978.

26. Nicholson, M. D., "A Review of Methods for Analyzing the Whipping Movement of Pipe-work," *Report No. RD/B/N4148,* CEGB, Berkeley Nuc. Labs., England, 1977.

27. Janssen, L.G.J., "Pipe Whip Analysis on the Bundle Tubes in a Sodium-Water Steam Generator," *Paper F 9/6,* 4th International Congress on Structural Mechanics in Reactor Technology, 1977.

28. Hibbitt, H. D. and Karlsson, B. I., "Analysis of Pipe Whip," *ASME Paper No. 79-PVP-122, 19-19.*

29. Mahin, S. A., Bertero, V. V., Chopra, A. K., and Collins, R., "Response of the Olive View Hospital Main Building During the San Fernando Earthquake," Earthq. Engng. Res. Ctr., *Report No. EERC 76/22,* University of California, Berkeley, 1976.

30. Mroz, Z., "On the Description of Anisotropic Workhardening," *J. Mech. Phys. Solids,* Vol. 15, pp. 163-175, Pergammon Press Ltd., Great Britain, 1967.

31 To be published.

32. Manjoine, M. J., "Influence of Rate of Strain and Temperature on Yield Stresses of Mild Steel," *J. Appl. Mech.,* Vol. II, A-211, 1944.

33. Mroz, Z., "An Attempt to Describe the Behavior of Metals under Cyclic Loads Using a more General Workhardening Model," *Acta Mechanica,* Vol. 7, 199-212, 1969.

34. Ziegler, H., "A Modification of Prager's Hardening Rule," *Quarterly of Applied Math.,* Vol. 17, 55, 1959.

35. Prager, W., "The Theory of Plasticity: A Survey of Recent Achievements," *Proc. Inst. Mech. Engrs.,* 169, 41-57, 1955.

36. Hill, R., **The Mathematical Theory of Plasticity,** Oxford University Press, 1950.

37. Shield, R. T. and Ziegler, H., "On Prager's Hardening Rule," ZAMP 9a (1958), 260-276.

38. Vijay, D. K. and Kozluk, M. J., "Pipe Whip Analysis of Unrestrained Piping Systems," *ASME Paper #80-C27-PVP-149.*

39. Hilber, H. M., Hughes, T.J.R., and Taylor, R. L., "Improved Numerical Dissipation of Time Integration Algorithms in Structural Dynamics," *Earthq. Engng. & Struct. Dyn.,* Vol. 5, pp. 283-292, 1977.

EARTHQUAKE ENGINEERING RESEARCH CENTER REPORTS

NOTE: Numbers in parentheses are Accession Numbers assigned by the National Technical Information Service; these are followed by a price code. Copies of the reports may be ordered from the National Technical Information Service, 5285 Port Royal Road, Springfield, Virginia, 22161. Accession Numbers should be quoted on orders for reports (PB --- ---) and remittance must accompany each order. Reports without this information were not available at time of printing. The complete list of EERC reports (from EERC 67-1) is available upon request from the Earthquake Engineering Research Center, University of California, Berkeley, 47th Street and Hoffman Boulevard, Richmond, California 94804.

UCB/EERC-77/01 "PLUSH - A Computer Program for Probabilistic Finite Element Analysis of Seismic Soil-Structure Interaction," by M.P. Romo Organista, J. Lysmer and H.B. Seed - 1977 (PB81 177 651)A05

UCB/EERC-77/02 "Soil-Structure Interaction Effects at the Humboldt Bay Power Plant in the Ferndale Earthquake of June 7, 1975," by J.E. Valera, H.B. Seed, C.F. Tsai and J. Lysmer - 1977 (PB 265 795)A04

UCB/EERC-77/03 "Influence of Sample Disturbance on Sand Response to Cyclic Loading," by K. Mori, H.B. Seed and C.K. Chan - 1977 (PB 267 352)A04

UCB/EERC-77/04 "Seismological Studies of Strong Motion Records," by J. Shoja-Taheri - 1977 (PB 269 655)A10

UCB/EERC-77/05 Unassigned

UCB/EERC-77/06 "Developing Methodologies for Evaluating the Earthquake Safety of Existing Buildings," by No. 1 - B. Bresler; No. 2 - B. Bresler, T. Okada and D. Zisling; No. 3 - T. Okada and B. Bresler; No. 4 - V.V. Bertero and B. Bresler - 1977 (PB 267 354)A08

UCB/EERC-77/07 "A Literature Survey - Transverse Strength of Masonry Walls," by Y. Omote, R.L. Mayes, S.W. Chen and R.W. Clough - 1977 (PB 277 933)A07

UCB/EERC-77/08 "DRAIN-TABS: A Computer Program for Inelastic Earthquake Response of Three Dimensional Buildings," by R. Guendelman-Israel and G.H. Powell - 1977 (PB 270 693)A07

UCB/EERC-77/09 "SUBWALL: A Special Purpose Finite Element Computer Program for Practical Elastic Analysis and Design of Structural Walls with Substructure Option," by D.Q. Le, H. Peterson and E.P. Popov - 1977 (PB 270 567)A05

UCB/EERC-77/10 "Experimental Evaluation of Seismic Design Methods for Broad Cylindrical Tanks," by D.P. Clough (PB 272 280)A13

UCB/EERC-77/11 "Earthquake Engineering Research at Berkeley - 1976," - 1977 (PB 273 507)A09

UCB/EERC-77/12 "Automated Design of Earthquake Resistant Multistory Steel Building Frames," by N.D. Walker, Jr. - 1977 (PB 276 526)A09

UCB/EERC-77/13 "Concrete Confined by Rectangular Hoops Subjected to Axial Loads," by J. Vallenas, V.V. Bertero and E.P. Popov - 1977 (PB 275 165)A06

UCB/EERC-77/14 "Seismic Strain Induced in the Ground During Earthquakes," by Y. Sugimura - 1977 (PB 284 201)A04

UCB/EERC-77/15 Unassigned

UCB/EERC-77/16 "Computer Aided Optimum Design of Ductile Reinforced Concrete Moment Resisting Frames," by S.W. Zagajeski and V.V. Bertero - 1977 (PB 280 137)A07

UCB/EERC-77/17 "Earthquake Simulation Testing of a Stepping Frame with Energy-Absorbing Devices," by J.M. Kelly and D.F. Tsztoo - 1977 (PB 273 506)A04

UCB/EERC-77/18 "Inelastic Behavior of Eccentrically Braced Steel Frames under Cyclic Loadings," by C.W. Roeder and E.P. Popov - 1977 (PB 275 526)A15

UCB/EERC-77/19 "A Simplified Procedure for Estimating Earthquake-Induced Deformations in Dams and Embankments," by F.I. Makdisi and H.B. Seed - 1977 (PB 276 820)A04

UCB/EERC-77/20 "The Performance of Earth Dams during Earthquakes," by H.B. Seed, F.I. Makdisi and P. de Alba - 1977 (PB 276 821)A04

UCB/EERC-77/21 "Dynamic Plastic Analysis Using Stress Resultant Finite Element Formulation," by P. Lukkunapvasit and J.M. Kelly - 1977 (PB 275 453)A04

UCB/EERC-77/22 "Preliminary Experimental Study of Seismic Uplift of a Steel Frame," by R.W. Clough and A.A. Huckelbridge 1977 (PB 278 769)A08

UCB/EERC-77/23 "Earthquake Simulator Tests of a Nine-Story Steel Frame with Columns Allowed to Uplift," by A.A. Huckelbridge - 1977 (PB 277 944)A09

UCB/EERC-77/24 "Nonlinear Soil-Structure Interaction of Skew Highway Bridges," by M.-C. Chen and J. Penzien - 1977 (PB 276 176)A07

UCB/EERC-77/25 "Seismic Analysis of an Offshore Structure Supported on Pile Foundations," by D.D.-N. Liou and J. Penzien 1977 (PB 283 180)A06

UCB/EERC-77/26 "Dynamic Stiffness Matrices for Homogeneous Viscoelastic Half-Planes," by G. Dasgupta and A.K. Chopra - 1977 (PB 279 654)A06

Preceding page blank

UCB/EERC-77/27 "A Practical Soft Story Earthquake Isolation System," by J.M. Kelly, J.M. Eidinger and C.J. Derham - 1977 (PB 276 814)A07

UCB/EERC-77/28 "Seismic Safety of Existing Buildings and Incentives for Hazard Mitigation in San Francisco: An Exploratory Study," by A.J. Meltsner - 1977 (PB 281 970)A05

UCB/EERC-77/29 "Dynamic Analysis of Electrohydraulic Shaking Tables," by D. Rea, S. Abedi-Hayati and Y. Takahashi 1977 (PB 282 569)A04

UCB/EERC-77/30 "An Approach for Improving Seismic - Resistant Behavior of Reinforced Concrete Interior Joints," by B. Galunic, V.V. Bertero and E.P. Popov - 1977 (PB 290 870)A06

UCB/EERC-78/01 "The Development of Energy-Absorbing Devices for Aseismic Base Isolation Systems," by J.M. Kelly and D.F. Tsztoo - 1978 (PB 284 978)A04

UCB/EERC-78/02 "Effect of Tensile Prestrain on the Cyclic Response of Structural Steel Connections, by J.G. Bouwkamp and A. Mukhopadhyay - 1978

UCB/EERC-78/03 "Experimental Results of an Earthquake Isolation System using Natural Rubber Bearings," by J.M. Eidinger and J.M. Kelly - 1978 (PB 281 686)A04

UCB/EERC-78/04 "Seismic Behavior of Tall Liquid Storage Tanks," by A. Niwa - 1978 (PB 284 017)A14

UCB/EERC-78/05 "Hysteretic Behavior of Reinforced Concrete Columns Subjected to High Axial and Cyclic Shear Forces," by S.W. Zagajeski, V.V. Bertero and J.G. Bouwkamp - 1978 (PB 283 858)A13

UCB/EERC-78/06 "Three Dimensional Inelastic Frame Elements for the ANSR-I Program," by A. Riahi, D.G. Row and G.H. Powell - 1978 (PB 295 755)A04

UCB/EERC-78/07 "Studies of Structural Response to Earthquake Ground Motion," by O.A. Lopez and A.K. Chopra - 1978 (PB 282 790)A05

UCB/EERC-78/08 "A Laboratory Study of the Fluid-Structure Interaction of Submerged Tanks and Caissons in Earthquakes," by R.C. Byrd - 1978 (PB 284 957)A08

UCB/EERC-78/09 Unassigned

UCB/EERC-78/10 "Seismic Performance of Nonstructural and Secondary Structural Elements," by I. Sakamoto - 1978 (PB81 154 593)A05

UCB/EERC-78/11 "Mathematical Modelling of Hysteresis Loops for Reinforced Concrete Columns," by S. Nakata, T. Sproul and J. Penzien - 1978 (PB 298 274)A05

UCB/EERC-78/12 "Damageability in Existing Buildings," by T. Blejwas and B. Bresler - 1978 (PB 80 166 978)A05

UCB/EERC-78/13 "Dynamic Behavior of a Pedestal Base Multistory Building," by R.M. Stephen, E.L. Wilson, J.G. Bouwkamp and M. Button - 1978 (PB 286 650)A08

UCB/EERC-78/14 "Seismic Response of Bridges - Case Studies," by R.A. Imbsen, V. Nutt and J. Penzien - 1978 (PB 286 503)A10

UCB/EERC-78/15 "A Substructure Technique for Nonlinear Static and Dynamic Analysis," by D.G. Row and G.H. Powell - 1978 (PB 288 077)A10

UCB/EERC-78/16 "Seismic Risk Studies for San Francisco and for the Greater San Francisco Bay Area," by C.S. Oliveira - 1978 (PB 81 120 115)A07

UCB/EERC-78/17 "Strength of Timber Roof Connections Subjected to Cyclic Loads," by P. Gülkan, R.L. Mayes and R.W. Clough - 1978 (HUD-000 1491)A07

UCB/EERC-78/18 "Response of K-Braced Steel Frame Models to Lateral Loads," by J.G. Bouwkamp, R.M. Stephen and E.P. Popov - 1978

UCB/EERC-78/19 "Rational Design Methods for Light Equipment in Structures Subjected to Ground Motion," by J.L. Sackman and J.M. Kelly - 1978 (PB 292 357)A04

UCB/EERC-78/20 "Testing of a Wind Restraint for Aseismic Base Isolation," by J.M. Kelly and D.E. Chitty - 1978 (PB 292 833)A03

UCB/EERC-78/21 "APOLLO - A Computer Program for the Analysis of Pore Pressure Generation and Dissipation in Horizontal Sand Layers During Cyclic or Earthquake Loading," by P.P. Martin and H.B. Seed - 1978 (PB 292 835)A04

UCB/EERC-78/22 "Optimal Design of an Earthquake Isolation System," by M.A. Bhatti, K.S. Pister and E. Polak - 1978 (PB 294 735)A06

UCB/EERC-78/23 "MASH - A Computer Program for the Non-Linear Analysis of Vertically Propagating Shear Waves in Horizontally Layered Deposits," by P.P. Martin and H.B. Seed - 1978 (PB 293 101)A05

UCB/EERC-78/24 "Investigation of the Elastic Characteristics of a Three Story Steel Frame Using System Identification," by I. Kaya and H.D. McNiven - 1978 (PB 296 225)A06

UCB/EERC-78/25 "Investigation of the Nonlinear Characteristics of a Three-Story Steel Frame Using System Identification," by I. Kaya and H.D. McNiven - 1978 (PB 301 363)A05

UCB/EERC-78/26 "Studies of Strong Ground Motion in Taiwan," by Y.M. Hsiung, B.A. Bolt and J. Penzien - 1978 (PB 298 436)A06

UCB/EERC-78/27 "Cyclic Loading Tests of Masonry Single Piers: Volume 1 - Height to Width Ratio of 2," by P.A. Hidalgo, R.L. Mayes, H.D. McNiven and R.W. Clough - 1978 (PB 296 211)A07

UCB/EERC-78/28 "Cyclic Loading Tests of Masonry Single Piers: Volume 2 - Height to Width Ratio of 1," by S.-W.J. Chen, P.A. Hidalgo, R.L. Mayes, R.W. Clough and H.D. McNiven - 1978 (PB 296 212)A09

UCB/EERC-78/29 "Analytical Procedures in Soil Dynamics," by J. Lysmer - 1978 (PB 298 445)A06

UCB/EERC-79/01 "Hysteretic Behavior of Lightweight Reinforced Concrete Beam-Column Subassemblages," by B. Forzani, E.P. Popov and V.V. Bertero - April 1979(PB 298 267)A06

UCB/EERC-79/02 "The Development of a Mathematical Model to Predict the Flexural Response of Reinforced Concrete Beams to Cyclic Loads, Using System Identification," by J. Stanton & H. McNiven - Jan. 1979(PB 295 875)A10

UCB/EERC-79/03 "Linear and Nonlinear Earthquake Response of Simple Torsionally Coupled Systems," by C.L. Kan and A.K. Chopra - Feb. 1979(PB 298 262)A06

UCB/EERC-79/04 "A Mathematical Model of Masonry for Predicting its Linear Seismic Response Characteristics," by Y. Mengi and H.D. McNiven - Feb. 1979(PB 298 266)A06

UCB/EERC-79/05 "Mechanical Behavior of Lightweight Concrete Confined by Different Types of Lateral Reinforcement," by M.A. Manrique, V.V. Bertero and E.P. Popov - May 1979(PB 301 114)A06

UCB/EERC-79/06 "Static Tilt Tests of a Tall Cylindrical Liquid Storage Tank," by R.W. Clough and A. Niwa - Feb. 1979 (PB 301 167)A06

UCB/EERC-79/07 "The Design of Steel Energy Absorbing Restrainers and Their Incorporation into Nuclear Power Plants for Enhanced Safety: Volume 1 - Summary Report," by P.N. Spencer, V.F. Zackay, and E.R. Parker - Feb. 1979(UCB/EERC-79/07)A09

UCB/EERC-79/08 "The Design of Steel Energy Absorbing Restrainers and Their Incorporation into Nuclear Power Plants for Enhanced Safety: Volume 2 - The Development of Analyses for Reactor System Piping,""Simple Systems" by M.C. Lee, J. Penzien, A.K. Chopra and K, Suzuki "Complex Systems" by G.H. Powell, E.L. Wilson, R.W. Clough and D.G. Row - Feb. 1979(UCB/EERC-79/08)A10

UCB/EERC-79/09 "The Design of Steel Energy Absorbing Restrainers and Their Incorporation into Nuclear Power Plants for Enhanced Safety: Volume 3 - Evaluation of Commercial Steels," by W.S. Owen, R.M.N. Pelloux, R.O. Ritchie, M. Faral, T. Ohhashi, J. Toplosky, S.J. Hartman, V.F. Zackay and E.R. Parker - Feb. 1979(UCB/EERC-79/09)A04

UCB/EERC-79/10 "The Design of Steel Energy Absorbing Restrainers and Their Incorporation into Nuclear Power Plants for Enhanced Safety: Volume 4 - A Review of Energy-Absorbing Devices," by J.M. Kelly and M.S. Skinner - Feb. 1979(UCB/EERC-79/10)A04

UCB/EERC-79/11 "Conservatism In Summation Rules for Closely Spaced Modes," by J.M. Kelly and J.L. Sackman - May 1979(PB 301 328)A03

UCB/EERC-79/12 "Cyclic Loading Tests of Masonry Single Piers; Volume 3 - Height to Width Ratio of 0.5," by P.A. Hidalgo, R.L. Mayes, H.D. McNiven and R.W. Clough - May 1979(PB 301 321)A08

UCB/EERC-79/13 "Cyclic Behavior of Dense Course-Grained Materials in Relation to the Seismic Stability of Dams," by N.G. Banerjee, H.B. Seed and C.K. Chan - June 1979(PB 301 373)A13

UCB/EERC-79/14 "Seismic Behavior of Reinforced Concrete Interior Beam-Column Subassemblages," by S. Viwathanatepa, E.P. Popov and V.V. Bertero - June 1979(PB 301 326)A10

UCB/EERC-79/15 "Optimal Design of Localized Nonlinear Systems with Dual Performance Criteria Under Earthquake Excitations," by M.A. Bhatti - July 1979(PB 80 167 109)A06

UCB/EERC-79/16 "OPTDYN - A General Purpose Optimization Program for Problems with or without Dynamic Constraints," by M.A. Bhatti, E. Polak and K.S. Pister - July 1979(PB 80 167 091)A05

UCB/EERC-79/17 "ANSR-II, Analysis of Nonlinear Structural Response, Users Manual," by D.P. Mondkar and G.H. Powell July 1979(PB 80 113 301)A05

UCB/EERC-79/18 "Soil Structure Interaction in Different Seismic Environments," A. Gomez-Masso, J. Lysmer, J.-C. Chen and H.B. Seed - August 1979(PB 80 101 520)A04

UCB/EERC-79/19 "ARMA Models for Earthquake Ground Motions," by M.K. Chang, J.W. Kwiatkowski, R.F. Nau, R.M. Oliver and K.S. Pister - July 1979(PB 301 166)A05

UCB/EERC-79/20 "Hysteretic Behavior of Reinforced Concrete Structural Walls," by J.M. Vallenas, V.V. Bertero and E.P. Popov - August 1979(PB 80 165 905)A12

UCB/EERC-79/21 "Studies on High-Frequency Vibrations of Buildings - 1: The Column Effect," by J. Lubliner - August 1979 (PB 80 158 553)A03

UCB/EERC-79/22 "Effects of Generalized Loadings on Bond Reinforcing Bars Embedded in Confined Concrete Blocks," by S. Viwathanatepa, E.P. Popov and V.V. Bertero - August 1979(PB 81 124 018)A14

UCB/EERC-79/23 "Shaking Table Study of Single-Story Masonry Houses, Volume 1: Test Structures 1 and 2," by P. Gülkan, R.L. Mayes and R.W. Clough - Sept. 1979 (HUD-000 1763)A12

UCB/EERC-79/24 "Shaking Table Study of Single-Story Masonry Houses, Volume 2: Test Structures 3 and 4," by P. Gülkan, R.L. Mayes and R.W. Clough - Sept. 1979 (HUD-000 1836)A12

UCB/EERC-79/25 "Shaking Table Study of Single-Story Masonry Houses, Volume 3: Summary, Conclusions and Recommendations," by R.W. Clough, R.L. Mayes and P. Gülkan - Sept. 1979 (HUD-000 1837)A06

UCB/EERC-79/26 "Recommendations for a U.S.-Japan Cooperative Research Program Utilizing Large-Scale Testing Facilities," by U.S.-Japan Planning Group - Sept. 1979(PB 301 407)A06

UCB/EERC-79/27 "Earthquake-Induced Liquefaction Near Lake Amatitlan, Guatemala," by H.B. Seed, I. Arango, C.K. Chan, A. Gomez-Masso and R. Grant de Ascoli - Sept. 1979(NUREG-CR1341)A03

UCB/EERC-79/28 "Infill Panels: Their Influence on Seismic Response of Buildings," by J.W. Axley and V.V. Bertero Sept. 1979(PB 80 163 371)A10

UCB/EERC-79/29 "3D Truss Bar Element (Type 1) for the ANSR-II Program," by D.P. Mondkar and G.H. Powell - Nov. 1979 (PB 80 169 709)A02

UCB/EERC-79/30 "2D Beam-Column Element (Type 5 - Parallel Element Theory) for the ANSR-II Program," by D.G. Row, G.H. Powell and D.P. Mondkar - Dec. 1979(PB 80 167 224)A03

UCB/EERC-79/31 "3D Beam-Column Element (Type 2 - Parallel Element Theory) for the ANSR-II Program," by A. Riahi, G.H. Powell and D.P. Mondkar - Dec. 1979(PB 80 167 216)A03

UCB/EERC-79/32 "On Response of Structures to Stationary Excitation," by A. Der Kiureghian - Dec. 1979(PB 80166 929)A03

UCB/EERC-79/33 "Undisturbed Sampling and Cyclic Load Testing of Sands," by S. Singh, H.B. Seed and C.K. Chan Dec. 1979(ADA 087 298)A07

UCB/EERC-79/34 "Interaction Effects of Simultaneous Torsional and Compressional Cyclic Loading of Sand," by P.M. Griffin and W.N. Houston - Dec. 1979(ADA 092 352)A15

UCB/EERC-80/01 "Earthquake Response of Concrete Gravity Dams Including Hydrodynamic and Foundation Interaction Effects," by A.K. Chopra, P. Chakrabarti and S. Gupta - Jan. 1980(AD-A087297)A10

UCB/EERC-80/02 "Rocking Response of Rigid Blocks to Earthquakes," by C.S. Yim, A.K. Chopra and J. Penzien - Jan. 1980 (PB80 166 002)A04

UCB/EERC-80/03 "Optimum Inelastic Design of Seismic-Resistant Reinforced Concrete Frame Structures," by S.W. Zagajeski and V.V. Bertero - Jan. 1980(PB80 164 635)A06

UCB/EERC-80/04 "Effects of Amount and Arrangement of Wall-Panel Reinforcement on Hysteretic Behavior of Reinforced Concrete Walls," by R. Iliya and V.V. Bertero - Feb. 1980(PB81 122 525)A09

UCB/EERC-80/05 "Shaking Table Research on Concrete Dam Models," by A. Niwa and R.W. Clough - Sept. 1980(PB81 122 368)A06

UCB/EERC-80/06 "The Design of Steel Energy-Absorbing Restrainers and their Incorporation into Nuclear Power Plants for Enhanced Safety (Vol 1A): Piping with Energy Absorbing Restrainers: Parameter Study on Small Systems," by G.H. Powell, C. Oughourlian and J. Simons - June 1980

UCB/EERC-80/07 "Inelastic Torsional Response of Structures Subjected to Earthquake Ground Motions," by Y. Yamazaki April 1980(PB81 122 327)A08

UCB/EERC-80/08 "Study of X-Braced Steel Frame Structures Under Earthquake Simulation," by Y. Ghanaat - April 1980 (PB81 122 335)A11

UCB/EERC-80/09 "Hybrid Modelling of Soil-Structure Interaction," by S. Gupta, T.W. Lin, J. Penzien and C.S. Yeh May 1980(PB81 122 319)A07

UCB/EERC-80/10 "General Applicability of a Nonlinear Model of a One Story Steel Frame," by B.I. Sveinsson and H.D. McNiven - May 1980(PB81 124 877)A06

UCB/EERC-80/11 "A Green-Function Method for Wave Interaction with a Submerged Body," by W. Kioka - April 1980 (PB81 122 269)A07

UCB/EERC-80/12 "Hydrodynamic Pressure and Added Mass for Axisymmetric Bodies," by F. Nilrat - May 1980(PB81 122 343)A08

UCB/EERC-80/13 "Treatment of Non-Linear Drag Forces Acting on Offshore Platforms," by B.V. Dao and J. Penzien May 1980(PB81 153 413)A07

UCB/EERC-80/14 "2D Plane/Axisymmetric Solid Element (Type 3 - Elastic or Elastic-Perfectly Plastic) for the ANSR-II Program," by D.P. Mondkar and G.H. Powell - July 1980(PB81 122 350)A03

UCB/EERC-80/15 "A Response Spectrum Method for Random Vibrations," by A. Der Kiureghian - June 1980(PB81 122 301)A03

UCB/EERC-80/16 "Cyclic Inelastic Buckling of Tubular Steel Braces," by V.A. Zayas, E.P. Popov and S.A. Mahin June 1980(PB81 124 885)A10

UCB/EERC-80/17 "Dynamic Response of Simple Arch Dams Including Hydrodynamic Interaction," by C.S. Porter and A.K. Chopra - July 1980(PB81 124 000)A13

UCB/EERC-80/18 "Experimental Testing of a Friction Damped Aseismic Base Isolation System with Fail-Safe Characteristics," by J.M. Kelly, K.E. Beucke and M.S. Skinner - July 1980(PB81 148 595)A04

UCB/EERC-80/19 "The Design of Steel Energy-Absorbing Restrainers and their Incorporation into Nuclear Power Plants for Enhanced Safety (Vol 1B): Stochastic Seismic Analyses of Nuclear Power Plant Structures and Piping Systems Subjected to Multiple Support Excitations," by M.C. Lee and J. Penzien - June 1980

UCB/EERC-80/20 "The Design of Steel Energy-Absorbing Restrainers and their Incorporation into Nuclear Power Plants for Enhanced Safety (Vol 1C): Numerical Method for Dynamic Substructure Analysis," by J.M. Dickens and E.L. Wilson - June 1980

UCB/EERC-80/21 "The Design of Steel Energy-Absorbing Restrainers and their Incorporation into Nuclear Power Plants for Enhanced Safety (Vol 2): Development and Testing of Restraints for Nuclear Piping Systems," by J.M. Kelly and M.S. Skinner - June 1980

UCB/EERC-80/22 "3D Solid Element (Type 4-Elastic or Elastic-Perfectly-Plastic) for the ANSR-II Program," by D.P. Mondkar and G.H. Powell - July 1980(PB81 123 242)A03

UCB/EERC-80/23 "Gap-Friction Element (Type 5) for the ANSR-II Program," by D.P. Mondkar and G.H. Powell - July 1980 (PB81 122 285)A03

UCB/EERC-80/24 "U-Bar Restraint Element (Type 11) for the ANSR-II Program," by C. Oughourlian and G.H. Powell July 1980(PB81 122 293)A03

UCB/EERC-80/25 "Testing of a Natural Rubber Base Isolation System by an Explosively Simulated Earthquake," by J.M. Kelly - August 1980(PB81 201 360)A04

UCB/EERC-80/26 "Input Identification from Structural Vibrational Response," by Y. Hu - August 1980(PB81 152 308)A05

UCB/EERC-80/27 "Cyclic Inelastic Behavior of Steel Offshore Structures," by V.A. Zayas, S.A. Mahin and E.P. Popov August 1980(PB81 196 180)A15

UCB/EERC-80/28 "Shaking Table Testing of a Reinforced Concrete Frame with Biaxial Response," by M.G. Oliva October 1980(PB81 154 304)A10

UCB/EERC-80/29 "Dynamic Properties of a Twelve-Story Prefabricated Panel Building," by J.G. Bouwkamp, J.P. Kollegger and R.M. Stephen - October 1980(PB82 117 128)A06

UCB/EERC-80/30 "Dynamic Properties of an Eight-Story Prefabricated Panel Building," by J.G. Bouwkamp, J.P. Kollegger and R.M. Stephen - October 1980(PB81 200 313)A05

UCB/EERC-80/31 "Predictive Dynamic Response of Panel Type Structures Under Earthquakes," by J.P. Kollegger and J.G. Bouwkamp - October 1980(PB81 152 316)A04

UCB/EERC-80/32 "The Design of Steel Energy-Absorbing Restrainers and their Incorporation into Nuclear Power Plants for Enhanced Safety (Vol 3): Testing of Commercial Steels in Low-Cycle Torsional Fatigue," by P. Spencer, E.R. Parker, E. Jongewaard and M. Drory

UCB/EERC-80/33 "The Design of Steel Energy-Absorbing Restrainers and their Incorporation into Nuclear Power Plants for Enhanced Safety (Vol 4): Shaking Table Tests of Piping Systems with Energy-Absorbing Restrainers," by S.F. Stiemer and W.G. Godden - Sept. 1980

UCB/EERC-80/34 "The Design of Steel Energy-Absorbing Restrainers and their Incorporation into Nuclear Power Plants for Enhanced Safety (Vol 5): Summary Report," by P. Spencer

UCB/EERC-80/35 "Experimental Testing of an Energy-Absorbing Base Isolation System," by J.M. Kelly, M.S. Skinner and K.E. Beucke - October 1980(PB81 154 072)A04

UCB/EERC-80/36 "Simulating and Analyzing Artificial Non-Stationary Earthquake Ground Motions," by R.F. Nau, R.M. Oliver and K.S. Pister - October 1980(PB81 153 397)A04

UCB/EERC-80/37 "Earthquake Engineering at Berkeley - 1980." - Sept. 1980(PB81 205 874)A09

UCB/EERC-80/38 "Inelastic Seismic Analysis of Large Panel Buildings," by V. Schricker and G.H. Powell - Sept. 1980 (PB81 154 338)A13

UCB/EERC-80/39 "Dynamic Response of Embankment, Concrete-Gravity and Arch Dams Including Hydrodynamic Interaction," by J.F. Hall and A.K. Chopra - October 1980(PB81 152 324)A11

UCB/EERC-80/40 "Inelastic Buckling of Steel Struts Under Cyclic Load Reversal," by R.G. Black, W.A. Wenger and E.P. Popov - October 1980(PB81 154 312)A08

UCB/EERC-80/41 "Influence of Site Characteristics on Building Damage During the October 3, 1974 Lima Earthquake," by P. Repetto, I. Arango and H.B. Seed - Sept. 1980(PB81 161 739)A05

UCB/EERC-80/42 "Evaluation of a Shaking Table Test Program on Response Behavior of a Two Story Reinforced Concrete Frame," by J.M. Blondet, R.W. Clough and S.A. Mahin

UCB/EERC-80/43 "Modelling of Soil-Structure Interaction by Finite and Infinite Elements," by F. Medina - December 1980(PB81 229 270)A04

UCB/EERC-81/01 "Control of Seismic Response of Piping Systems and Other Structures by Base Isolation," edited by J.M. Kelly - January 1981 (PB81 200 735)A05

UCB/EERC-81/02 "OPTNSR - An Interactive Software System for Optimal Design of Statically and Dynamically Loaded Structures with Nonlinear Response," by M.A. Bhatti, V. Ciampi and K.S. Pister - January 1981 (PB81 218 851)A09

UCB/EERC-81/03 "Analysis of Local Variations in Free Field Seismic Ground Motions," by J.-C. Chen, J. Lysmer and H.B. Seed - January 1981 (AD-A099508)A13

UCB/EERC-81/04 "Inelastic Structural Modeling of Braced Offshore Platforms for Seismic Loading," by V.A. Zayas, P.-S.B. Shing, S.A. Mahin and E.P. Popov - January 1981(PB82 138 777)A07

UCB/EERC-81/05 "Dynamic Response of Light Equipment in Structures," by A. Der Kiureghian, J.L. Sackman and B. Nour-Omid - April 1981 (PB81 218 497)A04

UCB/EERC-81/06 "Preliminary Experimental Investigation of a Broad Base Liquid Storage Tank," by J.G. Bouwkamp, J.P. Kollegger and R.M. Stephen - May 1981(PB82 140 385)A03

UCB/EERC-81/07 "The Seismic Resistant Design of Reinforced Concrete Coupled Structural Walls," by A.E. Aktan and V.V. Bertero - June 1981(PB82 113 358)A11

UCB/EERC-81/08 "The Undrained Shearing Resistance of Cohesive Soils at Large Deformations," by M.R. Pyles and H.B. Seed - August 1981

UCB/EERC-81/09 "Experimental Behavior of a Spatial Piping System with Steel Energy Absorbers Subjected to a Simulated Differential Seismic Input," by S.F. Stiemer, W.G. Godden and J.M. Kelly - July 1981

UCB/EERC-81/10 "Evaluation of Seismic Design Provisions for Masonry in the United States," by B.I. Sveinsson, R.L. Mayes and H.D. McNiven - August 1981

UCB/EERC-81/11 "Two-Dimensional Hybrid Modelling of Soil-Structure Interaction," by T.-J. Tzong, S. Gupta and J. Penzien - August 1981(PB82 142 118)A04

UCB/EERC-81/12 "Studies on Effects of Infills in Seismic Resistant R/C Construction," by S. Brokken and V.V. Bertero - September 1981

UCB/EERC-81/13 "Linear Models to Predict the Nonlinear Seismic Behavior of a One-Story Steel Frame," by H. Valdimarsson, A.H. Shah and H.D. McNiven - September 1981(PB82 138 793)A07

UCB/EERC-81/14 "TLUSH: A Computer Program for the Three-Dimensional Dynamic Analysis of Earth Dams," by T. Kagawa, L.H. Mejia, H.B. Seed and J. Lysmer - September 1981(PB82 139 940)A06

UCB/EERC-81/15 "Three Dimensional Dynamic Response Analysis of Earth Dams," by L.H. Mejia and H.B. Seed - September 1981 (PB82 137 274)A12

UCB/EERC-81/16 "Experimental Study of Lead and Elastomeric Dampers for Base Isolation Systems," by J.M. Kelly and S.B. Hodder - October 1981 (PB82 166 182)A05

UCB/EERC-81/17 "The Influence of Base Isolation on the Seismic Response of Light Secondary Equipment," by J.M. Kelly - April 1981 (PB82 255 266)A04

UCB/EERC-81/18 "Studies on Evaluation of Shaking Table Response Analysis Procedures," by J. Marcial Blondet - November 1981 (PB82 197 278)A10

UCB/EERC-81/19 "DELIGHT.STRUCT: A Computer-Aided Design Environment for Structural Engineering," by R.J. Balling, K.S. Pister and E. Polak - December 1981 (PB82 218 496)A07

UCB/EERC-81/20 "Optimal Design of Seismic-Resistant Planar Steel Frames," by R.J. Balling, V. Ciampi, K.S. Pister and E. Polak - December 1981 (PB82 220 179)A07

UCB/EERC-82/01 "Dynamic Behavior of Ground for Seismic Analysis of Lifeline Systems," by T. Sato and A. Der Kiureghian - January 1982 (PB82 218 926)A05

UCB/EERC-82/02 "Shaking Table Tests of a Tubular Steel Frame Model," by Y. Ghanaat and R. W. Clough - January 1982 (PB82 220 161)A07

UCB/EERC-82/03 "Experimental Behavior of a Spatial Piping System with Shock Arrestors and Energy Absorbers under Seismic Excitation," by S. Schneider, H.-M. Lee and G. W. Godden - May 1982

UCB/EERC-82/04 "New Approaches for the Dynamic Analysis of Large Structural Systems," by E. L. Wilson - June 1982 (PB83 148 080)A05

UCB/EERC-82/05 "Model Study of Effects of Damage on the Vibration Properties of Steel Offshore Platforms," by F. Shahrivar and J. G. Bouwkamp - June 1982

UCB/EERC-82/06 "States of the Art and Practice in the Optimum Seismic Design and Analytical Response Prediction of R/C Frame-Wall Structures," by A. E. Aktan and V. V. Bertero - July 1982 (PB83 147 736)A05

UCB/EERC-82/07 "Further Study of the Earthquake Response of a Broad Cylindrical Liquid-Storage Tank Model," by G. C. Manos and R. W. Clough - July 1982 (PB83 147 744)A11

UCB/EERC-82/08 "An Evaluation of the Design and Analytical Seismic Response of a Seven Story Reinforced Concrete Frame - Wall Structure," by F. A. Charney and V. V. Bertero - July 1982

UCB/EERC-82/09 "Fluid-Structure Interactions: Added Mass Computations for Incompressible Fluid," by J. S.-H. Kuo - August 1982

UCB/EERC-82/10 "Joint-Opening Nonlinear Mechanism: Interface Smeared Crack Model," by J. S.-H. Kuo - August 1982 (PB83 149 195)A05

UCB/EERC-82/11 "Dynamic Response Analysis of Techi Dam," by R. W. Clough, R. M. Stephen and J. S.-H. Kuo - August 1982 (PB83 147 496)A06

UCB/EERC-82/12 "Prediction of the Seismic Responses of R/C Frame-Coupled Wall Structures," by A. E. Aktan, V. V. Bertero and M. Piazza - August 1982 (PB83 149 203)A09

UCB/EERC-82/13 "Preliminary Report on the SMART 1 Strong Motion Array in Taiwan," by B. A. Bolt, C. H. Loh, J. Penzien, Y. B. Tsai and Y. T. Yeh - August 1982

UCB/EERC-82/14 "Shaking-Table Studies of an Eccentrically X-Braced Steel Structure," by M. S. Yang - September 1982

UCB/EERC-82/15 "The Performance of Stairways in Earthquakes," by C. Roha, J. W. Axley and V. V. Bertero - September 1982

UCB/EERC-82/16 "The Behavior of Submerged Multiple Bodies in Earthquakes," by W.-G. Liao - September 1982

UCB/EERC-82/17 "Effects of Concrete Types and Loading Conditions on Local Bond-Slip Relationships," by A. D. Cowell, E. P. Popov and V. V. Bertero - September 1982

UCB/EERC-82/18 "Mechanical Behavior of Shear Wall Vertical Boundary Members: An Experimental Investigation," by M. T. Wagner and V. V. Bertero - October 1982

UCB/EERC-82/19 "Experimental Studies of Multi-support Seismic Loading on Piping Systems," by J. M. Kelly and A. D. Cowell - November 1982

UCB/EERC-82/20 "Generalized Plastic Hinge Concepts for 3D Beam-Column Elements," by P. F.-S. Chen and G. H. Powell - November 1982